

**PROTECTION OF TRANSMISSION LINES SHARING THE
SAME RIGHT-OF-WAY**

BY

IONI T. FERNANDO

A Thesis

**Submitted to the Faculty of Graduate Studies
in Partial Fulfilment of the Requirements
for the Degree of**

DOCTOR OF PHILOSOPHY

**Department of Electrical and Computer Engineering
University of Manitoba
Winnipeg, Manitoba,
Canada**

(c) September, 1997



National Library
of Canada

Acquisitions and
Bibliographic Services

395 Wellington Street
Ottawa ON K1A 0N4
Canada

Bibliothèque nationale
du Canada

Acquisitions et
services bibliographiques

395, rue Wellington
Ottawa ON K1A 0N4
Canada

Your file Votre référence

Our file Notre référence

The author has granted a non-exclusive licence allowing the National Library of Canada to reproduce, loan, distribute or sell copies of this thesis in microform, paper or electronic formats.

The author retains ownership of the copyright in this thesis. Neither the thesis nor substantial extracts from it may be printed or otherwise reproduced without the author's permission.

L'auteur a accordé une licence non exclusive permettant à la Bibliothèque nationale du Canada de reproduire, prêter, distribuer ou vendre des copies de cette thèse sous la forme de microfiche/film, de reproduction sur papier ou sur format électronique.

L'auteur conserve la propriété du droit d'auteur qui protège cette thèse. Ni la thèse ni des extraits substantiels de celle-ci ne doivent être imprimés ou autrement reproduits sans son autorisation.

0-612-23601-3

**THE UNIVERSITY OF MANITOBA
FACULTY OF GRADUATE STUDIES

COPYRIGHT PERMISSION PAGE**

**PROTECTION OF TRANSMISSION LINES SHARING THE SAME
RIGHT-OF-WAY**

BY

IONI T. FERNANDO

**A Thesis/Practicum submitted to the Faculty of Graduate Studies of The University
of Manitoba in partial fulfillment of the requirements of the degree
of
DOCTOR OF PHILOSOPHY**

Ioni T. Fernando 1997 (c)

**Permission has been granted to the Library of The University of Manitoba to lend or sell
copies of this thesis/practicum, to the National Library of Canada to microfilm this thesis
and to lend or sell copies of the film, and to Dissertations Abstracts International to publish
an abstract of this thesis/practicum.**

**The author reserves other publication rights, and neither this thesis/practicum nor
extensive extracts from it may be printed or otherwise reproduced without the author's
written permission.**

TABLE OF CONTENTS



	Pages
Acknowledgments	viii
Abstract	ix
LIST OF FIGURES	x
LIST OF TABLES	xx
1. BACKGROUND AND INTRODUCTION	1
1.1 Background	1
1.2 Introduction	3
1.3 Scope	5
1.4 Overview of this Thesis	6

2. DISTANCE RELAY ALGORITHMS	8
2.1 Basic Operating Criteria of a Digital Distance Relay	8
2.1.1 Trip Characteristics	11
2.2 Data Processing Techniques	14
2.2.1 Sampling	16
2.2.2 Frequency Tracking	18
2.2.3 Low Pass Filtering	19
2.2.4 High Pass Filtering	19
2.2.5 Fourier Algorithm	20
2.2.6 Sequence Filtering	21
2.3 Supporting Elements to Distance Relay Algorithms	22
2.3.1 Over-Current Element	22
2.3.2 Directional Element	23
2.4 Organization of the Alpha Power Technology Relay	31
2.5 Summary	34
 3. ADVANCED POWER TECHNOLOGY RELAY LIBRARY FOR	
PSCAD/EMTDC™	35
3.1 PSCAD/EMTDC™ Relay Library of the APT Relay Elements	35
3.2 Data Processing Models and their Characteristics	37
3.2.1 Sampling Clock	37
3.2.2 Frequency Tracking Unit	38
3.2.3 Low-Pass Filter	40
3.2.4 High-Pass Filter	41
3.2.5 Sampler	46
3.2.6 Fast Fourier Transform (FFT)	47
3.2.7 Sequence Filter	49
3.2.8 Ground Impedance Element	50

3.2.9 Line Impedance Element	52
3.2.10 Directional Impedance Element	52
3.2.11 Zone Tripping Model	53
3.2.12 Data File Writer	54
3.2.13 Artificial Neural Network Model	55
3.3 Test Set-up	57
3.4 Summary	59
 4. SIMULATION MODELS	 60
4.1 Three-Phase Double Circuit Line Model	60
4.1.1 Transmission Line	61
4.1.2 Source and Transformers on Sending and Receiving Ends	65
4.2 Six-Phase Line Model	66
4.3 Summary	69
 5. PERFORMANCE OF IMPEDANCE RELAYS ON DOUBLE CIRCUIT LINES	 70
5.1 Introduction	70
5.2 Impedance Relay and its Settings	71
5.2.1 Trip Zone Settings	72
5.3 Impedance Trajectories for Different Types of Faults	74
5.3.1 Single Line to Ground Fault (a_1 -g)	74
5.3.2 Single Circuit Double-Line-to-Ground Fault (a_1 - b_1 -g)	78
5.3.3 Inter Circuit Double Line to Ground Fault (a_1 - b_2 -g)	80
5.3.4 Single Circuit Three-Phase-to-Ground fault (a_1 - b_1 - c_1 -g)	84
5.3.5 Inter Circuit Three-Phase-to-Ground Fault (a_1 - b_1 - c_2 -g)	84
5.3.6 Inter Circuit Four-Phase-to-Ground Fault (a_1 - b_1 - c_1 - a_2 -g)	87
5.3.7 Inter Phase Faults with no Ground Involvement	90

5.4	Observations	91
5.5	Proposed Improvement to Impedance Relays for Double Circuit Line Application	93
5.5.1	Modified Ground Impedance Trajectories	96
5.6	Summary of Relay Performance for Various Faults	100
5.7	Conclusions	101
6.	PERFORMANCE OF IMPEDANCE ELEMENTS ON SIX-PHASE TRANSMISSION LINES	102
6.1	Introduction	102
6.2	Impedance Relay and its Settings	103
6.3	Impedance Trajectories for Selected Fault Types	107
6.3.1	Single Line-to-Ground Fault (phase-a to ground)	107
6.3.2	Single Circuit Double Line to Ground Faults	111
6.3.3	Inter Circuit Double Line to Ground Fault	113
6.3.4	Single Circuit Three-Phase / Three-Phase-Ground Faults	119
6.3.5	Inter Circuit Three-Phase to Ground Faults	119
6.3.6	Four-Phase to Ground / Four-Phase Faults	126
6.3.7	Five-Phase to Ground / Five-Phase Faults	130
6.3.8	Six-Phase to Ground / Six-Phase Faults	130
6.4	Summary of Relay Performance for Various Faults	130
6.5	Effect of Pre-fault Operating Point on the Distance Relay Impedance Trajectories	133
6.5.1	Ground Faults	133
6.5.2	Ungrounded Faults	134
6.6	Conclusions	134

7. PROTECTION OF POINTE DU BOIS TRANSMISSION LINE	135
7.1 Rover-Pointe System Model.	136
7.1.1 Transmission Line	136
7.1.2 Pointe du Bois Terminal Station.	136
7.1.3 Rover Terminal Station.	138
7.2 Current Balance Algorithm	140
7.3 Test Set-up	141
7.4 Test Results	142
7.4.1 Single Line to Ground Fault	143
7.4.2 Remote Three-Phase Fault	145
7.4.3 Inter-Circuit Double Line Fault	148
7.5 Conclusions	148
 8. INTEGRATION OF ARTIFICIAL INTELLIGENCE TO THE APT RELAY	 150
8.1 Problem Identification	151
8.2 Artificial Neural Networks and their Properties	152
8.3 Applications of Neural Networks in Power System Protection	153
8.4 Selection of the ANN Architecture and Learning Rule	159
8.5 Selection of Network Topology	160
8.5.1 General Network Structure	160
8.5.2 Inputs and Outputs of the ANN	161
8.5.3 Activation Function of the Neurons	165
8.5.4 Learning Rule of the Network (Error Back-Propagation)	167
8.5.5 Training and Test Input-Output Data Vectors	169
8.5.6 Training and Test Data Generation	172
8.6 Conclusions	173

9. PERFORMANCE OF THE ANN TRAINED FOR DOUBLE CIRCUIT LINE APPLICATION	174
9.1 Training for Double Circuit Transmission Line Application	174
9.1.1 Scaling of Input Data	174
9.1.2 Network Structure and Training	176
9.2 Testing of the Neural Network	178
9.2.1 Criteria for Successful Diagnosis of Faulted Phases	178
9.3 Performance of the Trained Artificial Neural Network.	179
9.3.1 The Successful Response of the ANN to a Simple Line to Ground Fault	181
9.3.2 ANN Generates Short Duration ‘High’ Flags	182
9.3.3 ANN Response to Increased Distance to Fault	183
9.3.4 ANN is Insensitive to the Fault Inception Point on the Wave	185
9.3.5 Influence of Fault Resistance on the ANN Outputs	187
9.4 ANN Test Results	188
9.4.1 ANN Performance for Different Fault Locations	188
9.4.2 ANN Performance for Different Pre-Fault Operating Powers	191
9.4.3 ANN Performance for Different Fault Resistances	194
9.4.4 ANN Performance for Different Source Impedances	195
9.5 Comparison of the Trip Signals from the ANN and the APT Impedance Elements	196
9.6 Comparison of the Trip Signals from the ANN and the APT Single-Pole Trip Logic	202
9.7 Conclusions	204
 10. CONCLUSIONS AND FUTURE WORK	 206
10.1 Contributions	206
10.2 Future Work	207
10.3 Conclusions	209

REFERENCES	i
Appendix A:Positive Sequence Incremental Impedance Computations	A-i
A.1 Computation of the Positive Sequence Incremental Impedances for a Three-Phase Single-Circuit Transmission Line	A-i
A.2 Computation of the Positive Sequence Incremental Impedances for a Three-Phase Double-Circuit Transmission Line	A-v
Appendix B:Transmission Line Data and Conductor Configurations.....	B-i
B.1 McCalmont-Springdale Transmission Line Data	B-i
B.2 Pointe du Bois Transmission Line Data	B-iii
Appendix C:Validation Test of Pointe du Bois Transmission Line Model	C-i
C.1 Case Studies	C-ii
C.1.1 Case 94-0330.000	C-iii
C.1.2 Case 94-0410.000	C-ix
C.1.3 Case 94-0414.000	C-ix
C.1.4 Case 94-0608.000	C-xvi
C.1.5 Case 94-0608.001	C-xvi
C.1.6 Case 94-0608.002	C-xxii
C.1.7 Case 94-0617.000	C-xxviii
C.1.8 Case 94-0702.000	C-xxviii
C.2 Conclusions	C-xxx

Acknowledgments

I wish to express my sincere gratitude to Dr. P.G. McLaren for the guidance, advice and support extended during the course of this work. It is a true privilege to work with a leading researcher in the field. I also wish to thank my co-advisor Mr. A. Castro for the valuable guidance, Manitoba Hydro for their financial support, and the University of Manitoba for the research facilities provided for the project.

I am also very thankful to Dr. J. R. Lucas for the much needed direction given to pursue my doctoral studies. I acknowledge with greatest appreciation the valuable discussions and the information made available to me by the rest of the power research group at University of Manitoba. A special note of thanks is due to my colleague Dr. Rohitha Jayasinghe. I am also grateful to all my friends who have helped me in many different ways during the course of the study.

I also extend my heart felt gratitude to my dearest parents and my only sister for all the support given over the years. Finally, I take this opportunity to let my husband Pradeepa know that its you who has been the inspiration to further my studies to a doctoral degree.

Ioni T. Fernando.

Department of Electrical and Computer Engineering

University of Manitoba

September 18, 1997.

Abstract

The compact transmission configurations such as the double-circuit and multi-phase systems have emerged as a result of the search for compact and efficient systems with minimal environmental hazards. Protective relaying techniques are therefore, required to also evolve to provide adequate protection to such systems.

The latest well established numerical techniques have made protective relays very flexible, adaptable and cost effective. They also offer increased functionality in various applications. This thesis project proceeds to investigate the possible enhancements to a numerical distance relaying algorithm for application on double-circuit and six-phase transmission systems. Successful modifications and additions to the single ended relaying technique are recommended. The recommendations are also supported by the off-line simulation test results carried out on the EMTDC Electromagnetic Transient Simulation Program.

Finally, a neural network trained to identify the faulted phases is integrated to the distance algorithm in order to further improve the protection scheme on the double-circuit transmission line configuration.

LIST OF FIGURES

	Pages
Figure 2.1: Single line diagram of a typical transmission line with it's protective relays.	9
Figure 2.2: Typical zones of protection for a multi sectioned line.	12
Figure 2.3: 'mho' and 'quadrilateral' characteristics.	12
Figure 2.4: Typical ground impedance trajectories of the faulted phase for single line to ground faults at 70% and 100% distances.	13
Figure 2.5: A typical fault voltage and current waveforms.	15
Figure 2.6: Sequence of data processing elements for a simple 3f distance relay.	16
Figure 2.7: Original band limited signal spectrum and its periodically repeated versions as a result of sampling at Nyquist frequency.	17
Figure 2.8: Typical reach for zones 1 and 2 on a multi-section transmission line.	23
Figure 2.9: Incremental impedance plane.	25
Figure 2.10: A typical directional trip zone	26

Figure 2.11: Organization of the Alpha Power Technology relay.	33
Figure 3.1: The PSCAD/DRAFT icons of the APT relay library.	36
Figure 3.2: The icon of the Sampling Clock on the DRAFT canvas.	38
Figure 3.3: The icon of the frequency tracking unit, on the DRAFT canvas.	39
Figure 3.4: Low pass filter characteristics for sampling frequencies of 16, 32 and 64 samples per cycle of fundamental frequency.	40
Figure 3.5: PSCAD/DRAFT icon of the low-pass filter with its inputs.	41
Figure 3.6: Analog high pass filter characteristics.	42
Figure 3.7: PSCAD/DRAFT icon of the analog high-pass filter with its inputs.	44
Figure 3.8: Digital high pass filter characteristics.	45
Figure 3.9: PSCAD/DRAFT icon of the digital high-pass filter with its inputs.	46
Figure 3.10: PSCAD/DRAFT icon of the Sampler.	47
Figure 3.11: PSCAD/DRAFT icon of the Fast Fourier Transformation Model.	48
Figure 3.12: PSCAD/DRAFT icon of the Sequence Filter Model.	50
Figure 3.13: PSCAD/DRAFT icon of the Ground Impedance Element Model.	51
Figure 3.14: PSCAD/DRAFT icon of the Zone Trip Model.	53
Figure 3.15: PSCAD/DRAFT icon of the Data File Writer.	55
Figure 3.16: PSCAD/DRAFT icon of the Artificial Neural Network Model.	56
Figure 3.17: Set-up for testing the off-line relay model for its accuracy.	58
Figure 4.1: Simplified single line diagram of the 3-phase double circuit line.	60

Figure 4.2: Conductor configuration for the three-phase double circuit line.	61
Figure 4.3: Circuit connection for self impedance measurement on circuit #1	62
Figure 4.4: Circuit connection for mutual impedance measurement	64
Figure 4.5: Single line diagram of six phase transmission line model.	67
Figure 4.6: Conductor configuration for the 6-phase line.	68
Figure 5.1: Processing units of the impedance relay used in the study.	71
Figure 5.2: Trip zones of the impedance relays on McCalmont-Springdale double circuit line.	72
Figure 5.3: Trip zone of the directional impedance element on McCalmont- Springdale double circuit line.	73
Figure 5.4: Ground impedance relay trajectories of the faulted phase, for single line (a_1 -g) to ground faults at 10%, 80% and 90% distances.	74
Figure 5.5: Line impedance trajectories of circuits #1 & #2, for single line to ground (a_1 -g) faults at 10%, 80% and 90% distances.	75
Figure 5.6: Directional impedance trajectories of circuits #1 & #2., for single line to (a_1 -g) ground faults at 10%, 80% and 90% distances.	77
Figure 5.7: The directions and distances to the close-up and remote faults as seen by the directional element of the unfaulted line.	77
Figure 5.8: Ground impedance relay trajectories for the faulted phases, for double line to ground faults (a_1 - b_1 -g) at 10%, 80% and 90% distances.	79
Figure 5.9: Line impedance trajectories of a-b and c-a of the faulted circuit, for double line to ground faults (a_1 - b_1 -g) at 10%, 80% and 90% distances.	79
Figure 5.10: Directional impedance trajectories of the faulted and unfaulted circuits, for double line to ground faults (a_1 - b_1 -g) at 10%, 80% and 90% distances. .	80

Figure 5.11: Ground impedance trajectories of circuits #1 & #2, for a_1-b_2 -ground faults at 10%, 80% and 90% distances.	81
Figure 5.12: Line impedance trajectories of circuits #1 & #2, for a_1-b_2 -ground faults at 10%, 80% and 90% distances.	83
Figure 5.13: Directional impedance trajectories of circuits #1 & #2, for a_1-b_2 -ground faults at 10%, 80% and 90% distances.	84
Figure 5.14: Ground impedance trajectories of circuits #1 & #2, for $a_1-b_1-c_2$ -ground faults at 10%, 80% and 90% distances.	85
Figure 5.15: Directional impedance trajectories of circuits #1 & #2, for $a_1-b_1-c_2$ -ground faults at 10%, 80% and 90% distances.	86
Figure 5.16: Line impedance trajectories of circuits #1 & #2, for $a_1-b_1-c_2$ -ground faults at 10%, 80% and 90% distances.	87
Figure 5.17: Ground impedance trajectories of circuits #1 & #2, for four phase to ground faults at 10%, 80% and 90% distances. Faulted phases are $a_1-b_1-c_1-a_2-g$	88
Figure 5.18: Line impedance trajectories of circuits #1 & #2, for four phase to ground faults at 10%, 80% and 90% distances. Faulted phases are $a_1-b_1-c_1-a_2-g$	89
Figure 5.19: Directional impedance trajectories of circuits #1 & #2, for four phase to ground faults ($a_1-b_1-c_1-a_2-g$) at 10%, 80% and 90% distances.	90
Figure 5.20: The directional impedance trajectories for $a_1-b_1-c_2-g$ fault at 10% distance	91
Figure 5.21: Single line diagram of a double circuit system with a fault on one circuit: fraction of the line length to fault is 'l'.	93
Figure 5.22: Modified ground impedance trajectories of faulted phases, for a_1-b_1-g faults at 10%, 80% and 90% distances.	96

Figure 5.23: Modified ground impedance trajectories of faulted phases, for a_1 - b_2 - g faults at 10%, 80% and 90% distances.	97
Figure 5.24: Modified ground impedance trajectories of circuits #1 & #2, for a_1 - b_1 - c_2 - g faults at 10%, 80% and 90% distances.	98
Figure 5.25: Modified ground impedance trajectories of circuits #1 & #2, for a_1 - b_1 - c_1 - a_2 - g faults at 10%, 80% and 90% distances.	99
Figure 6.1: Single line diagram of the six phase transmission line model.	102
Figure 6.2: Processing units of the impedance relay used in the study for the six-phase transmission line configuration.	103
Figure 6.3: Trip zones of the ground/line impedance relays on McCalmont-Springdale six-phase line.	104
Figure 6.4: Trip zone of the directional impedance element on McCalmont-Springdale six-phase line.	105
Figure 6.5: Ground impedance trajectories of the faulted phase for single line to ground faults at 10%, 80% and 90% distances.	107
Figure 6.6: Magnitude of zero sequence currents in circuits #1 & #2, for single line to ground faults at 10%, 80% and 90% distances.	108
Figure 6.7: Line impedance trajectories for phases a-e for single line to ground faults at 10%, 80% and 90% distances.	109
Figure 6.8: Directional elements for circuit#1 and circuit #2, for single line to ground faults at distances 10%, 80% and 90%.	109
Figure 6.9: Modified ground impedance trajectories of the faulted phase, for single line to ground faults at 10%, 80% and 90% distances.	110
Figure 6.10: Ground elements of faulted phases, for faults at 10%, 80% and 90% distances.	111

Figure 6.11: Modified ground elements of faulted phases, for faults at 10%, 80% and 90% distances.	112
Figure 6.12: Some line impedance trajectories of the faulted circuit, for faults at 10%, 80% and 90% distances.	112
Figure 6.13: Ground elements of faulted phases, for faults at 10%, 80% and 90% distances.	114
Figure 6.14: Modified ground elements of faulted phases, for faults at 10%, 80% and 90% distances.	114
Figure 6.15: Directional elements for circuit#1 and circuit #2, for phases <i>a-b-ground</i> faults at distances 10%, 80% and 90%.	115
Figure 6.16: Ground impedance elements of faulted phases, for phases <i>a-b</i> faults at distances 10%, 80% and 90%.	116
Figure 6.17: Directional elements for circuit#1 and circuit #2, for phases <i>a-b</i> faults at distances 10%, 80% and 90%.	116
Figure 6.18: Ground elements of faulted phases, for faults at 10%, 80% and 90% distances.	117
Figure 6.19: The two line impedance elements which mis-operate for the <i>a-d-ground</i> fault at 10% distance.	118
Figure 6.20: Directional elements for circuit#1 and circuit #2, for phases <i>a-d-ground</i> faults at distances 10%, 80% and 90%.	118
Figure 6.21: Modified ground impedance elements of faulted phases, for <i>a-c-b-ground</i> faults at distances 10%, 80% and 90%.	122
Figure 6.22: Line impedance trajectories of phases <i>a-c</i> , for <i>a-c-b-ground</i> faults at distances 10%, 80% and 90%.	122
Figure 6.23: Ground impedance elements for faulted phases of one circuit, for <i>a-c-d-ground</i> faults at distances 10%, 80% and 90%.	124

Figure 6.24: Line impedance elements of faulted phases and directional impedance element, of the first circuit, for <i>a-c-d-ground</i> faults at distances 10%, 80% and 90%.	124
Figure 6.25: Ground impedance element for the faulted phase and the directional impedance element, of the second circuit, for <i>a-c-d-ground</i> faults at distances 10%, 80% and 90%	125
Figure 6.26: Modified ground impedance elements for faulted phases, for <i>a-c-d-ground</i> faults at distances 10%, 80% and 90%.	125
Figure 6.27: Categorization of different four-phase and four-phase-to-ground faults.	126
Figure 6.28: Ground impedance trajectories of phases a & c, for <i>a-c-b-d-ground</i> faults at distances 10%, 80% and 90%	128
Figure 6.29: Directional impedance trajectories of the two circuits, for <i>a-c-e-b-ground</i> faults at distances 10%, 80% and 90%	129
Figure 7.1: Simplified single line diagram of the modelled system	136
Figure 7.2: Single Line Diagram of the Pointe du Bois Terminal Station.	137
Figure 7.3: Zero Sequence network for l-g fault on circuit P3	138
Figure 7.4: Test set-up for testing the prototype APT relay using recorded fault waveforms.	141
Figure 7.5: Fault currents, trip signals, and ground impedance trajectory of the faulted phase for a single line to ground fault at 75% distance.	144
Figure 7.6: Fault currents, and the ground impedance trajectories of the faulted circuit for a three-phase to ground fault at the remote end. The fault is also cleared at the remote end five cycles after its inception.	146
Figure 7.7: Fault currents, and the relay trip signals of the faulted circuit for the same fault as in Figure 7.6.	147

Figure 7.8: Fault currents, ground impedance trajectory of the faulted phase, and the trip signals of a single circuit, for an inter-circuit double line fault at 75% distance.	149
Figure 8.1: Typical structure of an artificial neural network.	152
Figure 8.2: Input-output organization of the ANN.	164
Figure 8.3: Input and Output connections of a neuron.	165
Figure 8.4: The characteristics of the hidden and output neuron activation function	166
Figure 9.1: Block diagram of the relay elements and the neural faulted phase detector.	180
Figure 9.2: The ANN and target outputs for a phase a_1 -g fault at 10% distance to the measuring point.	181
Figure 9.3: ANN and target outputs for a a_1 - b_1 -g fault at 10% distance from the measuring point.	182
Figure 9.4: Comparison of the response time of ANN output for a_1 -g faults at different locations on the transmission line.	184
Figure 9.5: Instantaneous voltage and current of the faulted phase for a_1 -g fault at 10%, 40% and 80% distances.	185
Figure 9.6: ANN outputs for faulted phases during a_1 - b_1 - c_2 -g fault, with fault inception at six different points on the wave.	186
Figure 9.7: ANN output of phase-a1 for a a_1 -g fault with 0, 10 and 20 W fault resistance respectively.	187
Figure 9.8: ANN performance variation with distance to the fault: (a) Network operated for forward pre-fault power flow. (b) Network operated for reverse pre-fault power flows.	190

Figure 9.9: Comparison of ANN performance for pre-fault power flows of 90% and 100%. Same network weights are used.	191
Figure 9.10: Comparison of ANN performance for pre-fault operating levels of 90%, 80%, 70%, 60%, 50% and 40% of rated power flow.	193
Figure 9.11: Neural network performance for line faults and ground faults of various fault resistances.	194
Figure 9.12: Network performance variation for strong sources at receiving and sending ends.	196
Figure 9.13: Comparison of trip signals from the ANN and the zone trips of the APT impedance elements, for a a_1 -g fault at 10% distance.	198
Figure 9.14: Comparison of trip signals from the ANN and the zone trips of the APT impedance elements, for a a_1 - b_2 -g fault at 10% distance.	199
Figure 9.15: Comparison of trip signals from the ANN and the zone trips of the APT impedance elements, for a a_1 - b_1 - c_2 -g fault at 10% distance.	199
Figure 9.16: Comparison of trip signals from the ANN and the zone trips of the APT impedance elements, for a a_1 - b_1 - c_1 - a_2 -g fault at 10% distance.	200
Figure 9.17: Comparison of trip signals from the ANN and the zone trips of the APT impedance elements, for a a_1 - b_1 - c_2 fault at 10% distance.	200
Figure 9.18: Comparison of trip signals from the ANN and the zone trips of the APT impedance elements, for a a_1 - b_2 -g fault at 90% distance.	201
Figure 9.19: Comparison of trip signals from the ANN and the zone trips of the APT impedance elements, for a a_1 - b_2 fault at 90% distance.	201
Figure 9.20: Comparison of trip signals from the ANN and the single-pole trip logic of the APT relay algorithm, for a a_1 - b_2 -g fault at 10% distance.	203
Figure A.1: Positive sequence network of a three-phase single-circuit transmission line with a fault in front of the 'busbar M'.	A-i

Figure A.2: Positive sequence network of a three-phase single-circuit transmission line with a fault behind the busbar M	A-iii
Figure A.3: The double circuit transmission line and the positive sequence network impedances.	A-vi
Figure A.4: The Thevenin equivalent positive sequence incremental impedance network for the double circuit line in Figure A3, for a three phase to ground fault at F.	A-vi
Figure B.1: Conductor configuration for the three-phase double circuit line.	B-ii
Figure B.2: Conductor configurations of the Pointe du Bois transmission line (all lengths in meters)	B-iii

LIST OF TABLES

	Pages
Table 4.1: Self-impedances of the double circuit line	63
Table 4.1: Mutual impedances of the double circuit line	65
Table 4.1: Source Impedances	65
Table 4.1: Source impedances of the model measured at the HV bus	66
Table 4.1: Impedances of the six-phase line measured on the model.	68
Table 4.1: Equivalent Impedances of the sources and the transformers.	69
Table 5.1: Summary of relay performance on double-circuit lines for ground faults.	100
Table 4.1: Summary of relay performance on double-circuit lines for non-grounded faults.	101
Table 6.1: Phase orientation of faulted phases for various combinations of inter-circuit three phase faults.	120
Table 4.1: Summary of relay performance on six-phase lines for ground faults.	131

Table 4.1: Summary of relay performance on six-phase transmission line for non-grounded faults.	132
Table 8.1: Possible types of faults on a double circuit or six phase transmission line	170
Table 4.1: Source Impedances of the Transmission Network	172
Table 5.1: ANN inputs and their scaling factors for double circuit application.	175
Table B.1: Heights to Conductor Positions.	B-iv
Table B.2: Conductor Segment Information.	B-v
Table B.3: Comparison of Impedances for the transmission lines.	B-vii

CHAPTER 1

BACKGROUND AND INTRODUCTION

1.1 Background

Environmental concerns and questions of cost have led to investigating the possibilities of maximizing the power transmitted through any given right-of-way thereby introducing the concept of compact transmission line configurations. New developments of compact conductor configurations have been in general to minimize the tower dimensions, their visual impact, the transmission corridor and the electromagnetic field at ground level, while transmitting the required amount of power. A considerable amount of studies has been carried out to find the optimal conductor spacing [1] [2], and to investigate the design features of compact transmission towers, insulators and other physical structures [3 - 9].

Three-phase double circuit lines of the same voltage are commonplace in industrialized nations. Heightened concerns over low frequency electromagnetic fields have drawn interests to higher-phase order transmission systems. HVAC/HVDC hybrid systems are another attractive option, mainly due to the numerous advantages dc offers over ac in high voltage, long distance power transmission. Although most three phase double circuit lines operate at the same voltage level, some utilities have resorted to using different voltages on the parallel circuits erected on the same tower.

The benefit of the multi-phase transmission line is mainly due to the smaller phase angle between adjacent phases. This effectively reduces the voltage between adjacent conductors, making the conductor configurations, tower structures, and other associated equipment considerably more compact. Multi-phase systems (where the number of phases is a multiple of three) also offer complete compatibility with standard 3-phase systems. The possibility of upgrading 3-phase double circuit lines to 6-phase lines with minimal changes in the line structure and considerable increase in the possible thermal loading and surge impedance loading [14], makes 6-phase transmission a promising alternative for the future. Research on 6-phase transmission has progressed from the stage of feasibility studies to construction, testing, and analysis of prototype lines [10 - 14]. Therefore a considerable amount of work in designing terminal equipment, line construction, insulation coordination, and investigations on lightning performance has been reported. Effects of electric fields, radio interference, and corona on multi-phase transmission systems have also proved to be much better compared to 3-phase double circuit lines [12].

Lack of experience is no longer a drawback of HVDC transmission. Therefore utilities are actively investigating the possibility of upgrading appropriate existing lines to HVAC/HVDC hybrid transmission systems [18] [19]. Some studies on interactions between ac and dc systems report that hybrid effects are only significant below a critical distance between the two systems. This critical distance is observed to be a function of both systems' voltages and geometrical configuration of the transmission

corridor [18]. No significant limitations to increasing the proximity between the ac and dc lines have been observed other than a tolerable increase in the corona losses.

1.2 Introduction

With much research and investigation, compact transmission line models have proven to be a good solution to both economical and environmental concerns of the modern world. However, this concept brings in a new challenge to the transmission line protection problem. The conventional, high voltage transmission line protection schemes, such as

- current differential,
- distance,
- phase and amplitude comparators,

do not have self-sufficient capability to protect multi-circuit or multi-phase transmission lines under all possible contingencies. Therefore, in most reported multi-circuit/phase protection applications, the approach has been to use dissimilar schemes that overcome each others' deficiencies [20].

Most three-phase single circuit protection schemes fail during fault situations typical to multi-circuit lines. The following are some such situations that have to be carefully looked into when designing a protection scheme for a multi-circuit/phase transmission line.

Inter-circuit faults: A fault situation that can occur on any type of compact transmission configuration. (Even a six-phase circuit can be considered to consist of two three-phase circuits, which are of non-equal phase angles.) The optimal protection scheme would be able to handle such situations with minimal reduction to power transmission. It suggests that selective pole tripping be implemented for fault clearance.

Inter-circuit faults between different voltage levels: A fault condition that can only occur on parallel transmission lines with different voltage levels. Distance relay techniques fail under such fault conditions [20].

Mutual coupling of zero sequence currents: The zero sequence mutual coupling effects usually cause under or over reaching of distance relay elements, if not properly compensated. Therefore, it is necessary that the protection algorithms be designed with special consideration to accommodate the presence of zero sequence mutual coupling between circuits.

Communication Channels: In the case when communication channels are associated with the protection scheme, their security and dependability are of equal importance to the protective equipment. Compact transmission systems, must have the highest possible security and dependability because 100% of the power transfer between the two locations takes place on a single corridor. Consequences of a misoperation or a sympathy trip can be serious.

1.3 Scope

It is apparent that there is need for stand alone primary protective relays for application on compact transmission lines. Modern micro-processor based digital relays have the capability and the computing resources to cater to various complex network structures.

Driven by these factors, the objective of the study is to investigate the problems associated with using conventional (designed for three-phase, single circuit application) digital distance relay algorithms on selected compact configurations of transmission lines, during short circuit faults and also, to improve their adaptability to such systems. The transmission configurations under consideration are

- the double circuit with the same voltage levels and
- the six-phase transmission line types.

The Alpha Power Technology (APT) relay algorithms, designed and developed by *McLaren et al.* [24- 26], are particularly chosen as the base relay for the study. The APT relay is a digital distance relay that runs on a DSP (digital signal processing) board. The software algorithms utilize highly efficient data processing and computing techniques for implementing the relay functions. As with any other numerical relay, this too has the flexibility of modification and expansion. Thus, it is investigated for its potential applicability to transmission circuits with greater complexity.

As a result of the investigations, modifications to the relay algorithms are tested and recommended for improving their performance on the two compact transmission line

configurations mentioned above. The test results of a neural network, that can further improve the distance relay performance, are also presented. All the results reported are based on off-line simulation studies and tests on the prototype relay.

Research is confined to single-ended protection algorithms. The transmission lines considered in the study are two terminal long lines with equivalent sources on both ends. Off line analysis and testing of the power system performance are done on PSCAD/EMTDC™, the Electromagnetic Transient Simulation Program developed by the Manitoba HVDC Research Centre [30].

1.4 Overview of this Thesis

Chapter 2 reviews the distance relay algorithms in practice. It emphasises the digital signal processing techniques that are tested in the thesis and are used in the APT relay. Other supporting relay algorithms associated with distance relays are discussed as well.

Chapter 3 basically describes the exercise of establishing the accurate off-line models of the digital distance relay components, and other interfacing elements that were used in the study.

Chapter 4 describes the details of the double-circuit and six-phase, compact transmission line models. Also, the data for their circuit elements are presented. The end stations of both systems are named *McCalmont* and *Springdale* for reference purposes.

Having established the ground work, Chapters 5 and 6 examine the performance of the relay on the double-circuit and six-phase line configurations respectively. The modifications to the relay algorithms are also proposed in these chapters.

Initially, a transmission line of the Winnipeg Hydro transmission network was modelled to investigate the digital distance relay performance on it. The transmission line is a $69kV$, four-circuit line running on two sets of towers which are erected on the same right of way. Chapter 7 of the thesis discusses modelling of the Winnipeg Hydro, *Pointe du Bois* four-circuit transmission line and the APT relay performance tests carried out on it. However, due to the non-availability of system data to accurately model the entire *Pointe du Bois* system, and the modelling limitations of the twelve conductor line, investigations were also carried out on the two hypothetical transmission system models described in Chapter 4.

In Chapter 8, the concept of using a neural network for enhancing the relay performance is introduced. The nature of the problem, solved by artificial intelligence, and some neural network designing details are discussed.

Chapter 9 analyses the performance of a neural network trained to operate on the double-circuit line modelled in the study.

Finally, in Chapter 10, the contributions made through the investigations are summarized with a concluding note.

CHAPTER 2

DISTANCE RELAY ALGORITHMS

Relay algorithms are methods of converting voltage and current samples of a power system into measurements which can be used to make trip decisions for isolation of faults. Due to the increasing availability of inexpensive, light weight, programmable, and easily reproducible digital technology, micro-processor based relays are now being widely accepted for power system applications. This chapter covers some of the basics of digital distance relay techniques, with emphasis on those used in the Alpha Power Technology (APT) relay.

The issues discussed are:

- Basic operating criteria of a digital distance relay
- Data processing techniques
- Supporting elements to distance relays

2.1 Basic Operating Criteria of a Digital Distance Relay

Distance relays are commonly used for the protection of transmission line circuits. The operation of these relays is mainly based on the impedance measured at the relay point. The voltage to current ratio of the fundamental frequency components seen at the relay point is an indicator of the system's normal or fault condition.

Figure 2.1 shows a typical transmission line with its protective relays in a single line form. The three-phase currents and the three line-to-ground voltages are available at each line terminal.

Most digital distance relays for three-phase single circuit systems, use six impedance elements. Three of these elements are phase impedance elements and the other three are ground impedance elements

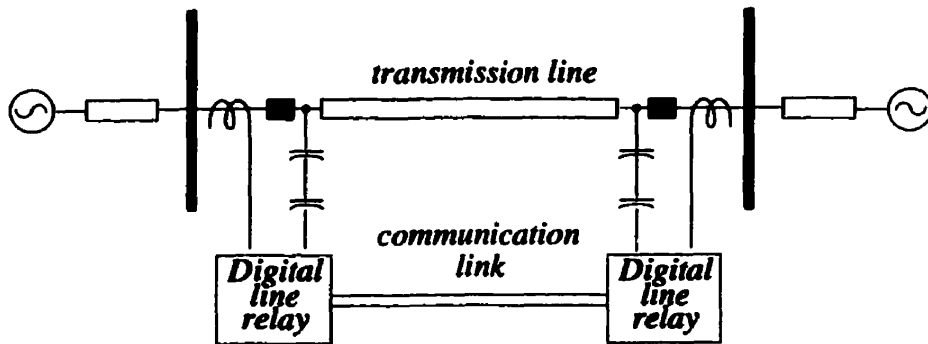


Figure 2.1: Single line diagram of a typical transmission line with its protective relays.

The impedances seen by the relays are [34]:

Phase Relays:

$$Z_{ab, bc, ca} = \frac{V_{ab, bc, ca}}{I_{a, b, c} - I_{b, c, a}} \quad 2.1$$

where, $V_{ab, bc, ca}$ = line voltages

$I_{a, b, c}$ = line currents at the relay point

Ground Relays:

$$Z_{a,b,c} = \frac{V_{ag,bg,cg}}{I_{a,b,c} + kI_0} \quad 2.2$$

where, $V_{ag,bg,cg}$ = phase voltages

$I_{a,b,c}$ = line currents

I_0 = zero sequence current at the relay point.

The zero sequence current compensation factor is;

$$k = \frac{Z_{l0} - Z_{l1}}{Z_{l1}} \quad 2.3$$

where, Z_{l1} = positive sequence impedance of the transmission line

Z_{l0} = zero sequence impedance of the transmission line.

Phase and ground impedances [given in equations 2.1 and 2.2] seen by the elements are evaluated for various fault conditions, small disturbances and normal operations, on simple three-phase, single circuit transmission lines [34].

These evaluations have shown that the impedances during normal operations mainly depend on the operating point of the system, and that they distinctly differ from those when the system is faulted. The values of the measured impedances during a system fault depend on the line, source, and fault impedances. They also depend on the

distance to the fault from the relay point. Therefore, the change of the impedances from the no fault zone to the fault zone is used to detect the system faults [34 - 35].

2.1.1 Trip Characteristics

Trip characteristics are the boundaries on the resistance-reactance (R-X) impedance plane, which define the zone within which the impedances seen at the relay point lie for all possible fault conditions on the protected transmission line. These characteristics are chosen not to include impedances resulting from faults on associated circuits or abnormal operating conditions.

All impedances which fall within the trip characteristics, will be detected by the relay. This results in the opening of relevant circuit equipment to isolate the fault.

In a practical relay, there is more than one protection zone. The first zone of protection normally covers 80% of the line starting from the relay location, and the second zone normally protects the remote 20% of the line and 20% into the next line section. Some relays also use a third protection zone which extends well beyond the protected line section. However, the APT relay uses only two zones of protection. Figure 2.2 shows typical zones of protection for a multi-sectioned line.

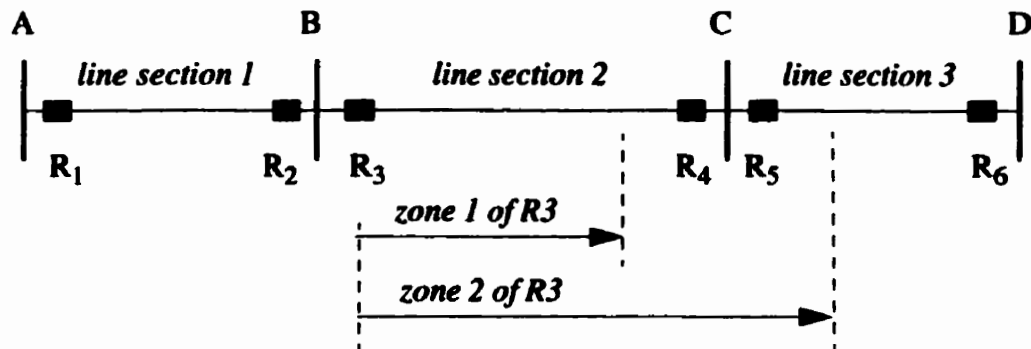


Figure 2.2: Typical zones of protection for a multi sectioned line.

It is required to have high speed clearance for the faults in the first zone and high reliability against tripping for all faults outside the protected area.

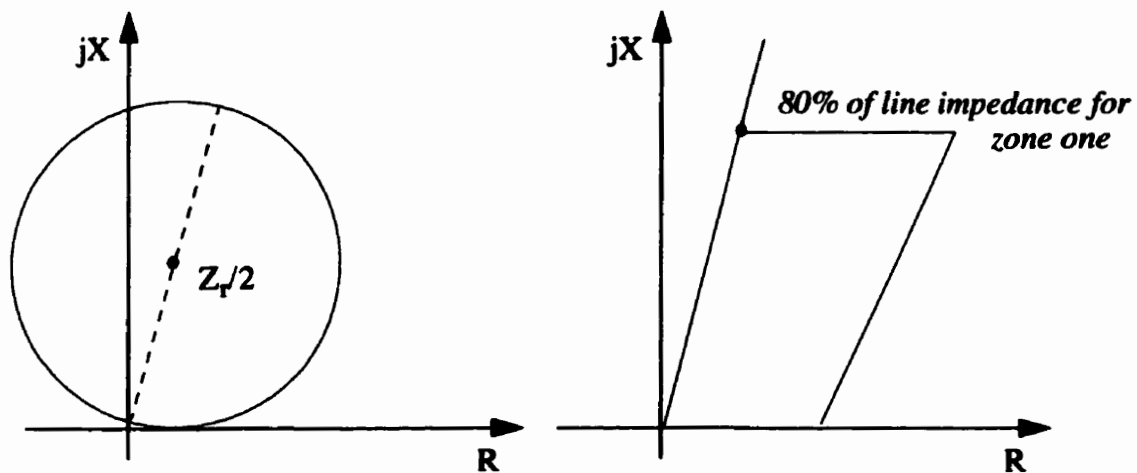


Figure 2.3: 'mho' and 'quadrilateral' characteristics.

The 'mho characteristic' shown in Figure 2.3 is one of the commonly used characteristics which satisfy the tripping criteria. It is a circular characteristic which

passes through the origin, with centre at $Z_r/2$. Z_r is a pre-defined replica impedance based on the extent of protection and the system parameters [34].

Figure 2.4 shows typical faulted phase impedance trajectories for single line to ground faults at distances 70% and 100% away from the relay point. The trajectory for the fault at 70% distance falls in zone one, while the trajectory for the fault at 100% distance is in zone two.

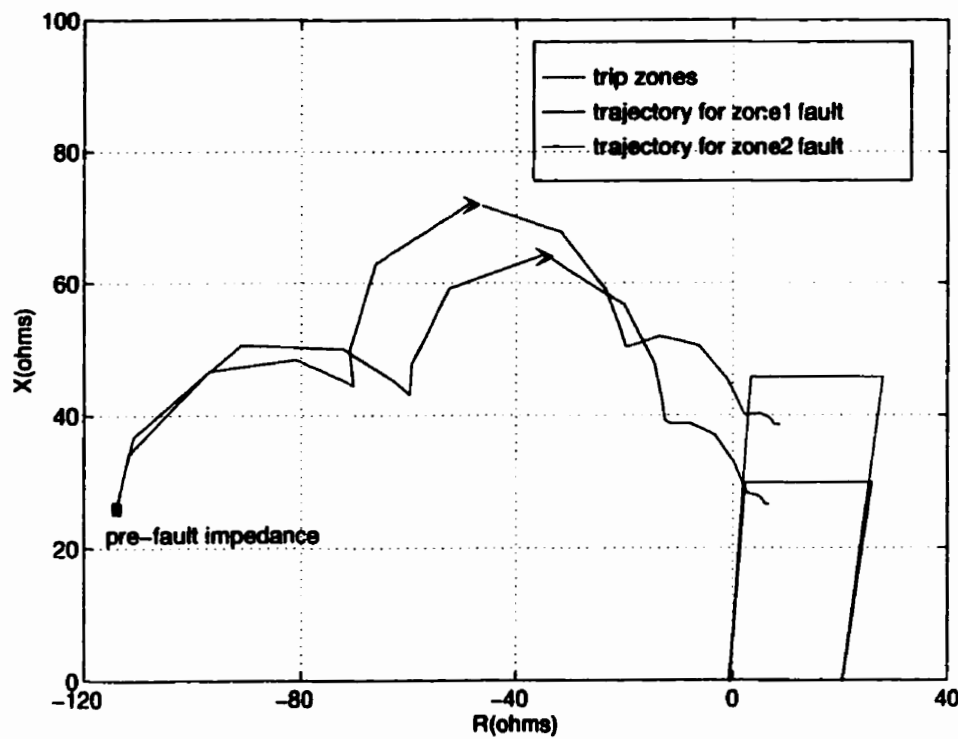


Figure 2.4: Typical ground impedance trajectories of the faulted phase for single line to ground faults at 70% and 100% distances.

Considering the impedances seen at the relay elements during fault conditions, the ideal characteristics should provide a close match to the area of the impedance plane containing all probable fault impedances. With such studies [17] it has been found

that this area needs to be a quadrilateral as shown in Figure 2.3. The coordinates depend on the extent of protection and the allowance for possible power swings, load encroachment, ground fault impedances (due to arcs and tower footing) etc.

With present day microprocessor based relays, the realization of such complicated characteristics has been greatly simplified.

2.2 Data Processing Techniques

Almost all the distance relay techniques demand the extraction of fundamental frequency components of currents and voltages at the measured point within less than two cycles of fundamental frequency, following a system fault. The voltages and currents following a fault fail to be pure sinusoidal signals, due to a variety of reasons.

The following are some major causes of waveform distortion:

- The dc component, introduced because of the fault inception angle, decays exponentially at a rate that depends on the line resistance and inductance (R and L).
- High frequency signals associated with the reflection of the surge waveforms at the fault and the bus bars.
- The non-linear nature of the fault arc.

Figure 2.5 shows typical voltage and current waveforms during faults.

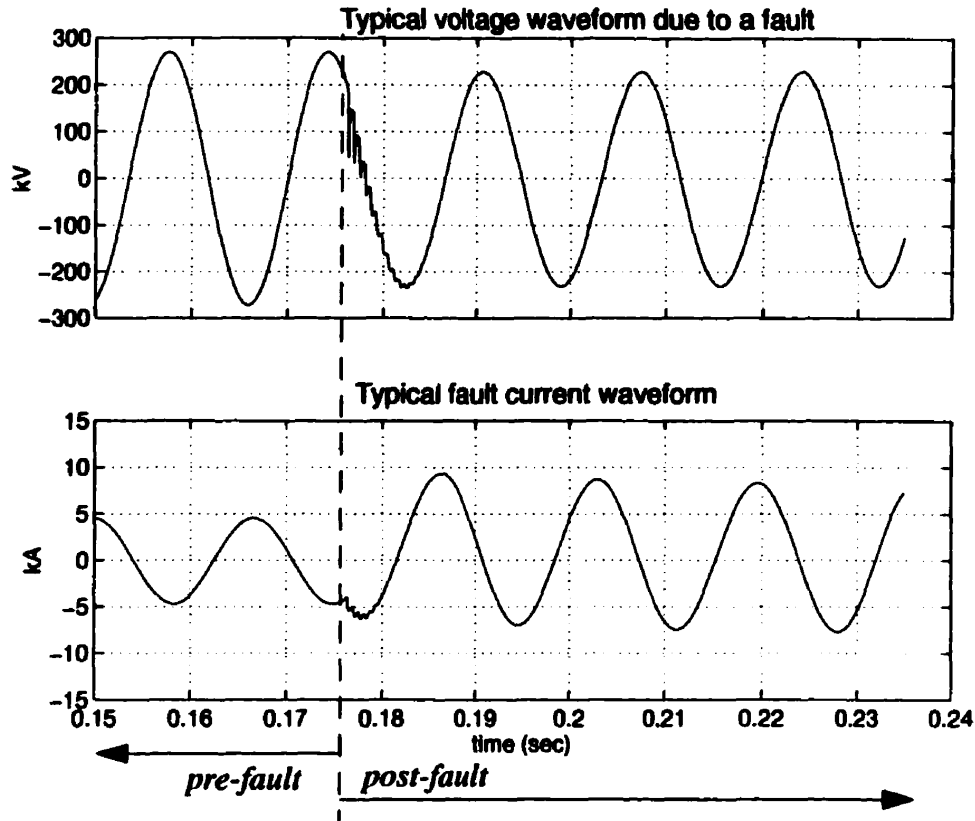


Figure 2.5: A typical fault voltage and current waveforms.

Selection of fast digital signal processing techniques, and their hardware and software implementation strategies, have become crucial due to the demanded high speed of operation of the relays. This sections covers the procedures and data extraction techniques used in the Alpha Power Technology (APT) relay [26].

The APT relay uses the well established discrete fourier transform method for determining the fundamental components of voltage and current waveforms. Figure 2.6 shows a block diagram of the sequence of data processing elements for three-phase voltage and current waveforms.

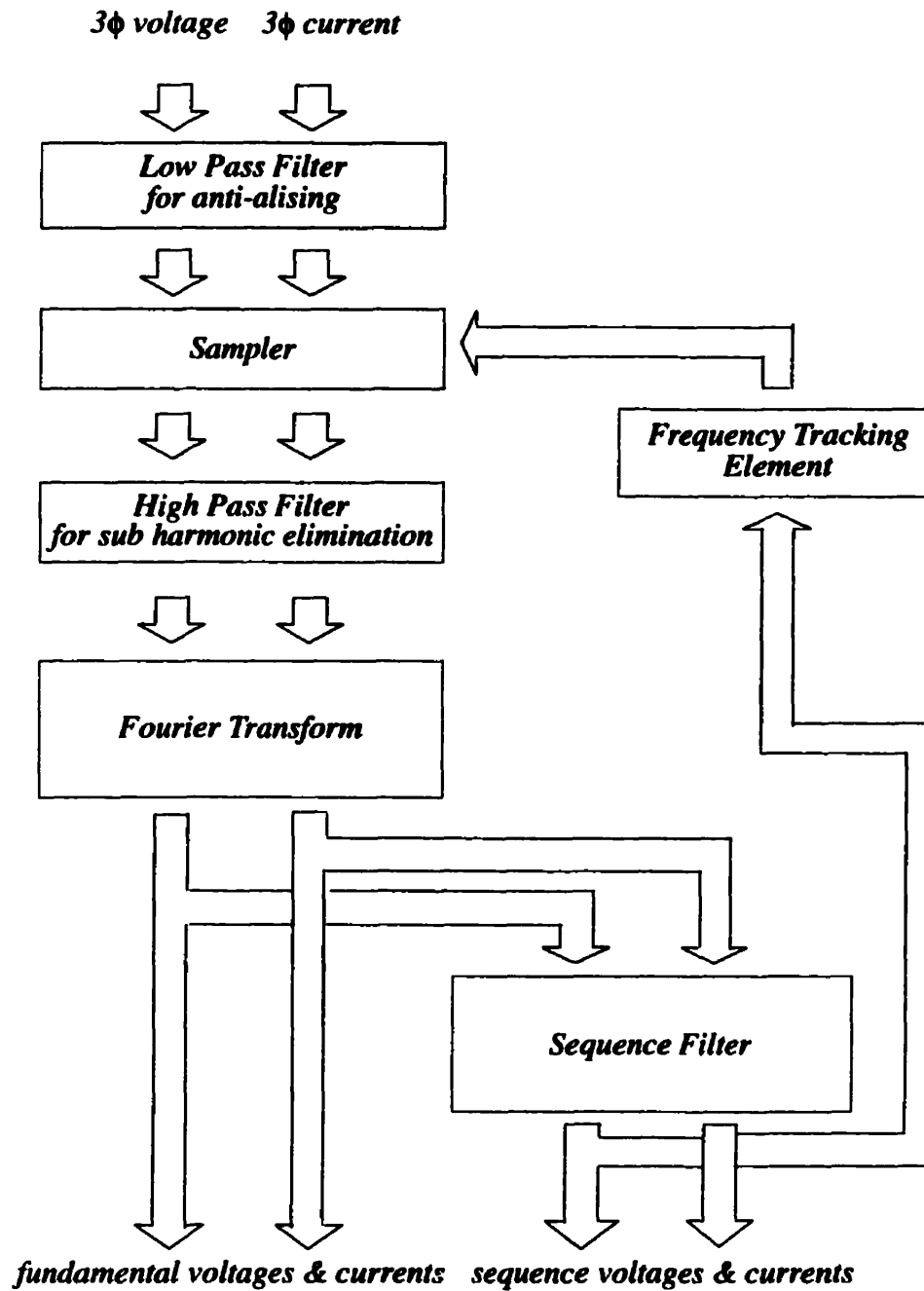


Figure 2.6: Sequence of data processing elements for a simple 3 ϕ distance relay.

2.2.1 Sampling

Analog to digital conversion of a signal can be described in terms of two separate operations. They are uniform sampling in time, and quantization in amplitude. In the sampling process, an

analog signal is sampled at uniform time intervals of T_s seconds. The samples, $x[n]$ of the continuous time signal $x[t]$ can be represented as

$$x[n] = x[nT_s]. \quad 2.4$$

The effect of the sampling process in the frequency domain is to create periodically repeated versions of the signal spectrum at multiples of the sampling frequency $f_s = 1/T_s$.

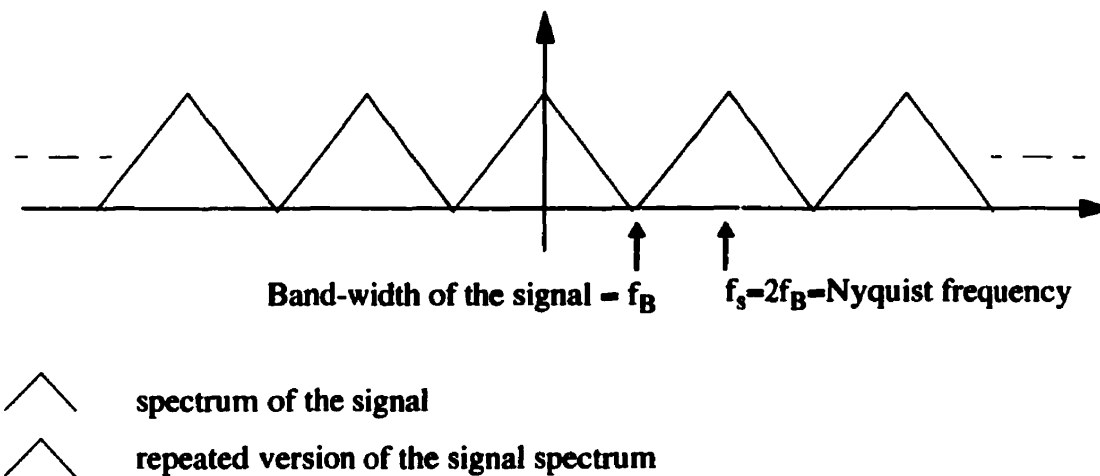


Figure 2.7 Original band limited signal spectrum and its periodically repeated versions as a result of sampling at Nyquist frequency.

Theoretically, the signal can be reconstructed exactly, if the repeated versions of the signal spectrum do not overlap. Thus the signal must be sampled at a rate greater than twice its bandwidth. Figure 2.7 shows the repetitions of the spectrum of the signal due to sampling at twice the band-width (Nyquist frequency) of the signal. Interference

between the adjacent versions of the signal spectrum is known as aliasing and it prevents accurate reconstruction of the signal [21].

The APT relay uses a sampling rate of 32 samples/cycle of the fundamental frequency. This selection of sampling frequency provides the required time for subsequent computations between samples. It also enables fast extraction of reasonably accurate, fundamental frequency information following a system fault. Frequency tracking techniques are used to keep sampling synchronized with the system frequency [refer to sections 2.2.2 and 3.2.2 for more details].

Thereafter, the signal samples are quantized in amplitude to a finite set of values. The possible number of quantization levels is determined by the resolution of the Analog-to-Digital (A/D) converter. The A/D converter of the present APT relay has a 11 bit resolution, i.e. 2^{11} quantization levels, with another bit for the sign.

2.2.2 Frequency Tracking

This is an element required to monitor the fundamental frequency of the system. The sampling rate is synchronized to the frequency being tracked and therefore errors due to fluctuations of system frequency are eliminated. The technique used in the APT relay is based on phase comparison. The change in system frequency is determined using the measured phase difference of the positive sequence bus voltage, at samples which are one cycle apart. The change in frequency is added, to update the measured system frequency. The updated frequency is used to adjust the sampling instants of the voltage and current waveforms. At least one cycle of system frequency is allowed

between two consecutive updates of measured frequency. This is the time required for the input quantity of the frequency tracking element, the positive sequence voltage, to stabilize following a change in system frequency.

2.2.3 Low Pass Filtering

The currents and voltages of the line are sensed through current transformers, voltage transformers or capacitive voltage transformers. These devices usually have limited frequency response, so that high frequency noise may not actually appear at the relay terminals. But on the other hand, the secondary side of these high-to-low value transducers may have resonance, or noise pick up, which adds components of other frequencies to the output signals. Therefore there must be adequate filtering, to band limit the signals made available at the relay terminals, to prevent aliasing. These ‘anti-aliasing filters’, usually are analog type with a cut-off frequency of less than half the sampling frequency, preceding the sampler.

The characteristics of the low pass filter used in the APT relay are provided in section 3.2.3. It is a Butterworth filter with a cut-off frequency of approximately 480 or 960 Hz, depending on the used sampling frequency (16 or 32 samples/cycle respectively).

2.2.4 High Pass Filtering

High pass filtering is required to filter any sub-harmonic frequencies and the exponential components that might be present in the waveforms. These filters can be of analog or digital type. A second order digital filter is used in the APT relay [find more details in section 3.2.4].

2.2.5 Fourier Algorithm

Fourier transform $X(f)$ of a time domain signal $x(t)$, gives the strength with which any frequency f is contained in the signal $x(t)$. In practice, the computation of the frequency spectrum on a digital computer can only be carried out using a finite set of samples of the time domain function. The fourier transform of such a sampled signal $x(nT_s)$, is given by:

$$X_d(f) = \sum_{n=-\infty}^{\infty} x(nT_s) e^{-j2\pi f n T_s} \quad 2.5$$

$X_d(f)$ is a periodic repetition of $X(f)$ with a period of $1/T_s$.

Furthermore, the continuous function $X_d(f)$ can only be computed at discrete points in the frequency domain. This leads to the Discrete Fourier Transform (DFT) given by:

$$X_{DFT}(k) = \sum_{n=0}^{N-1} x(nT_s) e^{-jk\left(\frac{2\pi}{N}\right)n}, \quad 2.6$$

where N is the number of samples for the chosen period T_s , and $k = 0 \dots (N/2)$. The number of samples N , in the period T_s , should be sufficient to compute the information, for reproduction of the original signal with acceptable accuracy for the given application.

The direct computation of the N-point DFT given in equation 2.6 requires N^2 multiplications. However, the number of computations can be dramatically reduced by exploiting the symmetrical properties of the quantities in equation 2.6. Fast Fourier Transform (FFT) [22] collectively refers to such computationally efficient algorithms that can be used to evaluate all the DFT's for all harmonics available.

Since the impedance calculations of the APT relay are based on the fundamental components of current and voltage, the algorithms only compute the DFT of the fundamental for $k = 1$. Thus, the instantaneous values of the voltage and current waveforms are converted to their phasor form.

2.2.6 Sequence Filtering

Fundamental components extracted using FFT techniques, as discussed in section 2.2.5, are sequence filtered to derive the zero, positive and negative sequence components X_0 , X_1 , X_2 of the waveforms. Symmetrical components of the three phase quantities X_a , X_b and X_c are given by:

$$\begin{bmatrix} X_0 \\ X_1 \\ X_2 \end{bmatrix} = \frac{1}{3} \begin{bmatrix} 1 & 1 & 1 \\ 1 & 1\angle 120^\circ & 1\angle -120^\circ \\ 1 & 1\angle -120^\circ & 1\angle 120^\circ \end{bmatrix} \cdot \begin{bmatrix} X_a \\ X_b \\ X_c \end{bmatrix}, \quad 2.7$$

where X stands for either a voltage or a current phasor.

This filter is used in the APT relay data processing algorithm in order to extract the sequence voltages and currents that are used in the subsequent computations of ground

impedances (equation 2.2) and directional impedance (equation 2.8). The positive sequence voltage is also used as an input in the frequency tracking element, discussed in section 2.2.2.

2.3 Supporting Elements to Distance Relay Algorithms

Over-current and directional elements are the basic supporting elements used in the APT relay.

2.3.1 Over-Current Element

This element is usually present to detect over-currents in the system due to various abnormal conditions. Digital over-current relays may have either inverse time or definite time characteristics. Normally there are two over-current elements. They are the *low-set* and *high-set* over-current elements.

Low set over-current elements: are used as “starter” elements, which prevent relay operation until current exceeds the set level. Thereby, they prevent mis-operation of impedance relays due to small disturbances on the system.

High set over-current elements: are used to cause an immediate trip in the case of excessive currents, independent of the detection by impedance elements, during close-up faults.

2.3.2 Directional Element

Impedance relays have trouble distinguishing forward and reverse faults when the fault is close to the measuring busbar. Both faults F_1 and F_2 in Figure 2.8 would result in a collapse of bus voltages at B. This causes the fault impedances to fall close to the origin of the trip zone in impedance relay elements of the relay R_3 , for both forward and reverse faults. Such confusion is eliminated by integration of a directional element which distinguishes the reverse and forward faults separately, thereby eliminating false trips for reverse faults.

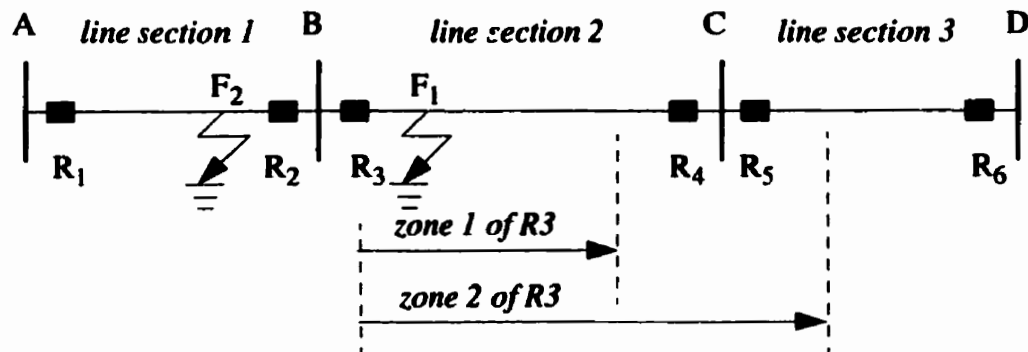


Figure 2.8: Typical reach for zones 1 and 2 on a multi-section transmission line.

There are various techniques used to identify the direction of faults. The positive sequence directional element used by the APT relay and a few other techniques are discussed in brief.

Positive Sequence Directional Element: This technique, which is implemented in the APT digital relay, uses the incremental positive sequence impedance measurement, given in equation 2.8, for distinguishing the direction of a fault [26].

$$\Delta Z_1 = \frac{\Delta V_1}{\Delta I_1} \quad 2.8$$

The incremental positive sequence voltage and current as seen at the relay location are the changes ΔV_1 and ΔI_1 caused by the inception of a disturbance on the system.

The incremental quantities at any given time t are:

$$\Delta V_1 = V_1(t) - V_1(t - nT) \quad 2.9$$

$$\Delta I_1 = I_1(t) - I_1(t - nT) \quad 2.10$$

where T is the period of the fundamental component.

It should be noted that V_1 and I_1 quantities are phasors.

The APT relay uses $n=5$, thus a change over a five cycle interval is computed.

A special feature of the element is that it freezes the pre-fault voltage and current in the event of a fault. A disturbance is detected by a zone trip of the impedance elements. The zone that detects a fault is also called the recorder zone because it triggers the recorder of the relay. This is a third zone that extends beyond the zone-two of ground and line impedance elements both in the forward and reverse directions. This is a precautionary measure to avoid infiltration of the fault data to the sample

window of pre-fault values. Thus, the directional trip signal lasts for longer than five cycles following a fault.

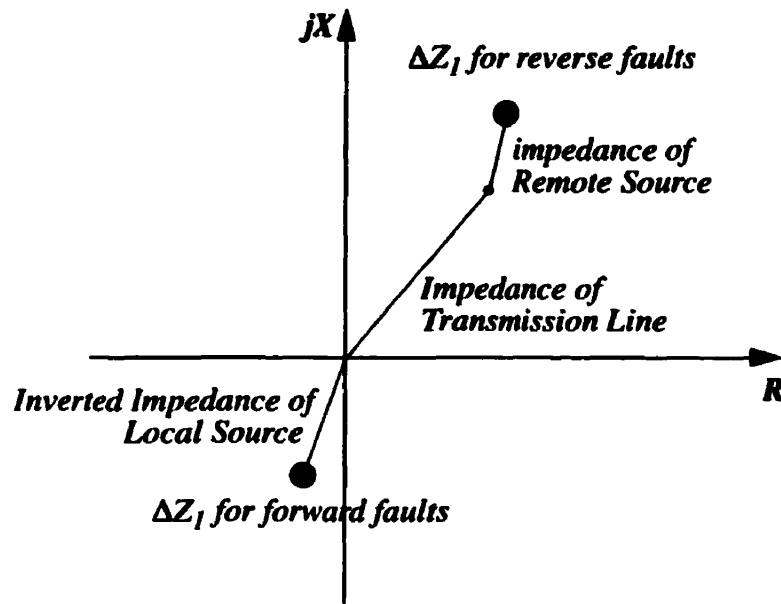


Figure 2.9: Incremental impedance plane.

When a change occurs, the incremental signal becomes non-zero. In the event of a forward fault, the incremental impedance computed becomes equal to the positive sequence impedance of the local source. See Appendix A for details of the incremental impedance computation for forward and reverse faults. The impedance however falls in the third quadrant of the incremental impedance plane as shown in Figure 2.9, affected by the direction of the measured current, which is normally into the transmission line. For a reverse fault the ratio ΔV_1 to ΔI_1 results in a value equal to the addition of the line and remote source impedances. Thus, the impedances clearly

lie in the third quadrant for forward faults and in the first quadrant for reverse faults, not including the origin. Therefore two very distinctly different regions are marked by forward and reverse faults on the impedance plane.

The incremental impedance computed is then checked for being inside a preset zone. The directional trip zone falls around the positive sequence impedance of the local source, as seen in Figure 2.10, with sufficient reactive and resistive clearance to increase the trip speed, as well as to account for other variations of the equivalent source impedance itself.

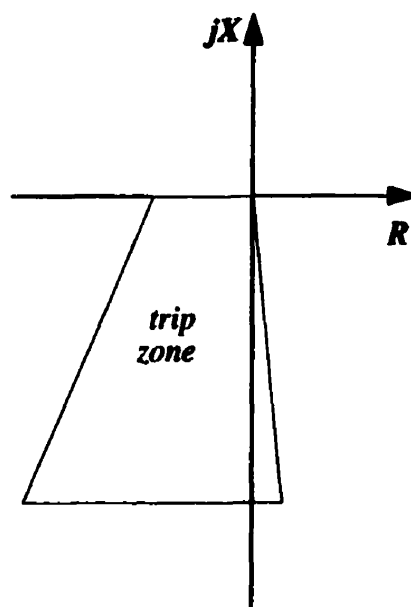


Figure 2.10: A typical directional trip zone

When there is no disturbance the incremental signals become very small and the computed impedance carries no meaning. Therefore, the directional trip signal is AND gated with any other impedance trip or pilot signal to operate the relay.

The most commonly used directional element is the polarized mho using memory or cross polarization. In static relays it is mostly implemented using phase or magnitude comparators. Other techniques are also derived using the deviation signals of voltage and current at the measuring busbar. The following are some such methods that have been proposed for application in numerical relays.

Amplitude Comparator Based Algorithm for Directional Comparison

Protection: This method is based on extracting the deviation signals of the voltage and phase shifted current at each terminal of the transmission line [27]. However, it only compares the amplitudes of the two signals for the directional decision. The voltage and current deviation signals caused by the inception of a fault are:

$$\Delta v = v - v_p, \quad 2.11$$

$$\Delta i = i - i_p, \quad 2.12$$

where v_p and i_p are pre-fault voltage and current.

For a forward fault:

$$\Delta v = -Z_{s1} \Delta i \quad 2.13$$

where Z_{s1} is the positive sequence source impedance of the local source. If phase shifting Δi by the angle of the source impedance Z_{s1} results in $\Delta i(\nu)$, then Δv and $\Delta i(\nu)$ have opposite signs for forward faults and same signs for reverse faults.

i.e. $|\Delta v + \Delta i(v)| < |\Delta v - \Delta i(v)|$ for forward faults and

$|\Delta v + \Delta i(v)| > |\Delta v - \Delta i(v)|$ for reverse faults.

Thus the quantity $|\Delta v + \Delta i(v)| - |\Delta v - \Delta i(v)|$ is used to determine the direction of faults.

When this type of scheme is used, each phase of the system is equipped with an amplitude comparator directional element. The current deviation signal is multiplied by a replica impedance to obtain the phase shifted deviation current signal.

General Phase Comparator Algorithm for Directional Comparison [28]: In this, the direction is simply obtained by the sign of the scalar product of the two phasors \overline{S}_1 and \overline{S}_2 .

$$\overline{S}_1 = \overline{\Delta I}_r \cdot -\overline{Z}_{ls} \quad 2.14$$

$$\overline{S}_2 = \overline{\Delta V}_r \quad 2.15$$

$\overline{\Delta V}_r$ and $\overline{\Delta I}_r$ being the incremental signals given in equations 2.9 and 2.10.

The incremental impedance is given by the following equations for forward and reverse faults (Appendix A).

For a forward fault (refer to Appendix A),

$$\frac{\Delta V_r}{\Delta I_r} = -Z_{ls}, \text{ or}$$

$$\frac{\Delta V_r}{\Delta I_r \cdot (-Z_{ls})} = 1 > 0$$

Here Z_{ls} is the impedance of the local source.

Similarly for a reverse fault,

$$\frac{\Delta V_r}{\Delta I_r} = Z_{tx} + Z_{rs}, \text{ or}$$

$$\frac{\Delta V_r}{\Delta I_r \cdot (-Z_{ls})} = \frac{Z_{tx} + Z_{rs}}{-Z_{ls}} < 0$$

where Z_{tx} is the impedance of the transmission line and Z_{rs} is the impedance of the remote source.

Therefore,

$$S_1 \cdot S_2 > 0 \text{ for forward faults and}$$

$$S_1 \cdot S_2 < 0 \text{ for reverse faults.}$$

Suffix r in the equations can denote the lines ab , bc , or ca for a system with phase sequence $a-b-c$.

Zero Sequence Current Polarized Directional Element. This identifies forward and reverse faults separately, based on the zero sequence ground current of the system. The algorithm is based on a measurement of the degree of polarization of the zero sequence current with reference to an input quantity [27].

The quantity that measures the polarization is given by:

$$T = |I_{POL}| \cdot |3I_0| \cdot \cos (\angle I_{POL} - \angle 3I_0) \quad 2.16$$

where I_{POL} is the polarizing quantity and I_0 is the zero sequence current.

Negative Sequence Voltage-Polarized Directional Element: Here the forward and reverse faults are identified based on the negative sequence impedance presented to the relay element. Two upper and lower threshold levels are used to determine the positioning of the negative sequence impedance and thereby the direction of the fault [27]. The negative sequence impedance computed is given by,

$$z_2 = \frac{Re [V_2 \cdot conjugate (1 \angle \theta_{L2} \cdot I_2)]}{|I_2|^2} \quad 2.17$$

where V_2 is the negative sequence voltage,

I_2 is the negative sequence current and

θ_{L2} is the line negative sequence impedance angle.

This is very similar to the positive sequence incremental impedance technique. However, here the quantity computed is the negative sequence incremental impedance.

Zero Sequence Voltage Polarized Directional Element: Similar to the algorithm in the above component, but uses the zero sequence impedance in place of the negative sequence quantity [27]. The zero sequence impedance computed is given by,

$$z_0 = \frac{Re [3V_0 \cdot conjugate (1 \angle \theta_{L0} \cdot 3I_0)]}{|3I_0|^2} \quad 2.18$$

where V_0 is the zero sequence voltage,
 I_0 is the zero sequence current and
 θ_{L0} is the line zero sequence impedance angle.

It should be noted that both the negative sequence polarized, and the zero sequence voltage polarized directional elements do not function properly under balanced fault conditions.

2.4 Organization of the Alpha Power Technology Relay

The organization of the Alpha Power Technology relay is shown in Figure 2.11. The APT digital distance relay uses the various data processing elements described in section 2.2 to extract the phasor components of the voltage and current waveforms supplied to the relay. The extraction of all the phasors is based on a moving window of data samples preceding to the time of measurement. These phasors are then used to compute the sequence components as discussed in section 2.2.6.

The phase voltages, currents and their sequence components are subsequently used in the impedance computations of the ground, line and directional elements (given by equations 2.2, 2.3 and 2.8 respectively). There are three ground impedance elements for phases a , b and c respectively. The line impedance elements are between phases a - b , b - c and c - a . There is only one directional impedance element, and it is operated

based on the incremental positive sequence impedance of the system. Each impedance is then checked for its positioning with respect to the corresponding trip zone (section 2.1.1).

Finally, the trip signals issued by all the ground, line and directional impedance elements are combined using a single trip logic to issue the trip signal to the local circuit breaker and the pilot signal to the remote relay. The logic expressions of the trip signals issued to the poles a , b , and c of the circuit breaker and the pilot signal can be approximated to be as follows.

$$trip_a = (G_a + L_{ab} + L_{ca}) \cdot dir \quad 2.19$$

$$trip_b = (G_b + L_{bc} + L_{ab}) \cdot dir \quad 2.20$$

$$trip_c = (G_c + L_{bc} + L_{ca}) \cdot dir \quad 2.21$$

$$pilot-signal = trip_a + trip_b + trip_c \quad 2.22$$

$trip_a$, $trip_b$ and $trip_c$ are the trip signals to the three poles of the local circuit breaker. G_a , G_b , and G_c denote the trip signals issued by the ground impedance elements. L_{ab} , L_{bc} , and L_{ca} are the trip signals of the line impedance elements. The directional impedance trip signal is denoted by dir .

As seen in the logic expressions, no trip signal is issued unless a directional trip is present. However a directional trip is prevented from causing any trips by itself. It should be noted that other logic functions are incorporated to implement appropriate delays for zone two trips.

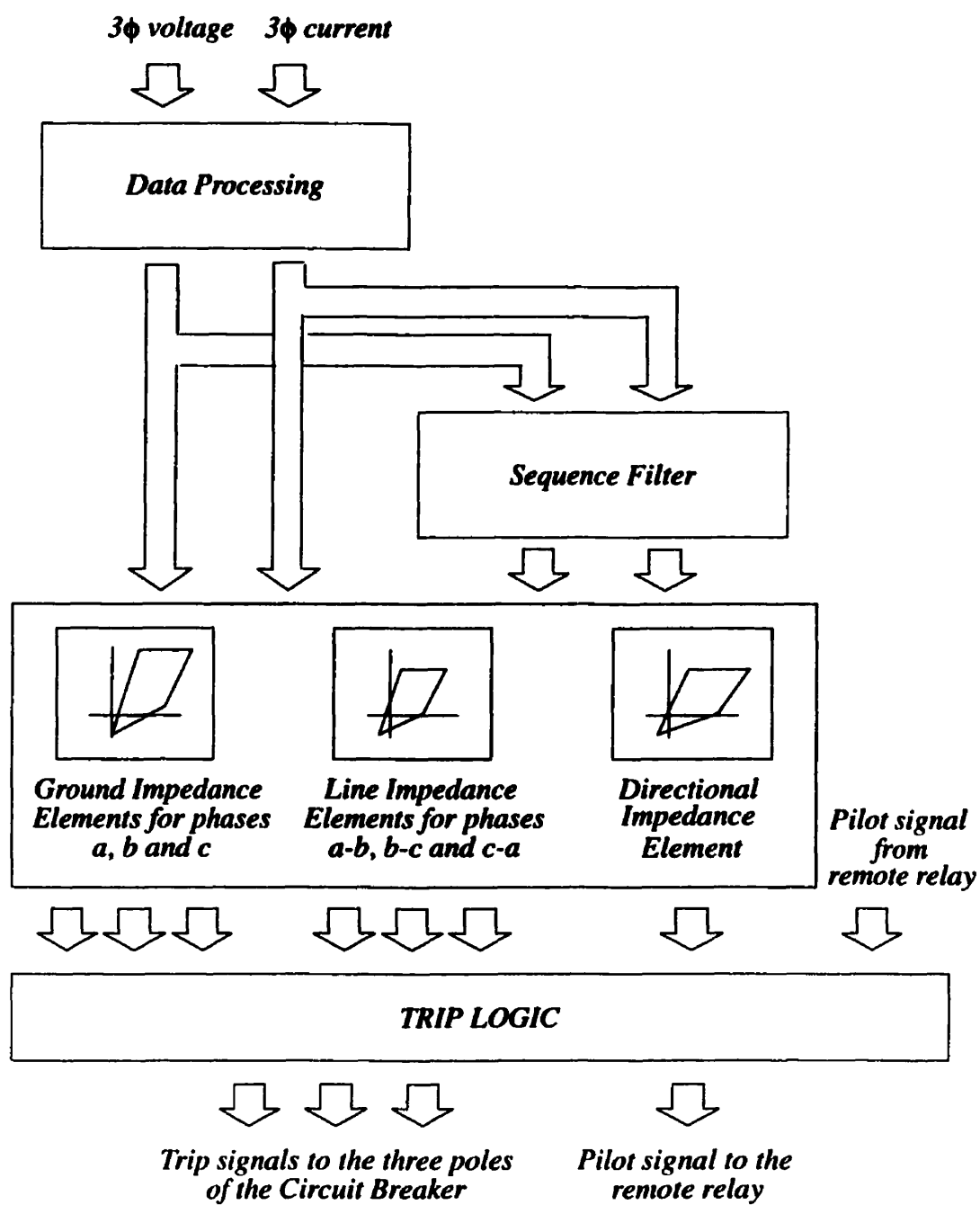


Figure 2.11: Organization of the Alpha Power Technology relay.

2.5 Summary

An overview of the distance protection techniques used in digital relays has been presented. The protection algorithms, data processing techniques and the organization of the APT relay algorithms have been described. The performance of this relay's algorithms are tested on complex transmission configurations. The test results are reported later, in Chapters 5 and 6.

CHAPTER 3

ADVANCED POWER TECHNOLOGY RELAY LIBRARY FOR PSCAD/EMTDC™

The important exercise of establishing the accurate off-line models of the Advanced Power Technology relay elements and the other interfacing components is described in this chapter. These models were used for off-line tests to determine its performance on double circuit and six-phase transmission line configurations. This chapter is dedicated to the description of the modelling techniques and the characteristics of various data processing elements which were developed for use on the PSCAD/EMTDC™ (Electromagnetic transient simulation program) simulation platform [30]. The relay model is available as one complete unit or as individual components of data processing elements. The data processing elements are combined to form the complete APT relay for a given application. This enables the user to investigate the internal parameters of each unit, in addition to the trip signals issued by the relay, during off-line tests.

3.1 PSCAD/EMTDC™ Relay Library of the APT Relay Elements

PSCAD is a graphical front end to the EMTDC Electromagnetic transient simulation program. The relay models therefore have their own graphical icons [30] which can be used on the PSCAD/DRAFT canvas for building a given system model.

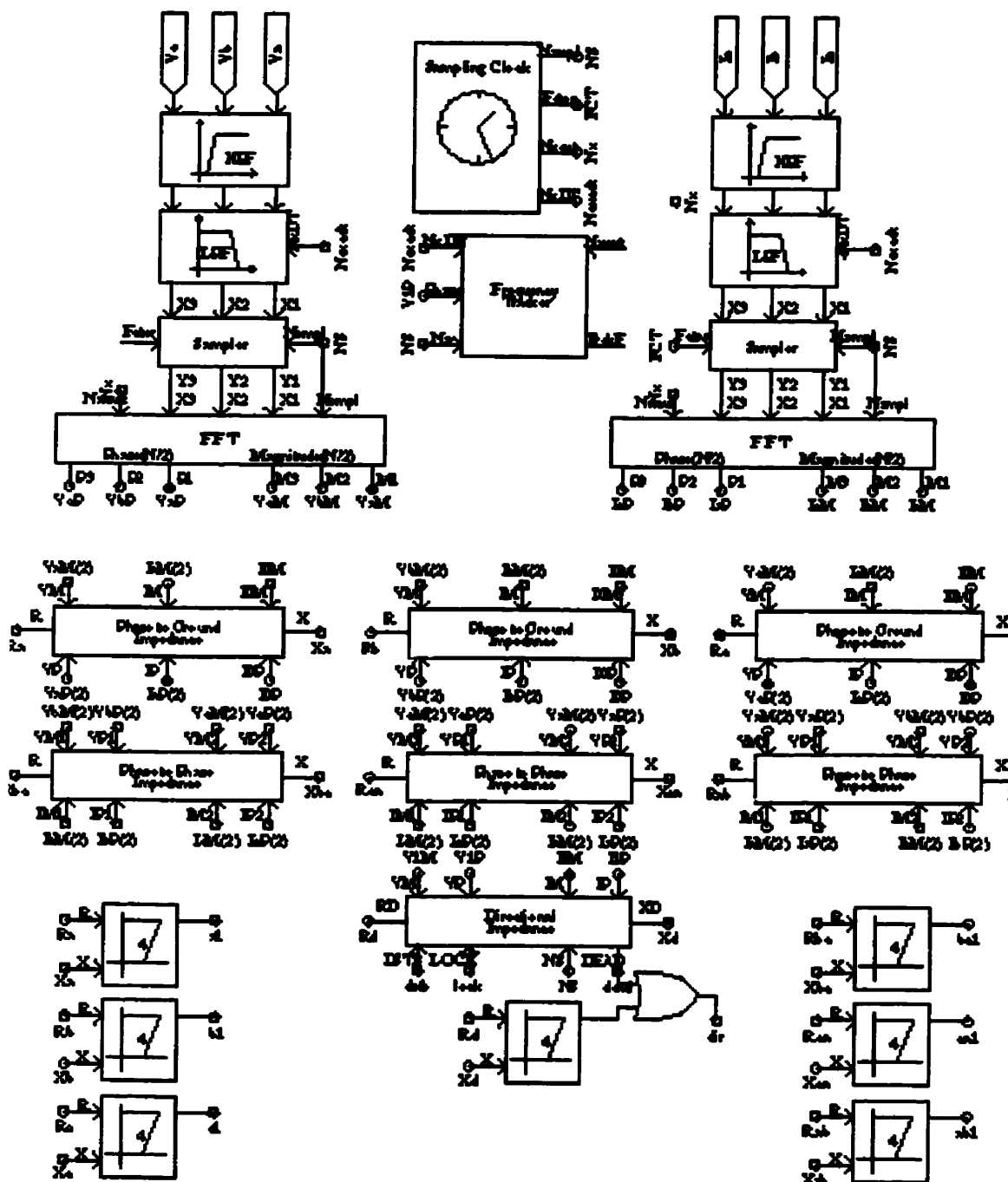


Figure 3.1: The PSCAD/DRAFT icons of the APT relay library.

Standard time domain simulation techniques are adopted for realizing the relay library. Additional modelling techniques such as interpolation are used to achieve increased accuracy, wherever necessary. The code for simulation is written in FORTRAN. All models were tested with the actual relay using a test set up described in section 3.3. Figure 3.1 shows the complete assembly of the APT relay data processing elements for a single circuit three phase line, without the trip logic [24].

3.2 Data Processing Models and their Characteristics

3.2.1 Sampling Clock

The clock governs the sampling instants by issuing a pulse to the sampler and other clock driven elements, while updating a counter on the number of samples per cycle. It also computes the ‘factor-of-interpolation’ required for correcting the error that is introduced due to a discrete time solution, particularly, for correcting the error introduced due to the sampling instants not being coincident with the computing instants of the time domain solution. Linear interpolation between computing times corrects for such errors.

The basic inputs to this element are the base frequency of the system and the sampling rate. It allows the user to choose between 16, 32 or 64 samples per cycle of the base frequency. It has four outputs which are inputs to the subsequent elements in the process. Figure 3.2 shows the icon of the clock as on the PSCAD/DRAFT canvas.

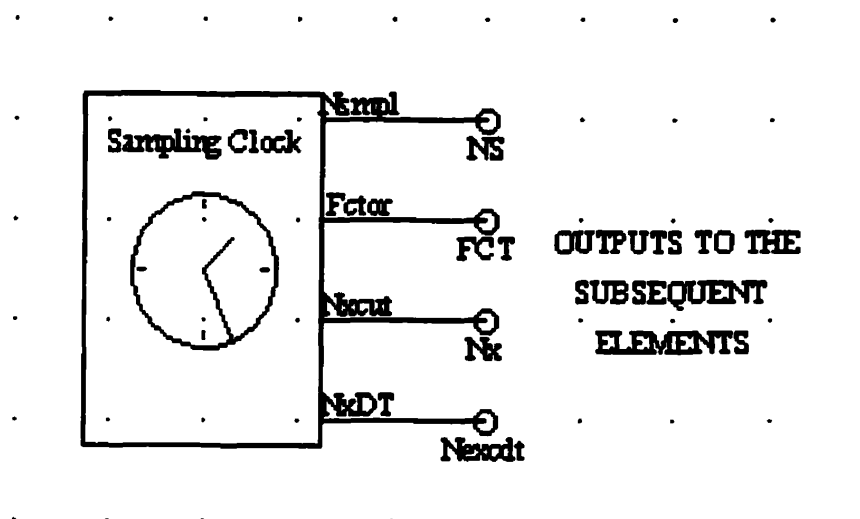


Figure 3.2: The icon of the Sampling Clock on the DRAFT canvas.

3.2.2 Frequency Tracking Unit

The sampling frequency of the data processing elements is synchronized to the system frequency. The frequency tracking unit tracks the frequency of the system to adjust the sampling interval accordingly. The difference in the phase of the positive sequence bus voltage computed in two consecutive cycles, is used to monitor the variations of the system frequency. Based on the computed difference in phase angle of the bus voltage, the sampling interval is corrected. Following a correction to the sampling interval, a cycle (of system frequency) of stabilizing time is allowed before another such correction is made. This is the time required for the data processing system to evaluate the system parameters accurately after a disturbance in the sampling interval. Note also that a correction to the sampling interval is approved only if the difference in measured phase angles of the bus voltage, at consecutive cycles, exceeds a preset

threshold. However, it freezes for any large changes (above a pre-set value) in the phase of the measured quantity as it implies a major disturbance of the system. The element returns to its active state when the phase angle between two consecutive sampling instants falls below a set value.

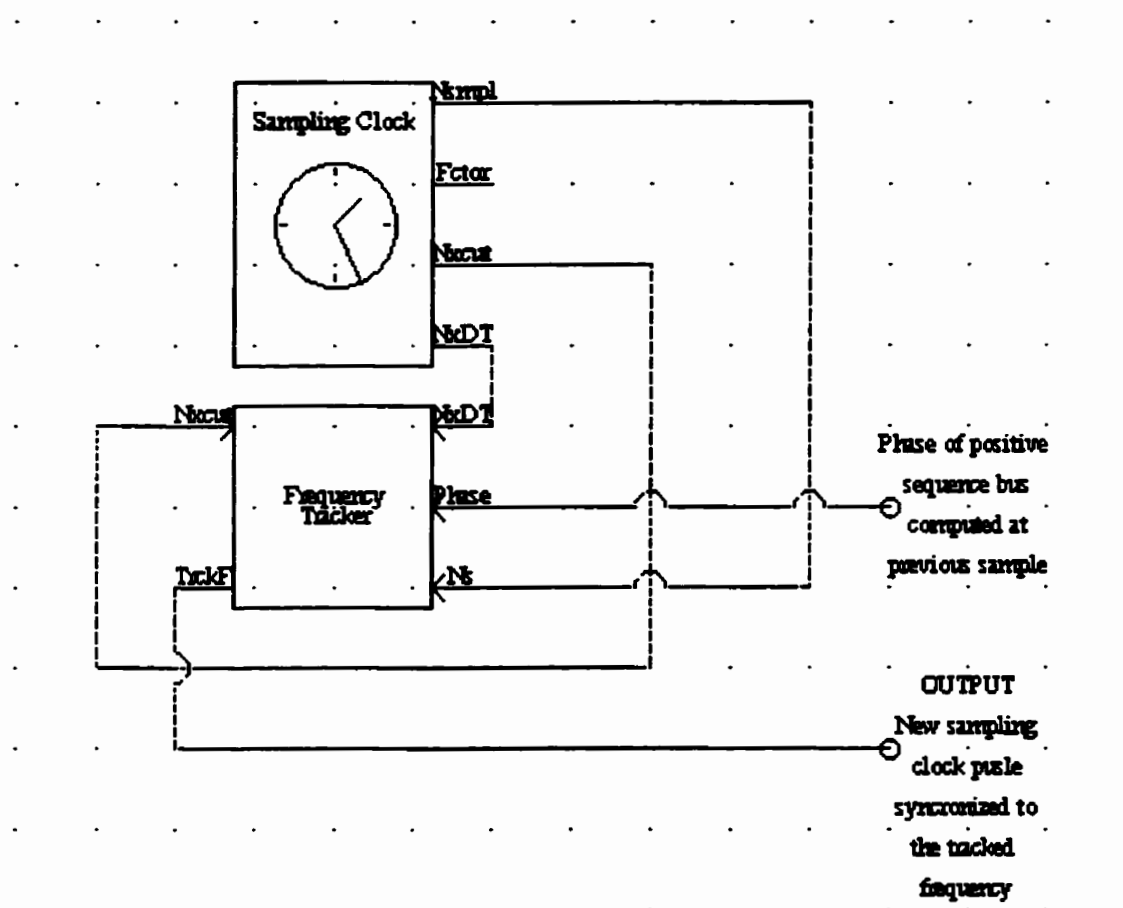


Figure 3.3: The icon of the frequency tracking unit, on the DRAFT canvas.

The PSCAD/DRAFT icon has four inputs, three are supplied by the sampling clock and the fourth is the phase angle of the positive sequence bus voltage computed at the

previous sample. Output is the clock pulse synchronized to the fundamental frequency of the positive sequence bus voltage.

3.2.3 Low-Pass Filter

This is an analog filter for filtering the higher order harmonics of the input signals, which would alias as low order harmonics when sampled. Therefore this is also called the anti-aliasing filter.

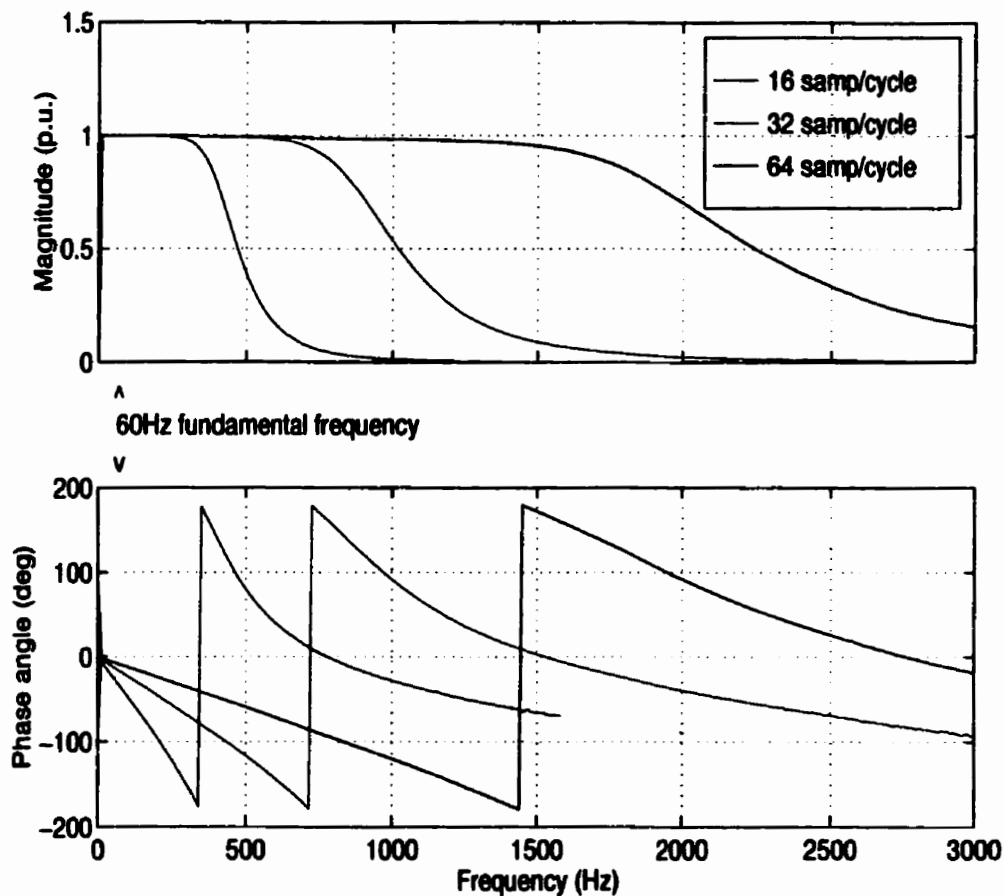


Figure 3.4: Low pass filter characteristics for sampling frequencies of 16, 32 and 64 samples per cycle of fundamental frequency.

The cut-off frequency of this fifth order Butterworth filter is dependent on the sampling rate of the digital scheme and the fundamental frequency of the system protected. The characteristics of the low-pass filter therefore differ according to the selected sampling frequency and the three possible characteristics for a system frequency of 60 Hz are shown in Figure 3.4. The characteristics show that the phase delay introduced by the low pass filter has an inverse relationship to the sampling rate.

Figure 3.5 shows the input signals and the input information on the cut-off frequency to the filter icon.

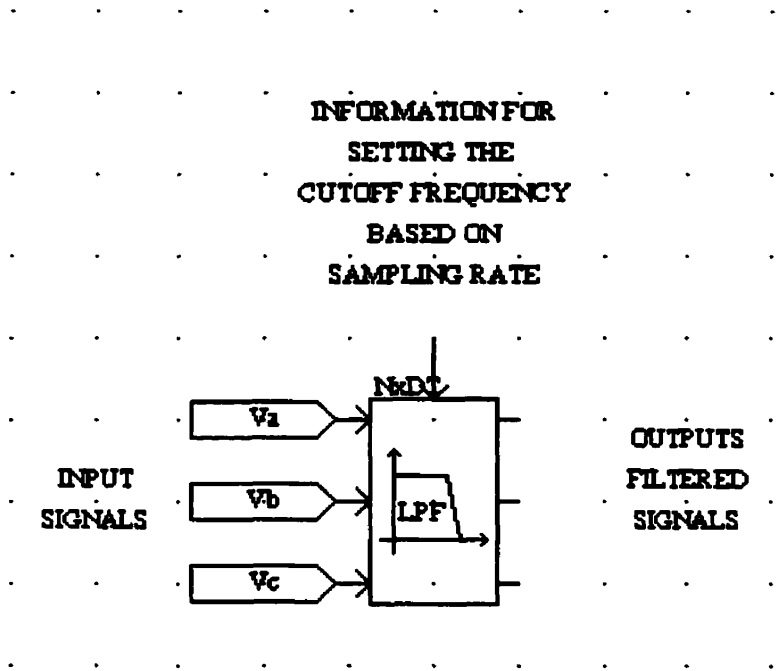


Figure 3.5: PSCAD/DRAFT icon of the low-pass filter with its inputs.

3.2.4 High-Pass Filter

The high pass filter is designed to eliminate the dc and sub-harmonic components in the input signals of the relay. An earlier version of the relay implementation consisted

of an analog high pass filter which was later replaced by a simpler but faster digital filter. Both filters were used in the studies carried out and are discussed in this section.

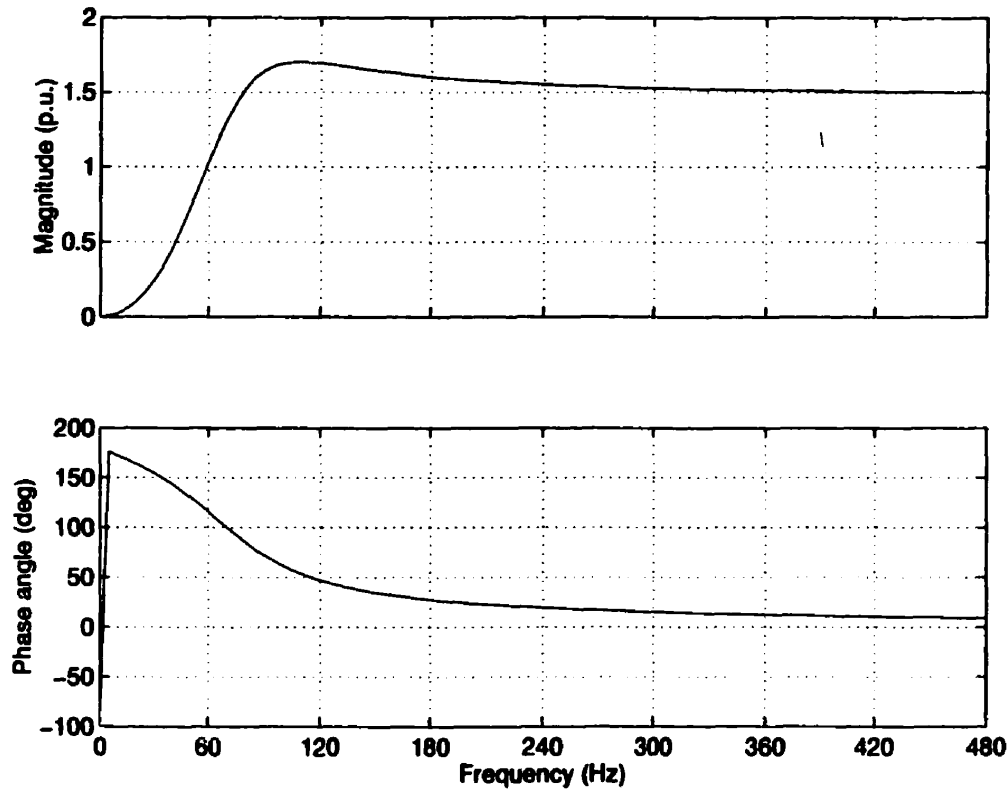


Figure 3.6: Analog high pass filter characteristics.

Ideally, the high pass filter characteristics require a sharp cut-off and a unity gain at the fundamental frequency. A filter with such characteristics introduces considerable delay to the output signal. Although increase in cutoff frequency results in higher speed or lesser delay, it also reduces the gain to less than unity at fundamental frequency. A compromise between the gain and the delay was reached with a filter that has a gain greater than one in the pass-band, but with a cut-off frequency such that the

gain near fundamental frequency remained at unity. The characteristics of the second order analog high pass filter used in the studies are shown in Figure 3.6.

The output signal subsequent to the low-pass filter is expected to have little or no harmonics higher than the filter cut-off frequency. Therefore the high pass filter gain was not a critical design concern. The filter has a delay of 116° at the fundamental frequency. As seen in Figure 3.1, the analog high pass filtering is the first stage of the signal processing sequence.

The transfer function of the analog high pass filter, in the Laplace domain is

$$TF(s) = \frac{G \cdot \left(\frac{s}{\omega_0}\right)^2}{1 + 2\zeta\left(\frac{s}{\omega_0}\right) + \left(\frac{s}{\omega_0}\right)^2}, \quad 3.1$$

where $G = 1.48216$,

$$\omega_0 = 1.27633 \times 2\pi \times 60,$$

$$\xi = 0.50349,$$

and $s = j\omega$.

The filter model for EMTDC has the normalized characteristics and therefore requires the base fundamental frequency for de-normalizing as an input, in addition to the input signals. The model can be set to filter up to three signals.

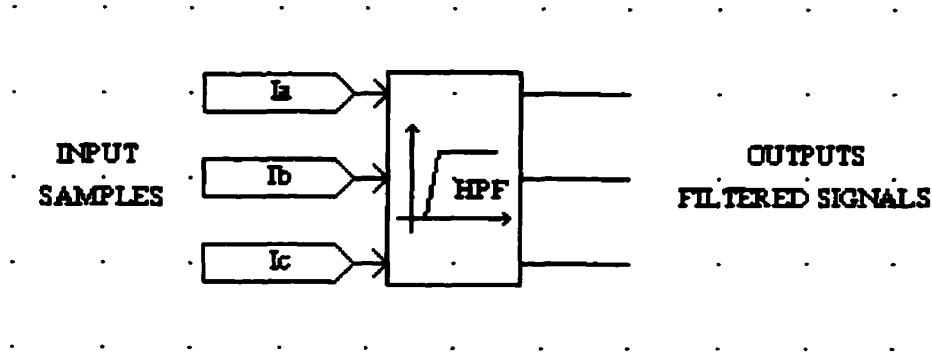


Figure 3.7: PSCAD/DRAFT icon of the analog high-pass filter with its inputs.

The analog filter was later replaced with a first order digital filter, which is placed after the sampler in the signal processing sequence. The transfer function of the filter in the z-domain is as given in, equation 3.2.

$$TF(z) = \frac{k_B(1 - z^{-1})}{1 - k_A z^{-1}}, \quad 3.2$$

where $k_A = 0.5929$,

$$k_B = 1.2974,$$

$$z^{-1} = e^{-j\omega T_s}, \text{ and}$$

$$T_s = \frac{1}{f_s}.$$

Sampling frequency f_s of the digital filter is 16 samples/cycle and has only a 52.1° phase shift at fundamental frequency. The characteristics shown in Figure 3.8 also

demonstrates its repetitive nature at multiples of sampling frequency, justifying the requirement of an anti aliasing filter in the processing sequence.

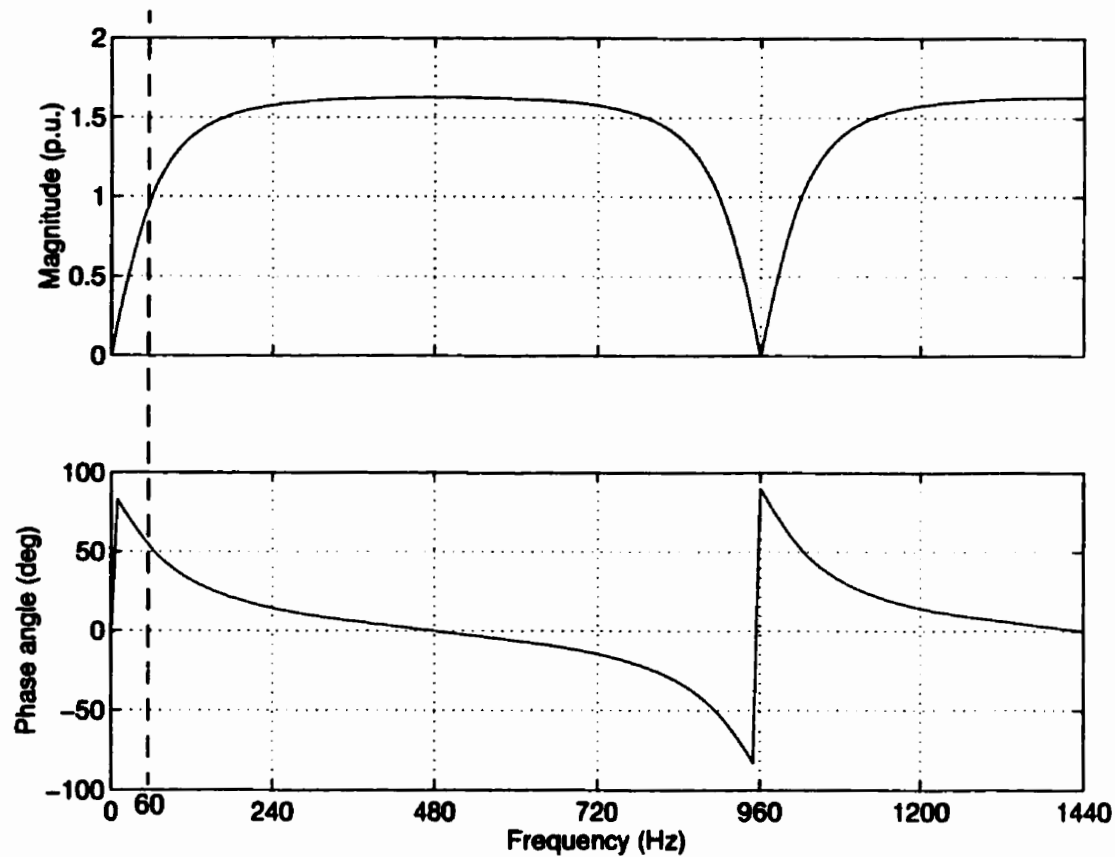


Figure 3.8: Digital high pass filter characteristics.

The DRAFT icon of the digital filter component is similar to that of the analog filter but with filter coefficients as the input parameters and an additional input from the clock, triggering the execution of the computational algorithm (Figure 3.9). The clock

pulses are issued at sampling instants. The outputs are held constant after a sampling instant till the next clock pulse is received.

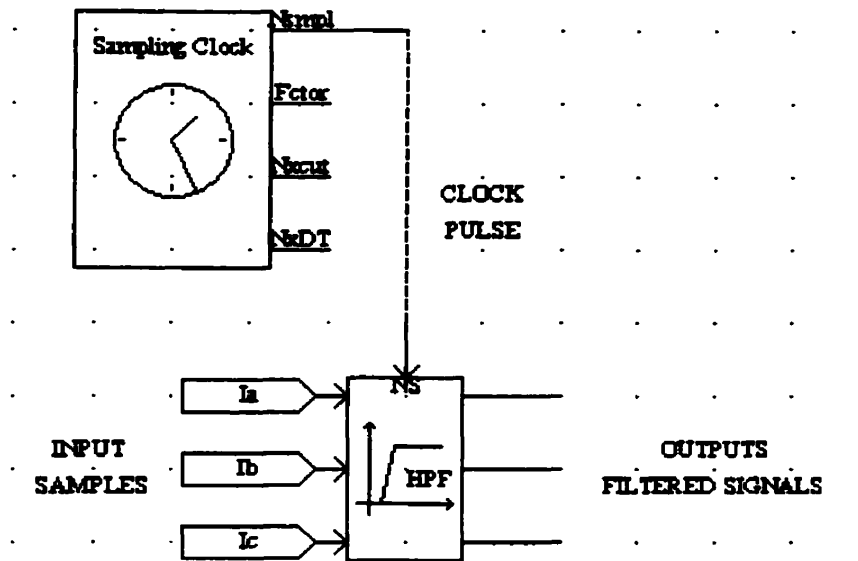


Figure 3.9: PSCAD/DRAFT icon of the digital high-pass filter with its inputs.

3.2.5 Sampler

The sampler samples and holds the input between sampling instants. This processing unit of the relay receives two other inputs from the sampling clock in addition to the data signals. The pulses issued by the clock trigger the sampling of inputs. The interpolated output ensures minimal errors due to the discrete time solution. Information on the interpolation factor is supplied by the clock element as well. The PSCAD/DRAFT icon can be set to sample up to three inputs.

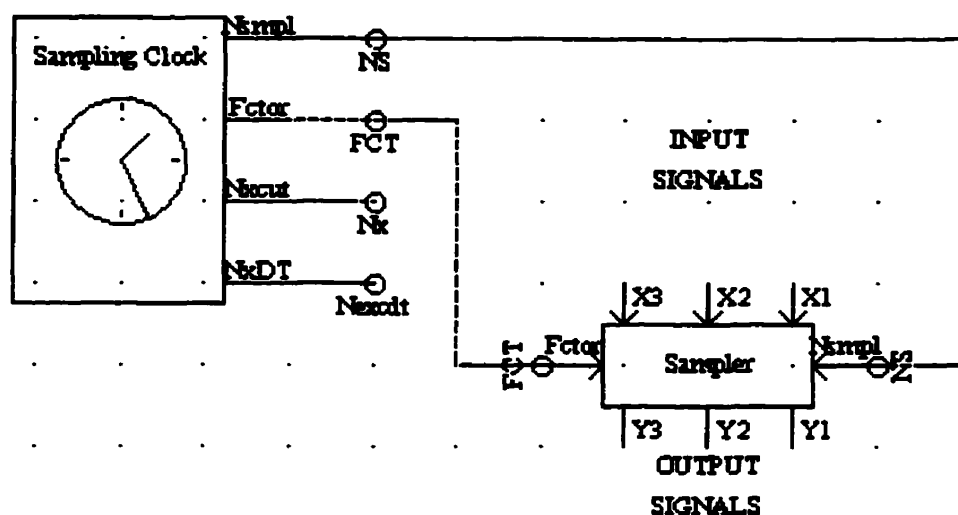


Figure 3.10: PSCAD/DRAFT icon of the Sampler.

3.2.6 Fast Fourier Transform (FFT)

Although the APT relay (the version used in this project) only requires the fundamental components to be extracted from the current and voltage waveforms, the fast fourier transform component modelled is a generic on-line frequency scanner which extracts harmonics up to half the sampling frequency. The computations in the model are based on 'Winograd Algorithm', a standard fast fourier transform (FFT) technique [23]. The computations use a moving window of data samples which represents a complete period of base frequency. Thus, the transients of a preceding period are captured in computations at any sampling instant. The sampling frequency set by the user, may be 16, 32, or 64 samples per cycle of fundamental frequency. It also determines the highest harmonic that can be accurately extracted from the input signals. The basis function for computation of the phase angle is a cosine waveform of

base frequency on a time axis starting at time zero. Therefore the FFT algorithm returns a zero phase for such input signals.

The DRAFT icon of the fast fourier transform model needs the information of sampling rate and the clock pulse indicating a sampling instant in addition to the input signals for execution of the algorithm. This model too can handle up to three input signals. Each output is an array of data containing information of fundamental and all other harmonics of interest, in their phasor form ($r\angle\theta$).

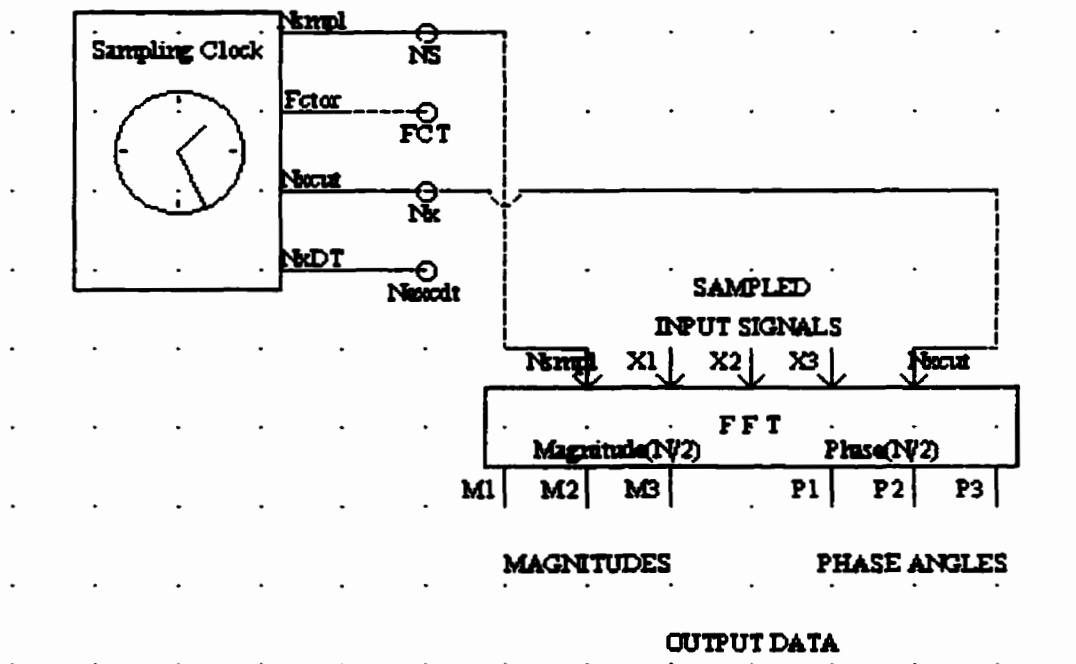


Figure 3.11: PSCAD/DRAFT icon of the Fast Fourier Transformation Model.

However, the algorithm used by the APT relay is different from the above. It is a very much more computationally efficient, pair FFT/DFT with oversampling-decimation techniques, which meets the requirements of both real-time signal processing and waveform recording purposes. In this technique the signals are oversampled with respect to the cut-off frequency of the anti-aliasing filter in order to minimize the aliasing effects. This same sampling rate is also used for recording waveforms with best possible resolution. Subsequently the sampled signals are decimated to a lower sampling rate for processing by the relay algorithm. The pair FFT/DFT algorithm had demonstrated considerable improvement in execution speed over the single FFT/DFT algorithm [25]. One to one correspondence in the FFT algorithm was not considered necessary for the off line model. Therefore, a generic algorithm which returned more harmonic information, although less computationally efficient, was used. Both algorithms give identical results for the fundamental component.

3.2.7 Sequence Filter

The sequence filter computes the magnitude and phase angle of the sequence components of the input signals. The inputs should be in the form of magnitude and phase angle of the fundamental component of the three phase quantity. The algorithm is executed at every computing instant of the simulation time grid. Therefore, the updating frequency of the outputs are naturally synchronized to the sampling frequency of the inputs.

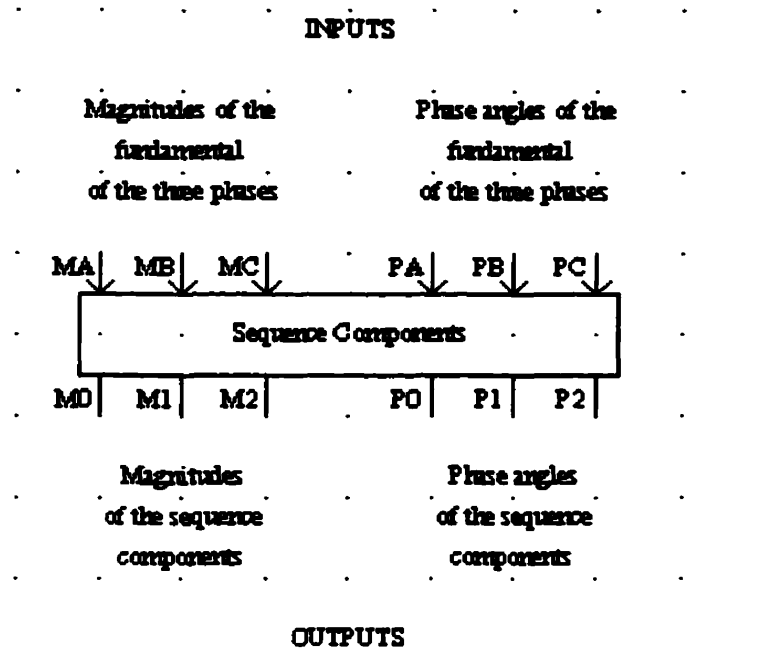


Figure 3.12: PSCAD/DRAFT icon of the Sequence Filter Model.

The processing units described in sections 3.2.1 to 3.2.7 are generic algorithms and are not limited in their use to simulation of protection algorithms. However, the models of the relay impedance elements and other decision making units, described in the following sections, are those of the APT relay. Therefore, they have little use in any other application other than simulation of digital distance protection algorithms.

3.2.8 Ground Impedance Element

The model uses inputs from both the fast fourier transform algorithm and the sequence filter for computing the impedance as given in equation 2.2. The fundamental components of voltage and current of a given phase as well as the zero sequence current computed by the sequence filter are inputs to the algorithm. Base frequency of

the signals and the zero sequence compensation factor k_0 are user defined inputs. The outputs are the resistive and reactive components of the computed impedance which correspond to a point on the impedance plane. The visual appearance of the DRAFT icon is shown in Figure 3.13. A distance relay model protecting a three phase circuit requires three such units for phases a , b and c separately.

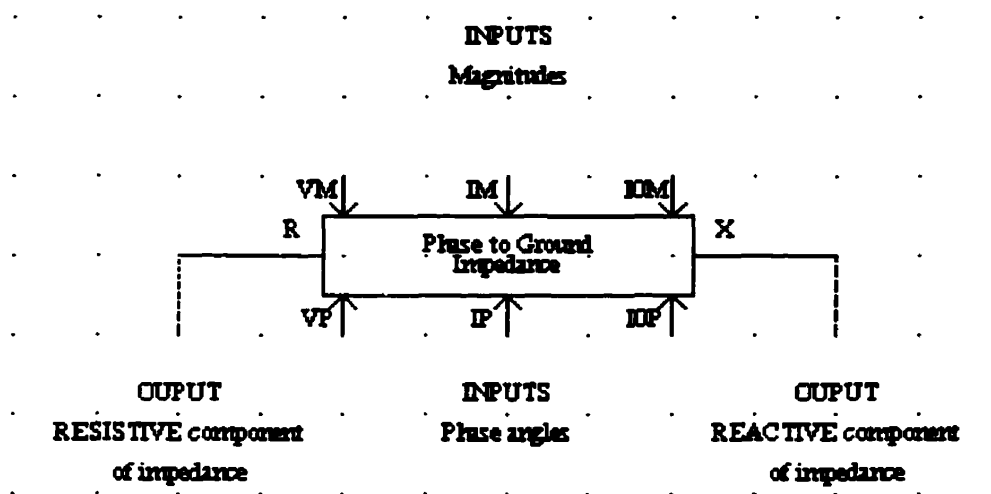


Figure 3.13: PSCAD/DRAFT icon of the Ground Impedance Element Model.

The ground impedance element for use in double circuit and six phase transmission configurations is a modified version of the above model with two more added inputs. It has the zero sequence current magnitude and phase angle of the parallel circuit as inputs as well as a second compensation factor k_m to compute the impedance as given in equation 5.2, later in CHAPTER 5.

3.2.9 Line Impedance Element

This element is very similar to the model described in section 3.2.8. It returns the resistive and reactive components of a line impedance. The inputs are the magnitudes and phase angles of the voltages and currents required to compute the impedance as given in equation 2.2.

3.2.10 Directional Impedance Element

This again computes the resistive and reactive components of the directional impedance computed as in equation 2.8. It requires the positive sequence voltage and current information and maintains a five cycle data buffer of the input information for use in its computations. If a disturbance on the system is detected the data buffer ceases to update. Thus the inputs corresponding to five cycles prior to the current time are locked at the pre-disturbance values. Therefore, the computed directional impedance remains indicating the directional impedance for the disturbance even when the system is into more than five cycles of disturbance. If the system returns to a second operating point after the disturbance, the directional impedances will not be accurate for five cycles till the data buffer is filled with the information of the new operating point. This model was intended for fault studies on various systems and does not accurately model the features during recovery from a disturbance. The PSCAD/DRAFT icon for the model is visually similar to the ground and line impedance elements. The inputs are the positive sequence voltage and current information, the sampling clock pulse and an input from other decision making elements indicating

system disturbances. The resistive and reactive elements of the directional impedance are the outputs.

3.2.11 Zone Tripping Model

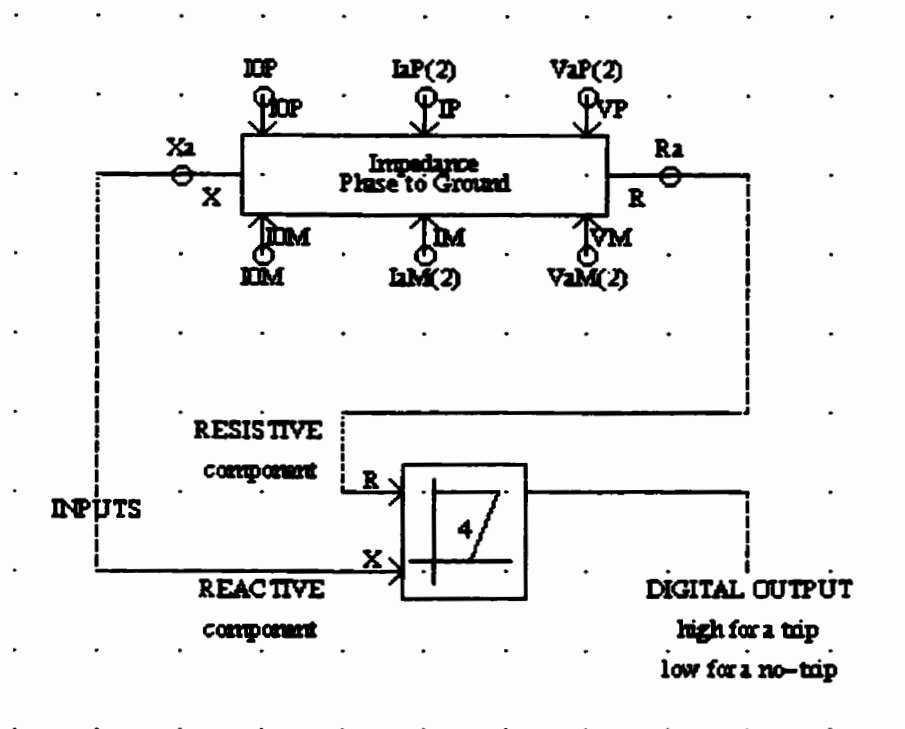


Figure 3.14: PSCAD/DRAFT icon of the Zone Trip Model.

The zone trip element returns the trip signal for the given impedance and the trip zone. The trip zone data are entered as preset data while the impedance is dynamically checked after each computation for its positioning in the impedance plane with respect to the trip zone. The output of the element is digital and is 'high' for a trip condition. A trigonometric algorithm is used for checking if the impedance is within the trip zone boundaries. The trip zone can be a polygon of up to eight vertices and is set to a four

by default. Each impedance computed using the ground, line or the directional impedance elements are fed into one or more zone trip elements for trip signals in the appropriate zone. Typically a relay protecting a single three phase circuit can have two such models for zones one and two, for each phase and line impedance. In addition there is another for the directional impedance.

The off-line fault studies were geared towards investigating the behaviour of the ground, line and directional impedance trajectories for various fault conditions on the selected transmission line configurations. Therefore, simulating the behaviour of individual decision making elements in the relay was sufficient to investigate the success of the relay operation for a given fault. It was also the intention to investigate the possibility of using other techniques such as artificial neural networks in parallel with the conventional elements, to aid the operation of the relay.

Some other simulation models that were used for studies on the use of Artificial Neural Networks (ANN) with the digital relay are also discussed.

3.2.12 Data File Writer

This is a model that generates a sampled data file of a pre-defined format. The data are written at every sampling instant while the file writer is enabled. Therefore, the model requires, as dynamic inputs, the data to be written to the file, a sampling clock pulse, and the write enable signal. There are also the number of inputs and the name of the file as preset inputs to the file writer. This model was developed to generate the required training data for various fault conditions, which were subsequently used for

training the fault detecting artificial neural network for a given transmission line configuration. The visual appearance of the DRAFT file writer icon with its inputs are shown in Figure 3.15. The data written at a given sampling instant are of input and output types and are written in the format compatible with the ANN training, Xerion Simulator. Therefore, the icon has the name 'Xerion' on it. A maximum of 50 input type and 25 output type of data can be written to the file at a given sampling instant.

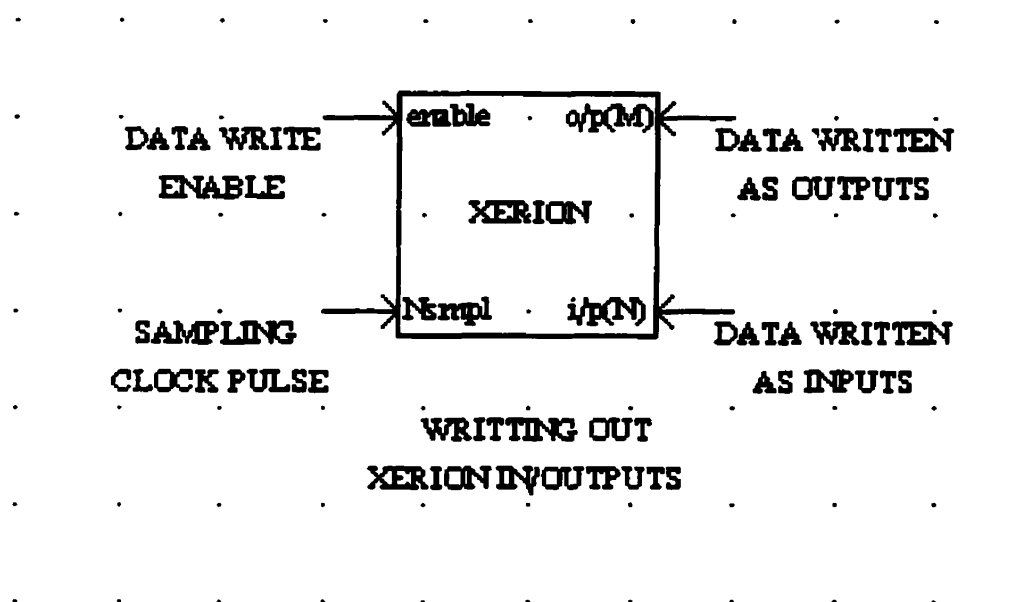


Figure 3.15: PSCAD/DRAFT icon of the Data File Writer.

3.2.13 Artificial Neural Network Model

This is a model of a feed forward neural network which has a pre-defined network structure described later in section 8.5.1. The input neurons in the model have a linear transfer function and the hidden and output neurons are fired using a logistic transfer

function given in equation 8.1. The weights of the network are read from a data file and the outputs are computed at every sampling instant. Outputs are available in both digital and analog forms, for the ease of testing. The fault detection capability of the trained networks for double circuit and six-phase line configurations were tested using this model. Basic three layer networks with different numbers of neurons can be simulated using this model with little modification to the code. The PSCAD/DRAFT icon of the ANN model is shown in Figure 3.16. The inputs and outputs are lumped to separate single arrays to maintain the compactness of the DRAFT icon.

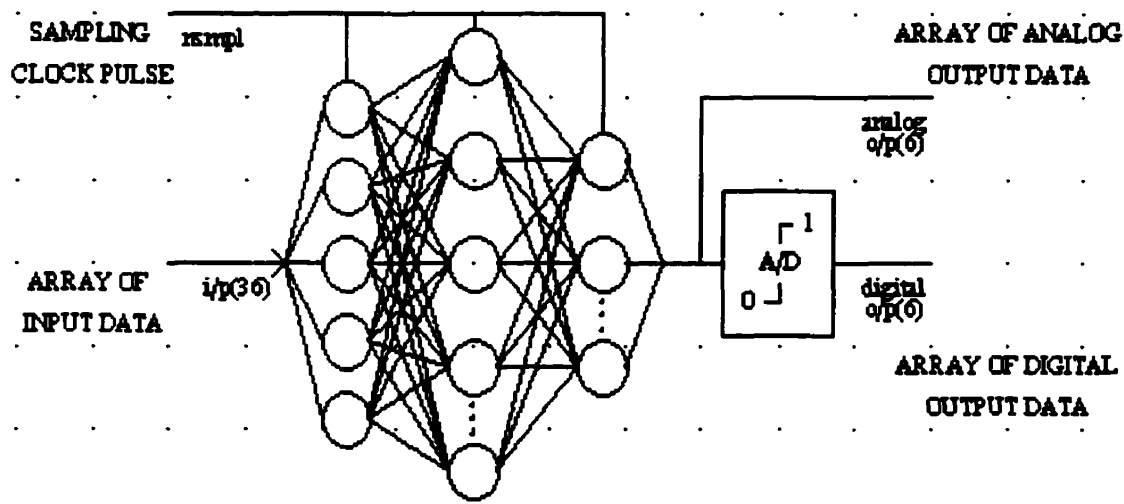


Figure 3.16: PSCAD/DRAFT icon of the Artificial Neural Network Model.

3.3 Test Set-up

The off-line relay model on the PSCAD-EMTDC simulation platform was verified for its accuracy after a series of tests that were conducted to compare its results with those of the APT relay for the same voltage and current waveforms. Figure 3.17 shows the test setup used to verify the accuracy of the off-line relay model. A single circuit transmission system modelled on PSCAD-EMTDC served as the test system. Voltage and current waveforms produced by the simulated system were recorded using a COMTRADE format recorder. Those waveforms were then transferred over the local area network to a playback simulator [30]. The playback simulator allows viewing of the waveforms and adjustment of output scaling to an appropriate level for input to the relay A/D (analog to digital) stage. For any given run the playback simulator initially repeats the pre-fault cycle of the waveforms continuously, until the fault is initiated by pushing a button on the playback simulator screen. It then plays the fault and repeats the last cycle of the waveforms for the preset period of time (typically 500 cycles).

When such waveforms are played at the relay, it produces a recording of the event, which can be viewed on-line by connecting a monitor to it. The display shows 300 ms of the voltage and current waveforms, the produced trip signals and the impedance trajectories with the trip zones. These same displays can also be viewed off-line using a “Wreshow” display program.

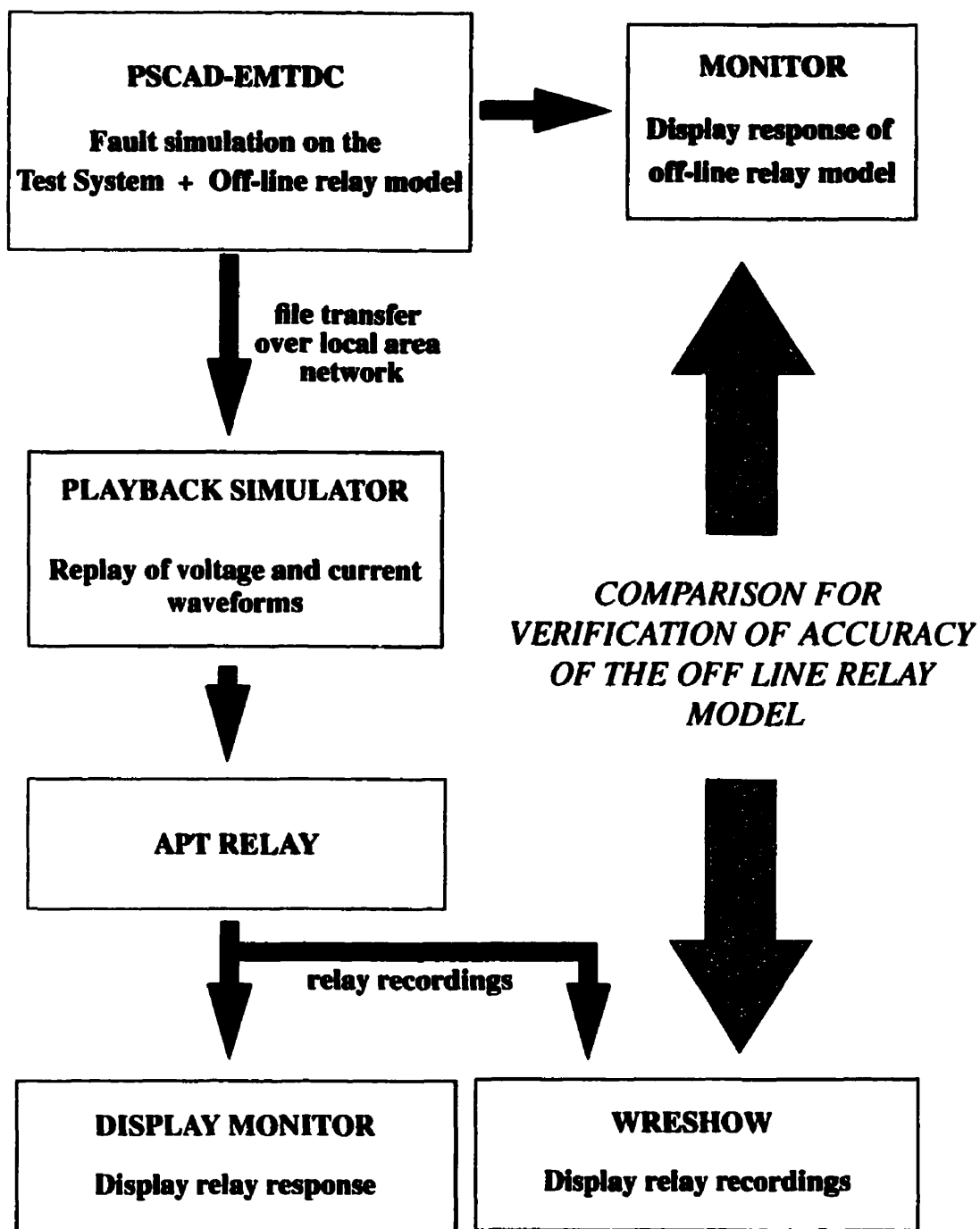


Figure 3.17: Set-up for testing the off-line relay model for its accuracy.

Thus the impedance trajectories of the off-line simulation relay model can be visually compared with those of the actual APT relay for the same test system waveforms. A series of such tests were carried out to verify the accuracy of the off-line relay model described in this chapter which was later used for investigation of its performance on two other transmission line configurations.

3.4 Summary

The characteristics and some important modelling details of all the measuring, data processing elements of the relay, and interfacing components have been presented. These models were later used to carry out the investigation of the relay performance on the two compact transmission line configurations.

CHAPTER 4

SIMULATION MODELS

Two system models were set up on PSCAD/EMTDC for the simulation studies. They are:

- A three-phase double circuit line and
- a six-phase line

Typical data were used to build the models and thus they are typical of their kind although hypothetical. This chapter discusses in detail the system parameters and the sources of data.

4.1 Three-Phase Double Circuit Line Model

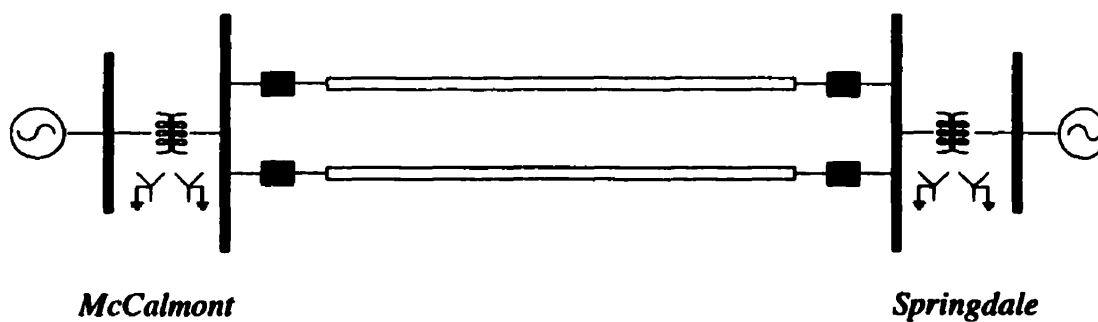


Figure 4.1: Simplified single line diagram of the 3-phase double circuit line.

The basic model consists of

- the 3-phase double circuit transmission line,
- the sending end equivalent source with a transformer,
- a load end transformer and an equivalent source.

4.1.1 Transmission Line

Published data of a transmission line tested for its power transfer capability under worst case conditions are used [15]. The tests reported are for both 3-phase double circuit, and 6-phase configurations. Some missing data necessary for the model were assumed based on normal practice. See Appendix B for details of the transmission line.

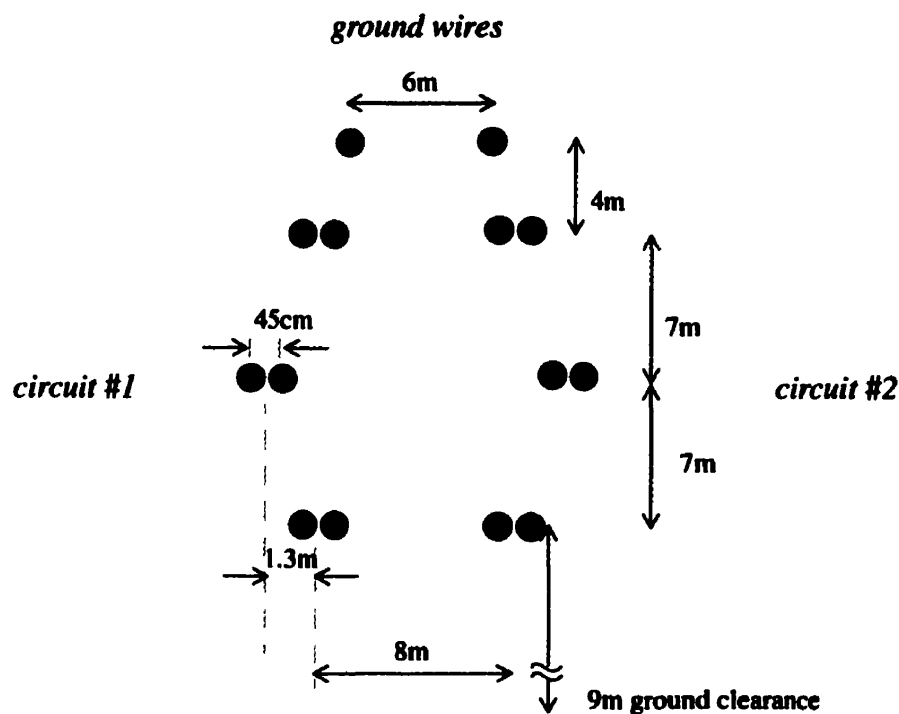


Figure 4.2: Conductor configuration for the three-phase double circuit line.

Measurement of Line Impedances:

For the measurement of line impedances, the double circuit line in the above configuration was terminated through a resistance and injected with positive, negative and zero sequence currents respectively. The circuit connection for self-impedance measurements is shown in Figure 4.3. The parallel circuit is disconnected from both the current source and the load for self-impedance measurements on any one of the circuits. Voltage to current ratio at the feeding end for respective phases are recorded in Table 4.1.

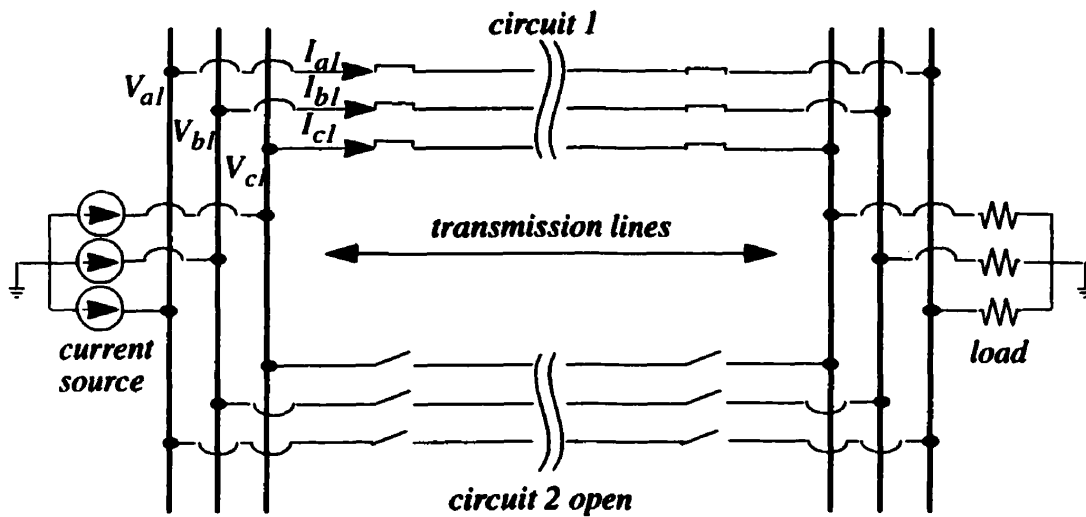


Figure 4.3: Circuit connection for self impedance measurement on circuit #1

Table 4.1: Self-impedances of the double circuit line

phase	positive seq. impedance (Ω)	negative seq. impedance (Ω)	zero seq. impedance (Ω)
<i>Za1</i>	<i>5.47 + j 37.8</i>	<i>5.47 + j 36.4</i>	<i>51.8 + j 122.0</i>
<i>Zb1</i>	<i>5.47 + j 37.8</i>	<i>5.47 + j 36.4</i>	<i>51.8 + j 122.0</i>
<i>Zc1</i>	<i>5.47 + j 37.8</i>	<i>5.47 + j 36.4</i>	<i>51.8 + j 122.0</i>
<i>Za2</i>	<i>5.47 + j 37.8</i>	<i>5.47 + j 36.4</i>	<i>51.8 + j 122.0</i>
<i>Zb2</i>	<i>5.47 + j 37.8</i>	<i>5.47 + j 36.4</i>	<i>51.8 + j 122.0</i>
<i>Zc2</i>	<i>5.47 + j 37.8</i>	<i>5.47 + j 36.4</i>	<i>51.8 + j 122.0</i>
<i>per phase self impedance</i>	<i>5.47 + j 36.4</i>	<i>5.47 + j 36.4</i>	<i>51.8 + j 122.0</i>

Impedances for the six phases are computed using:

$$Z_{a1,b1,c1,a2,b2,c2} = \frac{V_{a1,b1,c1,a2,b2,c2}}{I_{a1,b1,c1,a2,b2,c2}}, \quad 4.1$$

where $I_{a1,b1,c1}$ are the measured currents and $V_{a1,b1,c1}$ are the measured voltages as shown in Figure 4.3. $I_{a2,b2,c2}$ and $V_{a2,b2,c2}$ are currents and voltages from similar measurements on the second circuit.

One circuit is left disconnected from the current sources, as shown in Figure 4.4, for measurement of mutual impedances between circuits. The voltage induced at the open end of the second circuit due to unit current on the other is recorded in Table 4.2, for the three phases.

Mutual impedances are computed using:

$$Z_{a1a2,b1b2,c1c2} = \frac{V_{a1m,b1m,c1m}}{I_{a1,b1,c1}}, \quad 4.2$$

where $I_{a1,b1,c1}$ are the measured currents and $V_{a1m,b1m,c1m}$ are the measured voltages as shown in Figure 4.4.

Two 50 km line segments were connected in cascade for impedance measurements. Each segment was ideally transposed. This perfect balance in the phases is evident in the line impedance measurements.

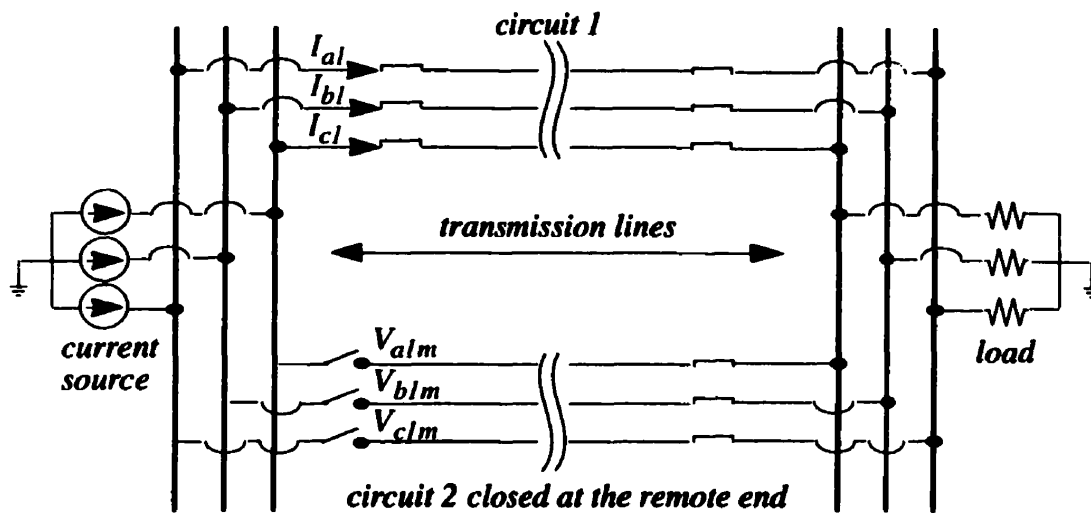


Figure 4.4: Circuit connection for mutual impedance measurement

Table 4.2: Mutual impedances of the double circuit line

	positive seq. impedance (Ω / phase)	negative seq. impedance (Ω / phase)	zero seq. impedance(Ω / phase)
<i>Zala2</i>	$0.0 + j 0.0$	$0.0 + j 0.0$	$47.6 + j 85.3$
<i>Zb1b2</i>	$0.0 + j 0.0$	$0.0 + j 0.0$	$47.6 + j 85.3$
<i>Zc1c2</i>	$0.0 + j 0.0$	$0.0 + j 0.0$	$47.6 + j 85.3$
<i>mutual impedance</i>	$0.0 + j 0.0$	$0.0 + j 0.0$	$47.6 + j 85.3$

4.1.2 Source and Transformers on Sending and Receiving Ends

Source impedances from a typical 6-phase system were adjusted to be used in the 3-phase double circuit line [15]. The sources are rated at a voltage of 345 kV and 3000 MVA, and the impedances are as given in Table 4.3. Some variations of the sources were achieved by changing the source impedances. The second set of data in Table 4.3 shows the source impedances for modelling the strong sources.

Table 4.3: Source Impedances

Source name	positive/negative seq. impedance in Ω	zero seq. impedance in Ω
<i>McCalmont</i>	$7.14 \angle 83.38^\circ$	$17.72 \angle 73.88^\circ$
<i>Springdale</i>	$3.32 \angle 80.51^\circ$	$10.47 \angle 74.36^\circ$
<i>McCalmont strong source</i>	$3.57 \angle 83.38^\circ$	$8.86 \angle 83.38^\circ$
<i>Springdale strong source</i>	$1.667 \angle 83.38^\circ$	$5.237 \angle 83.38^\circ$

Some details of the transformers at Dorsey converter station were used to derive typical data for the transformers on the model. Grounded Y-Y winding configuration with equal voltage levels of 345 kV for both primary and secondary are used for simplicity. The transformer core was modelled in order to be able to represent saturation effects if necessary. Transformers are rated at 3000 MVA for consistency with sources and the transmission line. Typical no load loss of 0.3% and positive sequence leakage reactance of 8% is assumed for the transformer model without saturation. The equivalent impedances of the sources and the transformers at both ends are shown in Table 4.4.

Table 4.4: Source impedances of the model measured at the HV bus

	Positive/negative seq. impedance (Ω /phase)	Zero seq. impedance (Ω /phase)
<i>McCalmont source + transformer</i>	10.33 $\angle 85.36^\circ$	20.80 $\angle 76.21^\circ$
<i>Springdale source + transformer</i>	6.48 $\angle 85.10^\circ$	13.60 $\angle 77.94^\circ$

4.2 Six-Phase Line Model

The model for the six-phase system remains very similar to the three-phase double circuit system configuration. Added to it are four transformers and two six-phase busbars.

Two delta-wye connected three-phase transformers at each end, one of each pair with reverse polarity are used to derive the required 60° phase shift. This arrangement breaks the zero sequence network at the transformers and provides the most straight

forward demonstration of operating parameters of a six-phase line, keeping the system as simple as possible for the fault analysis. The switching operations are performed on the six-phase side.

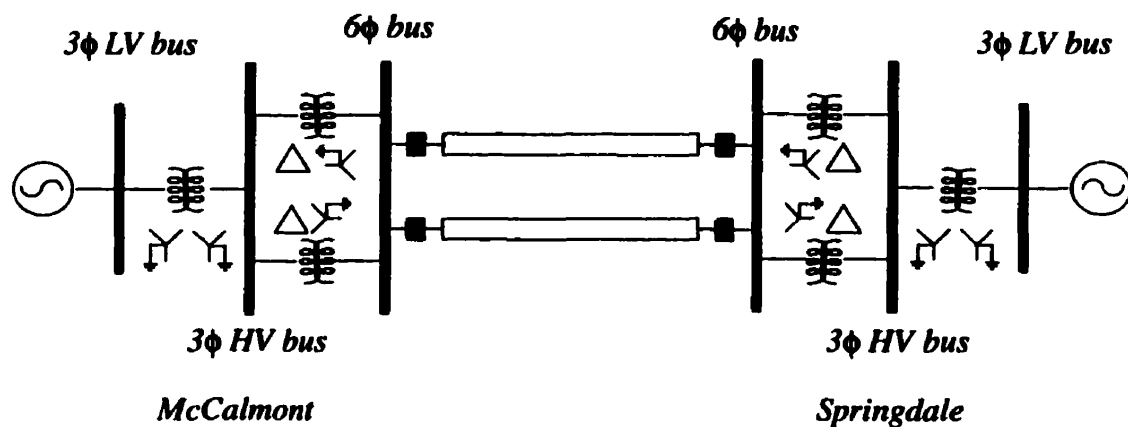


Figure 4.5: Single line diagram of six phase transmission line model.

A six-phase line has six phase-to-ground voltages and fifteen phase-to-phase voltages. These phase-to-phase voltages can not be reduced to a single set as with three-phase, because of the inherent angular differences between the various phase-ground voltages. Also, full transposition would destroy the phase relationship between adjacent conductors. Maximum compaction of a six-phase line results from adjacent phases being maintained at a 60° phase difference. Thus, the most which can be achieved in a circuit balance is a “roll transposition” where six conductors are rolled in position, allowing each conductor to occupy $1/6$ of the distance but maintaining the correct relative phasing [38]. No ground wires are used.

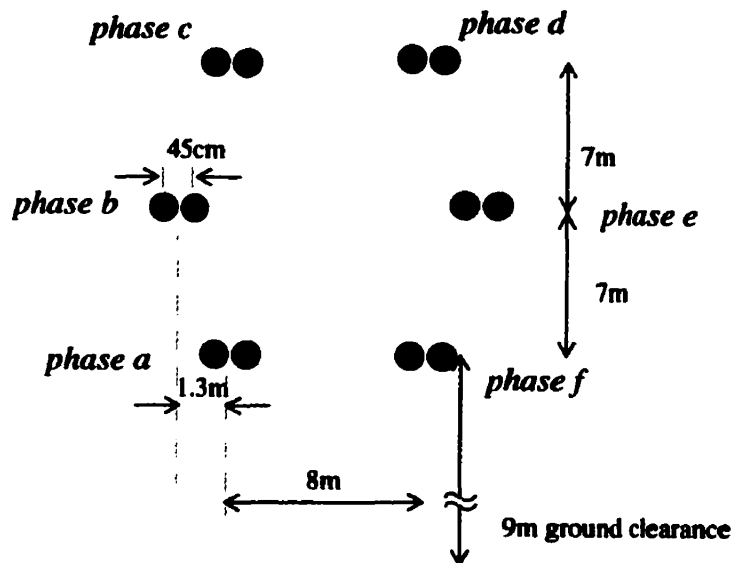


Figure 4.6: Conductor configuration for the 6-phase line.

The 100 km line consists of six segments of line. Each line segment is 16.67 km, with connections to allow transposition. Table 4.5 shows the measured self and mutual impedances of the line.

Table 4.5: Impedances of the six-phase line measured on the model.

Impedance measured on the model	Circuit 1 (consisting of phases a, c and e)	Circuit 2 (consisting of phases b, d and f)
<i>Positive sequence impedance (Ω/phase)</i>	$3.93 + j37.37$	$3.96 + j37.36$
<i>Negative sequence impedance (Ω/phase)</i>	$3.95 + j37.36$	$3.94 + j37.36$
<i>Zero sequence impedance (Ω/phase)</i>	$18.9 + j138.9$	$18.9 + j138.9$
<i>Zero sequence mutual impedance (Ω/phase)</i>	$16.2 + j114.3$	$16.2 + j114.3$

The equivalent sequence impedances of the source and the transformers as seen at the six-phase bus on the McCalmont and Springdale ends (see Figure 4.5) are as in Table 4.6.

With conductor data and the line configurations being the same for both three-phase double circuit and six-phase models, some difference is observed in the transmission line sequence impedances (as seen in Table 4.1, Table 4.2, and Table 4.5). This mismatch is due to the only difference in the models which is the type of transposition used. Three-phase configuration is with ideal transposition and the six-phase line is roll transposed for maintaining the required relative phase difference between adjacent conductors.

Table 4.6: Equivalent Impedances of the sources and the transformers.

Equivalent Impedance	McCalmont	Springdale
<i>Positive sequence (Ω/phase)</i>	<i>$1.74 + j12.6$</i>	<i>$1.74 + j11.8$</i>
<i>Negative sequence (Ω/phase)</i>	<i>$1.69 + j26.9$</i>	<i>$1.12 + j19.3$</i>
<i>Zero Sequence (Ω/phase)</i>	<i>$0.0 + j6.35$</i>	<i>$0.0 + j6.35$</i>

Due to the arrangement on the Δ -Y transformers, the negative sequence impedance seen at the six-phase bus differs from the positive sequence impedance.

4.3 Summary

The details of double-circuit and six-phase transmission system models have been presented. The performance of the APT relay discussed in the following chapters 5 and 6 is based on the tests carried out on these line models.

CHAPTER 5

PERFORMANCE OF IMPEDANCE RELAYS ON DOUBLE CIRCUIT LINES

5.1 Introduction

Impedance relays designed for 3-phase single circuit systems pose difficulty in application to 3-phase double circuit lines due to mutual effects, inter circuit faults etc. Simulation of different types of faults on a double circuit line and detailed observation of respective responses of impedance elements on each circuit gives better insight to the problem. This also aids in the identification of the causes of malfunction.

This chapter discusses

- the impedance relay model and it's settings for double circuit transmission line application,
- the impedance relay behaviour for selected fault conditions,
- analysis of causes of malfunction, and finally
- a proposal to improve the distance relay techniques for double circuit line applications.

5.2 Impedance Relay and its Settings

Figure 5.1 shows the block diagram of the data processing elements in the impedance relay used in this study.

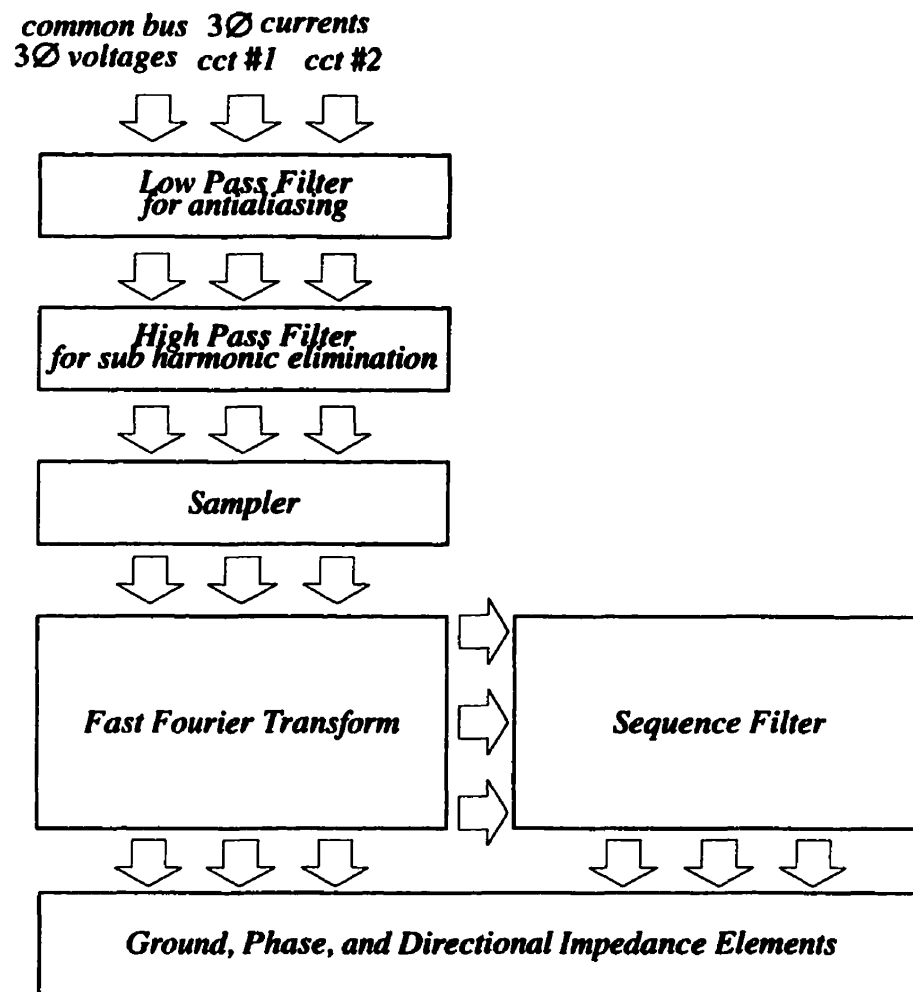


Figure 5.1: Processing units of the impedance relay used in the study.

Impedances seen by the phase and line elements are given by equations 2.1 and 2.2. The ground relay constant k given in equation 2.3 is computed as follows, based on impedances given in Table 4.1:

$$k = \frac{Z_{l0} - Z_{l1}}{Z_{l1}} = \frac{122.0 - 36.4}{36.4} = 2.35. \quad 5.1$$

5.2.1 Trip Zone Settings

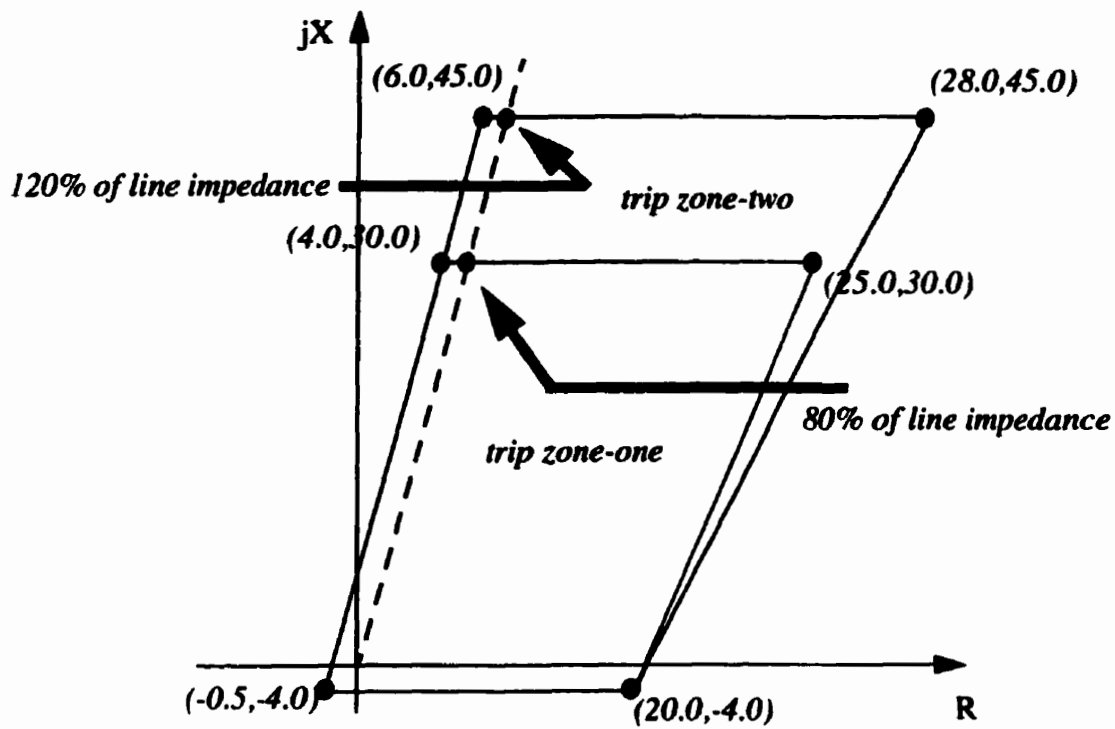


Figure 5.2: Trip zones of the impedance relays on McCalmont-Springdale double circuit line.

Four sided polygons as shown in Figure 5.2 are the trip zones one and two. Coordinates of the polygons are derived from 80% and 120% of the line impedance

for the primary and secondary protection respectively, with an allowance of 20~25 Ω of fault resistance. It also leaves a 10% safety margin at the boundaries near the origin.

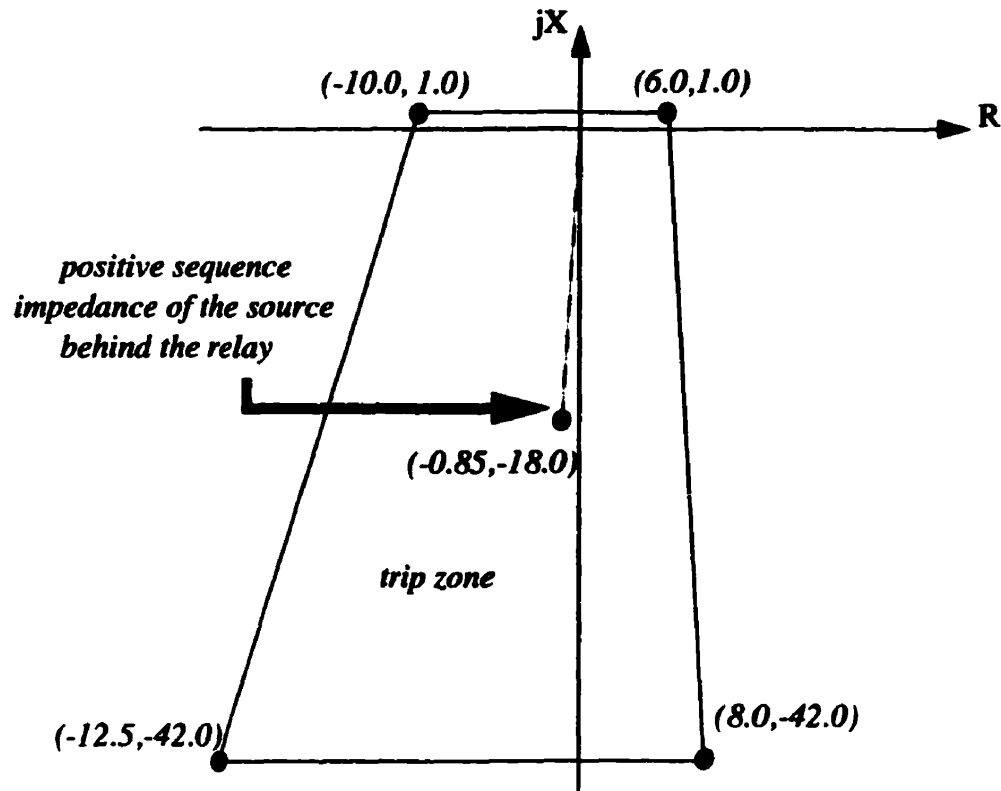


Figure 5.3: Trip zone of the directional impedance element on McCalmont-Springdale double circuit line.

The directional element of the relay has its own trip zone which is set to detect forward faults. A polygon, which can have independent resistive and reactive reach, has its coordinates set according to the likely range of positive sequence incremental impedance seen by the relay, as shown in Figure 5.3. It can be shown that on a double circuit line, the positive sequence incremental impedance fails to measure exactly the source impedance (Appendix A). Therefore, the zone boundary extends, to include over twice the impedance of the local source.

Two sets of impedance relays set up with the above mentioned parameters were simulated at the McCalmont end of the double circuit line model. Impedance trajectories seen by the ground, line, and directional elements for a set of selected fault conditions are discussed in the following section.

5.3 Impedance Trajectories for Different Types of Faults

5.3.1 Single Line to Ground Fault (a_1 -g)

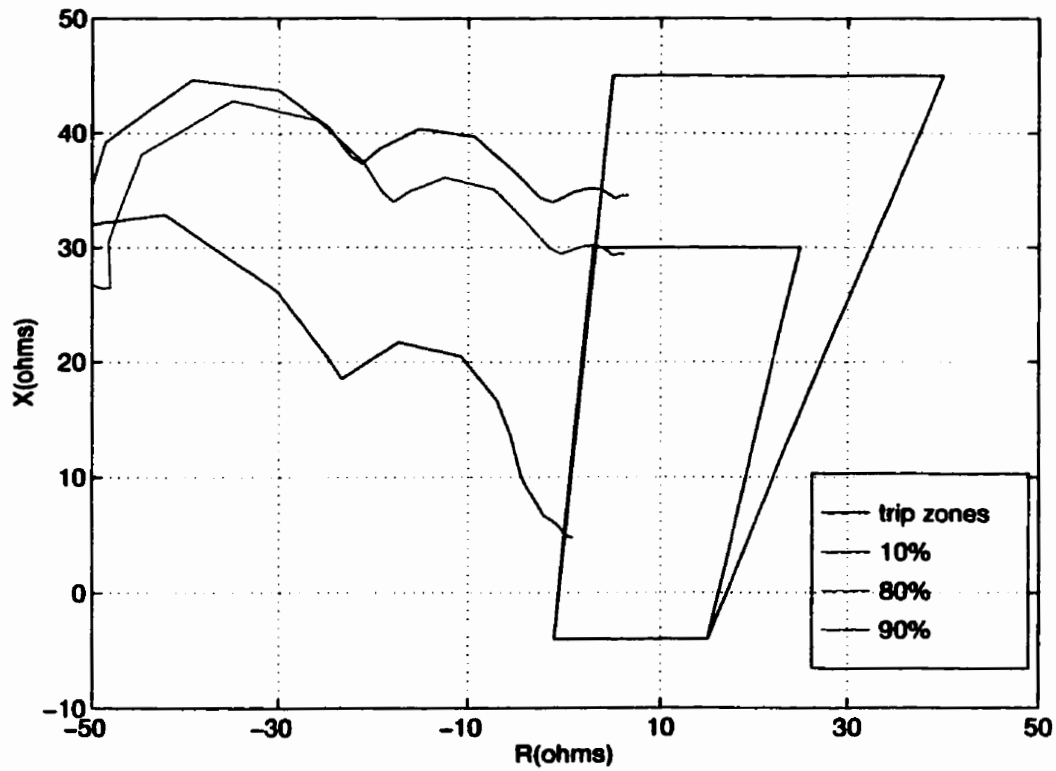


Figure 5.4: Ground impedance relay trajectories of the faulted phase, for single line (a_1 -g) to ground faults at 10%, 80% and 90% distances.

Figure 5.4 shows the comparison of ground impedance trajectories of the faulted phase for a single line-to-ground fault at three locations on the line. The faults simulated are 90%, 80%, and 10% down the transmission line. The faults at distances 10% and 90% are in zones one & two respectively, while the fault at 80% distance is falling on the boundary of the two zones as expected. Ground elements of the other two phases of the faulted circuit do not see impedances in the trip zones.

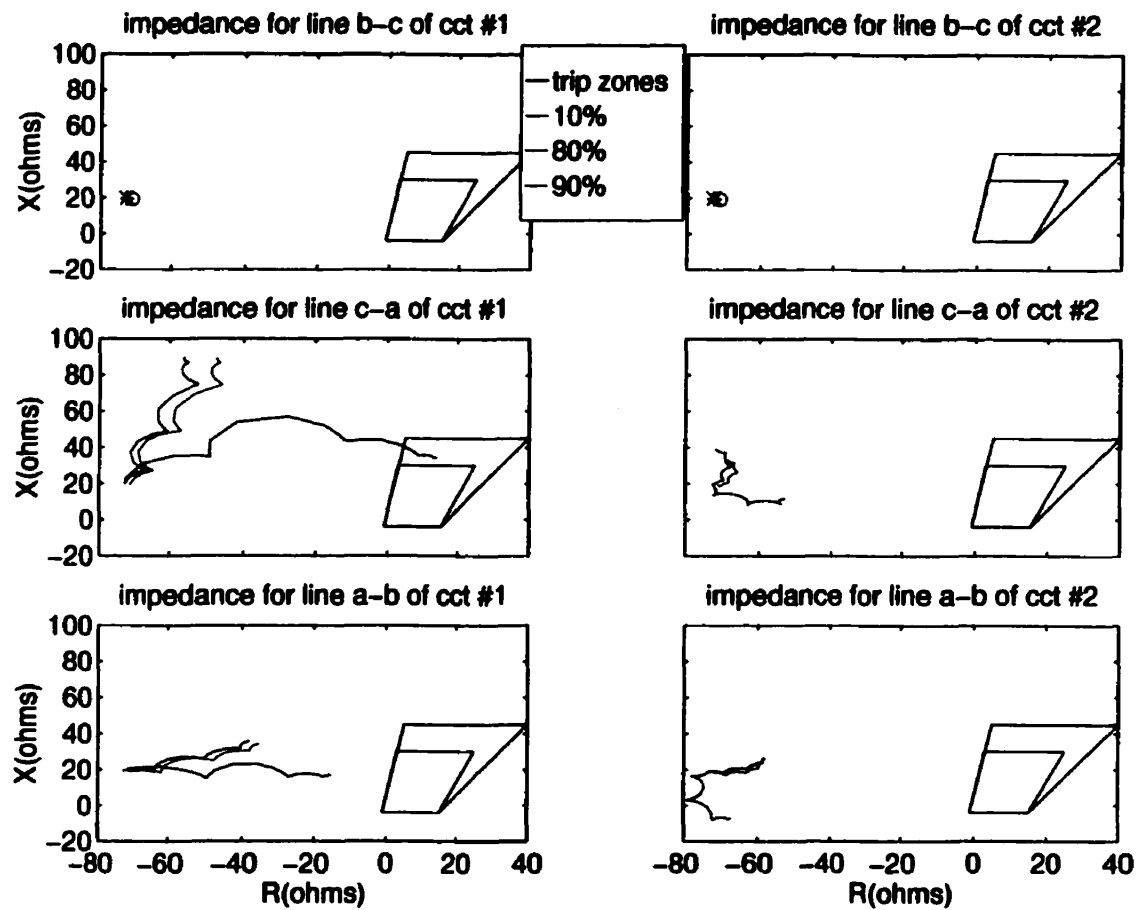


Figure 5.5: Line impedance trajectories of circuits #1 & #2, for single line to ground (a_1 -g) faults at 10%, 80% and 90% distances.

The line impedance element between phases c and a of circuit #1(Figure 5.5) detects the close up fault in zone-two. This is desirable as it can act as a back-up in the event the zone-one protection of the ground element fails. Also, this would not cause an undue immediate trip on phase- c , because of the time delay of a zone-two trip.

The dip in the bus voltage and the zero sequence mutual currents appear to have moved the impedances seen by the elements on the unfaulted parallel circuit from their normal operating point. The most influenced are the line impedances of $a-b$ and $c-a$ (Figure 5.5).

The impedance trajectories shown in Figure 5.6 are for the directional elements of the two circuits. All the three faults are seen as forward faults by the directional element of the first circuit. Therefore, they are all detected in the trip zone of the directional element as expected.

The directional element of the second circuit detects the far end faults as forward remote faults. The fault at 10% distance is appropriately detected as a backward fault (Figure 5.6). None of the faults are detected in the directional trip zone of circuit #2. Thus, the directional elements of both circuits detect and trip the correct circuit, for both zone-one and two, single line to ground faults. Figure 5.7 describes the direction and distance to the close-up and remote faults, seen by the directional element of the unfaulted line.

In general it is seen that the effects of bus voltage fluctuations and mutual currents for a single-line-to-ground fault are within safe regions not to cause any false trips.

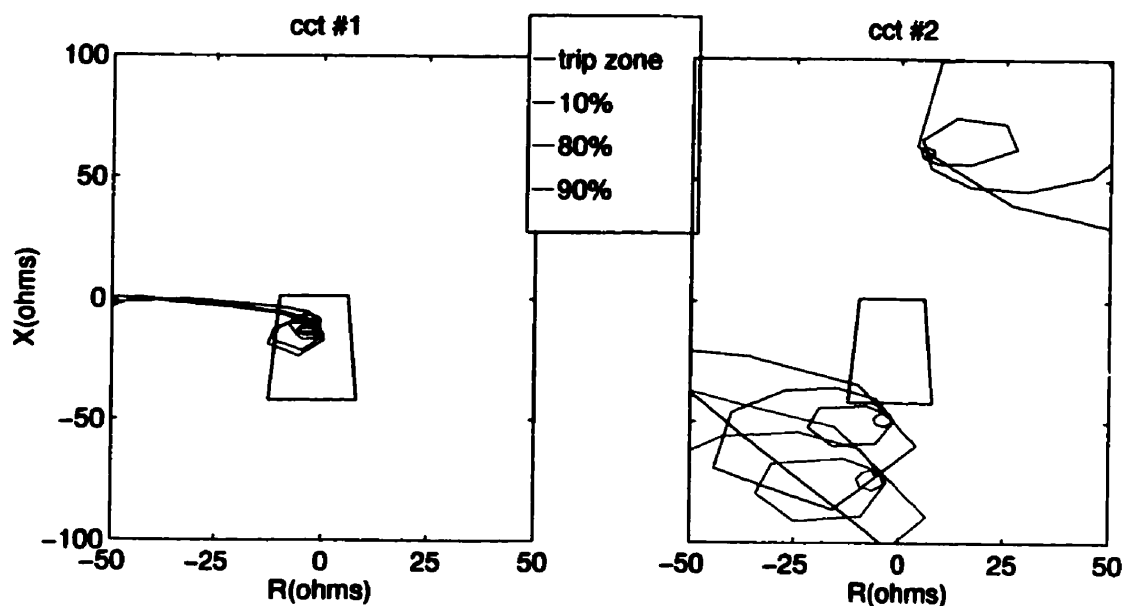


Figure 5.6: Directional impedance trajectories of circuits #1 & #2., for single line to (a₁-g) ground faults at 10%, 80% and 90% distances.

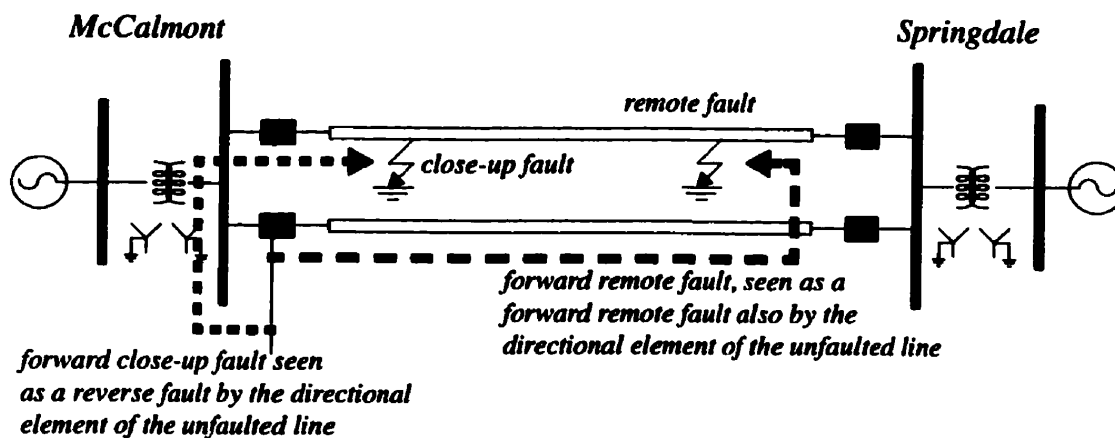


Figure 5.7: The directions and distances to the close-up and remote faults as seen by the directional element of the unfaulted line.

5.3.2 Single Circuit Double-Line-to-Ground Fault (a_1 - b_1 - g)

Figure 5.8 shows the ground impedance trajectories of the faulted phases for a single circuit double-line-to-ground fault. The faulted phases are phases a_1 and b_1 . Figure 5.9 shows two line impedance elements of the faulted circuit.

The ground and line elements corresponding to the faulted phases pick-up the faults in the appropriate zones of protection for the close up fault and the fault at 80% distance (Figure 5.8, Figure 5.9). The remote double line to ground fault at 90% distance does not move the ground impedance trajectory of phase- b in trip zone-two, but since the line impedance element detects it well in zone-two as expected, the relay issues a zone-two trip for such a fault. The close up fault causes a zone-one trip on the line element a - c , although phase c is unfaulted. This is a mis-indication of the actual fault situation, but does not cause any serious adverse effects as double line-to-ground faults should result in three pole tripping of the faulted circuit.

As in the single line-to-ground faults, the parallel circuit experiences fluctuations of impedance trajectories due to bus voltage variations and mutual effects, but remains well outside trip zones and therefore is not shown.

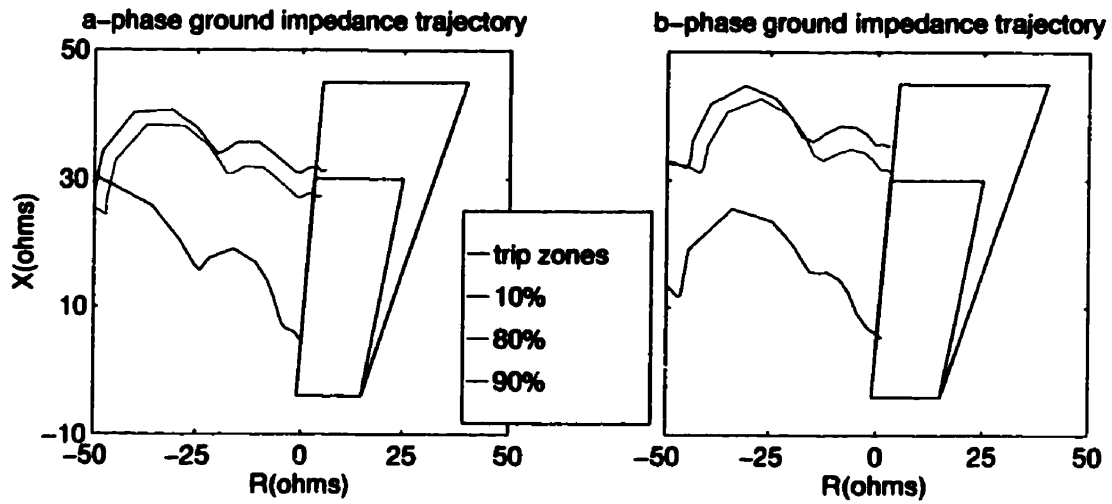


Figure 5.8: Ground impedance relay trajectories for the faulted phases, for double line to ground faults (a_1 - b_1 -g) at 10%, 80% and 90% distances.

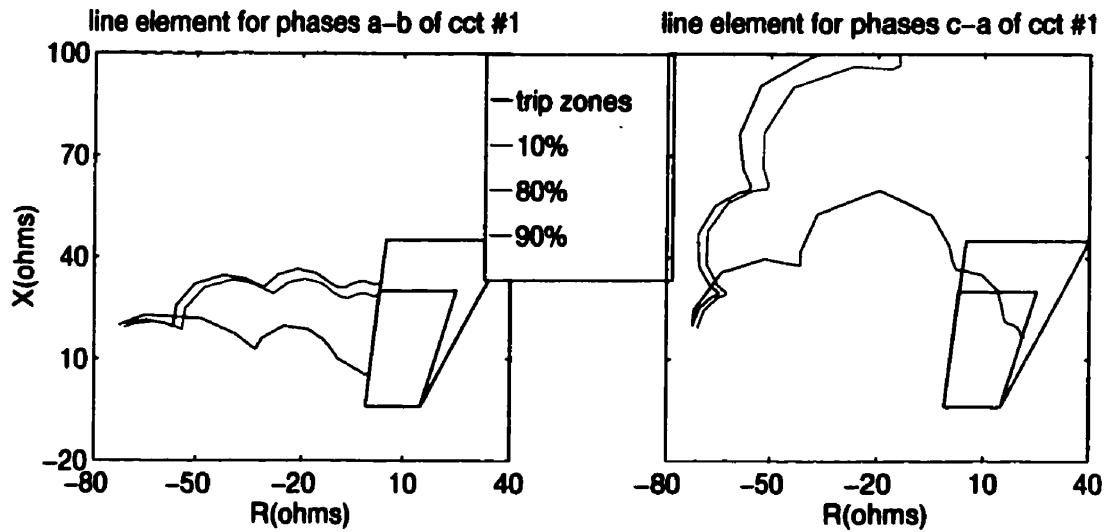


Figure 5.9: Line impedance trajectories of a-b and c-a of the faulted circuit, for double line to ground faults (a_1 - b_1 -g) at 10%, 80% and 90% distances.

The directional elements of the two circuits shown in Figure 5.10 behave the same as for a single line to ground fault, tripping the faulted circuit without any ambiguity.

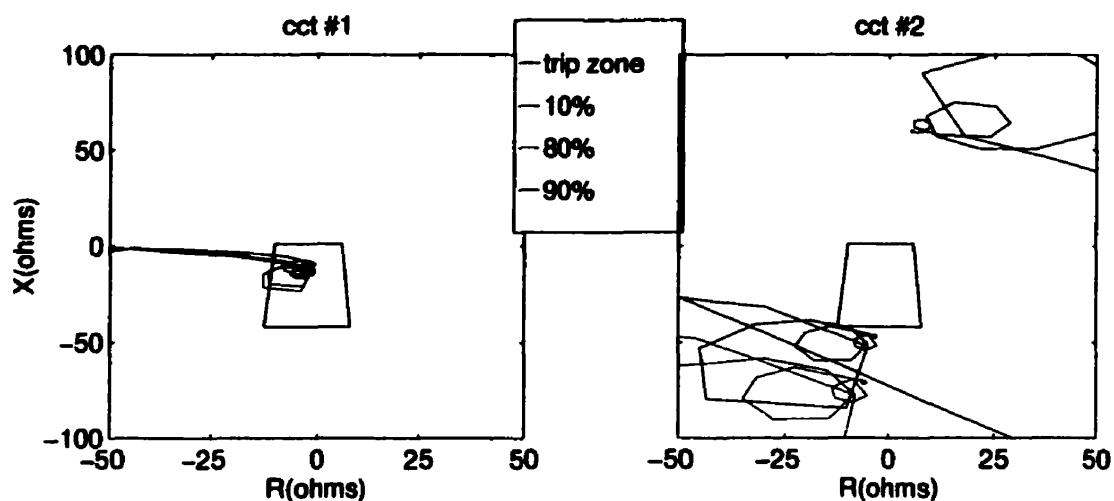


Figure 5.10: Directional impedance trajectories of the faulted and unfaulted circuits, for double line to ground faults (a_1 - b_1 -g) at 10%, 80% and 90% distances.

5.3.3 Inter Circuit Double Line to Ground Fault (a_1 - b_2 -g)

Inter-circuit faults cause the most serious mis-operation of the impedance elements. With reference to Figure 5.11, the ground impedance trajectories of phase- a in circuit #1 reaches zone-one for both close-up and remote faults. Those of phase- b on circuit #2 do not reach the trip zone at all for all three fault distances. The fault at 10% distance causes the impedance trajectories of phases b_1 and a_2 to move very close to zone-one which is also undesirable. As discussed in section 5.2, the compensation factor used in the ground impedance does not compensate for zero sequence mutual currents, resulting in under and over reach of ground impedances of phases a_1 and b_2 .

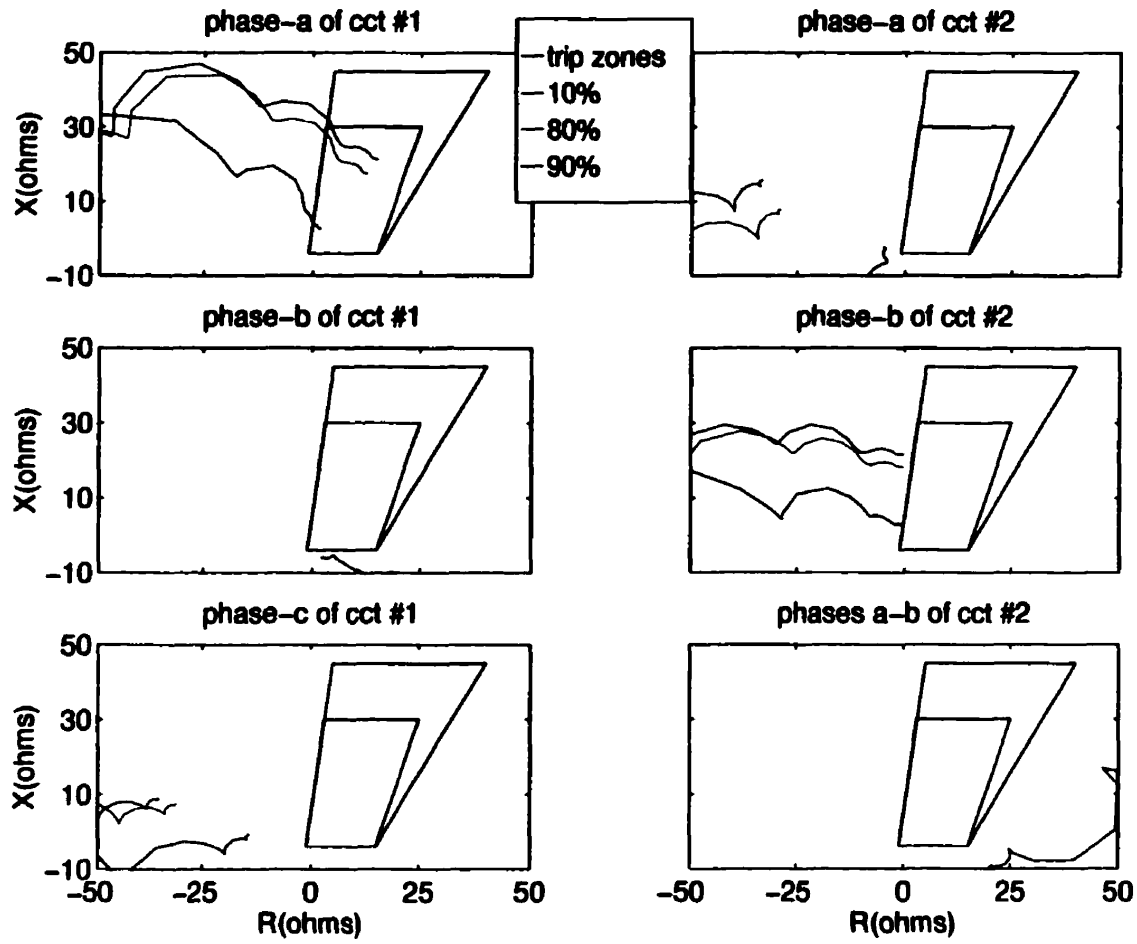


Figure 5.11: Ground impedance trajectories of circuits #1 & #2, for a_1 - b_2 -ground faults at 10%, 80% and 90% distances.

The solution to this problem is to modify equation 2.2, introducing a zero sequence mutual current compensation as follows [36].

Modified ground impedance computed:

$$Z_{a,b,c} = \frac{V_{a,b,c}}{I_{a,b,c} + kI_0 + k_m I_{om}}$$

Where the zero sequence current compensation factor is:

$$k = \frac{Z_0 - Z_1}{Z_1}, \text{ and}$$

the mutual zero sequence current compensation factor is:

$$k_m = \frac{Z_{om}}{Z_1}.$$

Z_0 , Z_1 , and Z_{om} are the zero sequence, positive sequence and the mutual zero sequence impedances of the transmission line.

The proof of the modified equation is given in section 5.5.

As seen in Figure 5.12, close-up faults move line impedances $c-a$ of circuit-one and $a-b$ of circuit-two in to the trip zones. This same situation, although not a problem in the case of a single circuit double line to ground fault (Figure 5.9 of Section 5.3.2), can lead to difficulty in this case, if single pole tripping is desired.

Directional elements of both circuits see all three faults as forward faults well inside the trip zone (Figure 5.13).

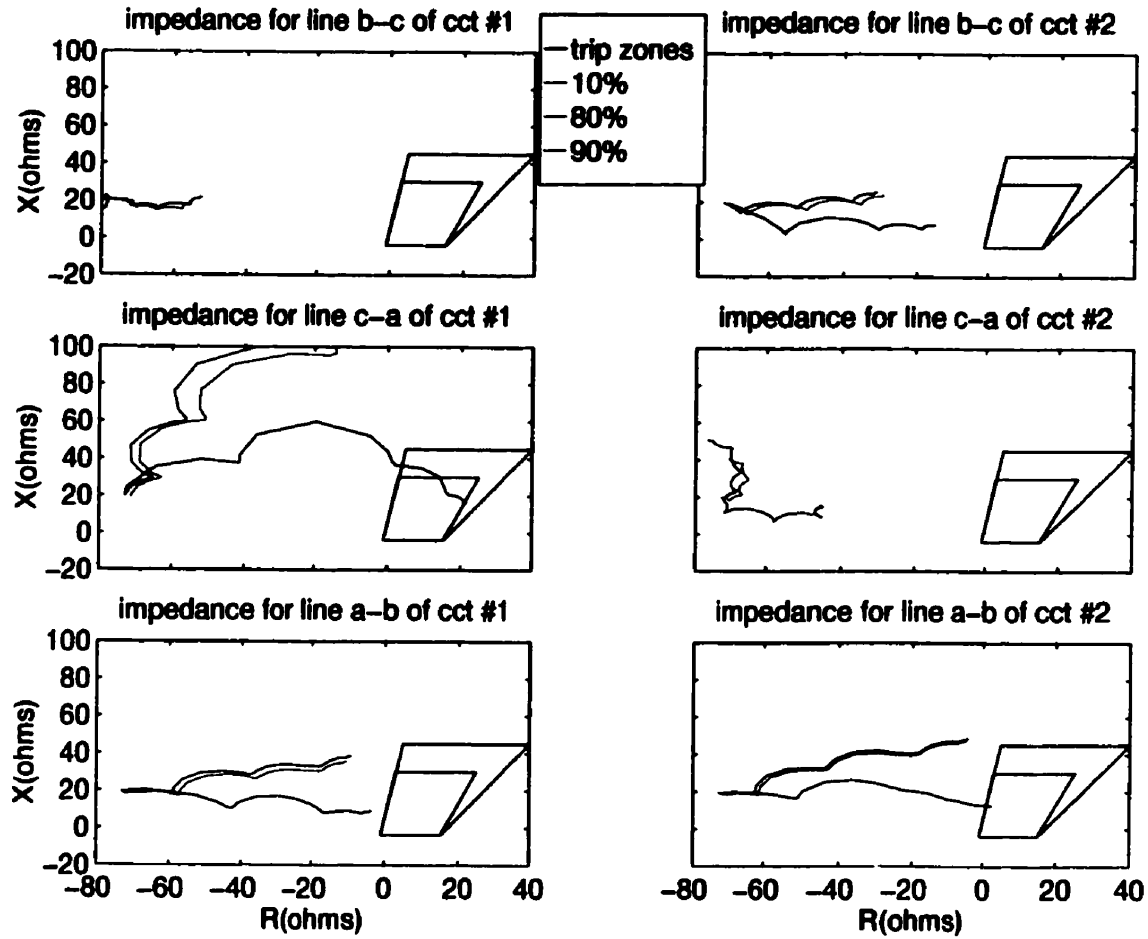


Figure 5.12: Line impedance trajectories of circuits #1 & #2, for a_1 - b_2 -ground faults at 10%, 80% and 90% distances.

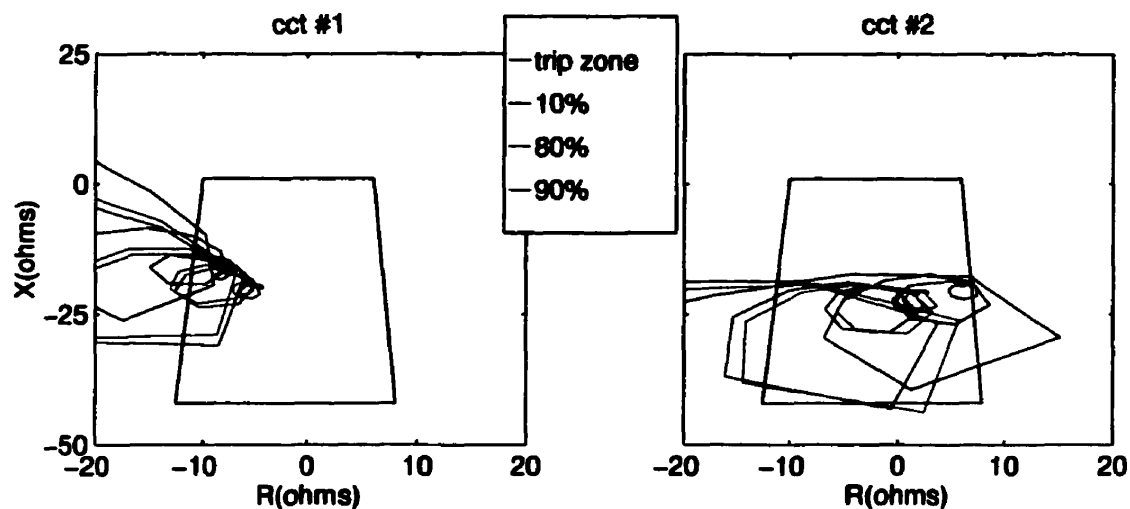


Figure 5.13: Directional impedance trajectories of circuits #1 & #2, for a_1-b_2 -ground faults at 10%, 80% and 90% distances.

5.3.4 Single Circuit Three-Phase-to-Ground fault ($a_1-b_1-c_1-g$)

Ground and line impedance elements for the faulted circuit pick up the fault in their respective zones as expected. Because the fault is symmetrical the zero sequence currents on both circuits are almost zero. Some movement of the measured impedances on the parallel circuit are detected due to the change in the bus voltage. However, they are safely outside the trip zones. Thus single circuit three phase faults on double circuit lines, do not pose any difficulty to a distance relay.

5.3.5 Inter Circuit Three-Phase-to-Ground Fault ($a_1-b_1-c_2-g$)

As in the case of the inter-circuit double-line-to-ground fault, here too the problems of over and under reach are detected (Figure 5.14, Figure 5.16). Also zone-one mis-

detection of line impedances for close up faults can cause problems for single pole tripping.

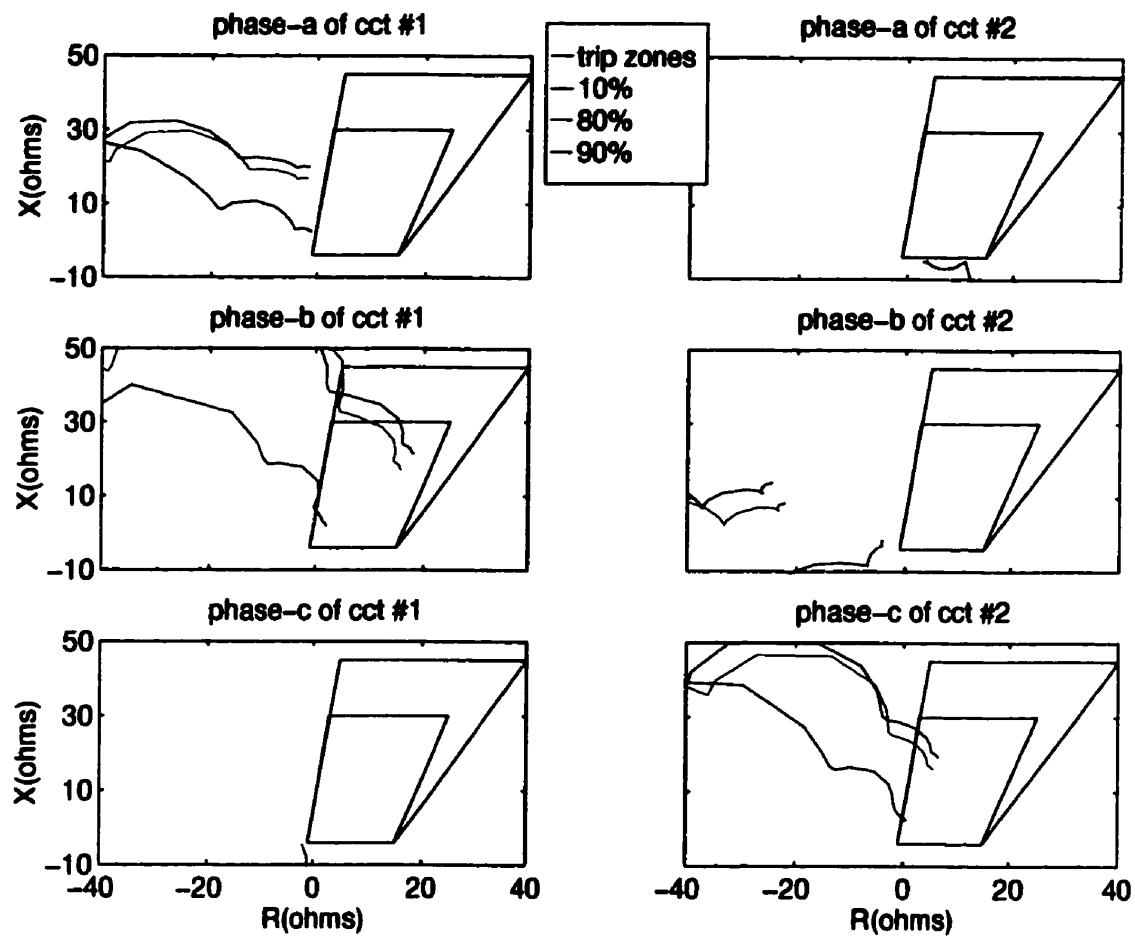


Figure 5.14: Ground impedance trajectories of circuits #1 & #2, for a_1 - b_1 - c_2 -ground faults at 10%, 80% and 90% distances.

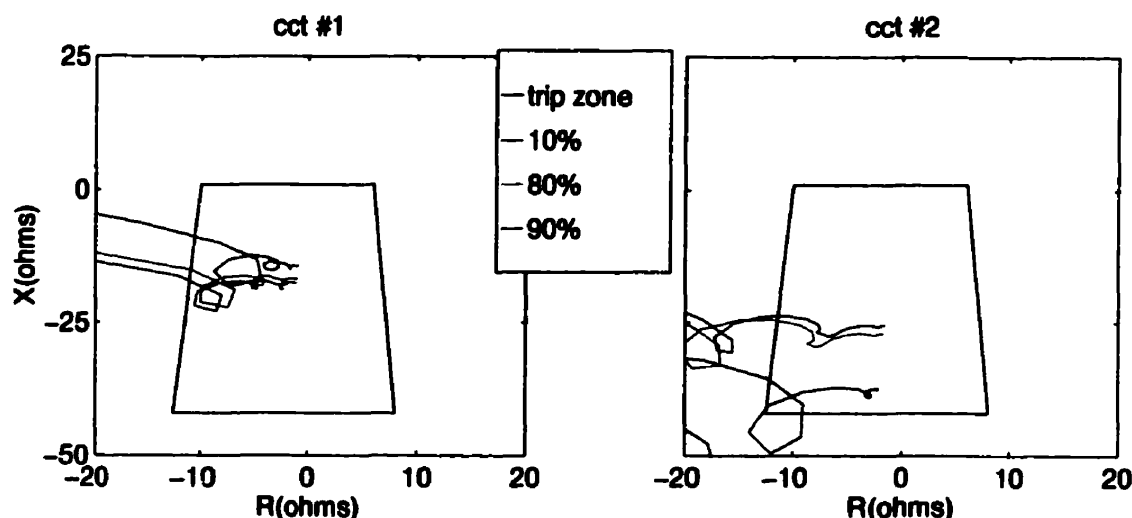


Figure 5.15: Directional impedance trajectories of circuits #1 & #2, for $a_1-b_1-c_2$ -ground faults at 10%, 80% and 90% distances.

The directional elements of both circuits shown in Figure 5.15 detect forward faults, causing directional trips on both circuits as required. However, the fault at 10% distance appears as a far end fault to the directional element of circuit #2, which only has one phase faulted to ground. This is a reflection of most of the fault current being confined to one circuit, while there is a considerable dip in the measured bus voltage. Apparently, this misoperation of the directional element is dominant for close-up faults.

Line impedance trajectories of the phases $a-b$ for circuit #1 are detecting the faults in the proper trip zones (Figure 5.16). However, the close-up fault is causing line elements c_1-a_1 and b_2-c_2 to trip as well. This results in opening all three phases of circuit-two unnecessarily.

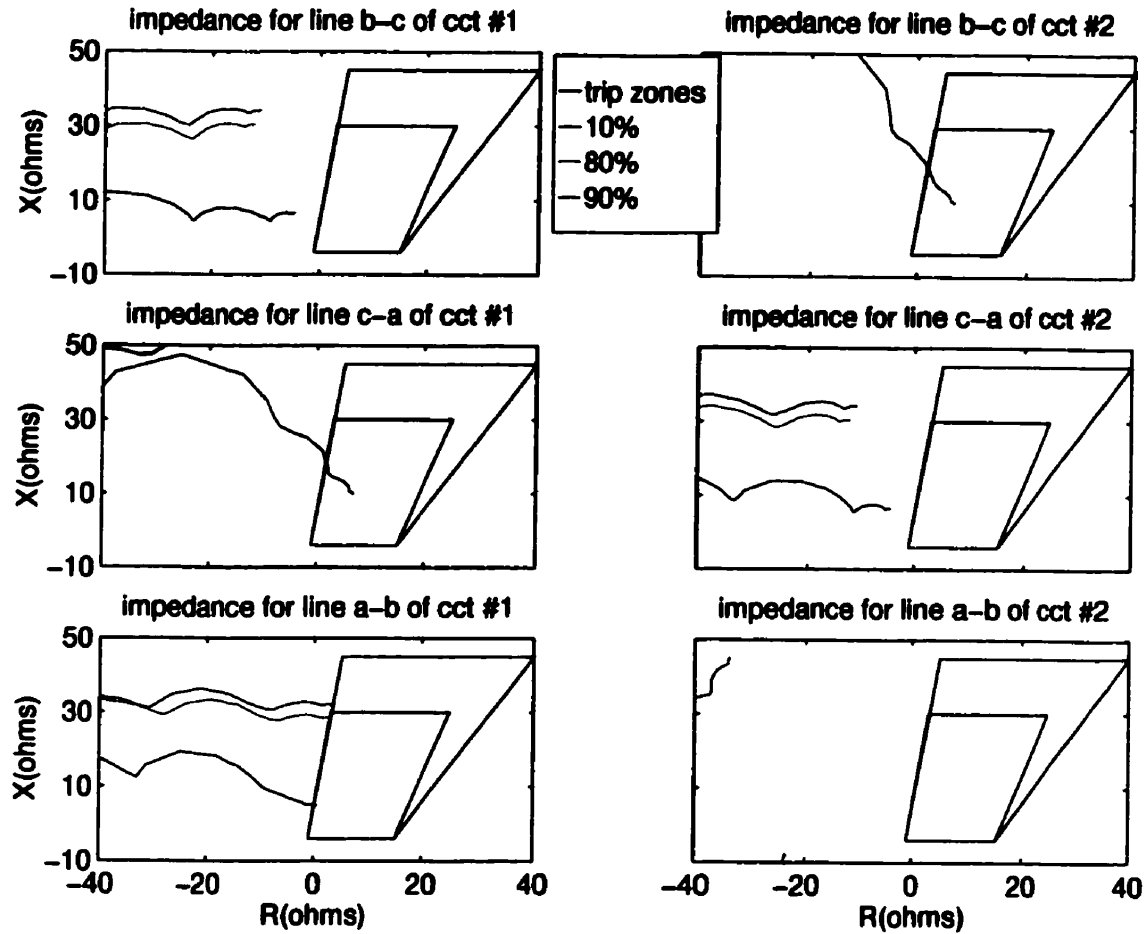


Figure 5.16: Line impedance trajectories of circuits #1 & #2, for $a_1-b_1-c_2$ -ground faults at 10%, 80% and 90% distances.

5.3.6 Inter Circuit Four-Phase-to-Ground Fault ($a_1-b_1-c_1-a_2-g$)

Line impedance elements for circuit #1 detect the faults accurately in their respective zones (Figure 5.18), while the phase elements suffer from under/over reach problems similar to those in the other inter-circuit faults discussed in the sections 5.3.3 and

5.3.5. Figure 5.17 shows the ground impedance elements, and Figure 5.18 shows the line impedance elements of the relays.

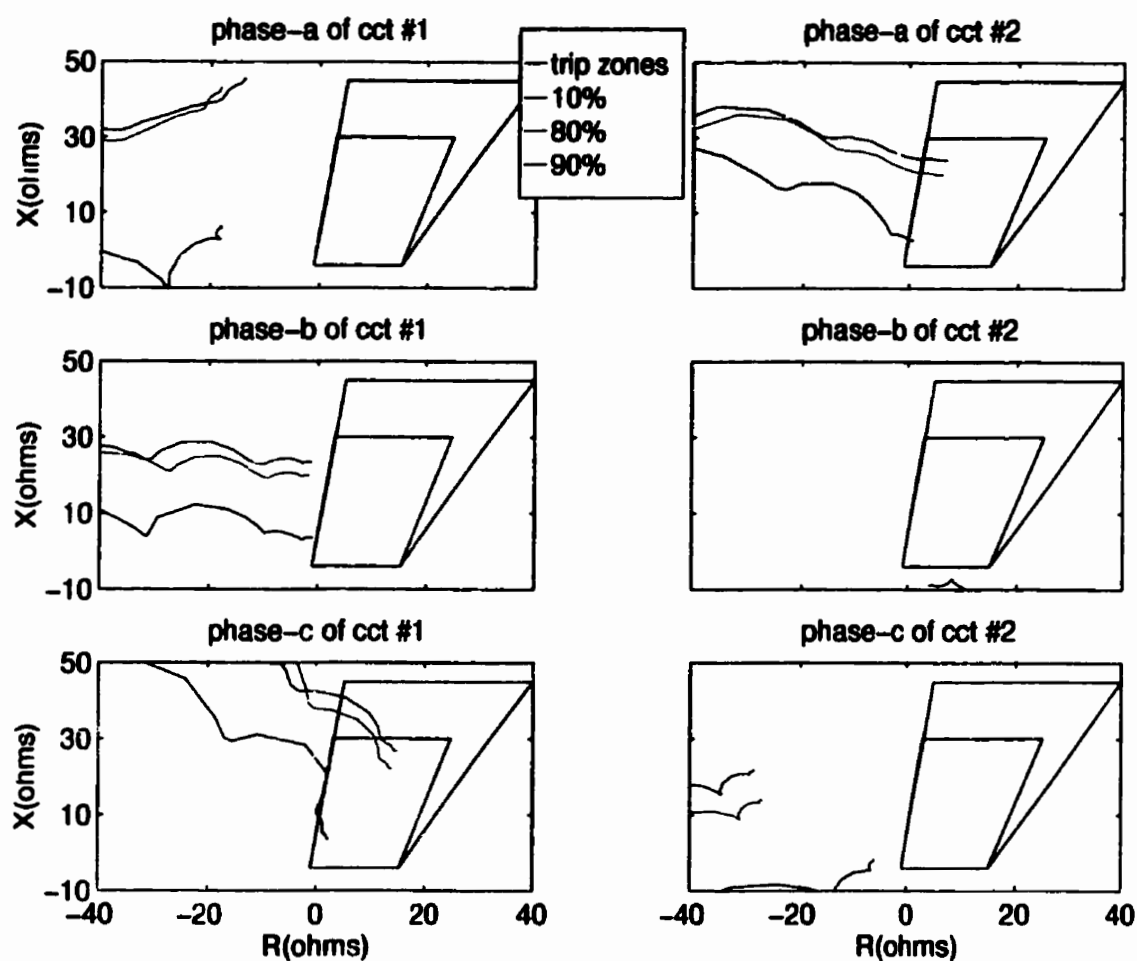


Figure 5.17: Ground impedance trajectories of circuits #1 & #2, for four phase to ground faults at 10%, 80% and 90% distances. Faulted phases are a_1 - b_1 - c_1 - a_2 - g .

Figure 5.19 shows the directional elements of the two circuits. Circuit #2, which has only one phase faulted to ground, is incapable of detecting the fault at 10% distance. Therefore, in this case the second circuit will not be tripped for close-up faults. But,

upon the clearance of the heavily faulted circuit, and the directional element resuming function, phase a_2 will also be tripped. However, this period may be sufficiently long to cause serious damage to the system, if it is not cleared by some other means.

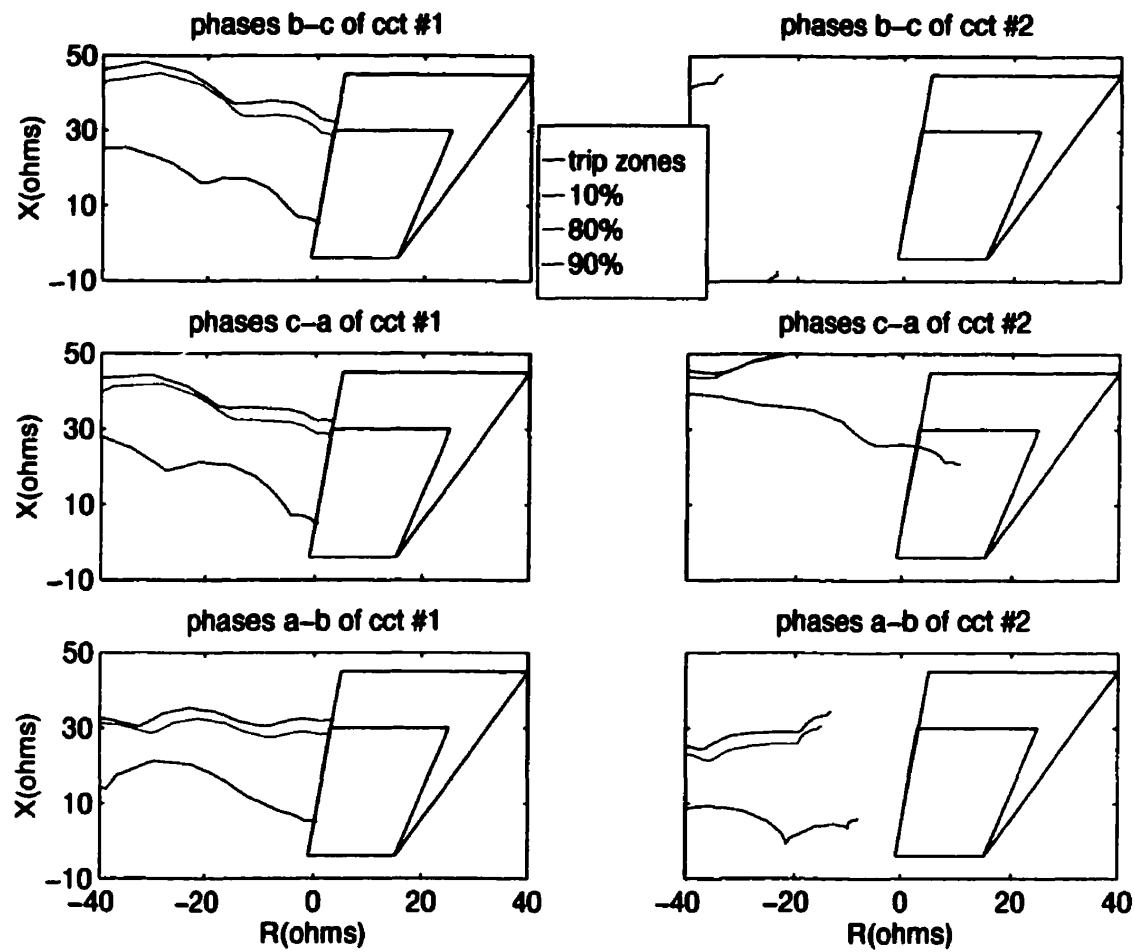


Figure 5.18: Line impedance trajectories of circuits #1 & #2, for four phase to ground faults at 10%, 80% and 90% distances. Faulted phases are a_1 - b_1 - c_1 - a_2 -g.

The movement of the directional impedance trajectories of the circuit with only one faulted phase is due to the relatively small fault current flowing in that circuit compared to the large drop in the bus voltage. The three phase fault on the parallel circuit is the reason for the high voltage drop on the common bus bar.

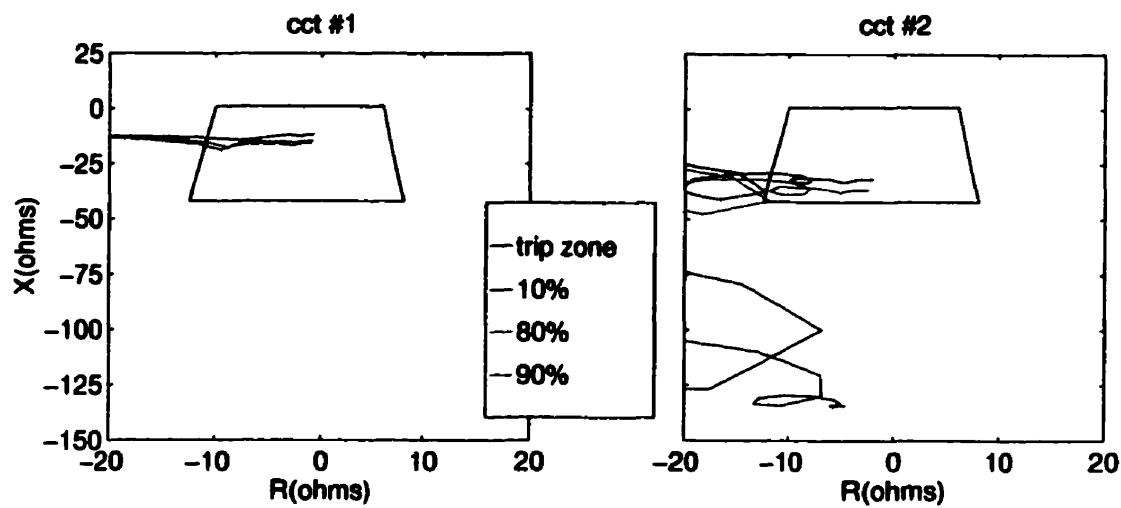


Figure 5.19: Directional impedance trajectories of circuits #1 & #2, for four phase to ground faults (a_1 - b_1 - c_1 - a_2 - g) at 10%, 80% and 90% distances.

5.3.7 Inter Phase Faults with no Ground Involvement

These can either be within a circuit or inter-circuit faults. Those faults that involve only one circuit do not cause mis-operation of impedance relays. Due to the absence of zero sequence currents the mutual effects are minimal. Bus voltage drop is the only cause of variation of impedance trajectories on the parallel circuit. These disturbances however are insufficient to cause any malfunction.

The impedances seen by the ground elements in the event of an inter-circuit fault without ground involvement is similar to, but higher than, those of the corresponding

ground faults. This is due to the appearance of the parallel circuit as a ground path with a higher impedance, to each individual impedance element. Therefore the ground impedance elements come in operation with less sensitivity. The operation of the line elements are proper and are as expected.

The behaviour of the directional elements for each fault without ground involvement are identical to that of their corresponding ground fault case.

5.4 Observations

It is seen that the bus voltage fluctuations and mutual currents have a significant effect on the impedances seen by some impedance elements. This implies that impedance relays on a system with a strong source would be less troubled, whereas, on the other hand, those with weak sources can suffer significant malfunctioning.

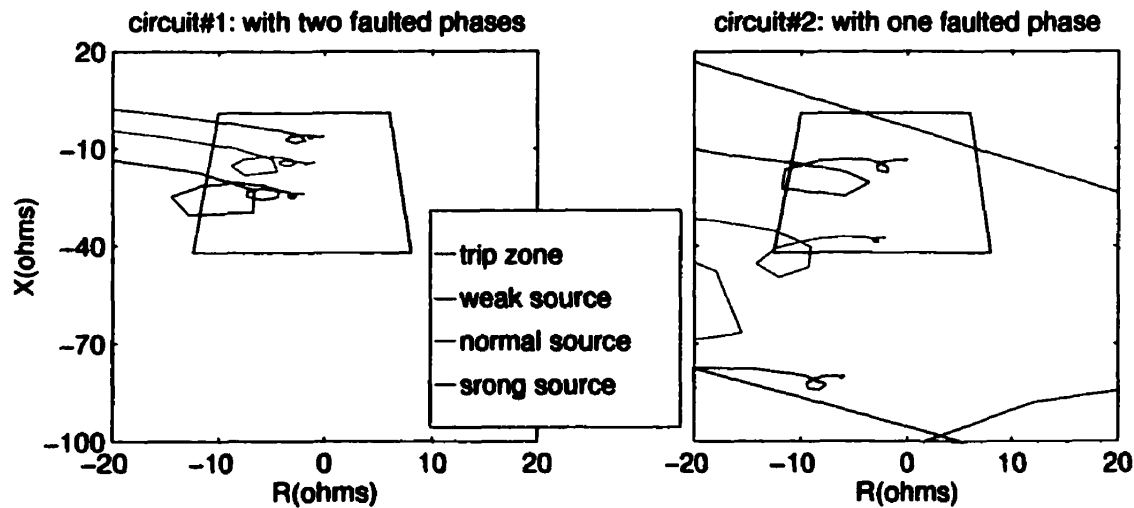


Figure 5.20: The directional impedance trajectories for a $a_1-b_1-c_2-g$ fault at 10% distance.

Figure 5.20 demonstrates such effects of source impedance on the directional impedance trajectory. For a three-phase-to-ground fault ($a_1-b_1-c_2-g$) at 10% distance the directional impedances fell well in the trip zone for both circuits, for the chosen source impedance (shown in blue) in the studies. However, the impedance trajectory of circuit #2 moves out of the trip zone when the source is made weaker for the same fault, whereas, with a stronger source it is moved further in to the zone.

The analysis of the performance of impedance elements on the double circuit line considered in this thesis shows that the elements corresponding to faulted phases are mostly troubled by the presence of mutual zero sequence currents. It is also apparent that relay elements of the faulted phases are not the only cause for deterioration of the relay performance. The sympathy trips due to mis-operated elements of the unfaulted lines have a considerable contribution as well. Such sympathy trips by a relay on a three-phase single-circuit transmission line is usually eliminated by the trip logic. However, the same trip logic is inadequate to perform that task on a double circuit transmission configuration. While a simple trip logic which can eliminate all the sympathy trips on a double-circuit configuration is not apparent, an alternate approach is investigated in this thesis to solve this problem. That is the use of a neural network to identify the faulted phases on a double circuit line, which can either validate or invalidate the trip signals issued by individual impedance elements. The neural faulted phase detector which is intended to operate in parallel with the rest of the impedance elements, is discussed in detail in CHAPTER 8 and CHAPTER 9.

5.5 Proposed Improvement to Impedance Relays for Double Circuit Line Application

The problems of over/under-reach can be overcome by compensating for mutual effects on faulted circuits, when calculating the ground impedance, in equation 2.2. The modified formula for ground impedance is given in equation 5.2.

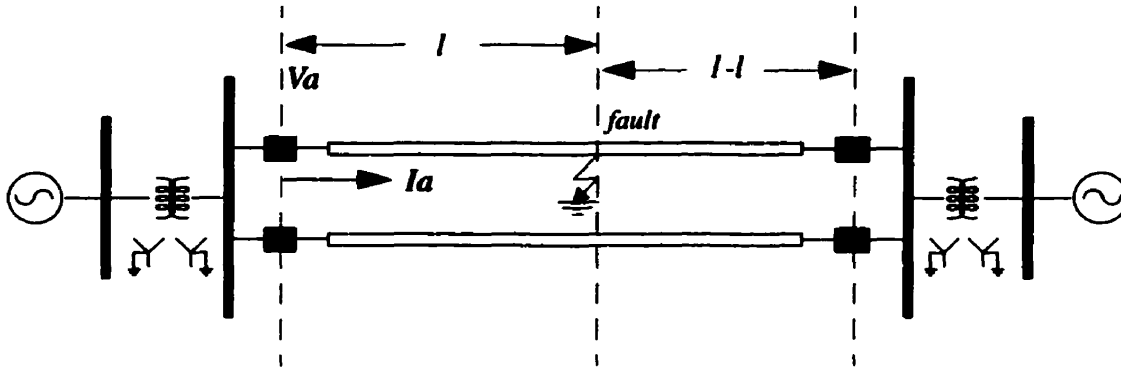


Figure 5.21: Single line diagram of a double circuit system with a fault on one circuit: fraction of the line length to fault is 'l'.

The voltage V_a at the relay on the faulted circuit is:

$$V_a = lZ_1I_1 + lZ_2I_2 + lZ_0I_0 + lZ_{0m}I_{om}$$

where I_0, I_1, I_2 are the zero, positive and negative sequence currents on the faulted circuit. I_{om} is the zero sequence current on the parallel circuit.

$$I_a = I_1 + I_2 + I_0$$

$$\frac{V_a}{I_a} = \frac{l \cdot (Z_1I_1 + Z_2I_2 + Z_0I_0 + Z_{0m}I_{om})}{I_1 + I_2 + I_0}$$

but $Z_1 = Z_2$;

$$\frac{V_a}{I_a} = \frac{l \cdot (Z_1 I_1 + Z_1 I_2 + Z_0 I_0 + Z_{0m} I_{om})}{I_1 + I_2 + I_0}$$

$$\frac{V_a}{I_a} = \frac{l \cdot Z_1 \cdot \left(I_1 + I_2 + \frac{Z_0}{Z_1} I_0 + \frac{Z_{0m}}{Z_1} I_{om} \right)}{I_1 + I_2 + I_0}$$

but $I_a = I_1 + I_2 + I_0$;

$$V_a = l \cdot Z_1 \cdot \left(I_0 + I_1 + I_2 + \left(\frac{Z_0}{Z_1} - 1 \right) I_0 + \left(\frac{Z_{0m}}{Z_1} \right) I_{om} \right)$$

$$V_a = l \cdot Z_1 \cdot \left(I_a + \left(\frac{Z_0}{Z_1} - 1 \right) I_0 + \left(\frac{Z_{0m}}{Z_1} \right) I_{om} \right)$$

Since the line impedance measured up to the fault is $l \cdot Z_1$ the impedance seen by the phase-a ground element is:

$$Z_a = \frac{V_a}{I_a + k I_0 + k_m I_{om}} \quad 5.2$$

where

$$k = \frac{Z_0 - Z_1}{Z_1} \quad 5.3$$

$$k_m = \frac{Z_{0m}}{Z_1} \quad 5.4$$

Z_0 , Z_1 , and Z_{0m} are the zero sequence, positive sequence and the mutual zero sequence impedances of the transmission line.

The ground impedance given in equation 5.2, will only be valid for the faulted circuit(s). They are detected on line using a zero sequence over-current element placed on each circuit. The non-uniform direction of the zero sequence current on the faulted circuit makes such computation for the unfaulted line more complex and dependant on the distance to fault. Therefore, the computation of the ground impedance for the unfaulted circuit remains unchanged as in equation 2.2. The error introduced by the mutual effects on the healthy line are minimal for faults approximately at the mid-point of the line. The error is maximum for faults on either ends of the parallel line. The zero sequence over current element identifies as faulted the circuits with zero sequence current greater than about 10% of the nominal secondary current of the current transformer.

5.5.1 Modified Ground Impedance Trajectories

In this section the corrected ground impedance trajectories for various faults are discussed.

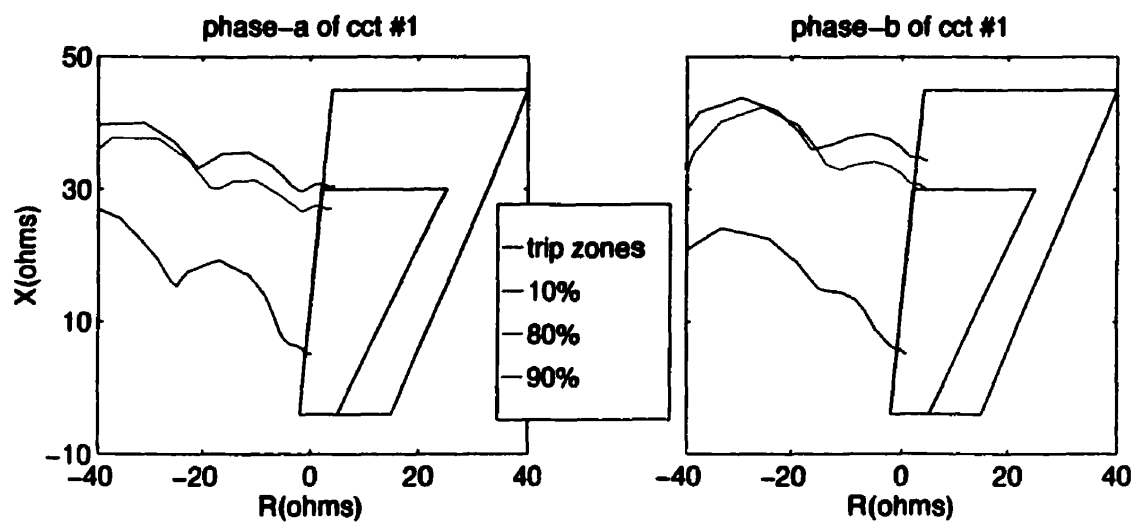


Figure 5.22: Modified ground impedance trajectories of faulted phases, for a_1-b_1-g faults at 10%, 80% and 90% distances.

With the modification, the phase- b ground impedance, shown in Figure 5.22, falls well in the correct trip zones. However, the apparent increase of sensitivity of the phase- a ground impedance element, (zone-one trip for fault at 80% distance, and the fault at 90% distance falling on the zone-one border) due to a current imbalance on the measuring bus remains incorrect. The modified ground impedance trajectories for a_1-b_2-g fault, $a_1-b_1-c_2-g$ fault and $a_1-b_1-c_1-a_2-g$ faults are shown in Figure 5.23, Figure 5.24 and Figure 5.25 respectively. They demonstrate significant improvement in performance.

Proper detection of all faults demanded a marginal increment in the boundaries of the trip zones which was done safely not to cause any sympathy trips.

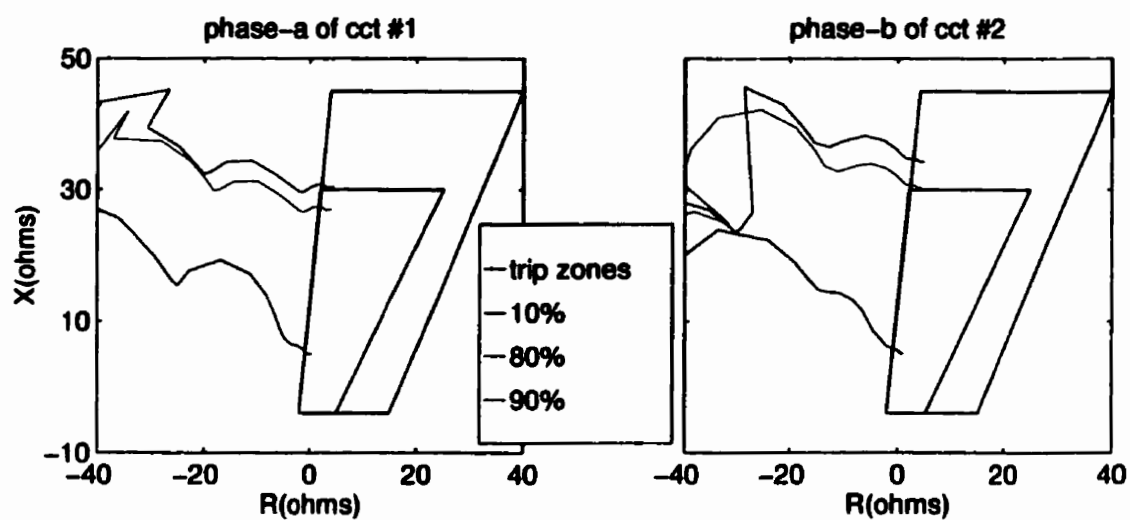


Figure 5.23: Modified ground impedance trajectories of faulted phases, for a1-b2-g faults at 10%, 80% and 90% distances.

The slight increase in sensitivity of some of the ground elements, caused by a system asymmetry, is visible for all other faults as well.

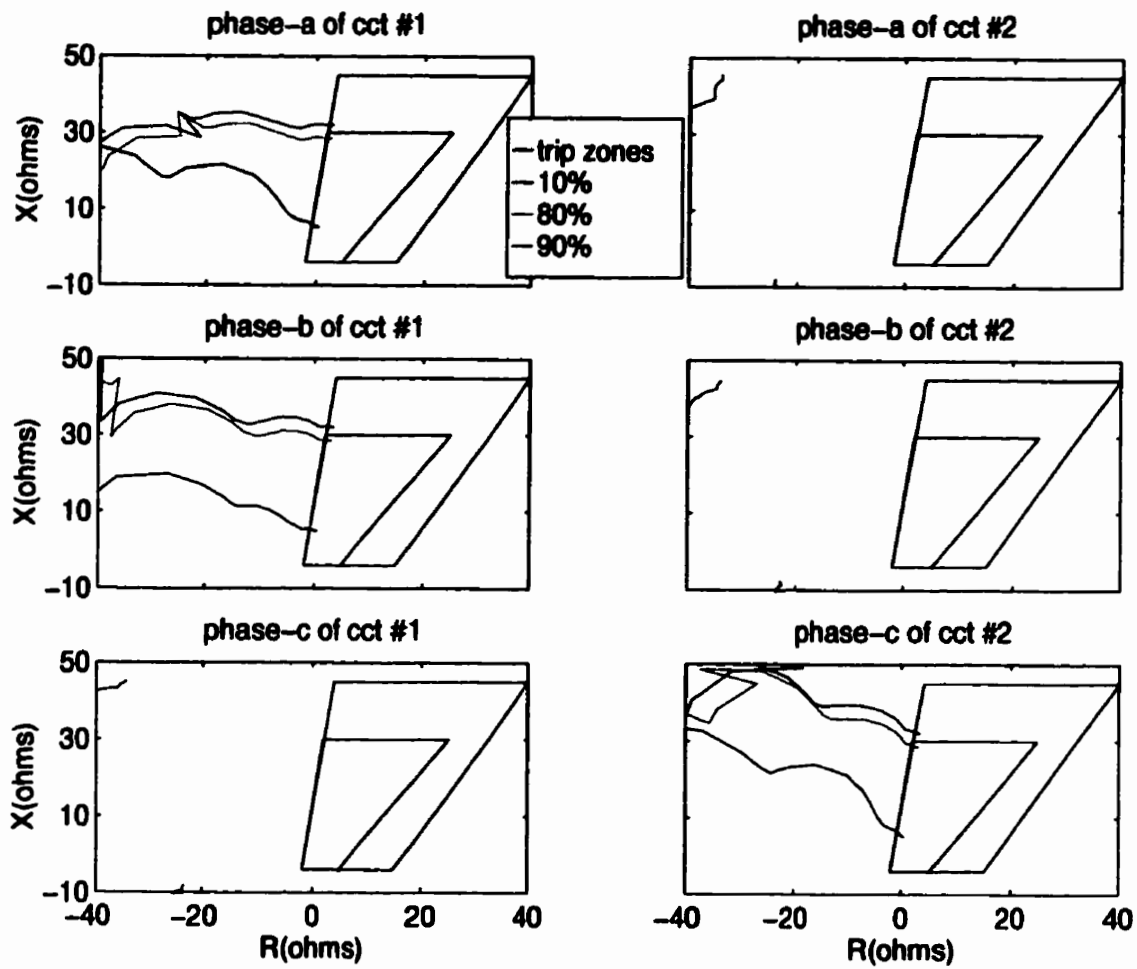


Figure 5.24: Modified ground impedance trajectories of circuits #1 & #2, for a1-b1-c2-g faults at 10%, 80% and 90% distances.

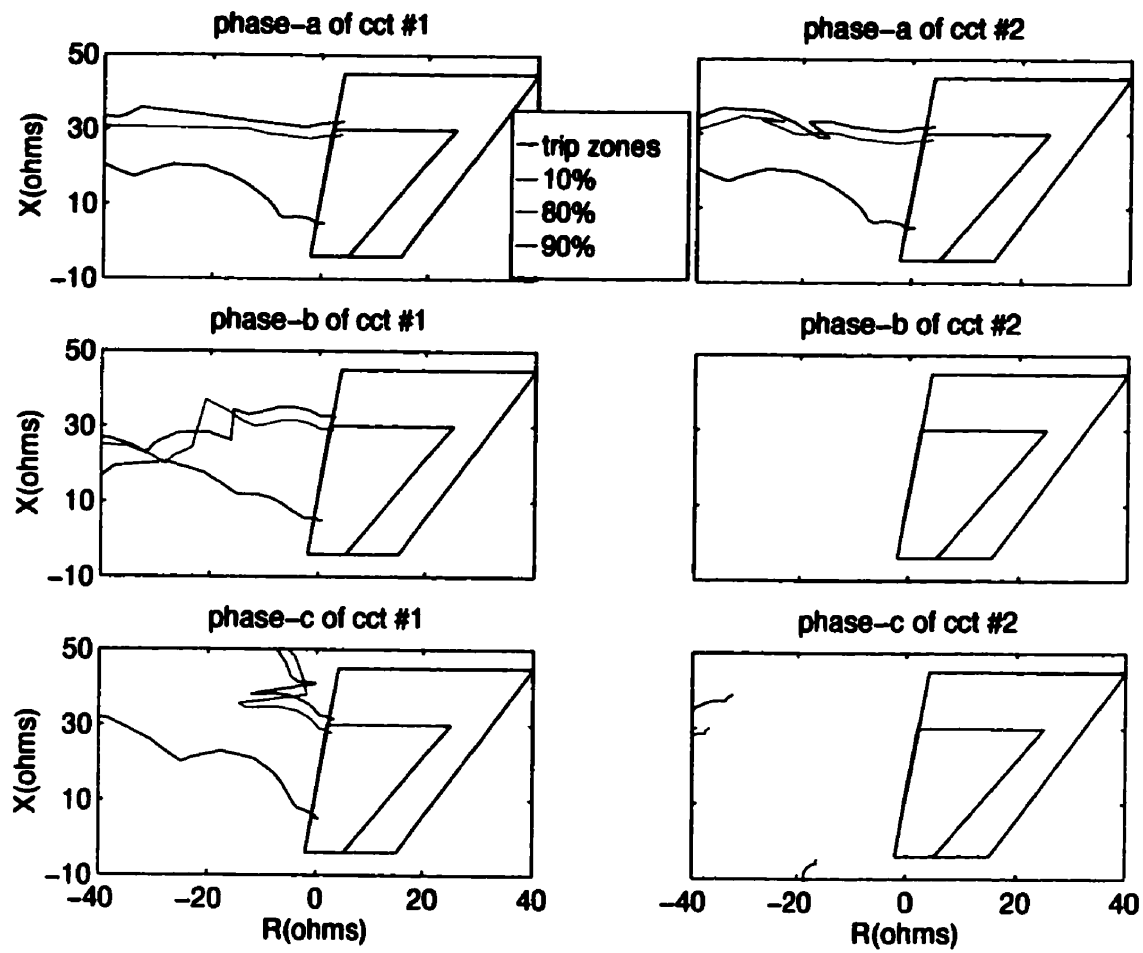


Figure 5.25: *Modified ground impedance trajectories of circuits #1 & #2, for a1-b1-c1-a2-g faults at 10%, 80% and 90% distances.*

5.6 Summary of Relay Performance for Various Faults

The tripped phases for various ground and non-ground faults that were analysed in the this chapter are summarized in Table 5.1 and Table 5.2 respectively.

Table 5.1: Summary of relay performance on double-circuit lines for ground faults.

Type of fault	Relay response for Zone 1, close-up faults	Relay response for Zone 2 remote faults
<i>Single line to ground fault</i>	<i>two phases of the faulted circuit are zone1 tripped</i>	<i>only the faulted phase is zone2 tripped</i>
<i>Double line to ground fault</i>	<i>all three phases of the faulted circuit are zone1 tripped</i>	<i>two phases of the faulted circuit are zone2 tripped</i>
<i>Inter-circuit double line to ground fault</i>	<i>two phases of both circuits are zone1 tripped</i>	<i>faulted phases of both circuits are zone2 tripped</i>
<i>Three line to ground fault</i>	<i>three phases of the faulted circuit are zone1 tripped</i>	<i>three phases of the faulted circuit are zone2 tripped</i>
<i>Inter-circuit three line to ground fault</i>	<i>all three phases of the circuit with two faulted phases and two phases of the other circuit are zone1 tripped</i>	<i>Only the faulted phases of both circuits are zone2 tripped</i>
<i>Inter-circuit four line to ground fault (three phases of one circuit and one phase of the other faulted)</i>	<i>only the three faulted phases of the circuit with three faulted phases are zone1 tripped</i>	<i>all the faulted phases of both circuits are zone2 tripped</i>
<i>Inter-circuit five line to ground fault</i>	<i>all three phases of both circuits are zone1 tripped</i>	<i>only the faulted phases are zone2 tripped</i>
<i>Six line to ground faults</i>	<i>all three phases of both circuits are zone1 tripped</i>	<i>all three phases of both circuits are zone2 tripped</i>

Table 5.2: Summary of relay performance on double-circuit lines for non-grounded faults.

Type of fault	Relay response for Zone 1, close-up faults	Relay response for Zone 2 remote faults
<i>Double line fault</i>	<i>faulted phases are zone1 tripped</i>	<i>faulted phases are zone2 tripped</i>
<i>Inter-circuit double line fault</i>	<i>no trip issued</i>	<i>no trip issued</i>
<i>Three phase fault</i>	<i>all faulted phases zone1 tripped</i>	<i>all faulted phases zone2 tripped</i>
<i>Inter-circuit three phase fault</i>	<i>all three phases of the circuit with two faulted phases and two phases of the other circuit are zone1 tripped</i>	<i>only the faulted phases of both circuits are zone2 tripped</i>
<i>Inter-circuit four line fault (three phases of one circuit and one phase of the other faulted)</i>	<i>only the three faulted phases of the circuit with three faulted phases are zone1 tripped</i>	<i>only the three faulted phases of the circuit with three faulted phases are zone2 tripped</i>
<i>Five phase faults</i>	<i>all three phases of both circuits are zone1 tripped</i>	<i>only the faulted phases are zone2 tripped</i>
<i>Six phase fault</i>	<i>all three phases of both circuits are zone1 tripped</i>	<i>all three phases of both circuits are zone2 tripped</i>

5.7 Conclusions

Over and under reach of ground impedance elements caused by the mutual zero sequence currents are largely corrected by the additional compensation introduced in the ground impedance computation. However, a simple trip logic cannot still eliminate mis-detection of unfaulted phases during certain fault situations such as inter-circuit three-phase-to-ground faults.

CHAPTER 6

PERFORMANCE OF IMPEDANCE ELEMENTS ON SIX-PHASE TRANSMISSION LINES

6.1 Introduction

A summary of a detailed fault study carried out for the purpose of investigating the performance of the impedance relay on a six phase transmission line is presented in this chapter. The faults selected for discussion are typical and representative of all possible problems associated with using conventional impedance elements of a distance protection scheme, on six phase lines. The studies were done on the six-phase system shown in Figure 6.1 maintaining a system operating point of 90% of rated power flow. The impact of the operating point on the impedance trajectories during various faults is also discussed, based on some tests, later in the chapter.

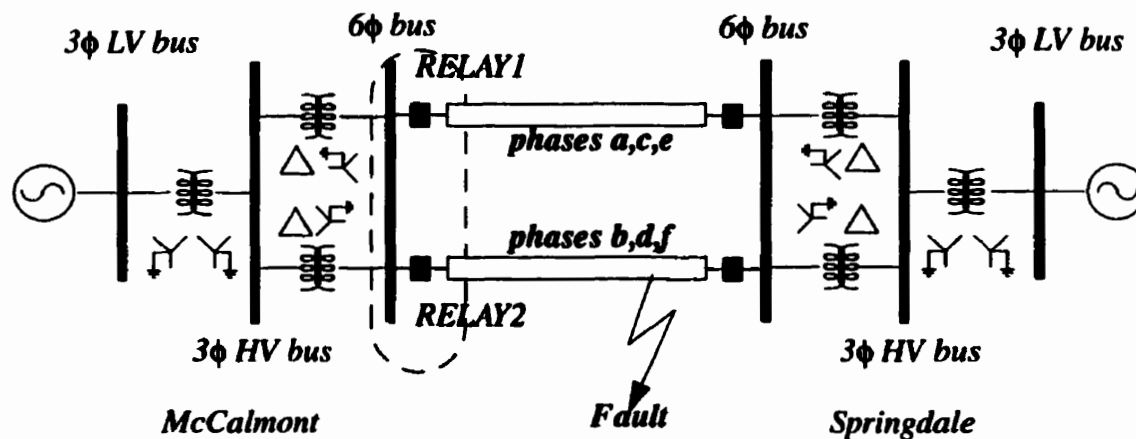


Figure 6.1: Single line diagram of the six phase transmission line model.

6.2 Impedance Relay and its Settings

The digital relay algorithms tested are those used in the Advanced Power Technology (APT) relay. It is tested in a context where two separate relays monitor the pair of three conductor circuits of the six-phase system on each side. It should be noted that the relays are at the six-phase busbar. Thus the voltages and currents monitored by relay1 are those of phases *a,c* and *e*, whereas phases *b,d* and *f* are monitored by relay2, as shown in Figure 6.1. Each relay has the voltages of the protected three phases of the circuit and all six currents available to it as system information, for performing the protective function of the circuit. Inputs and the data processing elements of the algorithm are shown in Figure 6.2.

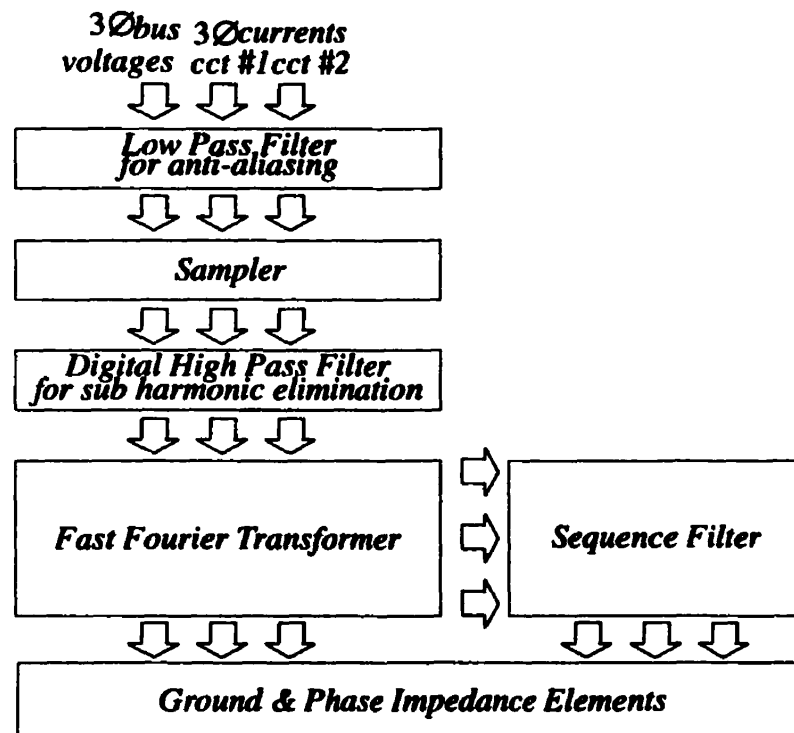


Figure 6.2: Processing units of the impedance relay used in the study for the six-phase transmission line configuration.

The analog high pass filter in Figure 5.1 is replaced with a digital filter to represent the data processing sequence as in the latest version of the APT relay software.

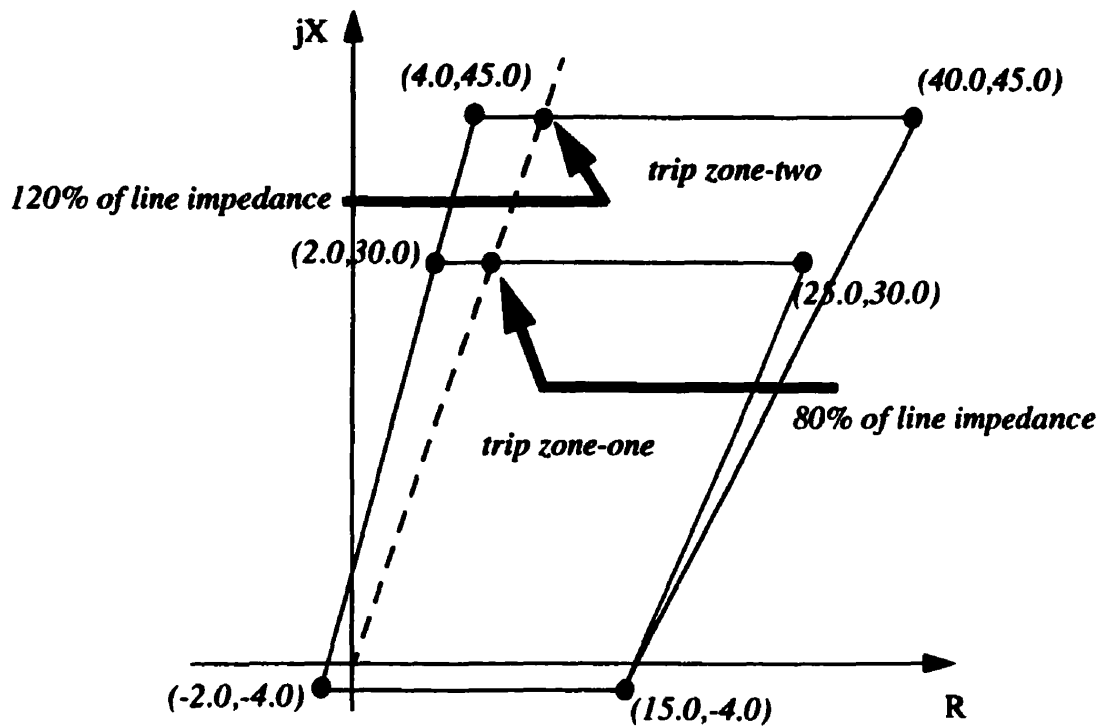


Figure 6.3: Trip zones of the ground/line impedance relays on McCalmont-Springdale six-phase line.

A simple four sided polygon defines the trip zones for all relay elements. The boundaries of the trip zones for the ground, phase and directional elements are set to suit the system impedances given in Table 4.5 and Table 4.6. The zone settings are chosen such that, on a three phase single circuit configuration, all faults at distances

less than 80% of the line length are detected in zone-one. The faults at distances within 80% and 120% of the line length are detected in zone-two.

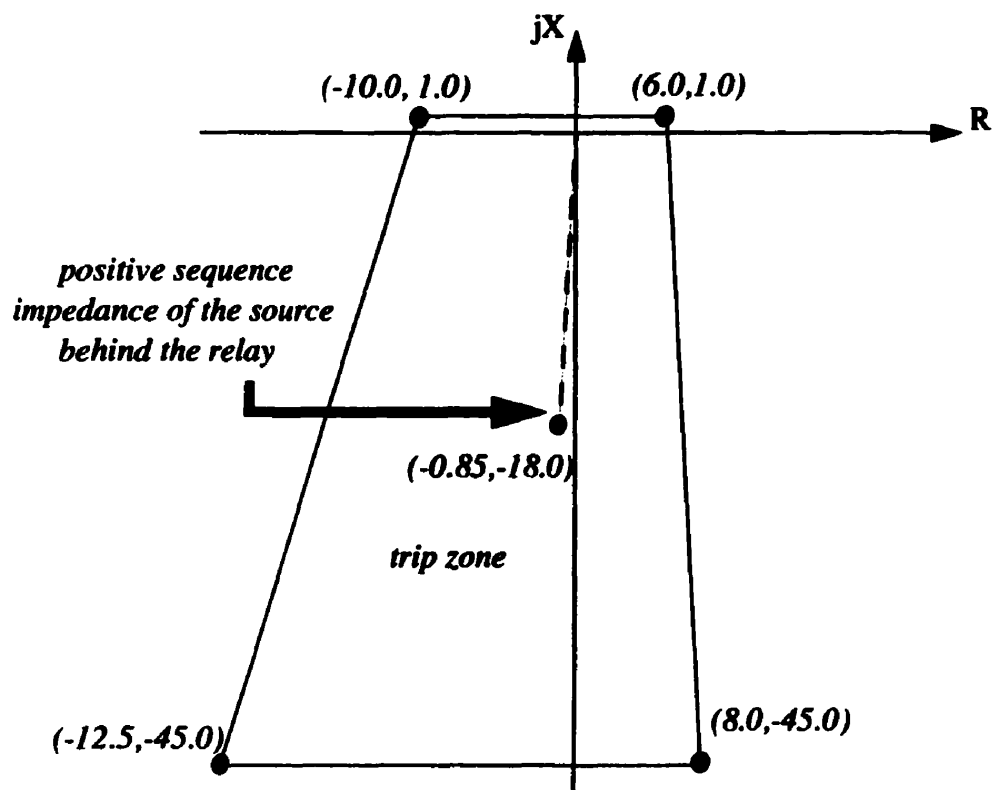


Figure 6.4: Trip zone of the directional impedance element on McCalmont-Springdale six-phase line.

The directional elements of both circuits also have identical trip zones due to the symmetry of the two circuits. The coordinates of the polygon for the directional trip zone is determined by the likely range of incremental positive sequence impedance of the six-phase system with a reasonable allowance for resistive reach. This is governed by the source impedance behind the relay and the possible imbalances that may be caused by various inter-circuit fault conditions on the transmission line. The zone details are shown in Figure 6.3 and Figure 6.4.

The following sections describe the behaviour of the ground, line and the directional impedance trajectories of the two distance relays placed on the two circuits of the six phase transmission line, for various fault situations. Although it is important to observe every impedance trajectory for all faults, only those of interest and unusual behaviour are shown for clarity. Trajectories for the same fault at distances 10%, 80% and 90% are shown on the same diagram so that the relay response for both close-up and remote faults can be directly compared.

Most of the errors in the ground impedances are due to the zero sequence mutual currents which are compensated in the calculation. The modified ground impedance is computed with proper compensation for the faulted circuit, as given in equation 5.2 whereas the computation for the unfaulted circuit is based on the conventional method in equation 2.2. A basic zero sequence over-current element on each circuit detects faulted circuit/circuits. The zero sequence over-current setting of about 1/6 of rated load current proved suitable for the McCalmont Springdale six-phase system, for all short circuit fault situations investigated. The modified ground impedance trajectories and their impact on the final trip decision by the distance relay for various types of faults are also discussed. It is seen that, with the modification, most of the mis-operations on the ground elements are eliminated.

The zero sequence and the zero sequence mutual current compensation factors (from equations 5.3 and 5.4) are given in equations 6.1 and 6.2 respectively.

$$k = \frac{Z_{I0} - Z_{I1}}{Z_{I1}} = \frac{140.18 \angle 82.25^\circ - 37.58 \angle 84^\circ}{37.58 \angle 84^\circ} = 2.73 \angle -2.37^\circ \quad 6.1$$

$$k_m = \frac{Z_{I0m}}{Z_{I1}} = \frac{115.44 \angle 81.93^\circ}{37.58 \angle 84^\circ} = 3.07 \angle -2.03^\circ \quad 6.2$$

6.3 Impedance Trajectories for Selected Fault Types

6.3.1 Single Line-to-Ground Fault (phase-a to ground)

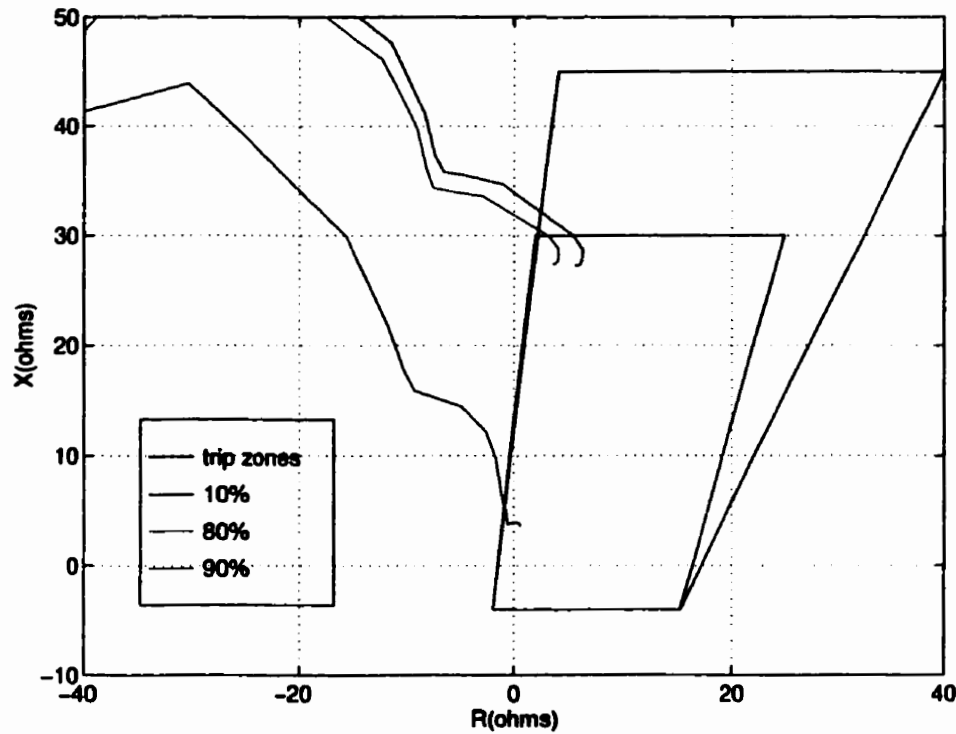


Figure 6.5: Ground impedance trajectories of the faulted phase for single line to ground faults at 10%, 80% and 90% distances.

The phase-a ground impedance trajectories for faults at 10%, 80% and 90% distances, are shown with the ground relay element trip zones. The impedance settles down to a

value of $(0.6 \Omega + j 3.8 \Omega)$ in the impedance plane for the close-up fault. This relates approximately to 10% of the positive sequence line impedance (given in Table 4.5) as expected. The reactance shown for a fault at 80% distance has an error of -8.5% with respect to the expected value of 30Ω on the reactance axis. The error in the indicated reactance for the far end (90% down the line) fault is -19%. This is sufficient to cause a zone-one trip, as seen in Figure 5.4.

Investigation of the zero sequence currents for the three cases discussed here, shows that the error is highest when the zero sequence current in the parallel circuit is comparable in magnitude to that of the faulted circuit (see Figure 6.6).

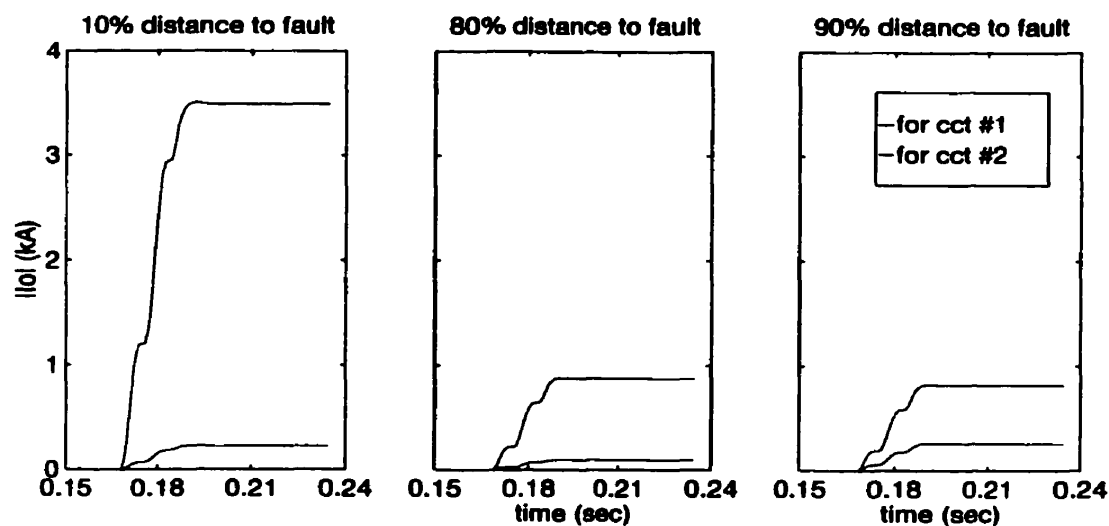


Figure 6.6: *Magnitude of zero sequence currents in circuits #1 & #2, for single line to ground faults at 10%, 80% and 90% distances.*

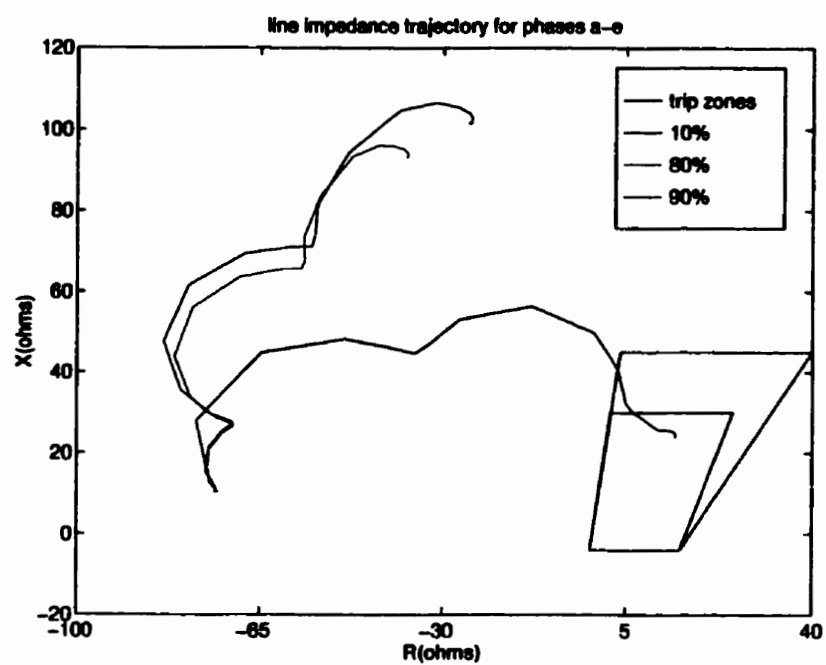


Figure 6.7: Line impedance trajectories for phases a-e for single line to ground faults at 10%, 80% and 90% distances.

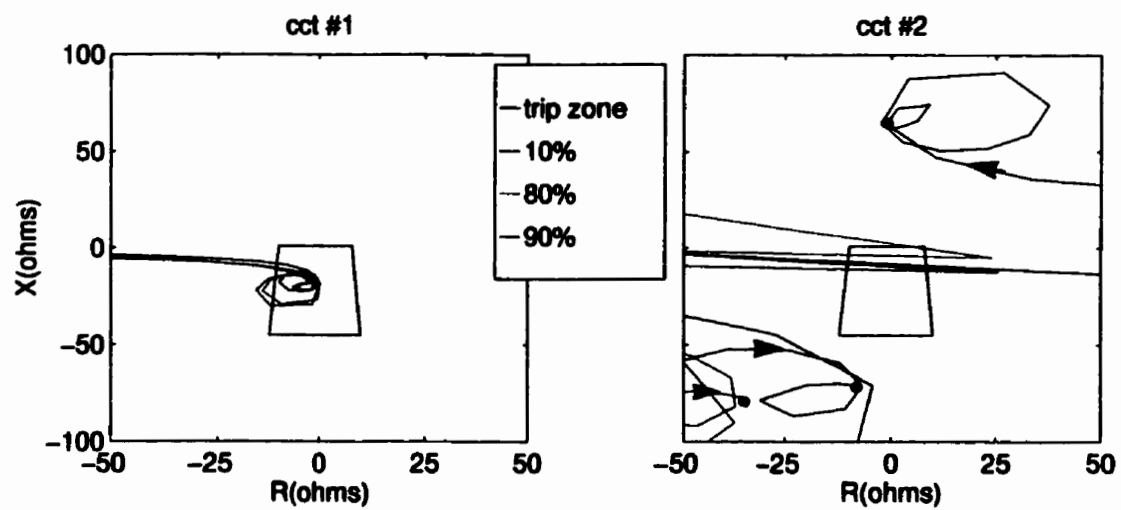


Figure 6.8: Directional elements for circuit#1 and circuit #2, for single line to ground faults at distances 10%, 80% and 90%.

The line impedance element for phases $e-a$ is tripping in zone-one for the close-up fault as seen in Figure 6.7. No other mis-operation is observed with the line impedance elements for the single line to ground fault.

The single line to ground faults are appropriately picked up by the directional elements of the faulted circuit as seen in Figure 6.8. The directional element of the unfaulted (second circuit) detects the close-up fault as a reverse fault and recognises both others as forward remote faults. However, they do not fall in the directional trip zone. The responses of the directional elements are similar to that of the three phase double circuit line discussed in section 5.3.1.

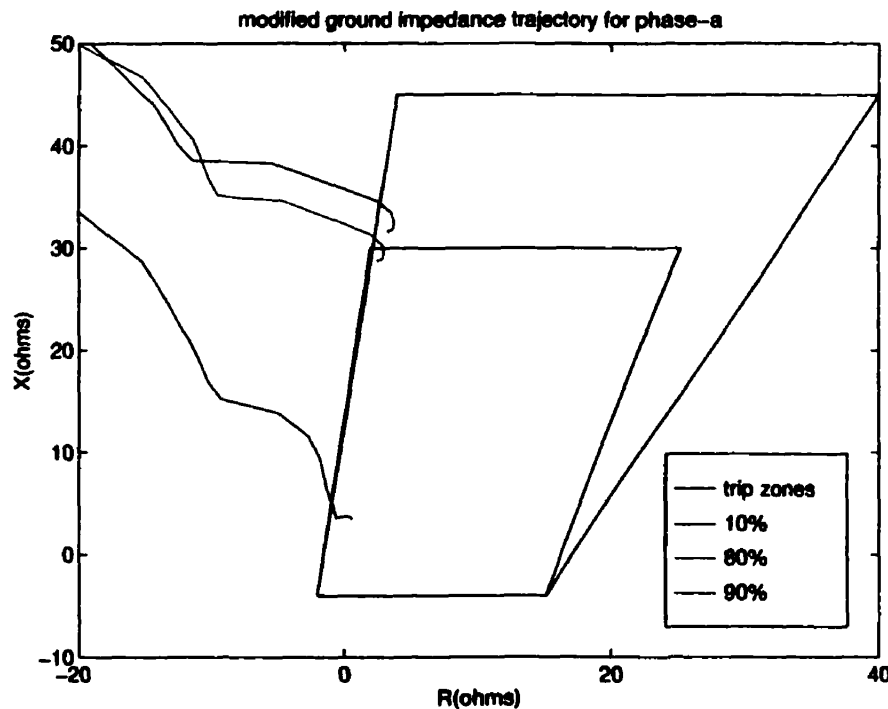


Figure 6.9: Modified ground impedance trajectories of the faulted phase, for single line to ground faults at 10%, 80% and 90% distances.

Thus for the fault at 10% distance, phase-*a* is appropriately tripped in zone-one. Phase-*e* is also tripped for the same fault due to the line element trip (Figure 6.7). The modified ground impedance trajectories of the faulted phase, shown in Figure 6.9, exhibit no errors. Therefore a zone-one trip on the faulted phase for remote faults is prevented

6.3.2 Single Circuit Double Line to Ground Faults

Phase *a-c-ground* Fault: This is a fault between two phases of the same circuit that are out of phase by 120° . Ground and line impedance trajectories for the *a-c-ground* fault are shown in Figure 6.10 and Figure 6.12. The ground impedance elements for both phases *a* and *c* mis-detect the remote faults as faults in zone-one.

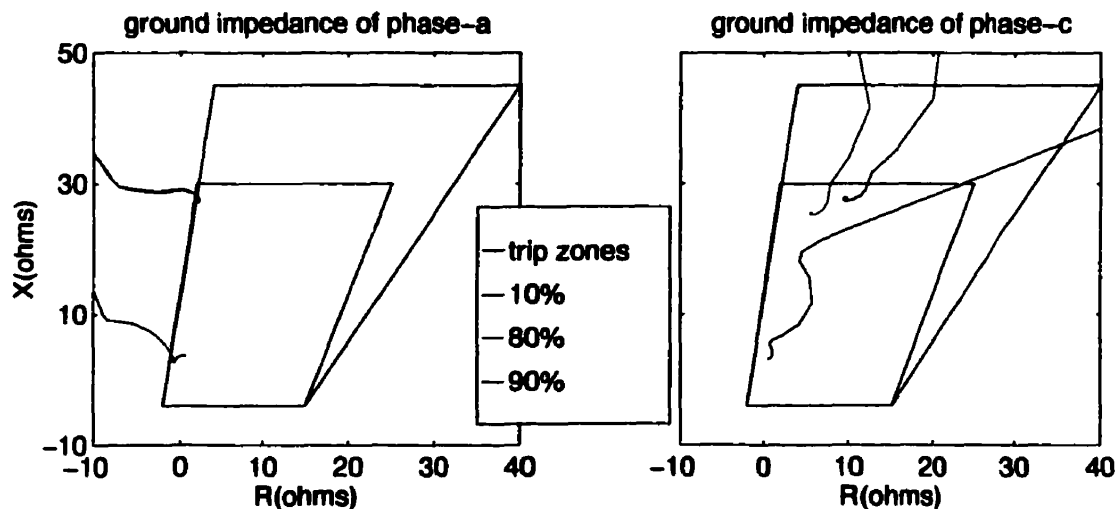


Figure 6.10: Ground elements of faulted phases, for faults at 10%, 80% and 90% distances.

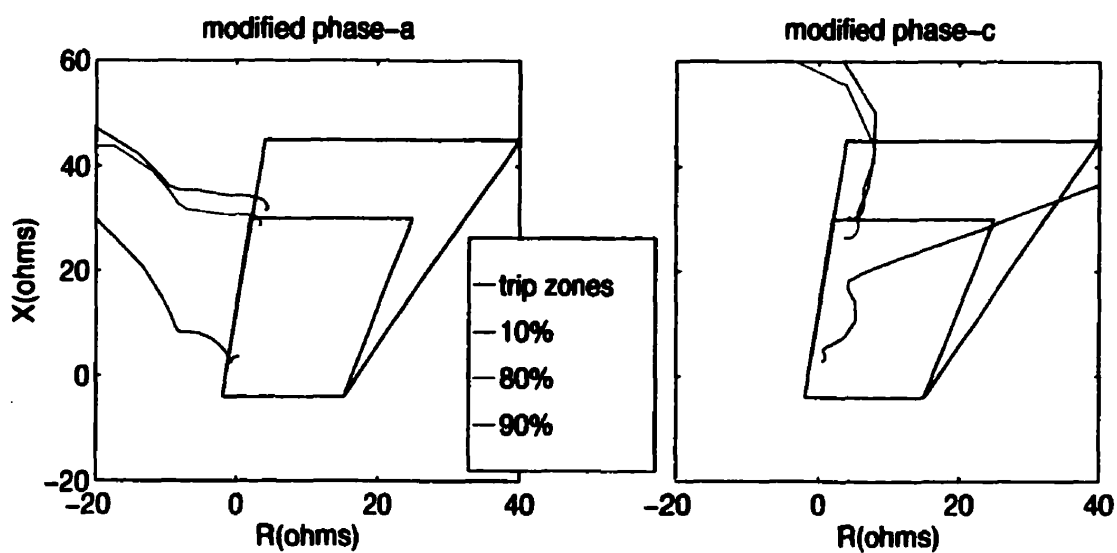


Figure 6.11: Modified ground elements of faulted phases, for faults at 10%, 80% and 90% distances.

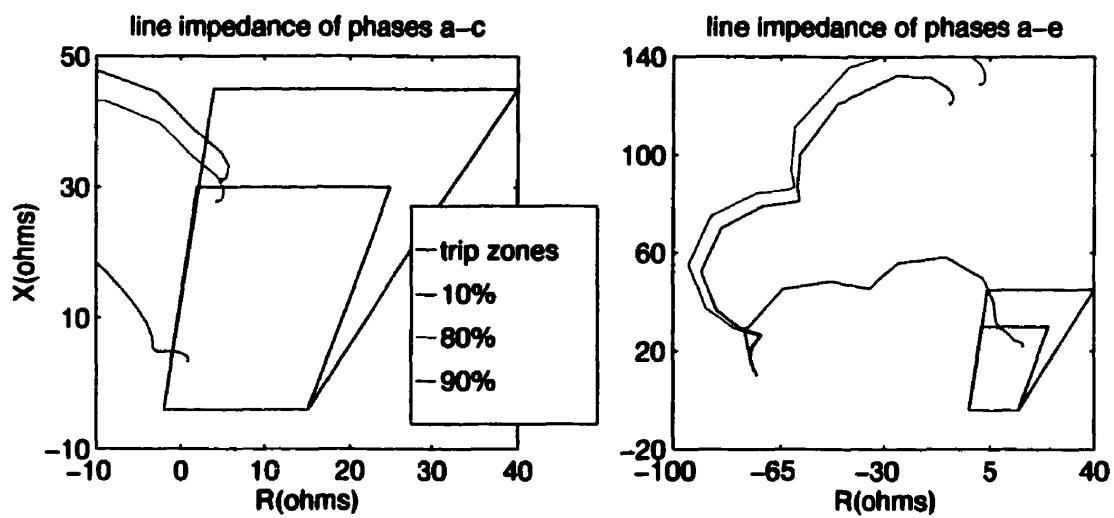


Figure 6.12: Some line impedance trajectories of the faulted circuit, for faults at 10%, 80% and 90% distances.

The line impedance element *a-c* picks up all faults in their respective zones as expected, while the line element for *a-e* is troubled again for close-up faults as in the case of a single line-to-ground fault. Some errors are visible in the modified ground impedances (Figure 6.11) which is most critical to faults falling in the borders of the trip zones. The directional elements detect the faults appropriately as in the case of a single line to ground fault.

However, since two phases, *a* and *c*, of the same circuit are faulted, phase *e* should also be tripped. Therefore, this mis-detection of the line element *a-e* does not result in any additional sympathy trips.

6.3.3 Inter Circuit Double Line to Ground Fault

In the six-phase configuration the inter-circuit double line to ground faults appear different to the distance relay depending on the phases involved in the fault. Therefore all possible combinations of such faults are discussed for clarity.

Phase *a-b-ground* Fault: This is an inter-circuit double line to ground fault. This fault involves two phases that are 60° apart in their respective phases, and are protected by different distance relays. The response of the ground and line impedance elements for such an inter circuit fault is observed to be different from an intra-circuit fault. As seen in , only phase-*a* ground impedance trajectories move into the trip zones, with more than 50% errors in the measured impedance. The line elements do not come in to operation since no two lines of the same circuit are faulted. Thus the distance relay is troubled by this category of faults in a six-phase system although the

directional element (Figure 6.15) functions properly detecting forward faults on both circuits. However, with the modified ground impedance elements, shown in Figure 6.13, the relay proves to be capable of handling this category of faults.

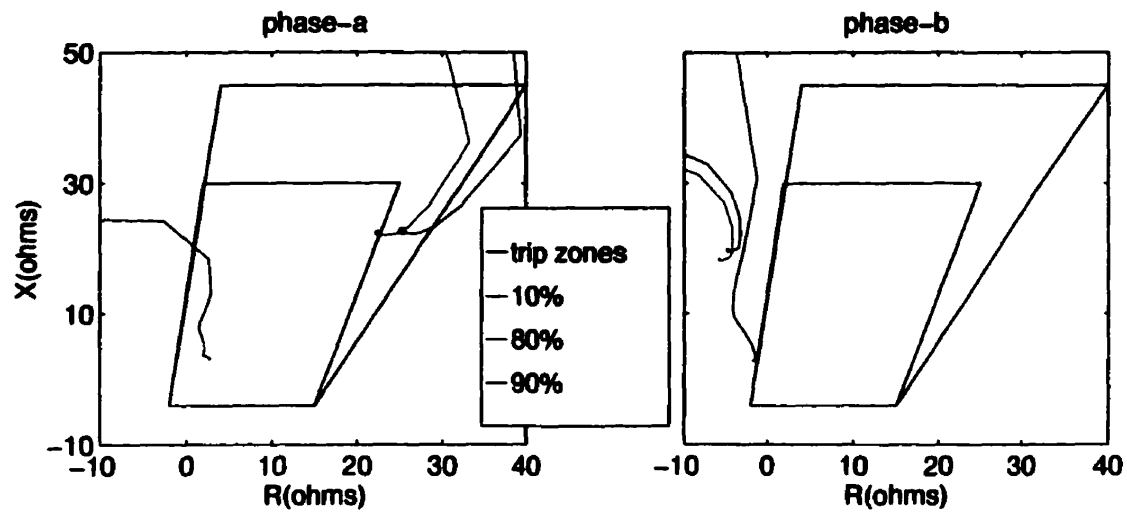


Figure 6.13 Ground elements of faulted phases, for faults at 10%, 80% and 90% distances.

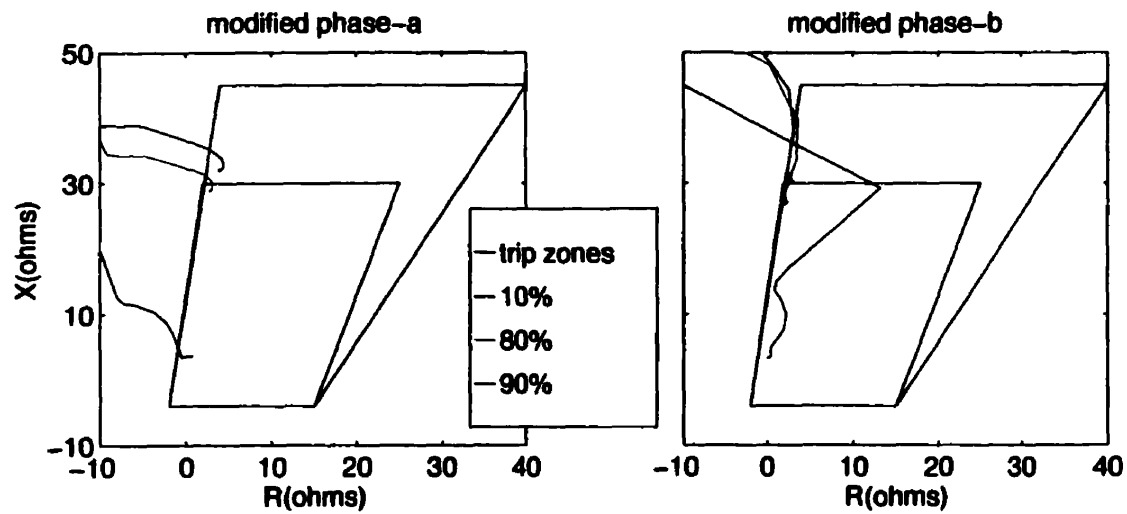


Figure 6.14 Modified ground elements of faulted phases, for faults at 10%, 80% and 90% distances.

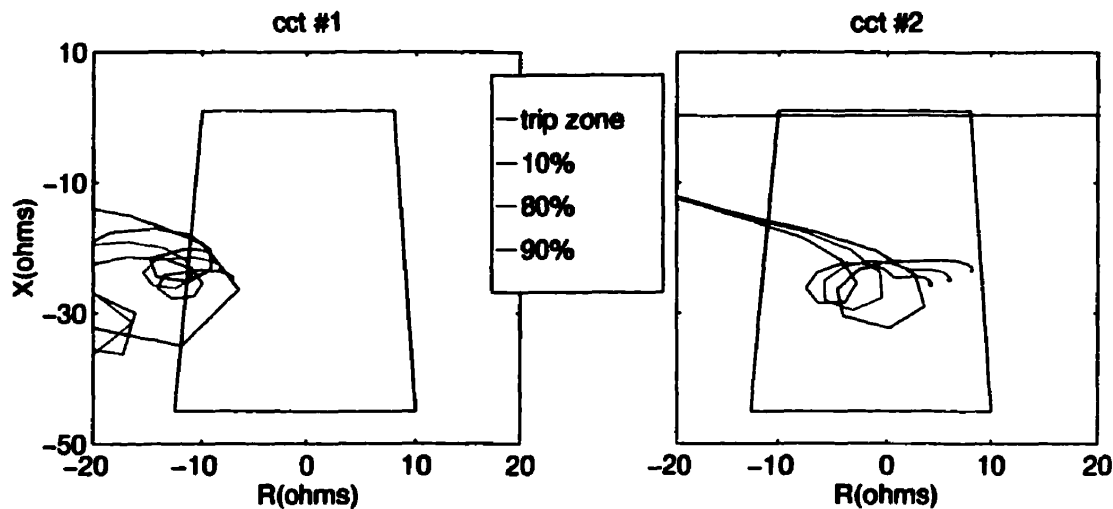


Figure 6.15: Directional elements for circuit #1 and circuit #2, for phases a-b-ground faults at distances 10%, 80% and 90%.

Phase *a-b* Fault: This is fairly different in nature to the corresponding ground fault. The voltage difference between the two phases at fault are small, independent of the fault inception point on the voltage waveform. Therefore, the disturbance caused by the line-line fault of this kind is insufficient to move ground impedance trajectories to their trip zones, except when the faults are close to the measuring busbar. Figure 6.16 shows one ground impedance trajectory moving to the trip zone for the close-up fault. Modifying the ground impedances with mutual zero sequence compensation moves all trajectories completely away from the trip zones. The line impedance elements do not see any fault, as no two lines of the same circuit are faulted. Only trajectories of the close-up faults cause a directional trip (Figure 6.17). Therefore, faults of this nature

are completely undetected by the distance relays with modified ground elements. Only close-up faults will be tripped.

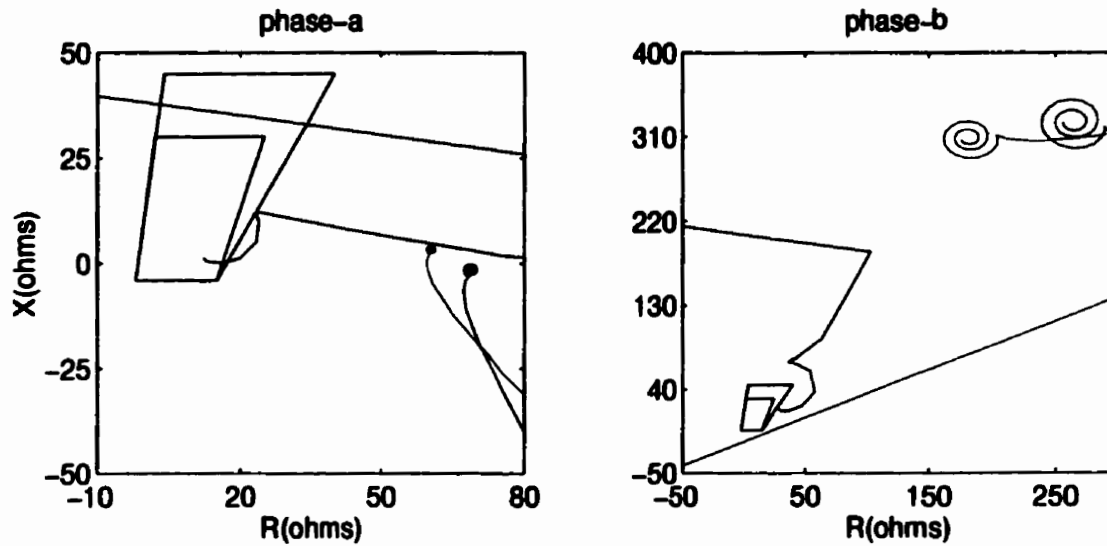


Figure 6.16: Ground impedance elements of faulted phases, for phases a-b faults at distances 10%, 80% and 90%.

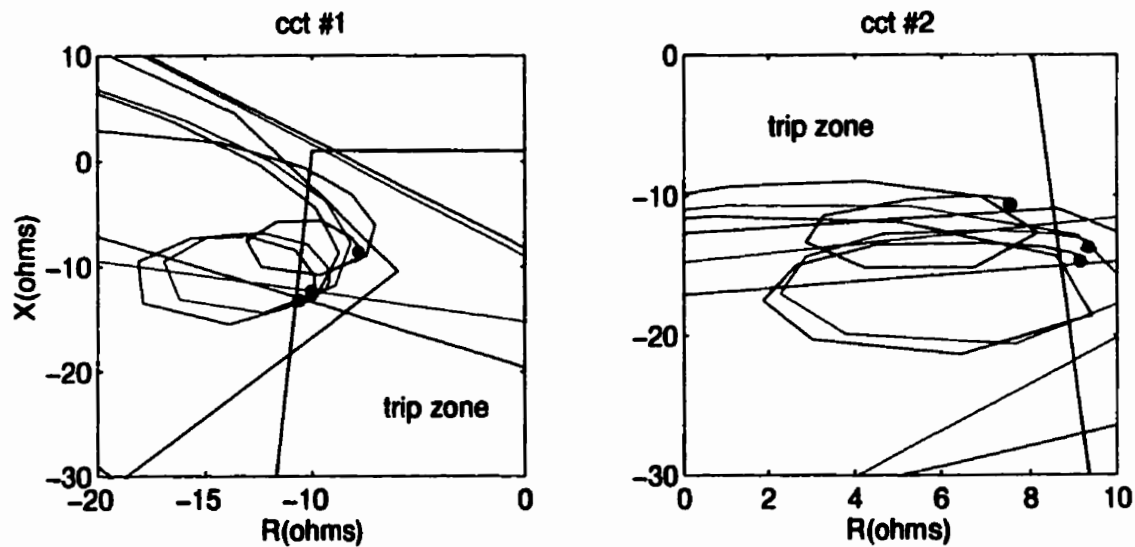


Figure 6.17: Directional elements for circuit #1 and circuit #2, for phases a-b faults at distances 10%, 80% and 90%.

Phase *a-d*-ground Fault: This inter-circuit double line to ground fault too involves two phases on different circuits but are of 180° phase shift. The ground impedance trajectories (in Figure 6.18) which move into zone-one for remote faults are corrected in the modified ground impedance element.

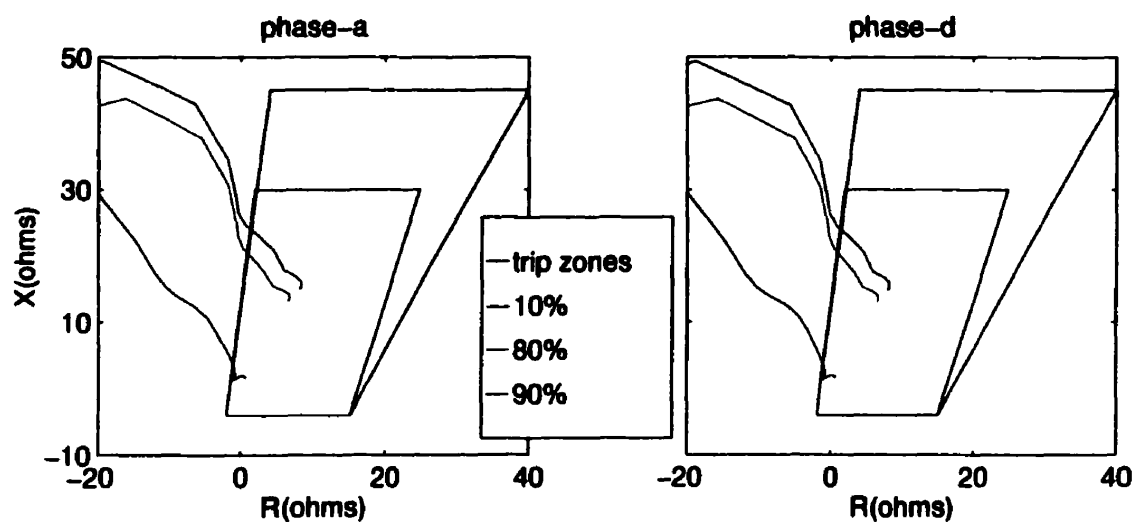


Figure 6.18: Ground elements of faulted phases, for faults at 10%, 80% and 90% distances.

Two line elements are also observed to mis-detect the close-up fault in zone-one (Figure 6.19). The directional elements shown in Figure 6.20 are not troubled in this case as well. The existing trip logic will result in tripping both circuits for a close-up fault of this type due to the mis-operated line impedance elements.

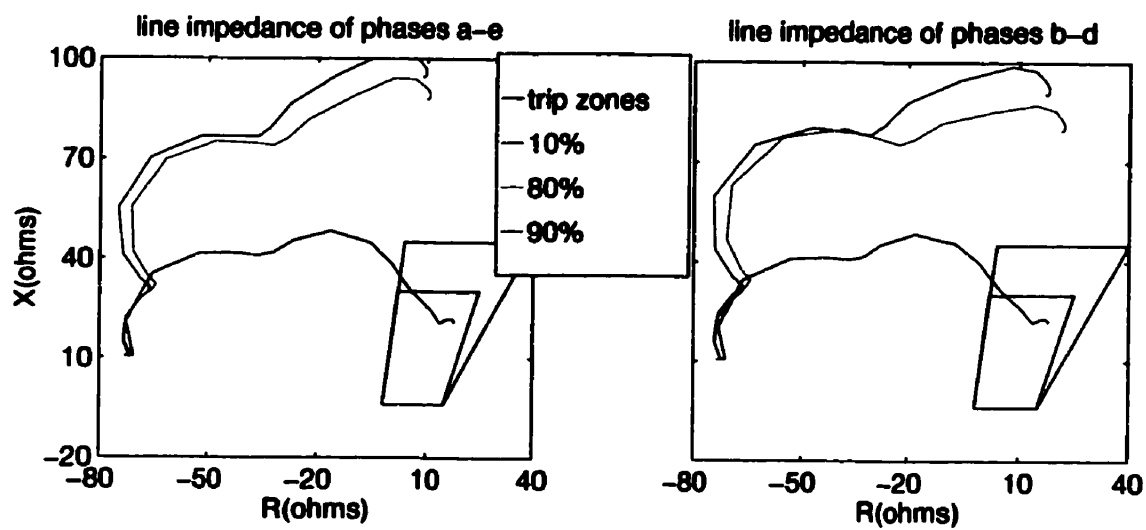


Figure 6.19: The two line impedance elements which mis-operate for the a-d-ground fault at 10% distance.

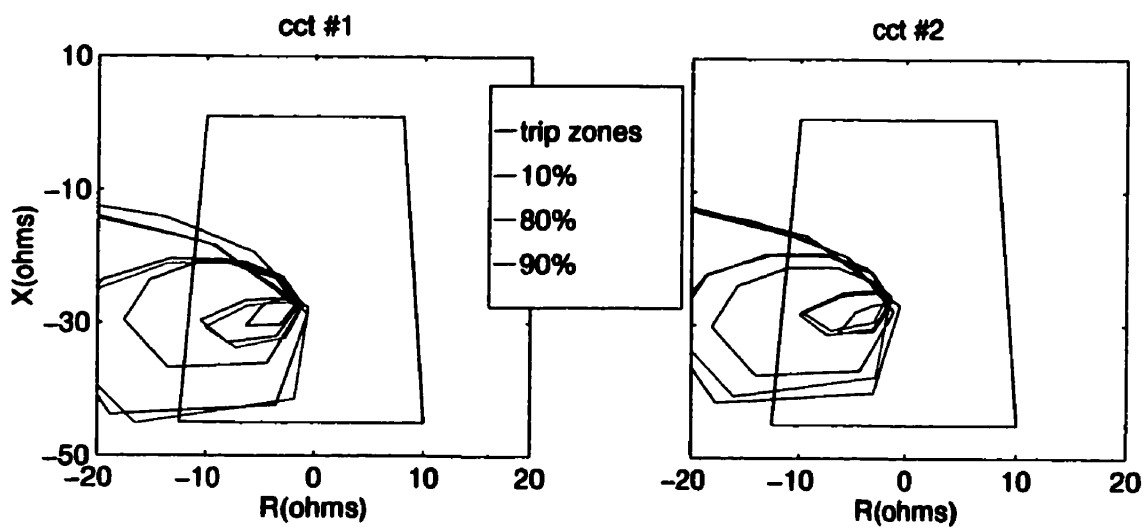


Figure 6.20: Directional elements for circuit#1 and circuit #2, for phases a-d-ground faults at distances 10%, 80% and 90%.

Phase *a-d* Fault: Because of the connection between two phases which are 180° apart, the zero sequence currents are as large as for the corresponding ground fault. Therefore the relay impedance elements see no difference between this and the corresponding ground (*a-d-ground*) fault. Thus for such a close-up fault both circuits will be tripped unnecessarily, whereas tripping just one phase of one circuit would be the ideal operation. The modified ground impedance elements of phases a and d pick up the faults in their respective zones

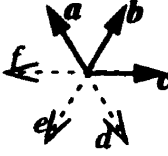
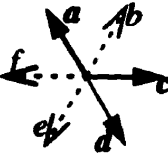
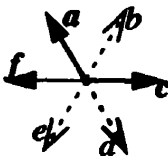
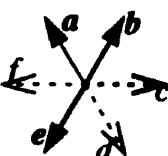


6.3.4 Single Circuit Three-Phase / Three-Phase-Ground Faults

These are faults that do not cause any complications to the relays, as the relay on the faulted circuit sees the simple three phase or three-phase to ground fault whereas the other one does not see any fault. They also do not result in any zero sequence currents, and therefore this makes the detection straight forward.

6.3.5 Inter Circuit Three-Phase to Ground Faults

The inter-circuit three phase to ground faults on a six-phase line can be classified into two basic categories, depending on the phase displacement of the three phases involved in the fault. Table 6.1 shows the possible combinations of phases for such faults with their relative phase orientation. The first and the sixth faults shown in the table have three neighbouring phases faulted. Impedance elements demonstrate similar behaviour for both these faults. The behaviour of the impedance trajectories for the other four faults appear similar as well.

Table 6.1: Phase orientation of faulted phases for various combinations of inter-circuit three phase faults.

Phases at fault		Phase angles of faulted phases with respect to phase-a		Phase sequence of faulted phases	Phasor diagram of faulted phases
cct#1	cct#2	cct#1	cct#2		
<i>a,c</i>	<i>b</i>	$0^\circ, -120^\circ$	-60°	$0^\circ, -60^\circ, -120^\circ$	
<i>a,c</i>	<i>d</i>	$0^\circ, -120^\circ$	-180°	$0^\circ, -120^\circ, -180^\circ$	
<i>a,c</i>	<i>f</i>	$0^\circ, -120^\circ$	$+60^\circ$	$0^\circ, -120^\circ, +60^\circ$	
<i>a,e</i>	<i>b</i>	$0^\circ, +120^\circ$	-60°	$0^\circ, -60^\circ, +120^\circ$	
<i>a,e</i>	<i>d</i>	$0^\circ, +120^\circ$	-180°	$0^\circ, -180^\circ, +120^\circ$	
<i>a,e</i>	<i>f</i>	$0^\circ, +120^\circ$	$+60^\circ$	$0^\circ, +120^\circ, +60^\circ$	

This similar behaviour of the impedance trajectories can be justified by their similar relative phase angles of the faulted lines. Therefore, two different inter circuit three phase to ground faults sufficiently demonstrate the complete spectrum of problems caused by such faults.

Phase *a-c-b-ground* Fault: The modified ground, and line impedance trajectories, for *a-c-b-ground* fault are shown in Figure 6.21 and Figure 6.22. It shows that the ground elements of the circuit with two faulted phases (elements of circuit *a, c, e*) do not detect the far-end faults even with compensation for zero sequence mutual current on the parallel circuit, since the currents are comparatively small in magnitude. But those faults are detected by the respective line impedance element, as shown in Figure 6.22. The directional impedances also fall in the trip zone for both close-up and remote faults. Therefore all three faulted phases are tripped appropriately. The apparent errors in the measured line and ground impedance will cause incorrect zone trips for most border-line fault distances.

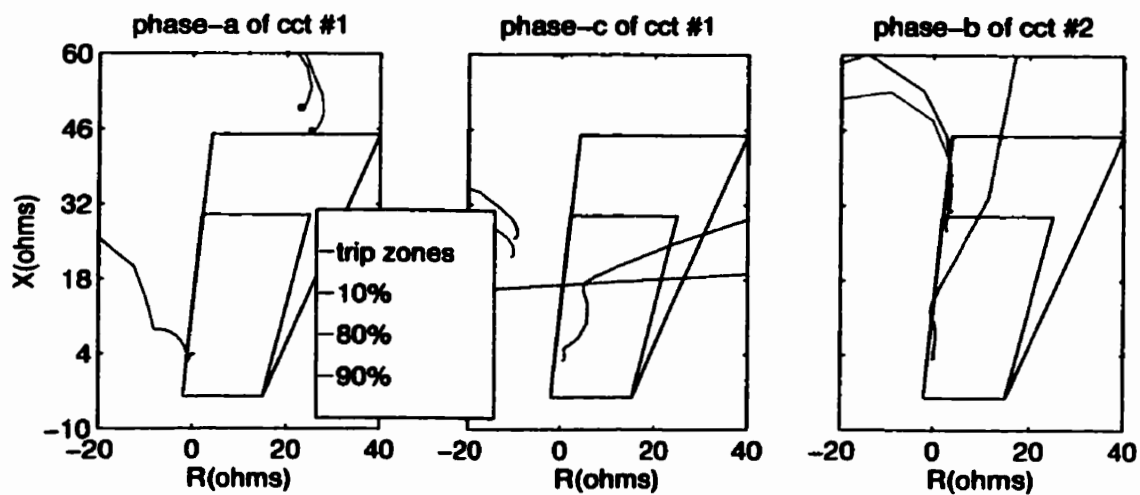


Figure 6.21: Modified ground impedance elements of faulted phases, for a-c-b-ground faults at distances 10%, 80% and 90%.

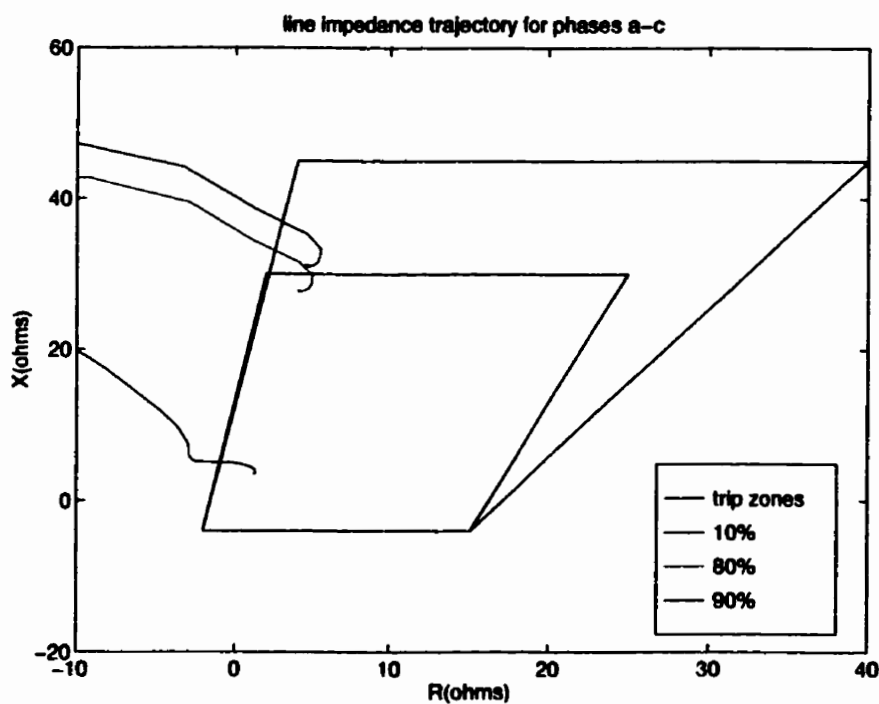


Figure 6.22: Line impedance trajectories of phases a-c, for a-c-b-ground faults at distances 10%, 80% and 90%.

Phase *a-c-b* Fault: The behaviour for line and directional impedance trajectories for the three phase fault without ground connection, is similar to that of the corresponding ground fault (*a-c-b-ground*). The imbalance caused by such inter circuit connection is insufficient to move the ground impedance trajectories to their trip zones on either of the circuits for far end faults. Therefore, only the circuit with two faulted conductors will be tripped and thus the fault will be cleared with minimal reduction in power flow. However, faults close to the measuring bus bar cause a trip of phase-*b* as well.

Phase *a-c-d-ground* Fault: This type of fault involves phases that are not displaced by equal angles and is representative of all such inter circuit three phase to ground faults. As shown in Figure 6.23 and Figure 6.25 one ground element of each circuit over reaches to zone-one for far-end faults. The line impedance element with two faulted phases detects the fault in their respective zones with the directional trip properly coming well in the trip zone for the same circuit (Figure 6.24). The directional impedance (Figure 6.25) of the circuit with one faulted phase falls outside the trip zone for close-up faults. Therefore, the circuit with a single faulted phase is not tripped for close-up faults, as the trip logic does not issue a trip to the circuit breaker without the directional element trip.

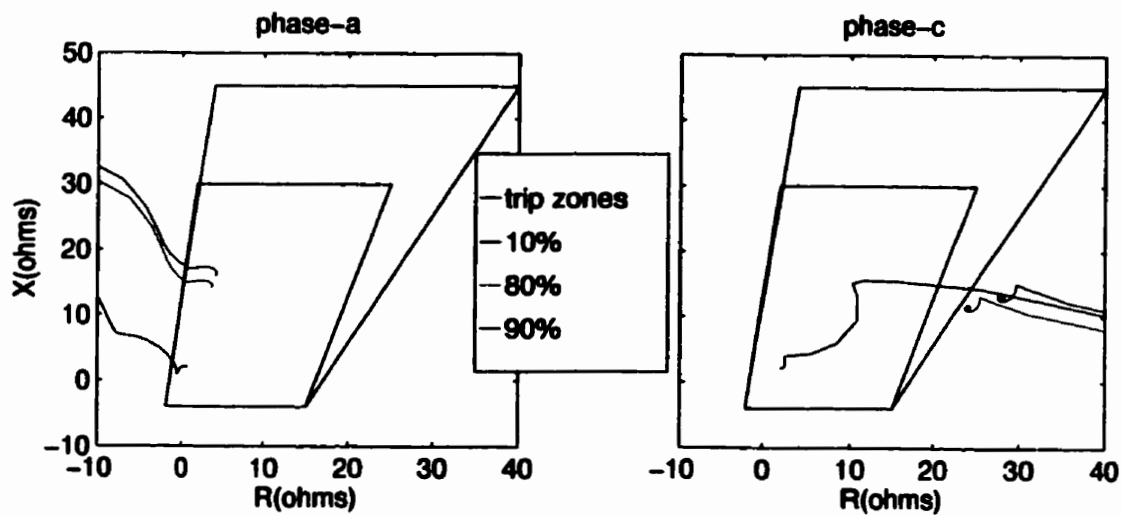


Figure 6.23: Ground impedance elements for faulted phases of one circuit, for a-c-d-ground faults at distances 10%, 80% and 90%.

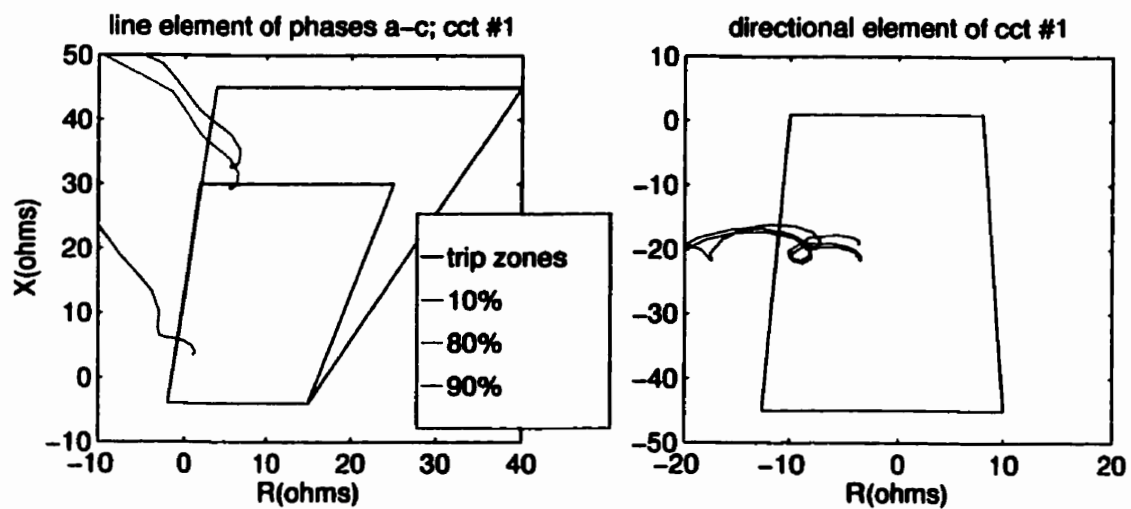


Figure 6.24: Line impedance elements of faulted phases and directional impedance element, of the first circuit, for a-c-d-ground faults at distances 10%, 80% and 90%.

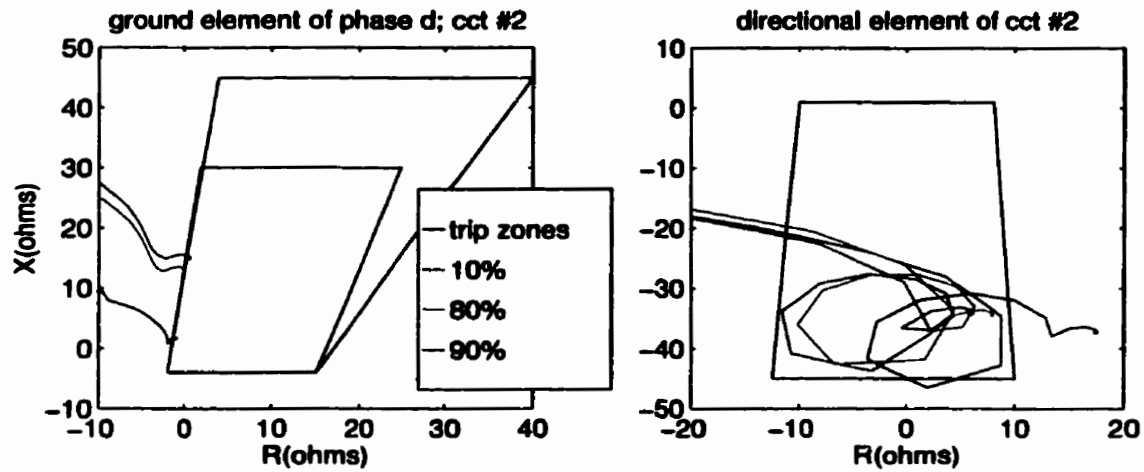


Figure 6.25: Ground impedance element for the faulted phase and the directional impedance element, of the second circuit, for a-c-d-ground faults at distances 10%, 80% and 90%

With the corrected ground impedance element shown in Figure 6.26, most of the mis-operations are rectified, except the close-up faults, for which only one circuit is cleared, due to the directional trip not being issued.

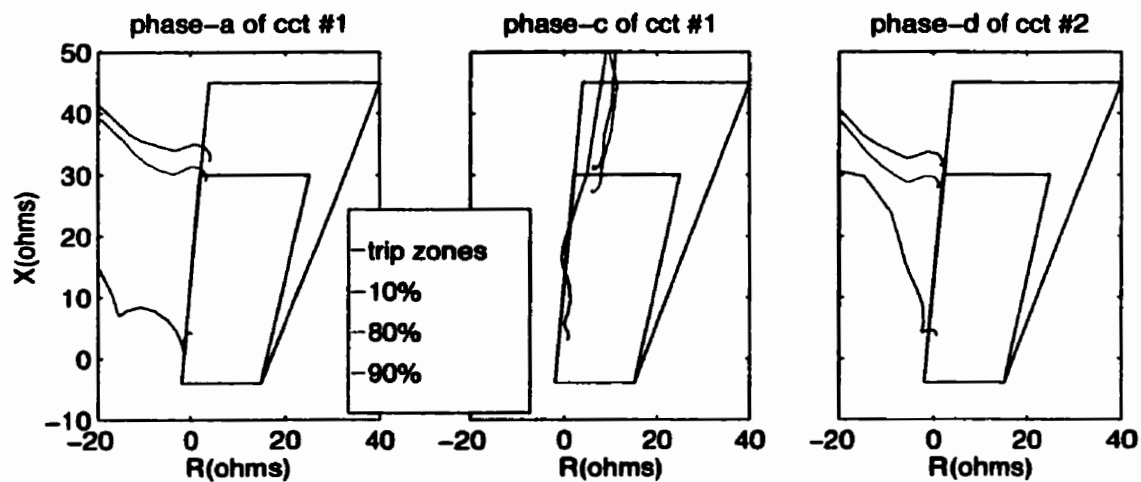


Figure 6.26: Modified ground impedance elements for faulted phases, for a-c-d-ground faults at distances 10%, 80% and 90%.

Phase *a-c-d* Fault: It is appropriate to investigate the behaviour of the relay elements for the same kind of faults with no ground involvement. The modified ground impedance trajectories of the circuit with one faulted line does not trip for the faults. Therefore, only one circuit will be tripped, clearing the fault and leaving the other in healthy operation for most of such faults.

6.3.6 Four-Phase to Ground / Four-Phase Faults

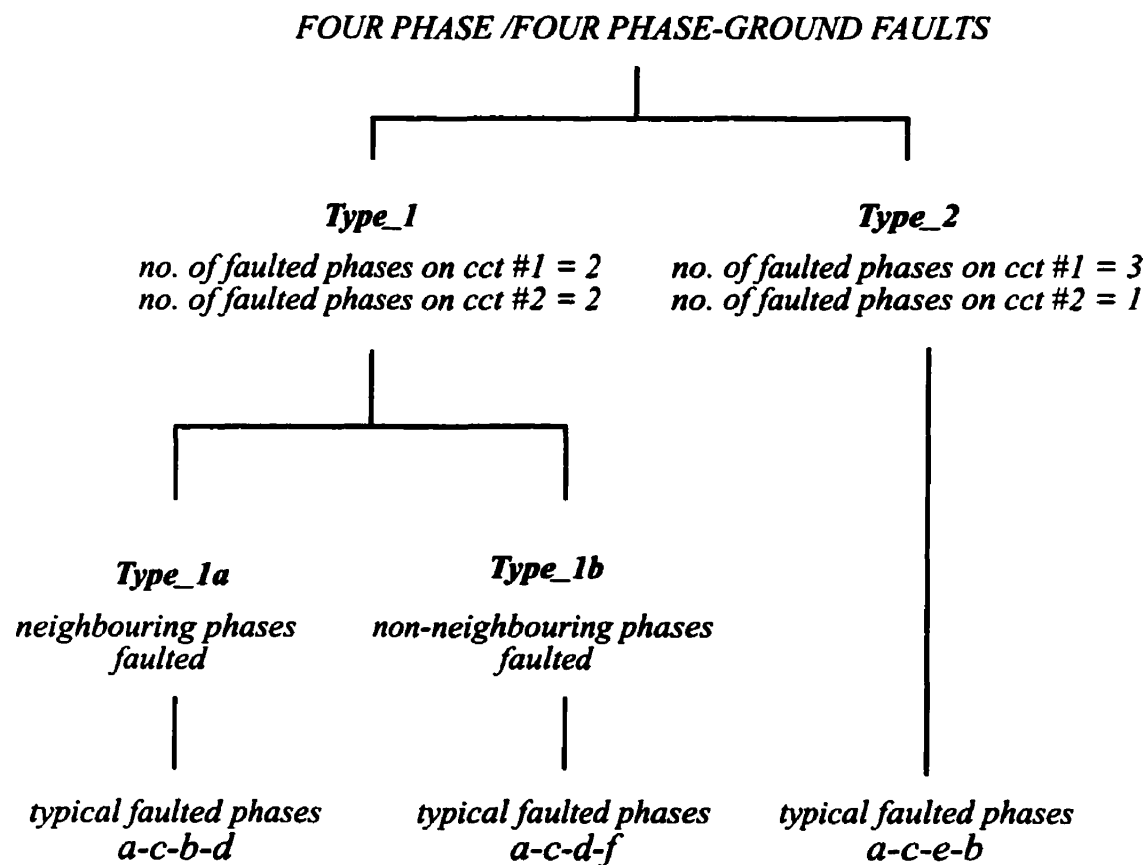


Figure 6.27: Categorization of different four-phase and four-phase-to-ground faults.

Four phase faults which involve both circuits can be categorized into three types based on the similarities of response of the relay elements to each of the faults.

- Those which involve two phases of each circuit.

This type can be further subdivided into two categories depending on the response of the distance relay elements for each fault type. Such similar behaviour can also be justified based on the relative phase orientation of the faulted phases.

- Those which involve three phases of one circuit and one of the other.

The three categories are named *type_1a*, *type_1b* and *type_2*, for the convenience of identification. Figure 6.27 shows the break down of these three types of four-phase faults.

The uncompensated ground impedance elements are unable to differentiate between the four-phase-ground faults from the four-phase faults due to the large zero sequence currents flowing in both cases. Close up faults move ground impedance trajectories of all the faulted phases into trip zone-one. But they either over reach to zone-one or fall outside the trip zones for remote faults. The ground impedance trajectories of phases *a* and *c* for *a-c-b-d-ground* fault at various distances shown in Figure 6.28 demonstrate the typical problems for such faults.

The compensated ground impedances are falling in their respective trip zones for the ground faults, whereas the behaviour differs between various types for non-grounded faults. *Type_1a* non-grounded faults have at least one of the ground impedances of each circuit move to trip zones with very little error in the fault impedance. *Type_1b*

faults are recognized as ground faults, in their respective trip zones. For faults of *type_2* the circuit with three faulted phases has the impedances move to the appropriate trip region. The ground element of the faulted line on the other circuit falls a little short of the trip zone boundaries. In general, compensated ground impedances eliminate the incorrect zone trip due to over reached ground impedance trajectories.

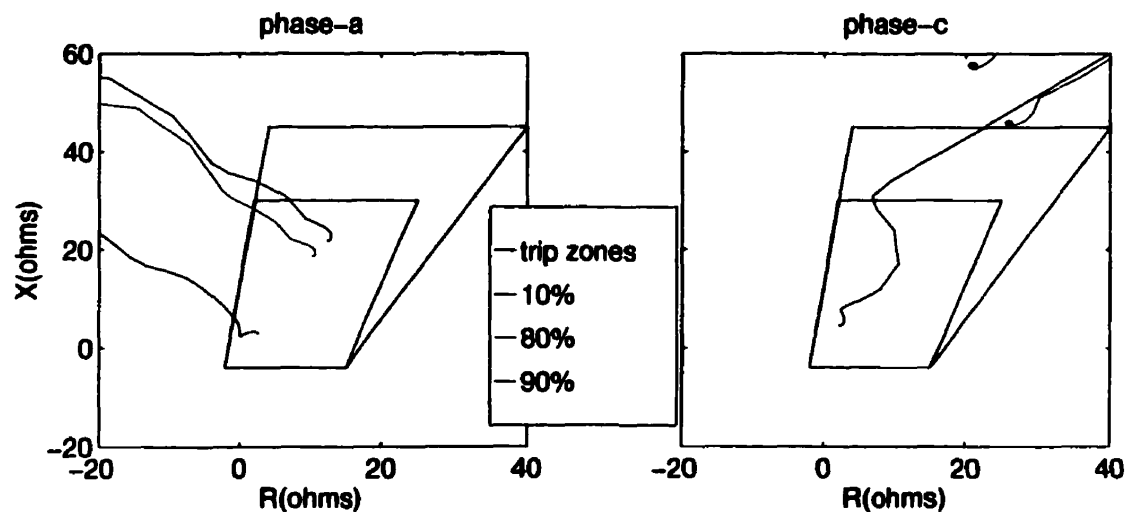


Figure 6.28: Ground impedance trajectories of phases a & c, for a-c-b-d-ground faults at distances 10%, 80% and 90%

The line impedances and the directional elements of both circuits operate without much trouble for faults of *type_1*. One of the three line impedances of each circuit move into the respective trip zones with small errors in the calculated line impedances, as expected for most of the faults. A few close-up faults cause a second line impedance of one of the circuits to move to trip zone-one. This mis-operation is not a problem as all three phases need to trip for a double-line fault on any circuit.

Therefore, in general *type_1a* and *type_1b* faults are well detected by the modified ground, line, and the directional elements causing trips on both circuits as required.

Type_2 faults are significantly different to *type_1* faults in terms of the response of the directional element. The circuit with one faulted phase does not have the directional trip operated for close up faults. Only those faults beyond about 90% distance move both directional impedances in the trip zone (Figure 6.29). The directional element of the circuit with smaller fault current is observed to suffer from this type of mis-operation typically in severe faults with unequal numbers of faulted phases on the two circuits. Therefore, initially, only three faulted phases or one circuit trips for a *type-2*, four-phase/four phase-ground fault. This should effectively clear a *type_2* ungrounded fault and subsequently trip the remaining faulted line for a ground fault.

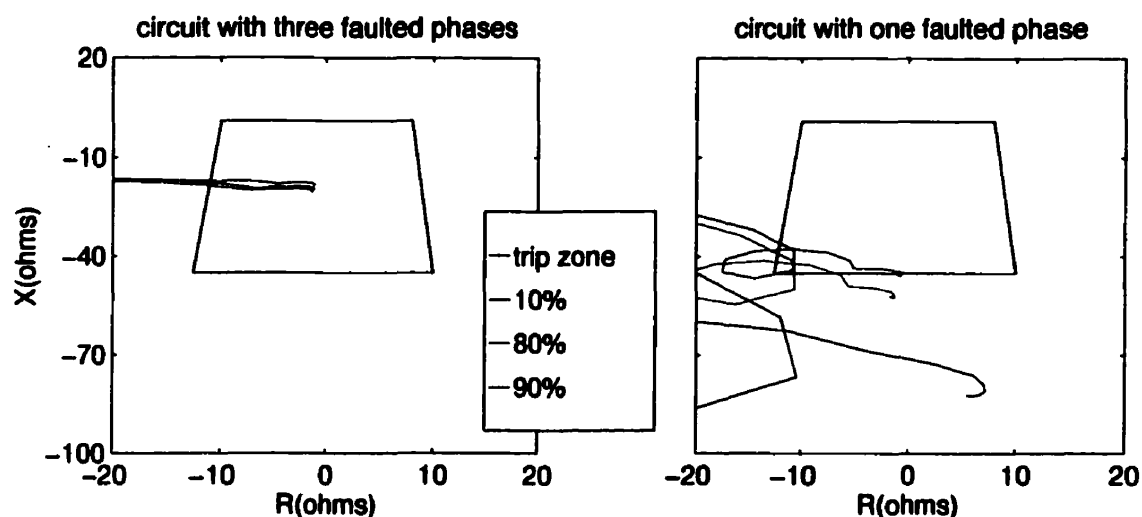


Figure 6.29: Directional impedance trajectories of the two circuits, for a-c-e-b-ground faults at distances 10%, 80% and 90%

6.3.7 Five-Phase to Ground / Five-Phase Faults

Here again, due to the heavy zero sequence currents flowing in both circuits, the relay elements do not differentiate ground faults from the non-ground faults.

The line impedance elements and the directional elements of both circuits operate as expected for all faults with minimal errors in the measured line impedances. But the ground impedances are troubled with heavy zero sequence currents, which are corrected to about 90% accuracy with compensation, for faults with ground involvement. The errors in the measured ground impedance for ungrounded faults remain high even with compensation, and cause incorrect zone trips. Thus, for faults involving five phases, some remote ungrounded faults are a zone-one trip whereas close-up faults are well detected.

6.3.8 Six-Phase to Ground / Six-Phase Faults

This type of fault is well handled by the distance relay impedance elements, as it does not generate heavy zero sequence currents. The ground impedance trajectories are identical for both ground and non-ground six-phase faults due to the inter connection between the two circuits appearing as the ground path for the non-ground fault.

6.4 Summary of Relay Performance for Various Faults

The tripped phases for various ground and non-ground faults that were analysed in the this chapter are summarized in Table 6.2 and Table 6.3 respectively.

Table 6.2: Summary of relay performance on six-phase lines for ground faults.

Type of fault	Relay response for Zone 1, close-up faults	Relay response for Zone 2 remote faults
<i>Single line to ground fault</i>	<i>two phases of the faulted circuit are zone1 tripped</i>	<i>only the faulted phase is zone2 tripped</i>
<i>Double line to ground fault</i>	<i>all three phases of the faulted circuit are zone1 tripped</i>	<i>two phases of the faulted circuit are zone2 tripped</i>
<i>Inter-circuit double line to ground fault (a-b-g)</i>	<i>two phases of one circuit and the faulted phase of the other circuit are zone1 tripped</i>	<i>faulted phases of both circuits are zone2 tripped</i>
<i>Inter-circuit double line to ground fault (a-d-g)</i>	<i>two phase of each circuit are zone1 tripped</i>	<i>the two faulted phases are zone2 tripped</i>
<i>Three line to ground fault</i>	<i>three phases of the faulted circuit are zone1 tripped</i>	<i>three phases of the faulted circuit are zone2 tripped</i>
<i>Inter-circuit three line to ground fault (a-c-b-g)</i>	<i>two phases of each circuit including the faulted phases are zone1 tripped</i>	<i>only the faulted phases of both circuits are zone2 tripped</i>
<i>Inter-circuit three line to ground fault (a-c-d-g)</i>	<i>phases a & c are zone1 tripped</i>	<i>all faulted phases are zone2 tripped</i>
<i>Inter-circuit four line to ground fault (type_1a)</i>	<i>five phases including the faulted phases of both circuits are zone1 tripped</i>	<i>all the faulted phases of both circuits are zone2 tripped</i>
<i>Inter-circuit four line to ground fault (type_1b)</i>	<i>all six phases are zone1 tripped</i>	<i>all the faulted phases of both circuits are zone2 tripped</i>
<i>Inter-circuit four line to ground fault (type_2)</i>	<i>only the three faulted phases of one circuit are zone1 tripped</i>	<i>all four faulted phases are zone2 tripped</i>

Table 6.2: Summary of relay performance on six-phase lines for ground faults.

Type of fault	Relay response for Zone 1, close-up faults	Relay response for Zone 2 remote faults
<i>Inter-circuit five line to ground fault</i>	<i>all three phases of both cir- cuits are zone1 tripped</i>	<i>only the faulted phases are zone2 tripped</i>
<i>Six line to ground faults</i>	<i>all three phases of both cir- cuits are zone1 tripped</i>	<i>all three phases of both cir- cuits are zone2 tripped</i>

Table 6.3: Summary of relay performance on six-phase transmission line for non-grounded faults.

Type of fault	Relay response for Zone 1, close-up faults	Relay response for Zone 2 remote faults
<i>Inter-circuit dou- ble line fault (a-b)</i>	<i>no trip issued</i>	<i>no trip issued</i>
<i>Inter-circuit dou- ble line to ground fault (a-d)</i>	<i>two phase of each circuit are zone1 tripped</i>	<i>the two faulted phases are zone2 tripped</i>
<i>Three phase fault</i>	<i>three phases of the faulted circuit are zone1 tripped</i>	<i>three phases of the faulted circuit are zone2 tripped</i>
<i>Inter-circuit three line fault (a-c-b)</i>	<i>two phases of each circuit including the faulted phases are zone1 tripped</i>	<i>only a & c phases are zone2 tripped</i>
<i>Inter-circuit three line to ground fault (a-c-d)</i>	<i>phases a & c are zone1 tripped</i>	<i>phases a & c are zone2 tripped</i>
<i>Inter-circuit four line fault (type_1a)</i>	<i>five phases including the faulted phases of both circuits are zone1 tripped</i>	<i>all the faulted phases of both circuits are zone2 tripped</i>

Table 6.3: Summary of relay performance on six-phase transmission line for non-grounded faults.

Type of fault	Relay response for Zone 1, close-up faults	Relay response for Zone 2 remote faults
<i>Inter-circuit four line to ground fault (type_1b)</i>	<i>all six phases are zone1 tripped</i>	<i>all the faulted phases of both circuits are zone2 tripped</i>
<i>Inter-circuit four line fault (type_2)</i>	<i>only the three faulted phases of one circuit are zone1 tripped</i>	<i>all four faulted phases are zone2 tripped</i>
<i>Inter-circuit five line to ground fault</i>	<i>all three phases of both circuits are zone1 tripped</i>	<i>only the faulted phases are zone2 tripped</i>
<i>Six line to ground faults</i>	<i>all three phases of both circuits are zone1 tripped</i>	<i>all three phases of both circuits are zone2 tripped</i>

6.5 Effect of Pre-fault Operating Point on the Distance Relay Impedance Trajectories

Various faults that were simulated were also repeated maintaining a few other pre-fault power flow conditions to investigate the effect of pre-fault system conditions on the distance relay impedance trajectories.

6.5.1 Ground Faults

Although the paths or the trajectories of the impedance elements differ due to the difference in the initial condition of the system, the final settling impedances for ground, line and directional elements are unaffected by the pre-fault operating point of the system for a given fault at a given distance.

6.5.2 Ungrounded Faults

The measured line and directional impedances during ungrounded faults are not affected by the pre-fault operating condition of the power system. However, due to the absence of the ground connection, the effect of pre-fault operating point seems to have a greater effect on the measured ground impedances. But this effect is not significant enough to cause any difference in the lines that are tripped for a given fault condition.

Therefore, for all practical purposes, pre-fault operating point has insignificant effect on the distance relay impedance measurements for a given short circuit fault.

6.6 Conclusions

The performance of the digital distance relay algorithms on the six-phase transmission line configuration was discussed with reference to various short circuit faults. Modification to the ground impedance algorithm has greatly improved its performance. However, the directional element in general is mis-operational for severe faults that confine most of the fault currents to one circuit. Thus, the faults that involve three or four phases, will not be detected by the distance relay.

CHAPTER 7

PROTECTION OF *POINTE DU BOIS* TRANSMISSION LINE

This chapter discusses the modelling of the *Pointe du Bois* line of the Winnipeg Hydro transmission network, and its protection using the digital distance relay under investigation (APT relay). Although the *Pointe* line is a four-circuit system, the protection studies on this line have been confined to only two circuits of the system. The other two parallel lines are left open circuited, simplifying the system to effectively a double-circuit line configuration. The protection of the two lines in operation have been considered in the context of a single relay monitoring both lines.

Exploiting the availability of all six currents of the two circuits for protection functions at one end, a current-balance protection algorithm has been incorporated in the distance relay. Section 7.4 discusses the heuristic design process of the current-balance algorithm and its performance. Thus, the results presented in this chapter demonstrate the performance of the APT relay which has been enhanced with both the modified ground impedance element discussed in section 5.5, and the current-balance algorithm described in section 7.2.

7.1 Rover-Pointe System Model.

The modelled system consists of two terminal stations, *Rover* and *Pointe du Bois*, connected by the 3-phase, four circuit, 69 kV transmission lines.

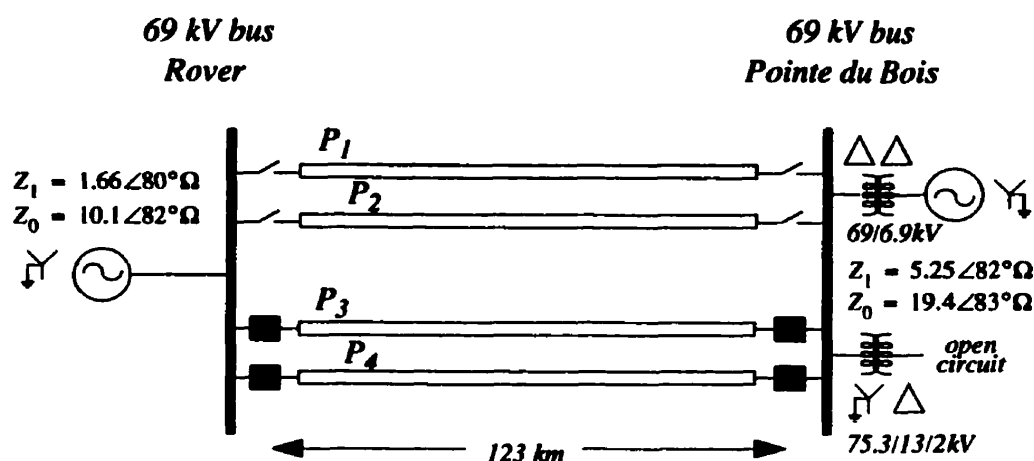


Figure 7.1: Simplified single line diagram of the modelled system

7.1.1 Transmission Line

The 69 kV three-phase transmission lines run on two sets of towers which are erected on the same right of way. These towers have varying configurations along the length of the line. The four circuits are named P_1 , P_2 , P_3 and P_4 .

The conductor configurations, the layout, the transmission line data, and the line impedances are provided in Appendix B.

7.1.2 Pointe du Bois Terminal Station.

Source impedances provided were as seen on the 69 kV bus, when all generators were 'ON'. They are as follows:

Zero Sequence Impedance: $2.41 + j19.28 \Omega$

Positive Sequence Impedance: $0.73 + j5.20 \Omega$

Short Circuit MVA: 770 MVA.

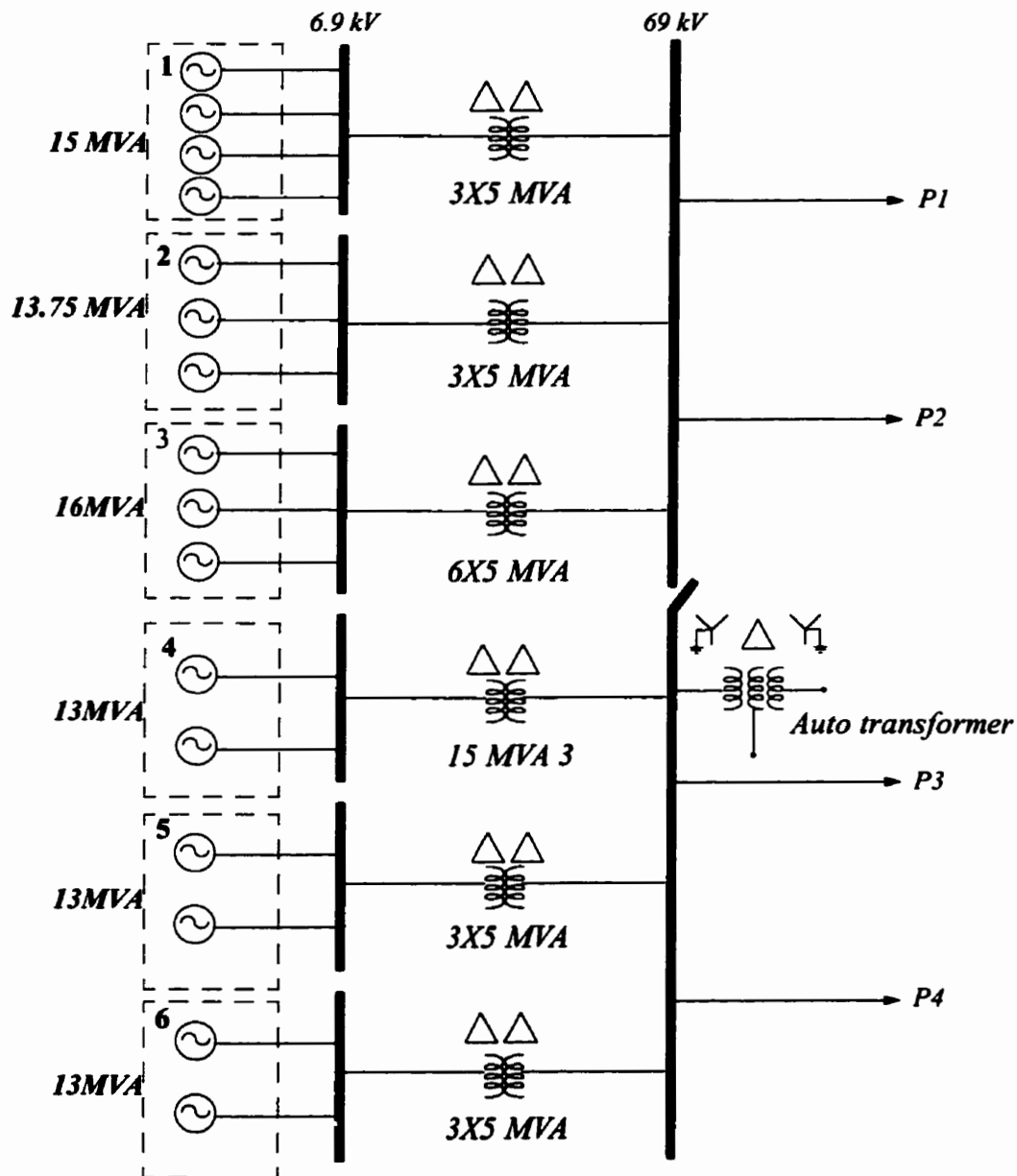


Figure 7.2: Single Line Diagram of the Pointe du Bois Terminal Station.

Since all the step-up transformers are delta-delta connected, the ground path is provided by the auto transformer on the 69 kV bus.

7.1.3 Rover Terminal Station.

The impedance and the single source is the Thevenin equivalent of the system beyond the 69 kV busbar at the Rover station, when all the generators are in service.

The zero sequence impedance of the Rover equivalent source was not provided. Data from a recording of a re-closure on a phase-*b* to ground fault on the P_3 circuit was used to derive this information. Data also shows that the circuit P_4 was not in service at the time of re-closure but does not provide information about the operating condition of the circuits P_1 and P_2 .

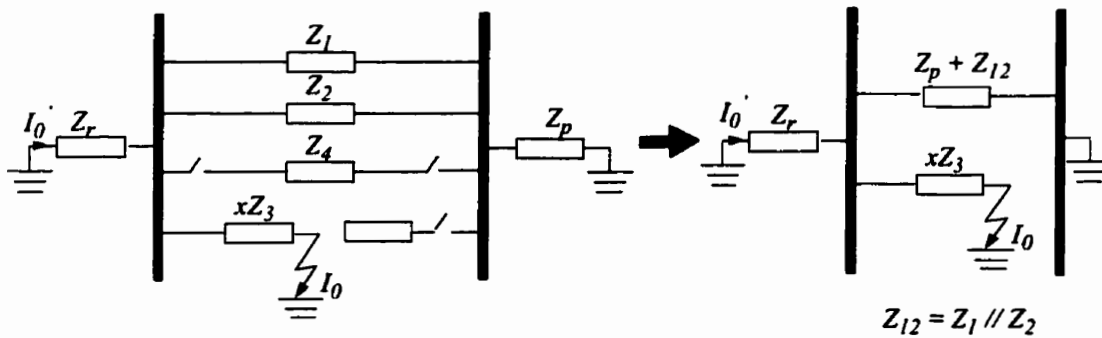


Figure 7.3: Zero Sequence network for l-g fault on circuit P3

Assuming the circuits P_1 and P_2 to be ON at the time of re-closure from the Rover end, on to the single phase fault, it can be shown that the zero sequence voltage to

current (on P_3) ratio can be taken to be the zero sequence equivalent source impedance at Rover. Figure 7.3 shows the zero sequence network of the system for the single line to ground fault.

$$I_0' = \frac{Z_{12}}{Z_r + Z_{12}} \cdot I_0$$

$$V_0 = -Z_r I_0' = -Z_r \left(\frac{Z_{12}}{Z_{12} + Z_r} \right) \cdot I_0$$

$$\frac{V_0}{I_0} = -Z_r \left(\frac{Z_{12}}{Z_{12} + Z_r} \right)$$

but since $Z_{12} \gg Z_r$

$$\frac{V_0}{I_0} \approx -Z_r \quad 7.1$$

Source data for the Rover equivalent source are as follows:

Positive sequence impedance: $0.2915 + j 1.6394 \Omega$

Short Circuit MVA: 2431 MVA

X/R Ratio: 5.6

Calculated zero sequence impedance of the Rover equivalent source:

$2.15 + j9.87 \Omega$

A prototype APT relay is installed on the *Pointe du Bois* transmission line at the *Rover* station. The relay is not connected to the circuit breakers. Fault recordings captured by this relay were made available for testing the model. Some of the validation tests are

given in Appendix C. The recordings also show that the relay has performed unsatisfactorily in several instances. The protection studies of the *Pointe* line was motivated by the need to improve the relay.

Thus, the Alpha Power Technology relay, with the modified ground impedance element described in section 5.5, was further enhanced with a current-balance algorithm for application on the *Pointe du Bois* double-circuit line model. As mentioned before, the four-circuit transmission line has been reduced to a double-circuit line by open circuiting the other two parallel lines P_1 and P_2 , throughout this study.

7.2 Current Balance Algorithm

Exploiting the availability of currents from both circuits, a current-balance algorithm is incorporated in the Alpha Power Technology relay with the modified ground impedance element. The current-balance algorithm consists of three elements, one for each phase which compares the amplitudes of the two phase currents and trips the line with the greater current. However, the trip is not issued if at least one of the phase currents and the positive sequence current of the circuit are not above a preset value. This preset value is typically about 10% of the secondary nominal current. Although simple and fast in operation a current-balance protection technique does not reach beyond the remote terminal. But, having combined with the modified distance relay for back-up capability, significant enhancement in the overall relay performance is achieved.

7.3 Test Set-up

Instead of using the off-line relay model, the prototype test relay (with the features to enhance double circuit line protection) with the testing peripherals was used on a model of the *Pointe* transmission line. The set-up used for testing the actual relay using simulated voltage and current waveforms is shown in Figure 7.4. The test relay was fed with signals from the *Rover* station busbar.

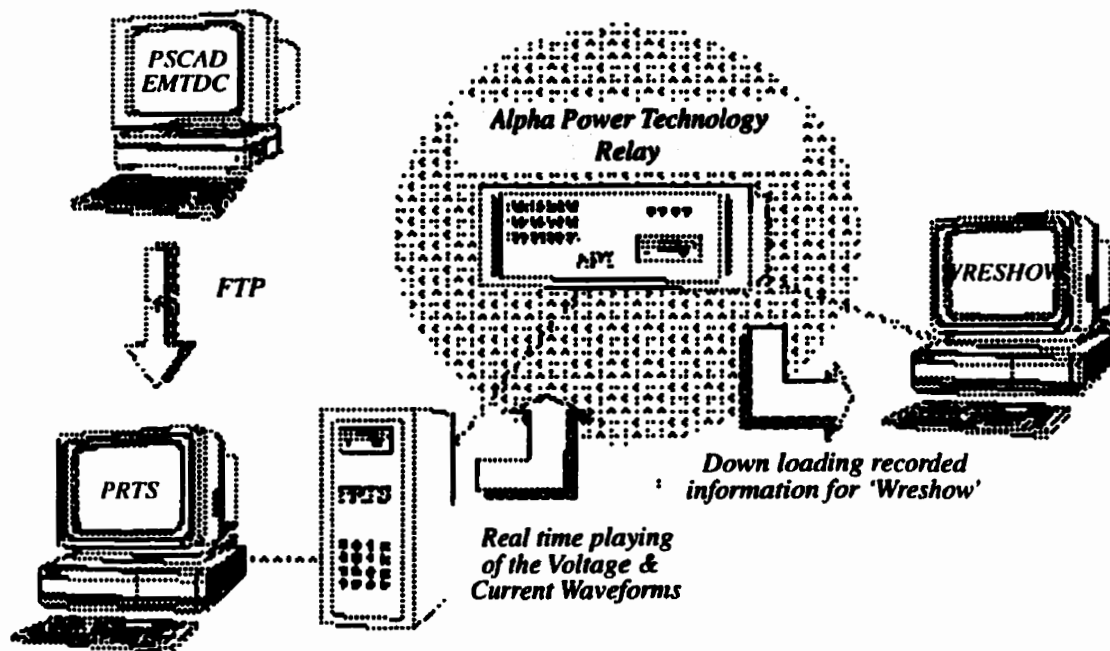


Figure 7.4: Test set-up for testing the prototype APT relay using recorded fault waveforms.

The fault current and voltage waveforms generated using PSCAD/EMTDC, are stored in a file using a simulated data recorder. This special formatted data file is transferred to the *Playback Real Time Simulator* (PRTS), using a file-transfer-protocol (ftp). The

playback simulator reads the data from the file, and plays the waveforms at the relay in real time. It also allows viewing and scaling of the waveforms to an appropriate level before being played at the relay. The PRTS is programmed to play the pre-fault cycle of the waveforms continuously until the key is pressed to initiate the fault. The PRTS then plays the fault and repeats the final cycle for a preset time.

On detection of a fault, the relay produces a recording of the event including the generated trip signals. If connected to a monitor an on-line display of 300ms of waveforms from both lines, as well as the computed impedance trajectories can be observed for any disturbance that triggers the recorder of the relay. Alternatively, for further analysis, the information recorded by the relay can be viewed using a “Wreshow” display program that runs on Windows. This test set-up, which has been developed by the power group at University of Manitoba, provides the facilities for extensive testing of the actual relay.

7.4 Test Results

The test cases chosen for presentation in this section are the critical cases in the design process of the current-balance algorithm on the double circuit line. The details of the algorithm before and after each test are discussed, in order to justify its final form. Note that, because of the availability of multiple transmission paths (P_1 , P_2 , P_3 , and P_4), the circuit breakers trip all three poles for any fault on a circuit.

7.4.1 Single Line to Ground Fault

Figure 7.5 shows recorded information for a single line to ground fault at 75% of line length captured using the 'Wreshow' display program. The top window shows the currents of the three phases on the faulted circuit. The middle window shows the trip signals issued by the current-balance, directional and ground impedance relay elements. The bottom window is the ground impedance trajectory of the faulted phase.

During the test phase, the directional element and the ground element of the faulted phase resulted in a distance relay trip of the faulted circuit. Since none of the impedance trajectories of the unfaulted line moved to the trip zones, the unfaulted line was not tripped by the distance element. However, the current-balance element which was set to operate comparing the amplitudes of the fundamental currents, tripped the unfaulted circuit. This was because of a momentary dip in the fundamental current on the faulted line immediately following the fault, as visible in the zoomed area of Figure 7.5. Apparently, the momentary fall of fundamental component is due to a phase reversal of fault current. As a corrective measure, the current-balance element was later modified to compare the root mean square (rms) currents, instead of the fundamental values.

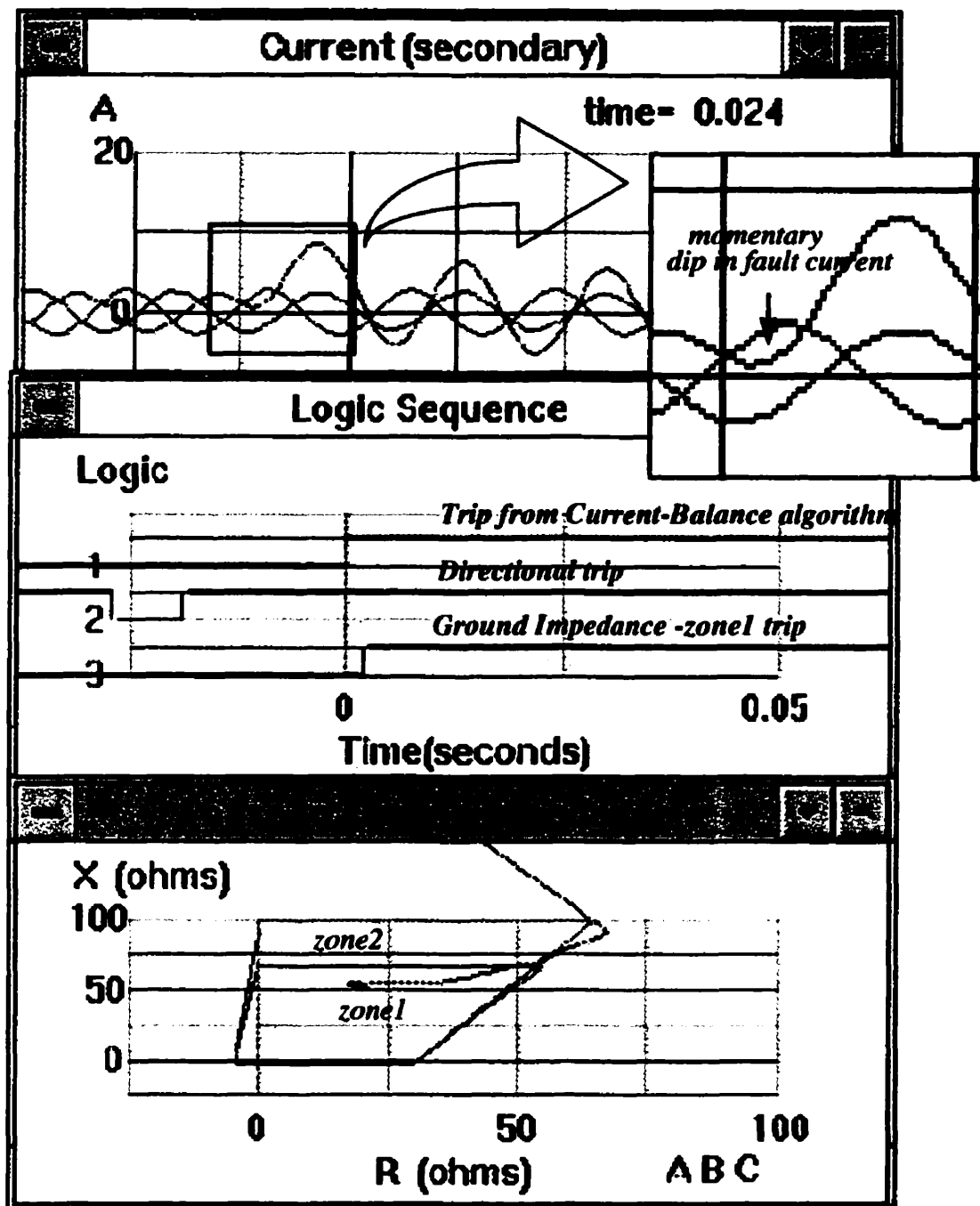


Figure 7.5: Fault currents, trip signals, and ground impedance trajectory of the faulted phase for a single line to ground fault at 75% distance.

7.4.2 Remote Three-Phase Fault

The current-balance element is not expected to differentiate between the faulted and healthy circuits for a fault at the remote end. However, the remote relay element should have no trouble tripping the faulted circuit. Subsequent to the remote trip, the current-balance element on the local end is expected to pick up the faulted circuit. In order to test the capabilities of the current-balance algorithms under these conditions, it was subjected to a three phase fault at the remote end which is cleared by the remote circuit breaker after five cycles of fault. Figure 7.6 shows the currents of the unfaulted circuit with its ground impedance trajectories for the three phase fault as seen by the local relay. Figure 7.7 shows the currents and the trip signals of the local relay on the faulted line for the same fault.

The local current-balance element comes in operation detecting a sufficiently large differential current after the fault is cleared at the remote end. However, it trips the wrong circuit when it is operated based on the rms currents. Close observations of the currents on both circuits (zoomed in areas of Figure 7.6 and Figure 7.7) showed that the rms current of the unfaulted circuit is greater than that of the faulted line for a brief period following the fault clearance by the circuit breaker at the remote end, again due to a phase reversal.

Thus modifying the current-balance logic to trip only if both rms and fundamental differential currents were higher than set values, made it more robust to post-fault and clearance transients. The trip signals shown in Figure 7.7 are for the corrected current-balance element.

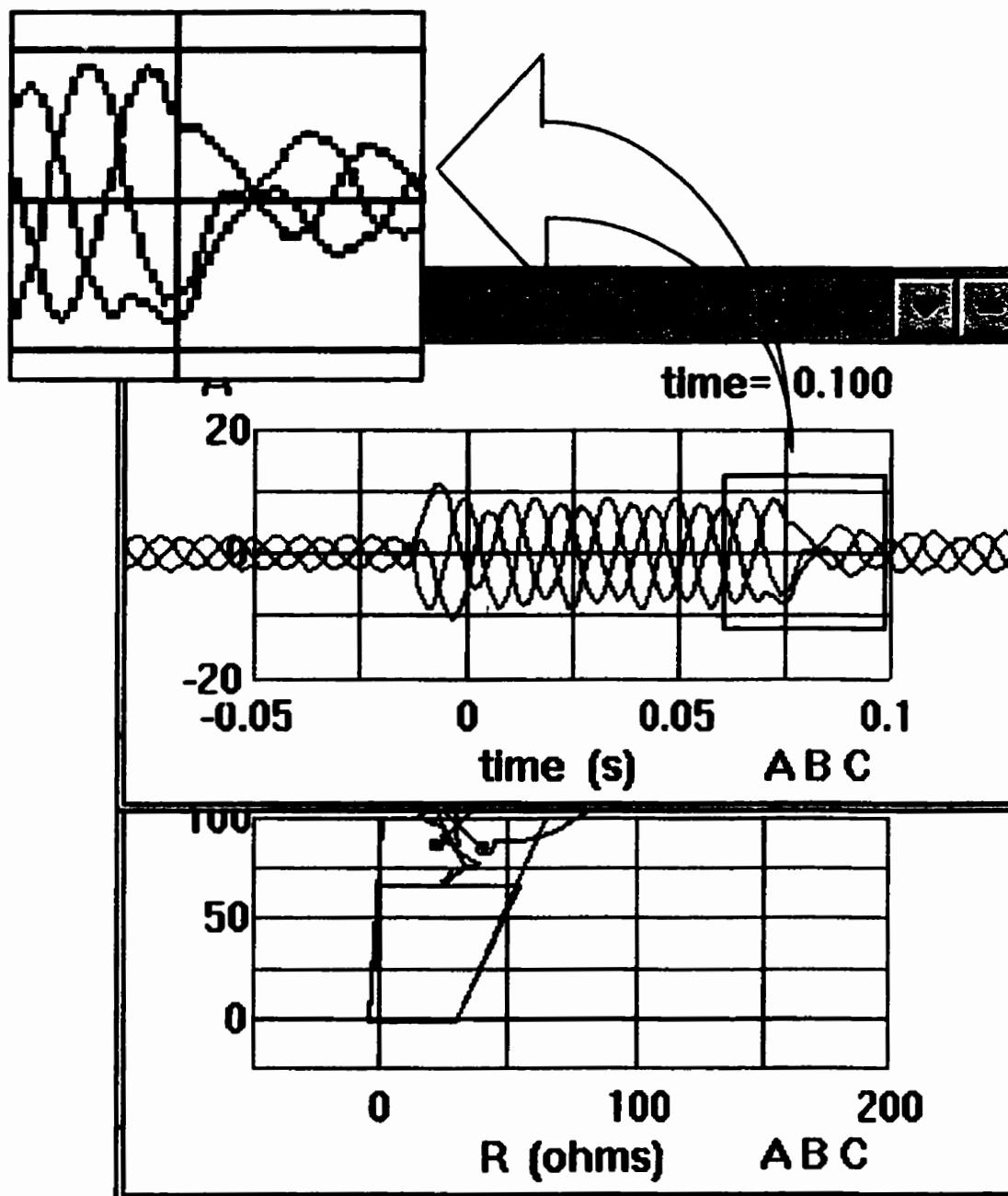


Figure 7.6: Fault currents, and the ground impedance trajectories of the faulted circuit for a three-phase to ground fault at the remote end. The fault is also cleared at the remote end five cycles after its inception.

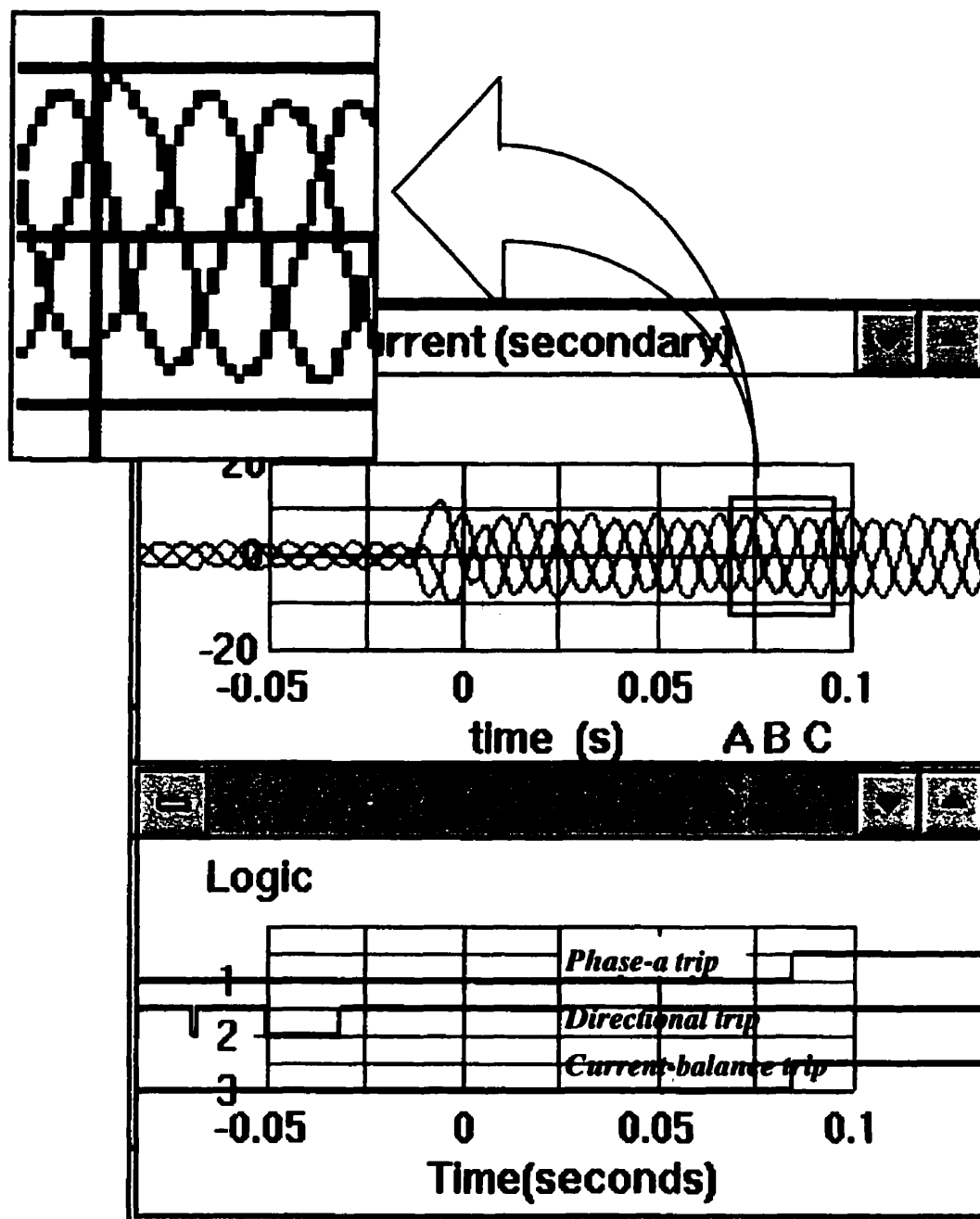


Figure 7.7: Fault currents, and the relay trip signals of the faulted circuit for the same fault as in Figure 7.6.

7.4.3 Inter-Circuit Double Line Fault

Figure 7.8 shows the current waveforms, ground impedance trajectory for the faulted phase, and the trip signals issued by the relay on the same circuit, for an inter-circuit double line fault at 75% distance of the transmission line.

This inter-circuit, phase- a_1 to phase- b_2 fault is presented to demonstrate the improvement in the protection function and the speed of relay trip due to the added current-balance protection algorithm.

As seen in the figure the ground impedance trajectory does not get in the trip zone for the given settings. However, the current-balance algorithm trips the faulted phase within a time period less than half a cycle following the fault.

7.5 Conclusions

Significant improvement in both the protection function, and the speed of operation has been achieved by the use of a current-balance algorithm with the far reaching distance algorithm for back-up on the *Pointe du Bois*, P_1 , P_2 transmission lines. Only the software of the APT relay was modified for the recommended enhancement of the relay.

The original contributions by *Prof. P.G. McLaren* and *Dr. H. Liu* during the studies on the *Pointe* line are gratefully acknowledged.

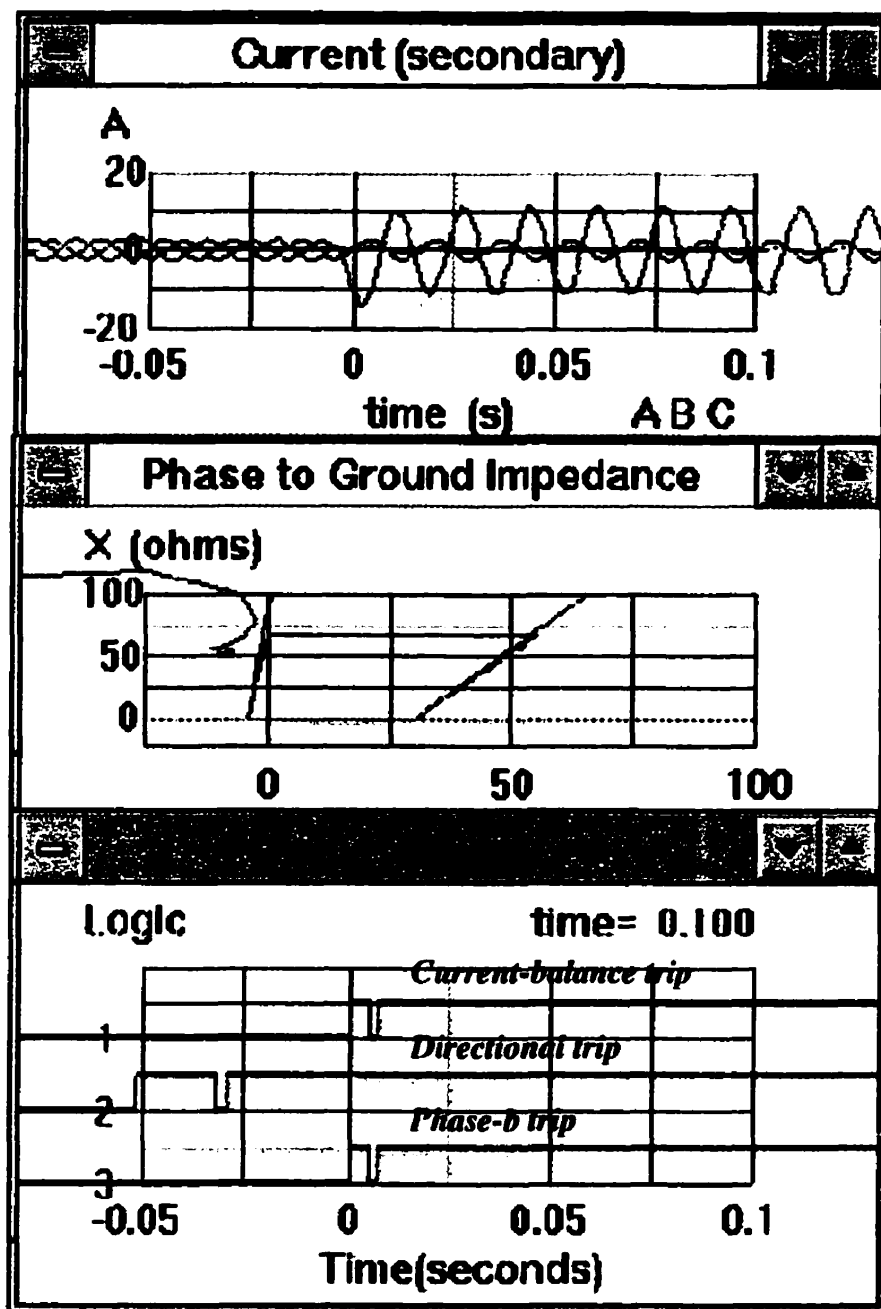


Figure 7.8: Fault currents, ground impedance trajectory of the faulted phase, and the trip signals of a single circuit, for an inter-circuit double line fault at 75% distance.

CHAPTER 8

INTEGRATION OF ARTIFICIAL INTELLIGENCE TO THE APT RELAY

The detailed observation of the performance of the impedance relays on the double circuit and six phase transmission lines showed that the impedance trajectories of the unfaulted lines are the most influenced by the presence of another parallel transmission line. Those impedance elements corresponding to the faulted phases, in most cases, detected the fault in its correct zone with proportional distances. The ambiguity was mostly due to the mis-operation of the impedance elements of unfaulted phases. Therefore, it is apparent that an independent element which identifies the faulted phases without ambiguity can greatly improve the security of the relay for multi circuit line applications.

This chapter identifies the problem to be solved by an independent data processing element. Also, it discusses its nature and proposes integration of an artificial neural network to the distance relay to improve detection of faulted phases on the multi circuit transmission lines. The design details of the network with various selection criteria are described as well.

8.1 Problem Identification

A distance relay consists of several impedance and over current elements integrated together for making the trip decision under fault conditions. Each such element is a data processing unit that functions based on a selected set of voltage and current information. From the results of Chapters 5 and 6, it is apparent that this method of sectioned data processing has lead to difficulties in identifying certain fault conditions on multi circuit transmission lines. Proposed modification to the ground impedance computation in Chapters 5 and 6 is an attempt to enrich the information available to some processing units in order to enhance their functional capabilities. Although it has significantly improved the reliability of the relay, security still remains to be improved. An alternate approach is to process all locally available voltages and currents in a single unit to identify the faulted phases. This unit should be capable of optimally compressing the large number of voltage and current data, recognizing the pattern of the waveforms, and finally classifying as required, the faulted phases. It is also required that this unit be able to function for:

- all operating power levels and topologies of the system
- all fault types at various distances on the transmission line,
- various fault resistances and fault inception points.

Considering the non-availability of an explicit input-output relationship for the problem, its pattern recognition and classification nature, and the unit's expected wide domain of operation, an Artificial Neural Network (ANN) is proposed to perform this task.

Thus, for application to multi circuit lines, the ANN should analyse the bus voltages and line currents in real time to identify the faulted phases.

8.2 Artificial Neural Networks and their Properties

The Artificial Neural Network (ANN) architecture basically consists of input nodes, units called neurons in hidden and output levels which are inter-connected with branches of different weights.

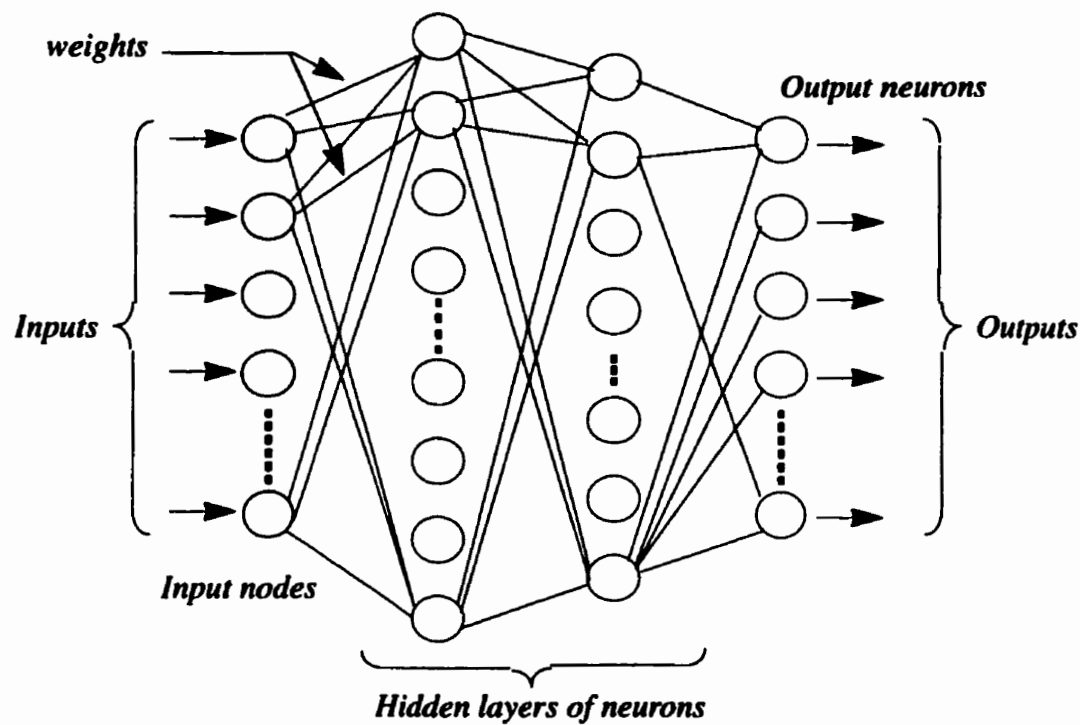


Figure 8.1: Typical structure of an artificial neural network.

Each neuron is a data processing element. An ANN can therefore be considered as a distributed information processing structure, interconnected with unidirectional signal channels. Each processing element branches out to many collateral connections,

carrying a weighted output to the next set of processing units. The processing taking place in a neuron is completely local and depends only on the present values of inputs to it. Therefore, neural networks are inherently parallel in their architecture, with an attractive feature of very low computational times. Its power, in various applications, also lies in its ability to capture very complex, implicitly related input-output maps given through a set of examples, rather than an explicit relationship. The shape of the map between inputs and outputs is altered by adjusting the weights through a learning process. A properly designed and trained ANN is able to generalize, rather than just recognize cases similar to those used as training data.

In general, neural computing has been found to be of great use in applications where a large number of statistically distributed inputs are to be optimally mapped to a few outputs through data compression and clustering. They also have been found to be tolerant to fairly high levels of noise or error in inputs [51- 52].

8.3 Applications of Neural Networks in Power System Protection

A considerable amount of work has been published on the use of artificial neural networks in the area of power system protection and recognition of transient events. This section discusses some such applications highlighting the important features of neural computing exploited in each case. It is also expected to draw attention to the type of network topologies and the input vectors used in each application.

Neural Network Approach to Fault Classification for High Speed Protective

Relaying [45]. The paper reports encouraging results on fault classification for a transmission line using neural networks. The classification of the fault is done after detecting a fault on the system. Therefore, the classification module, which consists of feed forward neural networks, is preceded by the detection module and is reported to be capable of classifying the detected disturbances to one of the ten possible types of short circuit faults on a three phase transmission line. It is also able to recognize no fault situations associated with disturbances. In the event a fault is detected, a second set of neural networks are used to further categorize it to an arcing or a non-arcing type of fault.

The inputs to the neural networks are reported as raw samples of voltages and currents of all three phases at the relay point. The network has been trained using the error back propagation rule with a large number of training sets generated off-line, using the NETOMAC (electromagnetic transient simulation software) simulation software. The test results presented, which are also based on off-line simulations, seem to demonstrate good accuracy and confirm the ability of the artificial neural networks to classify faults on transmission systems based on raw, sampled voltage and current data. It also demonstrates that the neural network topology needed for such applications are fairly simple and could result in very high speed relay techniques due to their parallel nature of computation.

Multi Neural Network Based Fault Area Estimation for High Speed Protective Relaying [46]. This paper reports continuation of the work reported in [45]. A third module of a neural network based fault area estimator is added to the protective relay described in [45]. It uses the knowledge provided by the fault classifier and the feature vectors, formed by voltage and current trails following a fault, as inputs to estimate the fault area. The three layer feed forward network used for this purpose is also reported to be trained using the error back propagation rule. The paper also emphasises the importance of careful selection of a feature vector of voltages and currents in order that the number of inputs be contained within manageable limits while all important information still is captured in the input vector. Here again the input feature vector consists of consecutive samples of voltages and currents of faulted lines. The fault area estimator provides the information on the zone the fault had occurred in so that the trip signal can be issued with appropriate time grading.

This application demonstrates the large error tolerance feature of the neural networks and their ability to define the transform within their weights, that extracts the important features of the input signals to map to the desired outputs. The comparison of the neural network outputs to the conventional techniques reports considerable improvement in the speed of fault area estimation. The authors also report the confirmation of the fact that the quality of the classification is not dependant on a transmission line model but rather the neural net topology, training set, and the choice of the learning rule.

Adaptive Distance Protection of a Double Circuit Line Using Artificial Neural Nets [43]. This paper describes the use of artificial neural networks to adaptively change the setting of a distance relay on a double circuit line, thereby reducing the necessary safety margins and increasing the selectivity of the relay which avoids over-tripping and sympathy trips. The distance relay usually computes the impedance based on the voltage and current information available, and trips if this computed value is less than a preset value of impedance. A non-adaptive preset value of the impedance is normally based on the worst case scenario and has a large safety margin. The neural network is used to compute a correction factor for the preset impedance setting based on the operating mode of the parallel transmission circuit and the power flow in the system. This estimation of the correction factor is done while the system is in the healthy state.

A feed forward neural network trained using the error back propagation rule is reported to perform satisfactorily for the selected system. Although details of the exact network topology and the inputs to the network are not made available, it is clear that the network is operated on line with information of voltages, currents, power flow and the operating mode of the parallel line. The network clearly is not intended for recognizing the transients of the system. However, it certainly reports to be able to characterise the steady state operating point of the system at a given instant.

The paper demonstrates the ability of using feed forward neural networks for adaptively setting trip zones on distance relays and their ability to map input output relationships which are of indeterministic nature.

The Application of Neural Network Techniques to Adaptive Auto-Reclosure in Protection Equipment [44]. This describes an application of a feed forward neural network to identify the transient and permanent faults on a system. The knowledge provided by the neural network is to be used for developing adaptive auto re-closing features of circuit breakers of a given system. The classification enables one to determine if the circuit breakers should be re-closed or not following incidence of a fault. In the case of transient faults, the neural network also determines the successful re-closing time depending on the nature of the fault. It is stated that the sending end voltage, which is directly affected by arcing faults, has sufficient features which are recognized by the neural network for successful identification of such faults.

The inputs are reported to be pre-processed as an attempt to simplify the neural network topology. The error back propagation rule has been used to train the network with batches of training data which have been produced off-line using the EMTP simulation program. The tests which had also been on a test set generated off-line had given 100% accuracy.

The findings reported in this paper demonstrate the use of a feed forward neural network with back propagation training rule and pre-processed input data vectors for recognizing the differences in transient events successfully.

Detect and Classify Faults Using Neural Nets [47]. The paper proposes the use of a neural network to detect and classify faults on a system with both short and mutually coupled transmission lines. The input vector is a sliding window of raw voltage and

current samples. It reports the use of a neural computation which embodies a special algorithm of classical pattern recognition, that does data self-organizing through unsupervised learning. This is also reported to be both trained and tested on off-line EMTP simulations of the network. The tests are reported to be more than 90% accurate.

The application exploits a strong feature of neural computing, which is the ability to produce a few outputs from a large number of inputs, a process of optimal topological mapping through functional approximations, data compressing and clustering. However, it does not use the standard feed forward architecture.

Impulse Test Fault Diagnosis on Power Transformers Using Kohonen's Self-Organizing Neural Network [48]. The work reported is an example of neural networks being used to identify transients due to faults on power transformers. The application uses Kohonen's self organizing neural nets which are usually capable of training unsupervised, and are also known to perform well in classification tasks. The classical approach to locating a failure occurring on a power transformer during impulse tests, are reported to require expert evaluators who base their judgment on reasoning related to concepts of travelling waves. Preliminary investigations and tests have shown that neural networks can successfully be applied to the classification of signals resulting from impulse tests on power transformers for fault diagnosis.

8.4 Selection of the ANN Architecture and Learning Rule

As a result of customizing networks for specific applications over the years of advances in the artificial neural network technology, many types of network architecture have been developed. It has repeatedly been observed that different network structures and learning parameters can substantially affect the performance with regard to generalization, learning speed etc. [40], [41]. Yet there are no analytical or empirical approaches which can reliably assist network designing for any application. Therefore, designing the optimal neural network with the most suitable architecture and topology for the problem in hand is not a straight forward task.

The selection criteria for the proposed type and topology of the neural network, to be integrated to the distance relay, for multi-circuit applications is largely based on

- reported similar applications and
- reported findings on the behaviour of various neural network architecture and topology.

By far the most popular choice for practical application is the feed-forward network architecture trained with error-back propagation rule. The studies described in section 8.3 directly relate to protection applications, and also demonstrate the successful use of ANN methodology in recognition of transient events [42- 48]. In these cases as well, the use of the popular feed forward network architecture is apparent. Therefore, the same architecture with error-back propagation training is considered suitable for

the single ended digital distance relay scheme proposed for multi-circuit applications, without much investigation of the other types.

8.5 Selection of Network Topology

8.5.1 General Network Structure

Although, ‘feed forward’ is a very large class of networks, a vast majority of applications use simple structures with one to three hidden layers and fully connected units. In addition, typically one learning rate is used for all connection weights. This leaves the choice of the number of hidden layers as the next unresolved design decision.

It is known that one of the major parameters that influence the generalization capabilities of a classifier neural network is its complexity [49]. The number of weights can be used as a measure of the network complexity for all practical purposes. Reference [50] reports results of investigations on comparative performance of three and four layer feed forward networks which are of comparable complexity. (Three layer networks are those with a single hidden layer. Those with double hidden layers are named four layer networks)

- Three layer networks report to have better generalization ability particularly when trained on an incomplete set of training data. This is perceived as a commonly encountered situation in most real world applications.

- Three layer networks on average have better ability to train than four layer networks of comparable complexity to training sets of various statistical distributions.
- Three layer networks do better classification or identification of a given problem, on average.
- Four layer networks train easily if the number of neurons in the two hidden layers are nearly equal in number.
- The initial choice of weights in a four layer network have been found to have more pronounced influence on the final network performance. This is attributed mostly to the problem of the weight vector being trapped in local minima, during the error minimization process. Thus, three layer networks are again found to be superior in their ability to find the global optimal in the training process, for the given problem, independent of the starter weights.
- Due to the difference in the structure the three and four layer networks have been found to parameterize a given problem differently.

The above reported general comparisons of the two topologies were the basis for selecting a single hidden layer structure for the proposed neural network.

8.5.2 Inputs and Outputs of the ANN

Most of the information needed to identify the disturbances and transients in a system is contained in the voltage and current waveforms. However, un-processed raw data

often tend to have noise and redundant information. Also, preprocessing input data simplifies the network and it then trains more quickly [44]. Therefore the fundamental frequency component of the processed voltage and current waveforms shown in Figure 8.2 were selected as one set of inputs to the ANN. The fault voltages and currents are not only dependant on the characteristics of the fault but also the pre-fault operating point of the system. Therefore, the inputs to the ANN at any given time should contain both fault and pre-fault information for accurate decision making. Thus, the ANN to be trained for detection of faulted phases was designed with 36 and 48 inputs for double circuit and six-phase configurations respectively. They are the magnitudes and phases of the fundamental voltages and currents, with and without a two cycle delay for each quantity as shown in Figure 8.2. Two cycles is about the minimum possible delay which avoids the mix of pre-fault and fault data in the same window during the intended decision making time.

It should be noted that this selection of inputs utilizes the data preprocessing units available in the impedance relay algorithm tested for double circuit, and six-phase applications without additional computational burden.

The ANN is required to detect faulted phases. Thus, six simple binary outputs each corresponding to a phase of the circuit were considered suitable for the task. A level 'high' indicates a fault on the phase whereas a level 'low' is for un-faulted operation. The analog output is quantized to derive the digital form. All outputs falling below or equal to 0.5 are classified as 'low' whereas those greater than 0.5 are defined as 'high'.

All inputs were considered necessary to determine the state of each individual phase on the circuit during a fault. But the network has to parameterize the fault differently to produce the outputs of faulted phases to that of un-faulted phases. For this reason, six parallel networks, one for each output, was considered suitable. All six networks share the same inputs and produce a binary output each, which corresponds to one phase of the circuit. The output indicates if the corresponding phase is faulted or otherwise.

The ANN shown in Figure 8.2 has full connection between inputs and hidden units. But only a sixth of the hidden units connect to one output. Thus, this operates as six parallel networks that share the same inputs.

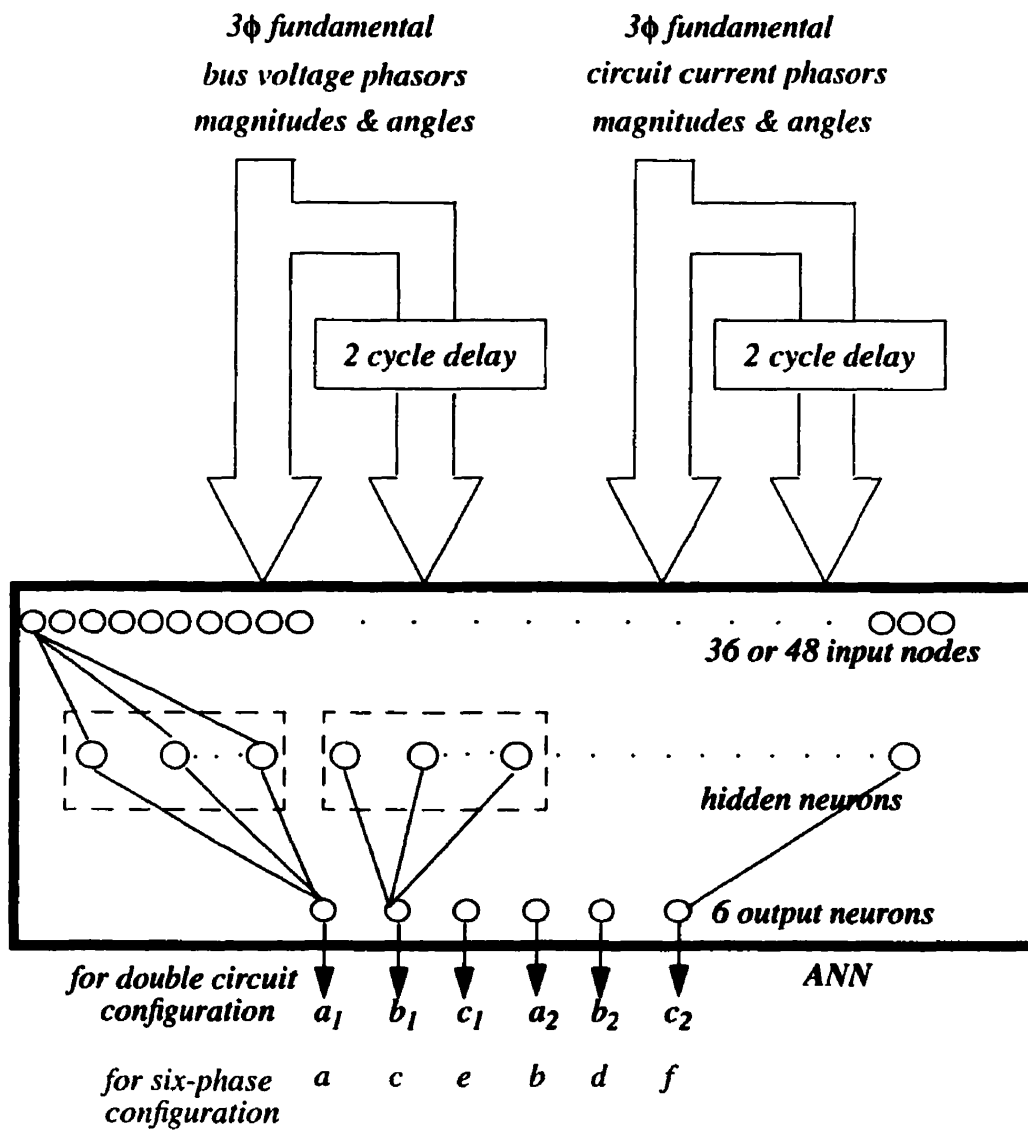


Figure 8.2: Input-output organization of the ANN.

8.5.3 Activation Function of the Neurons

The inputs shown in Figure 8.2 are simple nodes which simply pass the input to their output.

Any hidden or output neuron has its connections coming from the preceding layer and is connected through weights as shown in Figure 8.3. The output is determined by a differentiable, non-linear activation function. The activation of each of the inputs is multiplied by an associated weight. They are all added to one another and to a weighted bias to form the input to the firing rule.

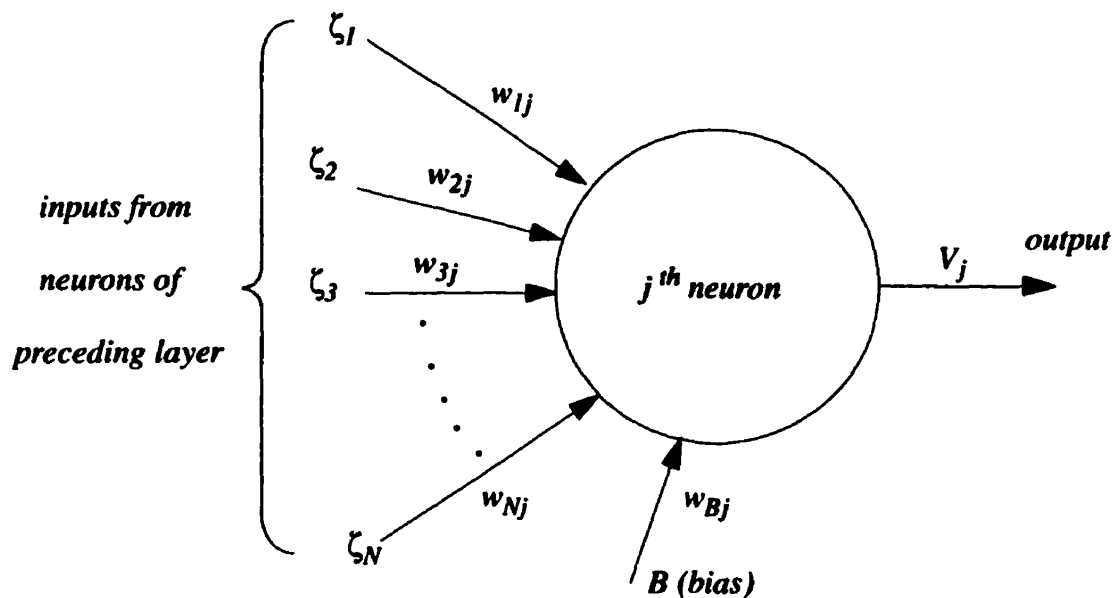


Figure 8.3: Input and Output connections of a neuron.

The firing rule used is a logistic function given in equation 8.1 [53]. The total activation of the j^{th} neuron in the hidden layer due to the input vector μ is given by:

$$h_j^\mu = \left(\sum_{i=1}^N w_{ij} \cdot \zeta_i \right) + w_{Bj} \cdot B$$

Therefore, the output of the j^{th} hidden unit is:

$$V_j = \frac{1}{1 + \exp \left\{ - \left[\left(\sum_{i=1}^N w_{ji} \cdot \zeta_i \right) + w_{Bj} \cdot B \right] \right\}} \quad 8.1$$

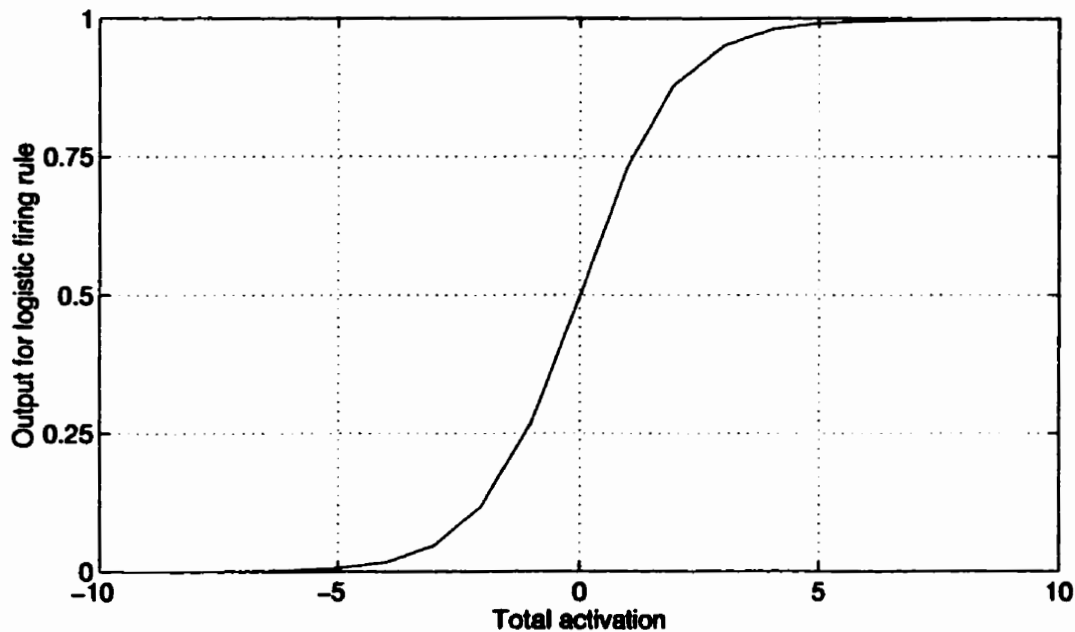


Figure 8.4: The characteristics of the hidden and output neuron activation function

The characteristics of the activation function show that the output function saturates to either '1' or '0' within a very small span of the input. For best characterization of the input vector, the total activation of every neuron in the network has to be within non-saturable limits. This criteria can be closely met with pre-scaling of the inputs within -

1 and 1. Since the worst case scenario is different for each input, close investigation of such situations was required to compute appropriate pre-scaling factors.

8.5.4 Learning Rule of the Network (Error Back-Propagation)

In order for a neural network to learn a certain relationship, data sets describing that relationship must be presented. Such a data set consists of the input vector and the associated target output vector. A good training set represents the full range of expected inputs and desired outputs. The network learns its connection weights by minimizing the square error of the outputs. The error is the difference between the actual and target outputs of the training sample.

Training initialises with a given set of seed weights to the network. It then trains by adjusting the weights of each connector propagating backwards. The technique exploits gradient information of the error function.

For an input vector μ the error function E_μ is:

$$E_\mu = \frac{1}{2} \cdot \sum_z (t_{\mu z} - o_{\mu z})^2$$

where $t_{\mu z}$ is the desired output of pattern μ and $o_{\mu z}$ is the actual network output. Error

E for all patterns in the training set is the sum of all pattern errors.

$$E = \sum_\mu E_\mu = E(w)$$

Minimisation of the error E is the task of a gradient search. The weight updating process follows the direction of negative gradient and the change in weight w_{ij} is as follows.

$$\Delta w_{ij} = -\eta \cdot \frac{\partial E}{\partial w_{ij}} \quad 8.2$$

Learning rate η , is the gradient or the rate of descent towards the minima in the error hyper plane, computed by the line search technique used. There are many line searching techniques [51] that can be used such as steepest descent, conjugate gradient, quasi Newton, based on the first derivative of the activation function.

From these many possibilities the ‘Conjugate Gradient’ minimization was chosen to train the network. This technique is proven to be suited for a variety of multi-dimensional minimization problems. More importantly, it is also a method which generally needs far less tuning on the initial learning parameters for fast and proper convergence [53].

Thus, for any given layer of weights, the required change in a weight for error minimization is a function of the learning rate, the input patterns, the target outputs and the existing values of weights. Thus, weights can be updated by recursive calculation of weight changes, moving backwards in the network from output layer to the input layer. This process is iterated until the total error reduces within a satisfactory limit.

8.5.5 Training and Test Input-Output Data Vectors

Training and test samples are an input-output vector, containing examples from the complete domain of pre-fault operating and fault conditions of the system for which the network is supposed to be functional. The training vector is presented to the network for adjusting its weights. When the network is trained the test data are presented for testing the network performance. For best performance of the network it is understood that the training set be representative of all possible fault and non-fault conditions of the system.

However, the parameters that determine voltage and current levels at measuring points, during faults on a transmission system, are continuous quantities. For the purpose of generating finite sets of training and test data, these parameters were quantized as discussed below

Distance to Fault. Faults simulated for generating the training data were at distances varying from 0% - 100% down the transmission line, in steps of 10%. Thus eleven discrete points on the transmission line were set up to simulate faults.

Fault Inception Point on the Waveform. Six equidistant points (by phase angle) of fault inception on a voltage waveform were chosen to generate data for the training set.

Fault Resistance. Three different fault resistances were considered They were 0Ω , 10Ω and 20Ω . The highest ground resistance considered is approximately 50% of the total line impedance.

Type of Faults. Restricting the study to only short circuit faults the number here is discrete, finite, and manageable without further simplification. Table 8.1 shows the possible types of faults on a double circuit or a six phase transmission line.

Quantization process of continuous variables reduces the possible infinite number of faults to a finite set of:

$$11 \times 6 \times 3 \times 120 = 61,280$$

cases for a given pre-fault operating point. However, only a randomly selected 1000 faults made up the initial training data set. Another 1000 cases contributed to the test data.

Table 8.1: Possible types of faults on a double circuit or six phase transmission line

Fault type	possible combinations
<i>single line to ground</i>	<i>6</i>
<i>double line to ground</i>	<i>15</i>
<i>three line to ground</i>	<i>20</i>
<i>four line to ground</i>	<i>15</i>
<i>five line to ground</i>	<i>6</i>
<i>six line to ground</i>	<i>1</i>
<i>double line</i>	<i>15</i>
<i>three line</i>	<i>20</i>
<i>four line</i>	<i>15</i>
<i>five line</i>	<i>6</i>
<i>six line</i>	<i>1</i>
Total possible combinations	120

The voltages and currents on a network, resulting from a fault, depend on its pre-fault operating point as much as on the conditions of the fault itself. However, information of a given operating condition can be readily made available to the relay unit. Therefore, a set of network weights is trained only within a small range of pre-fault operating conditions. Many such sets of weights may then be required to make the network functional for the complete domain of operating conditions. Adaptive on-line switching between different sets of weights for different ranges of pre-fault operating conditions considerably reduces the complexity of the task assigned to the network. This in turn reduces the complexity of the network structure and the training process. Changing the point of pre-fault operation changes the values of the input data, but does not change the nature of the problem itself. Therefore, the network structure that trains for a given operating range of the system is almost guaranteed for its trainability for any other range of operating conditions. However, due to the differences in the magnitudes of the inputs, at various operating conditions, the same weights can not be expected to give the best of performances in the entire operating domain. Nevertheless, it is worth while testing a trained set of weights for a wider range of operating conditions. Appropriate adjustment of simply the pre-scaling factors could improve the performance within some ranges.

The following are some other parameters that influence the voltages and currents on the system during a fault. They also determine the pre-fault operating point of the transmission system.

Direction of Power Flow. Two separate sets of training and test data were generated for two directions of power flow, into (also referred to as ‘forward’ direction in this document), and out of (reverse) the relay.

Pre-Fault Power Flow. Only the operating power level of 90% of the system rating was included in the training set presented to the network.

Source Impedances. Training data was only generated for one set of source impedances. However, the network was tested for stronger and weaker sources.

Table 8.2: Source Impedances of the Transmission Network

Impedance	McCalmont	Springdale
<i>Positive Sequence</i>	$7.14 \angle 83.38^\circ$	$3.332 \angle 80.51^\circ$
<i>Zero Sequence</i>	$17.72 \angle 73.88^\circ$	$10.474 \angle 74.36^\circ$

8.5.6 Training and Test Data Generation

Training and test data were produced on the PSCAD/EMTDC™ simulation tool for the double circuit model described in section 4.1. The model was set up to run to its steady state operation of 90% rated forward power flow, and simulate any of the possible 61,280 types of faults.

The network is meant to detect the faults on the fly as they appear. Therefore, it has to be presented with both no-fault and fault data for training. From every simulated case, a 2.5 cycle window of sampled input-output data vectors contributed to build the complete training set. Half a cycle of the window consisted of the pre-fault data,

whereas the rest were of the fault. All the input data are in their phasor form. Thus, with a sampling rate of 16 samples per/cycle, 40 data vectors added to the training set from each simulated fault.

8.6 Conclusions

The fundamental design details and the basic setting up to train the artificial neural network that is expected to aid the distance relay on a double-circuit transmission configuration is established. Reported applications of neural networks and the finding of the behaviour of neural computing techniques are used to keep the network structure simple.

The neural network, which is expected to operate in parallel with the rest of the impedance elements, uses the fundamental voltage and current phasors derived from the same data pre-processing units of the APT relay. Because the faulted phases will then be detected by the two independent units, the impedance relays and the neural network, a simple trip logic can be developed to identify those phases which are detected as faulted by both units. Thus, a more confident trip decision, which will eliminate most of the sympathy trips due to the mis-operated impedance elements of the distance relay, can be made. Although the trip logic to be used is not discussed in this thesis, the idea of using the neural network is to simplify the needed trip logic.

CHAPTER 9

PERFORMANCE OF THE ANN TRAINED FOR DOUBLE CIRCUIT LINE APPLICATION

The initial design details of the artificial neural network that is proposed to aid the distance relay functions on double circuit or six phase configurations were established as discussed in CHAPTER 8. This chapter discusses exclusively the training process of a candidate feed forward network structure to perform the intended task of recognizing faulted phases on a double circuit transmission line configuration. It also presents the testing criteria used, which defines a successful and non-successful diagnosis of faulted phases, and finally the detailed performance test results of the ANN under various conditions.

9.1 Training for Double Circuit Transmission Line Application

9.1.1 Scaling of Input Data

A detailed investigation of the voltages and currents for different worst case fault conditions was carried out to decide on scaling factors which confine the input magnitudes within -1 and 1 for the activation function used (discussed in section 8.5.3). Table 9.1 shows the inputs of the ANN and their respective scaling factors.

Table 9.1: ANN inputs and their scaling factors for double circuit application.

Input description	# of inputs	Scaling factor
<i>Magnitudes of the fundamental bus voltages in kV Phases a, b and c (phase-ground)</i>	3	1/250
<i>Phase angles of the fundamental bus voltages in radians Phases a, b and c (phase-ground)</i>	3	1/ π
<i>Magnitudes of the fundamental currents for circuits #1&2, in kA Phases a1, b1, c1, a2, b2 and c2</i>	6	1/18
<i>Phase angles of the fundamental currents for circuit #1&2, in radians Phases a1, b1, c1, a2, b2 and c2</i>	6	1/ π
<i>2 cycle delayed Magnitudes of the fundamental common bus voltages in kV Phases a, b and c (phase-ground)</i>	3	1/250
<i>2 cycle delayed Phase angles of the fundamental common bus voltages in radians Phases a, b and c (phase-ground)</i>	3	1/ π
<i>2 cycle delayed Magnitudes of the fundamental currents for circuits #1&2, in kA Phases a1, b1, c1, a2, b2 and c2</i>	6	1/18
<i>2 cycle delayed Phase angles of the fundamental currents for circuits #1&2, in radians Phases a1, b1, c1, a2, b2 and c2</i>	6	1/ π

9.1.2 Network Structure and Training

The successful performance of a neural network lies in its ability to generalize the problem well. Generalization ability is influenced by the size and efficiency of the training set, the network structure and the complexity of the problem itself [52].

Clearly, the two factors to be manipulated for best results are the training set and the number of hidden units in the neural network. A large number of weights in comparison to the amount of information presented in the training data, tends to lead the network to memorize training data. Memorisation is essentially a look up table formed through the training vectors, which implies that the input-output mapping is not smooth enough for generating acceptable outputs for inputs other than those in the training set. On the other hand, the number of weights need to be large enough to parameterize the characteristic features of the training patterns that produce outputs with acceptable accuracy.

The training set consisting of one thousand randomly chosen fault cases, each contributing 40 pattern vectors, was initially chosen as the training set to construct the neural network for double circuit application. The faults in the training set were simulated maintaining the same pre-fault operating power flow of the transmission system. However, the initial attempts of training using this training set, with various numbers of hidden neurons, proved to be ineffective due to the excessive amount of redundant information. This resulted in poor convergence of the error function and prolonged training durations.

Therefore, selecting an efficient training set which well represented the problem was another trial and error process that had to be done hand in hand with choosing the suitable number of hidden units for the network.

The network that trained with acceptable accuracy for double circuit application has 20 hidden units per each output neuron. As discussed in section 8.5.2, the complete network that performs successfully to diagnose the faulted phases on the *McCalmont-Springdale* double circuit transmission system therefore required 32 inputs, 120 hidden neurons, and 6 output neurons.

The set of faults which resulted in zero sequence currents above a certain threshold for the two independent circuits as well as for all six phases, qualified as a satisfactory training set. These cases were picked from the thousand faults that made up the initial training set.

For pattern-classification using large redundant data bases, the pattern-by-pattern approach of training tends to be orders of magnitudes faster. However, in the process it also has the tendency to unlearn or forget the patterns presented earlier. Therefore, the technique of batch learning was adopted in this case even at the expense of longer training times.

The neural network simulation tool used, XERION, was configured to train the designed feed forward network using the PSCAD/EMTDCTM generated voltage and current information. The interfacing component described in section 3.2.12. converted the sampled and scaled voltage and current inputs to the XERION compatible format.

The entire training set was generated through repetitive execution of the fault cases on PSCAD/EMTDC models of the transmission system.

9.2 Testing of the Neural Network

The neural network simulator provides a batch testing feature to a given test data set. In that, the total error for the entire test data set is computed as an estimation of the ANN performance. Clearly such a number, which is intended for dynamic performance, is largely inadequate for evaluation of the network performance. Therefore, the ANN was modelled on the PSCAD/EMTDC package for testing its performance on a case by case basis, for a chosen set of test data.

9.2.1 Criteria for Successful Diagnosis of Faulted Phases

Performance of the neural network is considered successful if the network outputs corresponding to the faulted phases go 'high' within two cycles from the inception of the fault. However, in the cases where 2 or 3 phases of a circuit are faulted, 2 or 3 outputs turning 'high' is considered successful performance. For example, if only the outputs for phases a_1 and b_1 were 'high' for a $a_1-b_1-c_1-g$ fault, the network outputs are considered valid. This validation is based on the fact that, having two faulted phases to ground on a circuit makes three pole trip of the circuit compulsory.

For the same reason, ANN detecting all three phases as faulted for a double line to ground fault is valid as well. However, if the network detects all three phases as faulted for an inter-circuit double line fault, it is considered a mis-operation. In such a situation, single pole tripping may really clear the fault and allow for two phase

operation of the circuit, whereas mis-detection of three faulted phases violates such flexibility.

In the event that at least one phase of the circuit is detected in its 'high' state for longer than half a cycle continuously, the network is considered to have recognized a fault with sufficient confidence. In response to such a detection, the delayed inputs of the voltages and currents to the network are frozen. This is done in order to speed up the rest of the decision making process of the network by helping to maintain the pre-fault operating point information unchanged.

9.3 Performance of the Trained Artificial Neural Network.

Figure 9.1 shows the block diagram of the digital distance relay with its neural computing module proposed for double circuit application. The diagram shows the data processing modules and decision making elements of the digital distance relay. The logic that combines the trip signals is not shown.

In this section, simulation results for a number of faults are presented to demonstrate both successful and mis-operations of the artificial neural network which operates in parallel with the rest of the impedance elements in the distance protection scheme. Other details concerning its performance on the double circuit transmission configuration are also discussed.

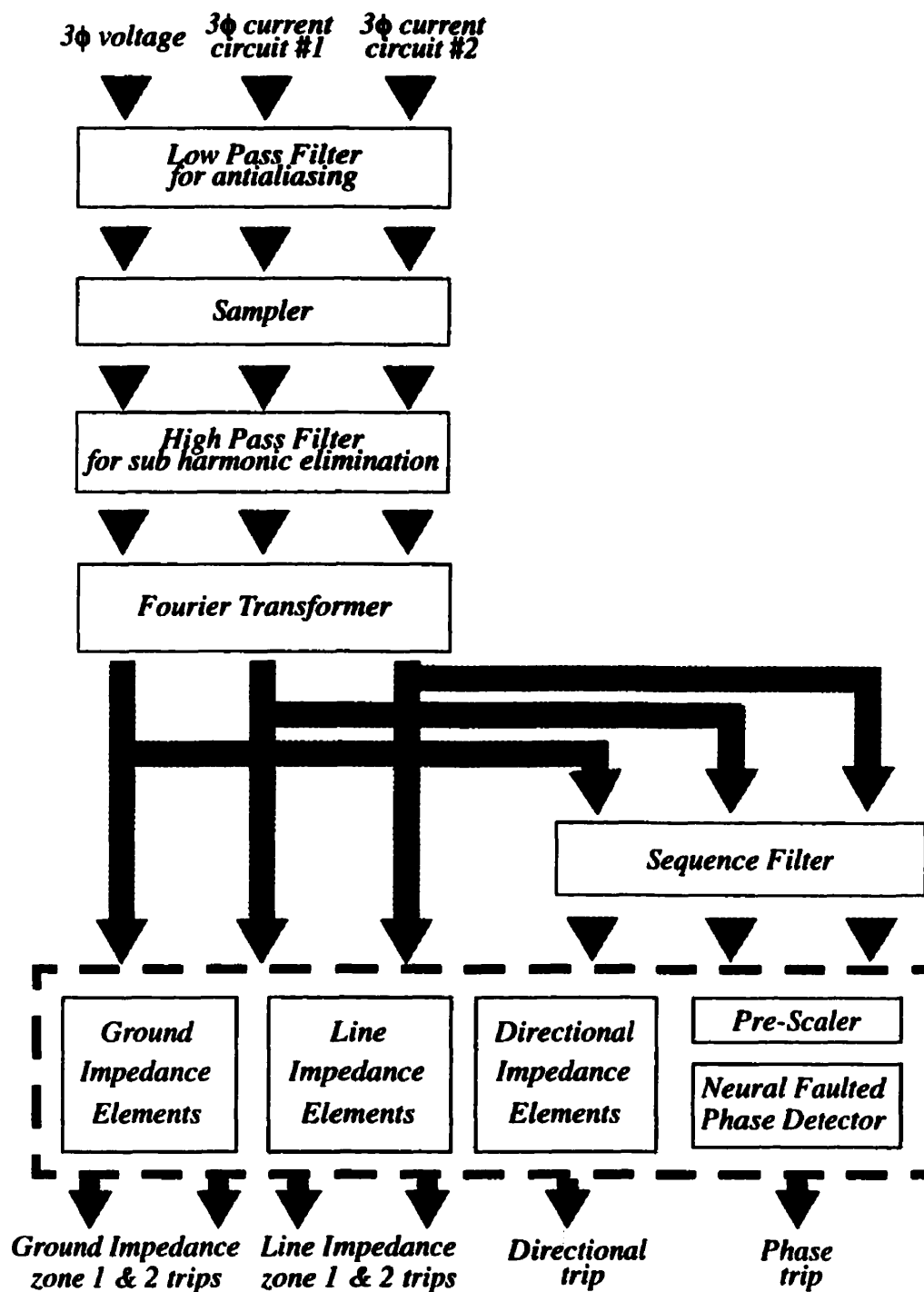


Figure 9.1: Block diagram of the relay elements and the neural faulted phase detector.

9.3.1 The Successful Response of the ANN to a Simple Line to Ground Fault

Figure 9.2 shows the outputs of the artificial neural network against the target outputs for a simple a_1 -g fault at 10% distance to the measuring point. The fault is simulated while the system is operating at the 90% rated power level. The time axis is marked zero for the time of incidence of the fault. The target output for phase a_1 is indicating a 'high' state immediately following the fault. The ANN output for phase a_1 goes 'high' within less than 1/2 a cycle of the fundamental frequency, and stays 'high' continuously denoting a fault on phase a_1 . The rest of the outputs remain in the 'low' state as expected.

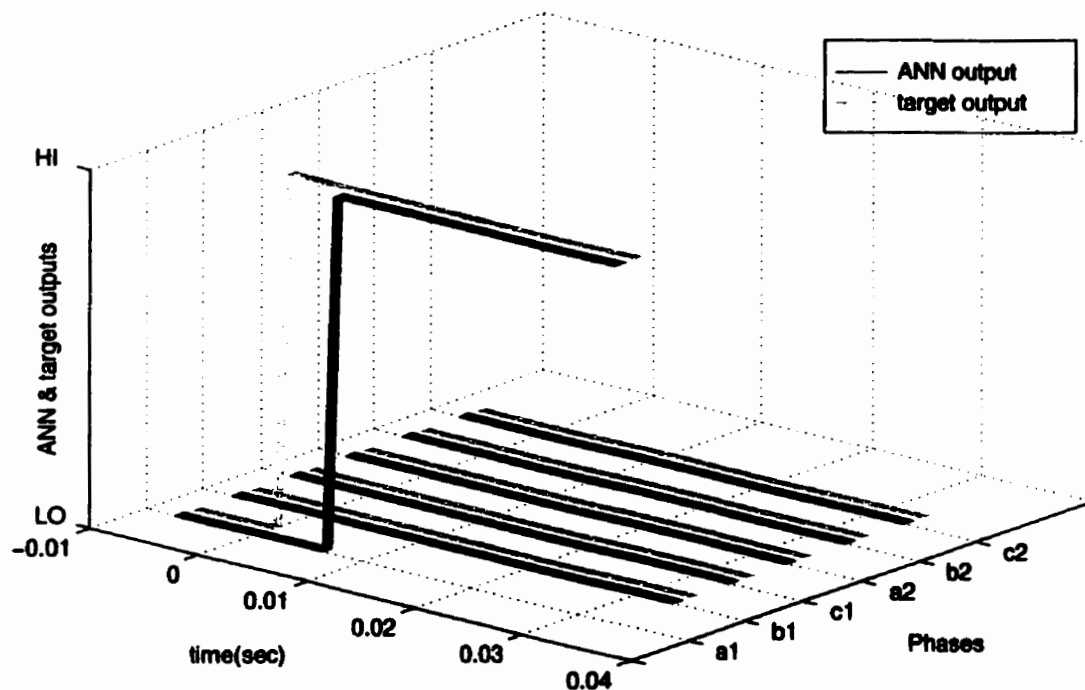


Figure 9.2: The ANN and target outputs for a phase a_1 -g fault at 10% distance to the measuring point.

9.3.2 ANN Generates Short Duration 'High' Flags

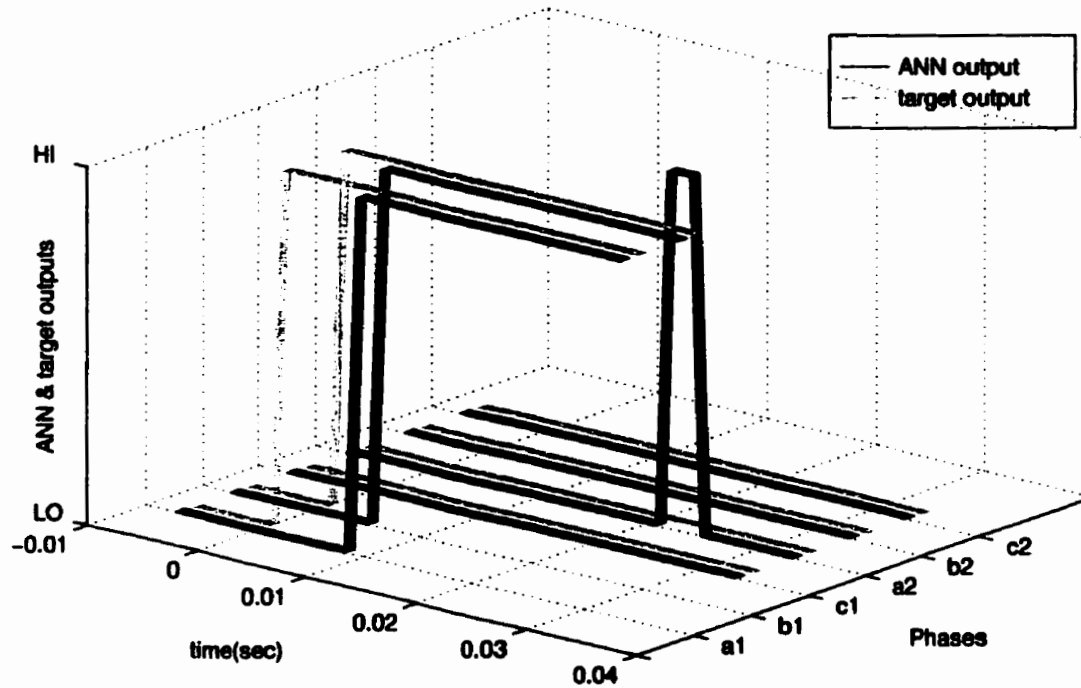


Figure 9.3: ANN and target outputs for a a_1 - b_1 -g fault at 10% distance from the measuring point.

Figure 9.3 shows the ANN response to a a_1 - b_1 -g fault. The faulted phases a_1 and b_1 are detected by the ANN within half a cycle. Also, about 2 cycles following the fault a short duration 'high' flag appears for the output of phase a_2 , which only lasts for less than 5 samples. This type of mis-operation is observed in some other fault situations as well. In most such cases the high pulse only lasted for less than five samples. Observing the inputs to the ANN during these sudden short high pulses revealed that, the sudden rapidly changing nature of the phase angle inputs was the dominant cause.

The rapid variations are the changes of angles from 360^0 to 0^0 . However, it was also observed that such mis-operations occurred even when all inputs were smoothly varying, and they can simply be attributed to the ANN error itself, which can easily be rectified with a block averaging technique.

The discontinuous nature of the phase angles may be eliminated by using the cosine or the sine function of the angle as the input. This not only provides smooth continuity, but also the required pre-scaling to the inputs. Although such a pre-scaler introduces additional non-linearity to the problem, it may improve the dynamic performance of the ANN. However, this is an idea that was not experimented in this thesis.

Pulses of short duration can be ignored in the trip logic by attaching a timer with each ANN output. Thus separating the more confidently detected faulted phases from the less confidently detected ones is not an impossible task. This is especially true when the short pulses occur about a cycle later than the rest of the high outputs, and therefore the influence of the mis-detection on the final trip decision is minimal. Therefore, adding to the performance criteria, the ANN detecting the faulted phases, even with short high pulses that do not last longer than 6 samples, is considered a successful operation.

9.3.3 ANN Response to Increased Distance to Fault

In order to investigate the general trend of the network response time for varied fault distances, the same fault was simulated at different locations on the transmission line.

Figure 9.4 shows the phase- a_1 output of the network for the same a_1 -ground fault at distances 10%, 40% and 80% respectively against the target output.

The ANN responds with a delay of about 6 samples for the fault at 10% distance. The response time is increased to 7 and 8 samples for distances 40% and 80% respectively. This is a typical example of the general trend of ANN response time with the distance to fault. Faster response is observed for close-up faults, the same as for the impedance elements of the distance relay.

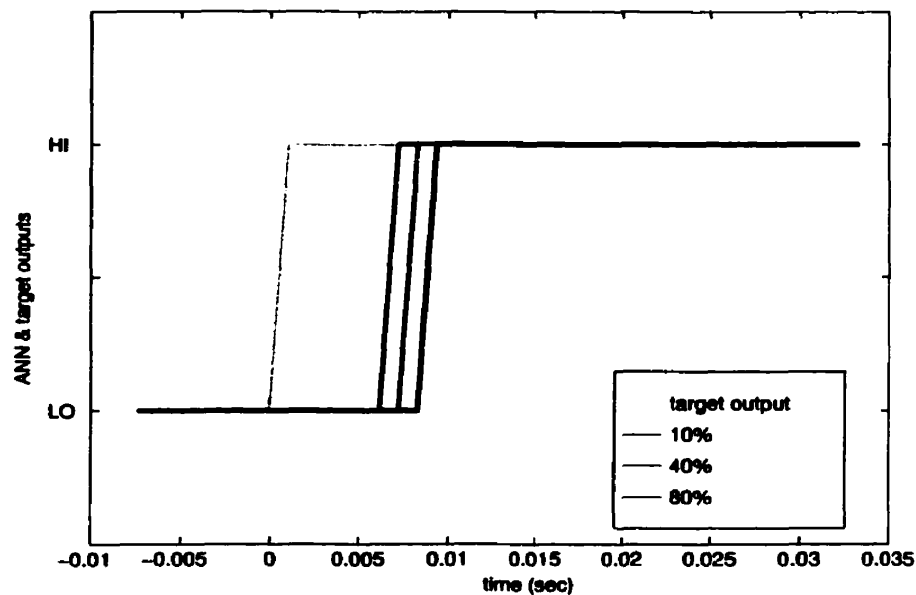


Figure 9.4: Comparison of the response time of ANN output for a_1 -g faults at different locations on the transmission line.

Figure 9.5 shows the voltage and current waveforms at the relay point for the same a_1 -g fault, for different fault distances. The smaller changes in the currents and voltages explain the longer response time of the ANN for remote end faults.

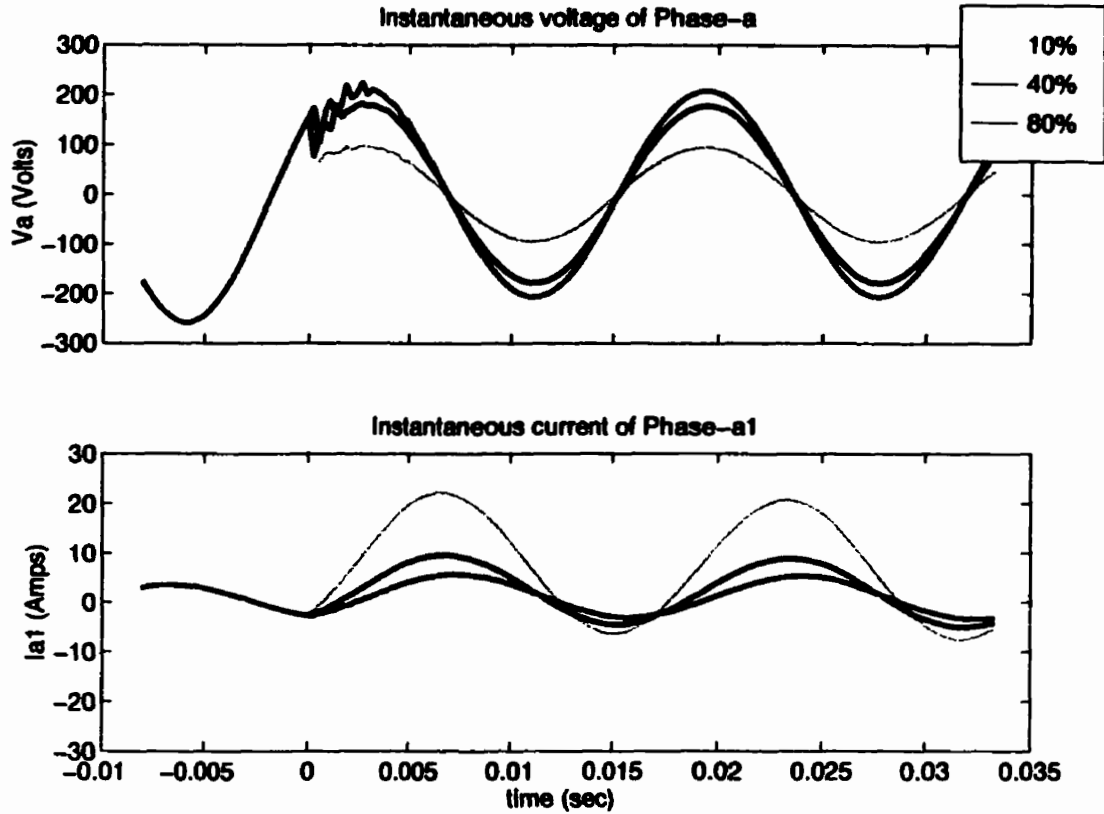


Figure 9.5: Instantaneous voltage and current of the faulted phase for a_1 -g fault at 10%, 40% and 80% distances.

9.3.4 ANN is Insensitive to the Fault Inception Point on the Wave

The neural network outputs were found to be almost independent of the point of fault inception on the wave. The fault a_1 - b_1 - c_2 -g has three faulted phases. Figure 9.6 shows the outputs for the faulted phases, during the a_1 - b_1 - c_2 -g fault, with onset at six different points on the wave. The outputs of the unfaulted phases stay 'low'

continuously. This is a typical response which makes it apparent that the outputs are unchanged for varied fault inception points.

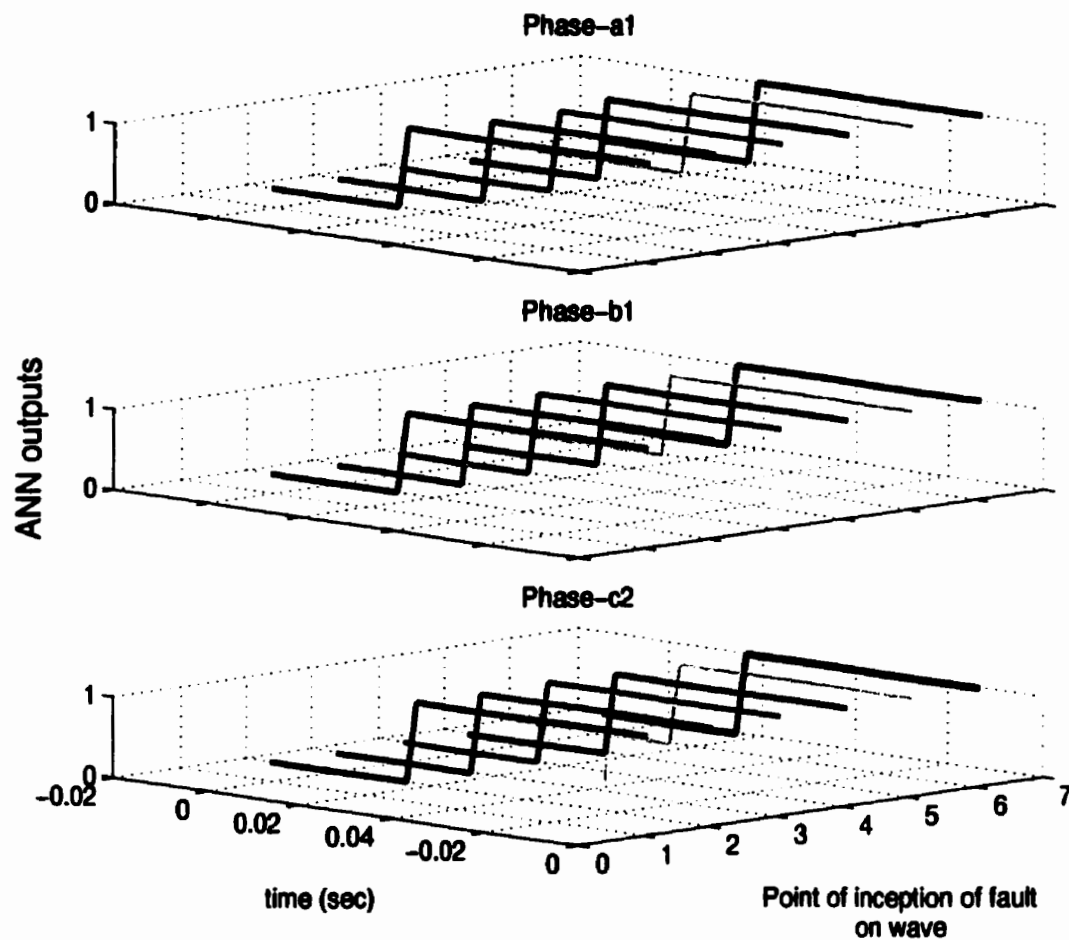


Figure 9.6: ANN outputs for faulted phases during a_1 - b_1 - c_2 -g fault, with fault inception at six different points on the wave.

The exponentially decaying dc component following a fault is very much dependent on the point of fault inception. However, the inputs to the network are the fundamental

voltages and currents of the system at the relay point. Thus, this parameter, justifiably, has little or no influence on its performance.

9.3.5 Influence of Fault Resistance on the ANN Outputs

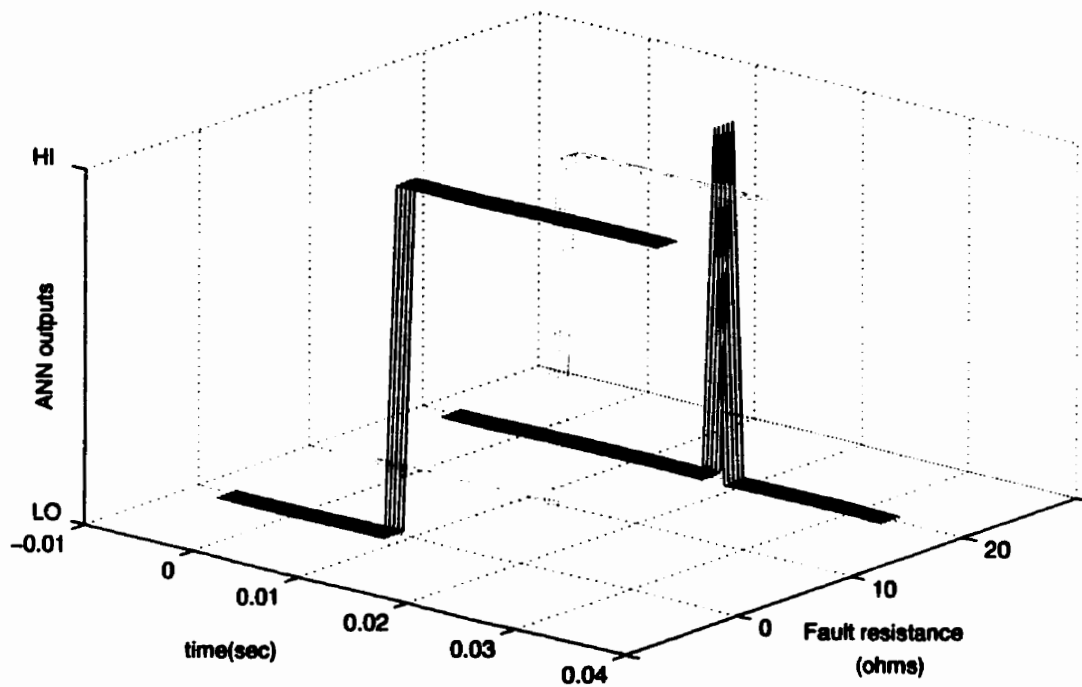


Figure 9.7: ANN output of phase-a₁ for a a₁-g fault with 0, 10 and 20 Ω fault resistance respectively.

As can be seen in Figure 9.7, the fault resistance has a distinct influence on the ANN output. The ANN output indicates the fault 9 sampling intervals following the incidence of the fault, for zero fault resistance, whereas it is delayed by 4 more sampling intervals when the fault resistance increases to 10 Ω . Further increase to a 20 Ω fault resistance results in a non-sustained 'high' pulse for the faulted phase

output. According to the test criteria the latter is considered an unsuccessful operation of the ANN.

The voltage and current waveforms following a fault largely depend on the fault impedance and it is reflected in the neural network outputs.

9.4 ANN Test Results

As discussed in section 8.5.5, two separate sets of weights were trained for forward and reverse power flows on the double circuit transmission system. The training data for both networks were generated maintaining a pre-fault operating condition of 90% rated power flow.

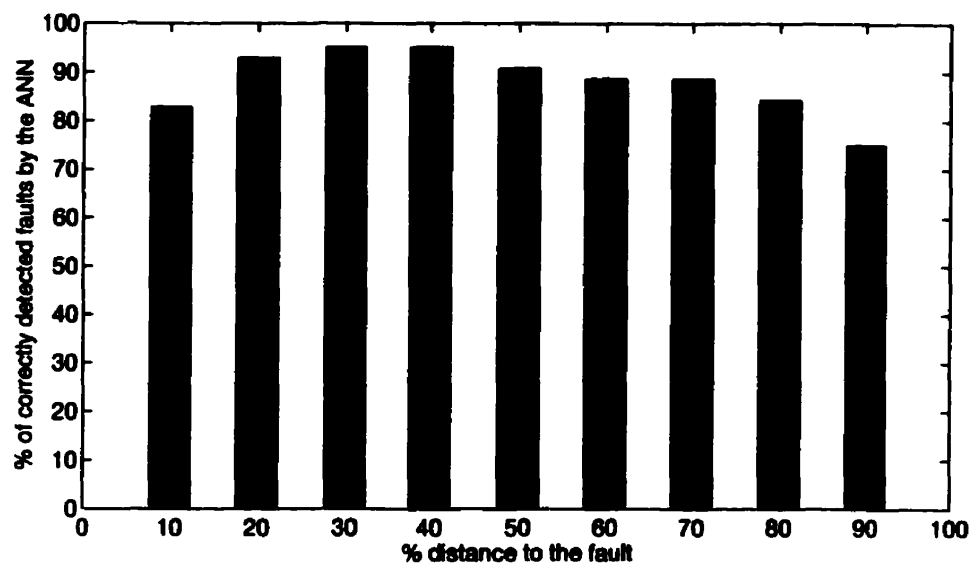
This section discusses their general performance under various fault situations. The performance investigations are based on a large test set of a thousand randomly generated fault cases. The test set was ensured not to consist of any fault cases from the training set, in order that the networks' generalization ability be properly tested.

9.4.1 ANN Performance for Different Fault Locations

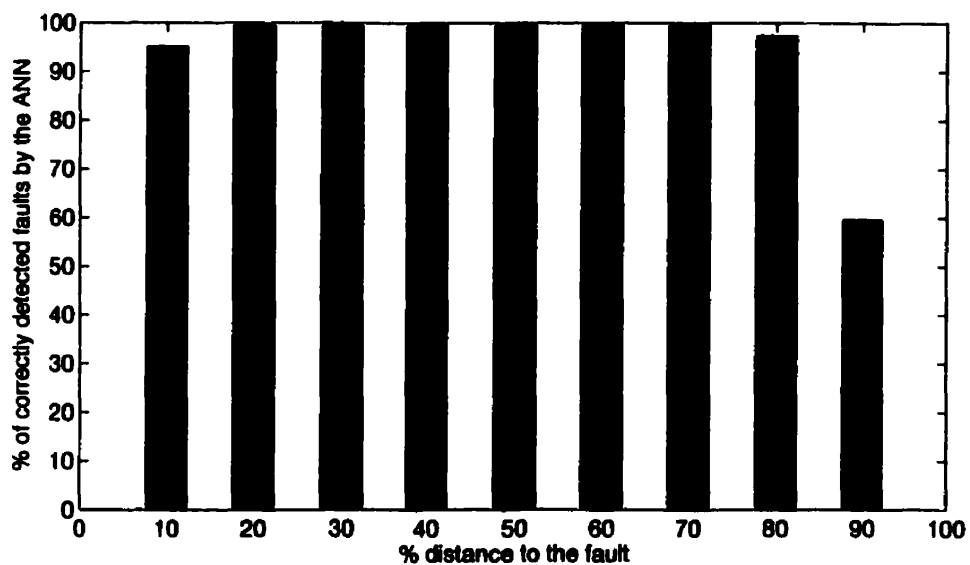
The artificial neural network was tested for its performance, maintaining the same pre-fault power flow on the transmission line. A thousand test faults simulated were at distances varying from 10% to 90% along the transmission line. Figure 9.8, shows the percentage of successful operations by the ANN, for faults at various distances. It is seen that the best performance of the ANN is when the fault occurs close to mid-way of the transmission line. The performance for remote faults deteriorates due to changes

in the inputs to the ANN being of low magnitudes. Thus, it fails to accurately pick all the faulted phases on the system. This however, is not a critical problem as the remote end relay can be expected to detect those faults with higher accuracy. The close up faults tend to cause large changes in the inputs of the ANN. Such large changes in inputs seem to appear to the ANN as much more severe faults than they are. Therefore, close-up faults cause the ANN to detect healthy phases as faulted as well. Thus the deteriorated performance of the ANN for close-up faults is not a reflection of poor reliability but of poor security.

It is also evident that the overall performance of the network trained for reverse pre-fault power flow is better than the network trained for forward power flows. Although the same network structure, selection criteria of training set, and the test criteria were maintained the same for both, there is a fundamental difference in the inputs to the two networks during a fault. The network used for forward pre-fault power flow, experiences a power reversal at the inception of fault, and the one used for reverse power flow does not. The differences in the performances of the two networks is attributed to this reason. However, the overall distance relay scheme on the transmission network will have two relays on either end, one on forward power flow mode and the other on reverse. In which case they can compensate for each others performance. Pre-scaling the phase inputs to the network using sine or cosine functions may help eliminate the differences in the two networks as well. However, as mentioned before, it is only a technique foreseen as a possible improvement to the network performance, and was not experimented with during the course of the project.



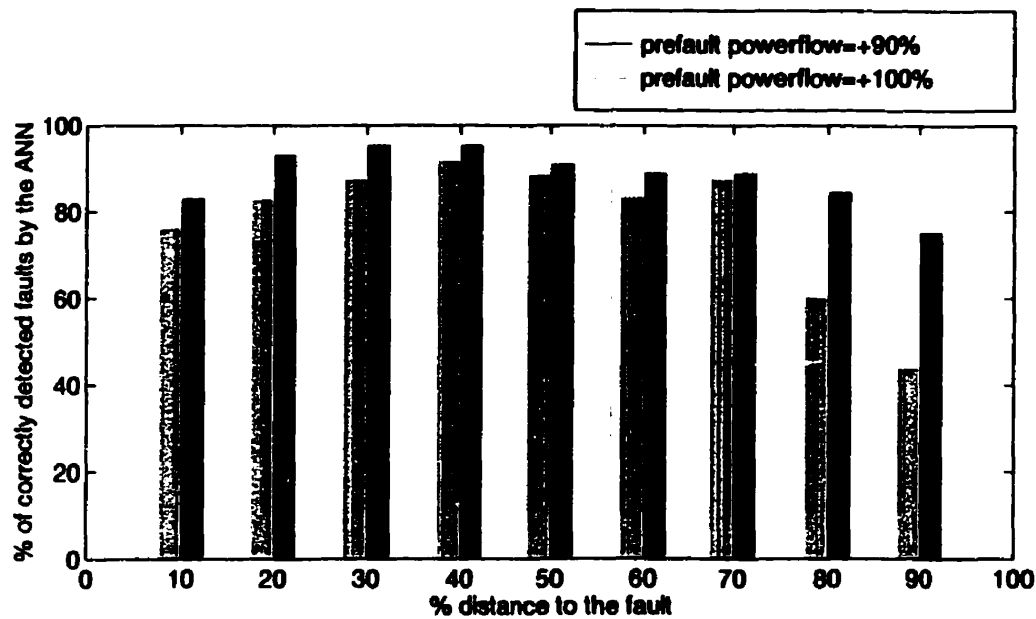
(a) Network for forward pre-fault power flows



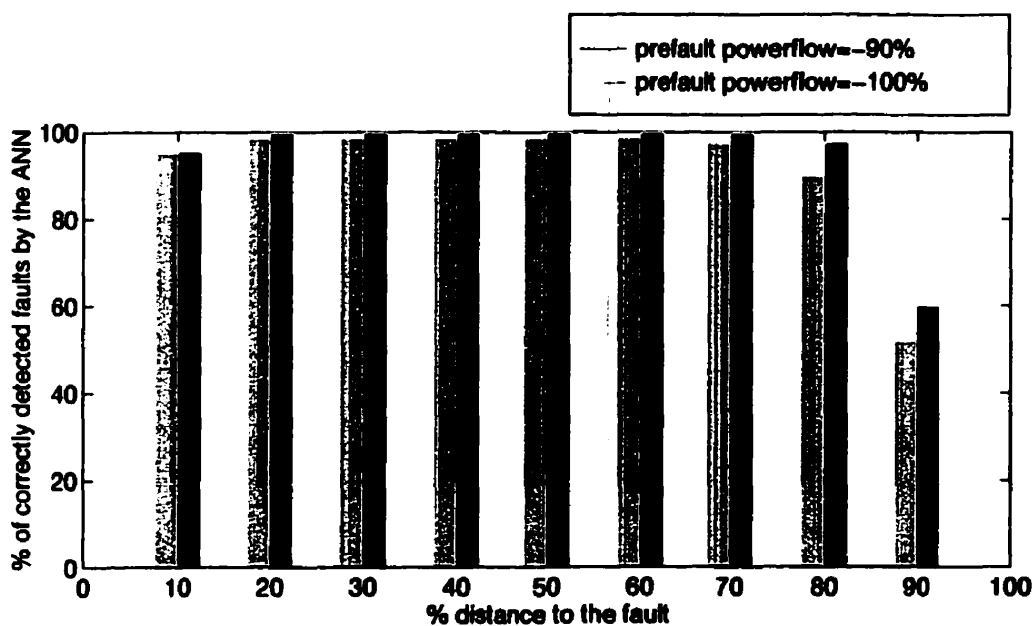
(b) Network for reverse pre-fault power flows

Figure 9.8: ANN performance variation with distance to the fault: (a) Network operated for forward pre-fault power flow. (b) Network operated for reverse pre-fault power flows.

9.4.2 ANN Performance for Different Pre-Fault Operating Powers



(a) Network for forward pre-fault power flows



(b) Network for reverse pre-fault power flows

Figure 9.9: Comparison of ANN performance for pre-fault power flows of 90% and 100%. Same network weights are used.

Although the network weights were trained with faults simulated while the transmission system delivered 90% of the rated power, it was also tested for its performance for other levels of prefault operating power flows. Changing the pre-fault operating point mostly scaled the inputs to the ANN proportionately and therefore, the weights trained for 90% power level were still able to perform with some accuracy for power flows around it. Figure 9.9 demonstrates the network performance for a 10% increase in the prefault power flow levels. Figure 9.10 shows the general performance for various other prefault operating points, as the distance to fault varies. The performance analysis is based on a sample of a thousand test fault cases at each level of pre-fault power flow. The tests are performed separately for forward and reverse neural networks.

The performance analysis in Figure 9.10, shows very poor performance for 40% prefault power flow levels. Therefore as suggested at the design stage, a second set of weights for lower power levels is necessary.

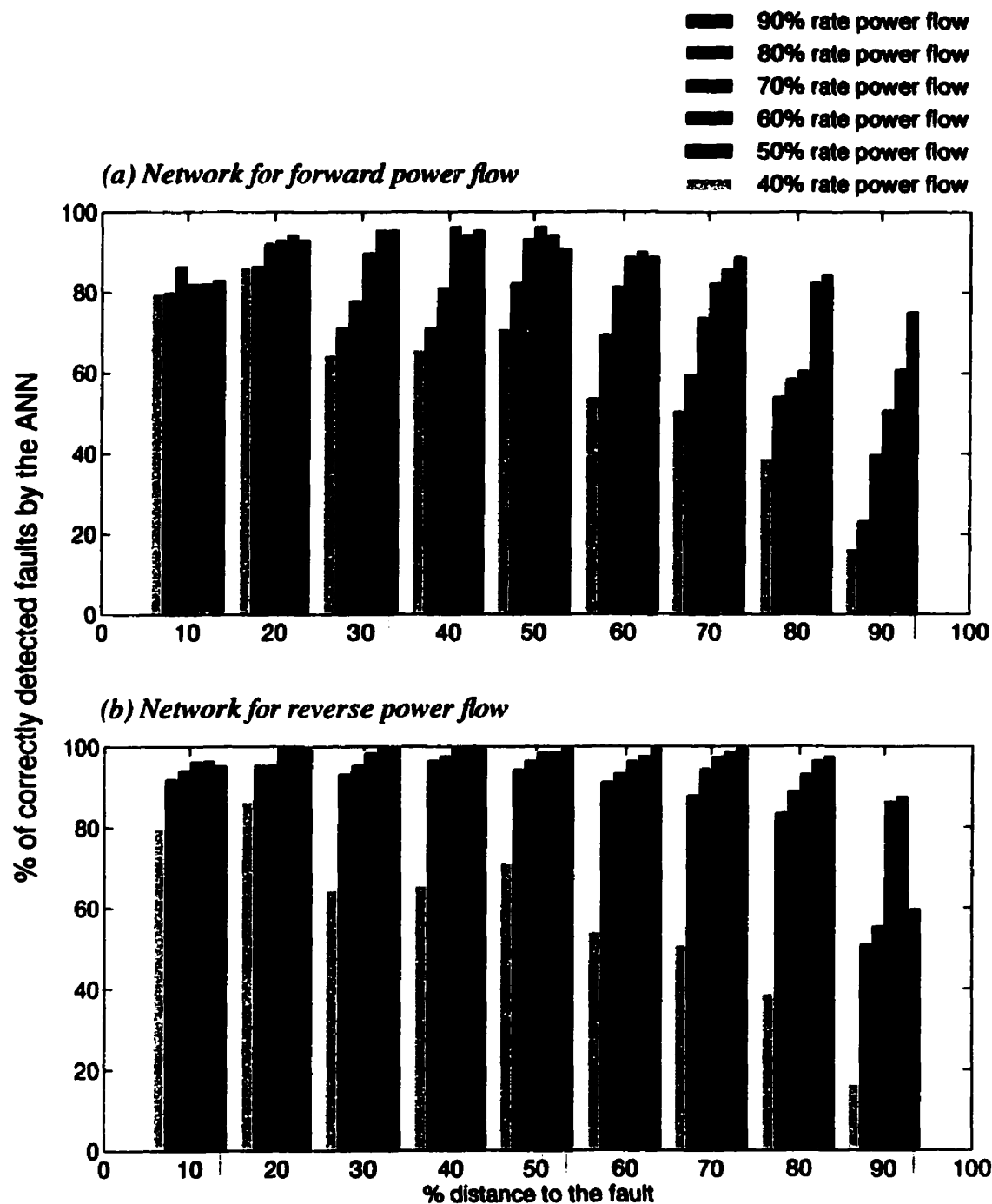


Figure 9.10: Comparison of ANN performance for pre-fault operating levels of 90%, 80%, 70%, 60%, 50% and 40% of rated power flow.

9.4.3 ANN Performance for Different Fault Resistances

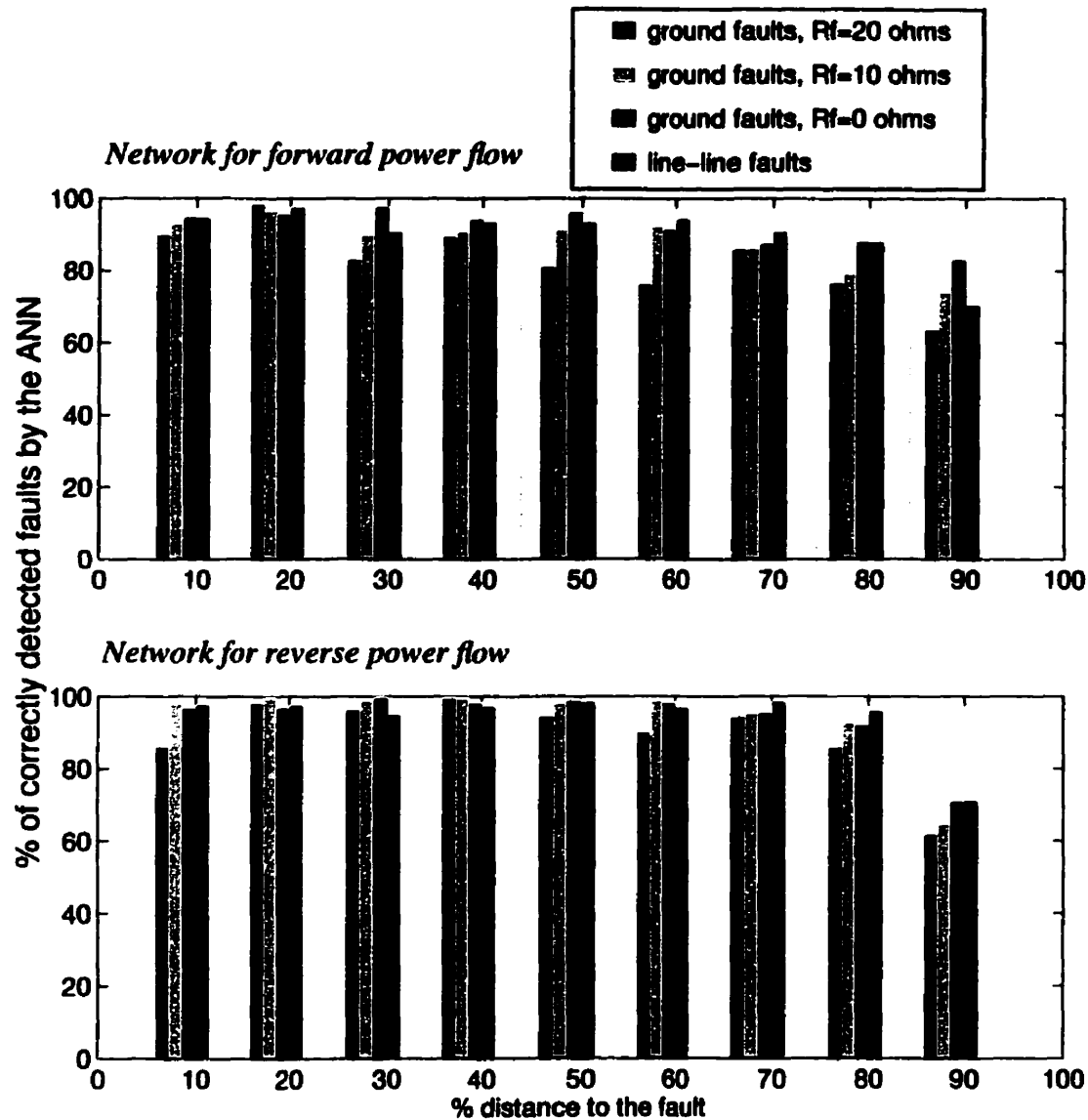


Figure 9.11: Neural network performance for line faults and ground faults of various fault resistances.

In section 9.3.5, it was shown that the network response times were increased with the increase in fault resistance. The same trend is observed in the general performance analysis, where the performance drops with the increase of fault resistance. The

percentages are based on the network performance for all pre-fault power levels of 100% to 50% of the rating, i.e. is a total of six thousand test cases, for each network.

Note that for line-line faults and ground faults of zero fault resistance, the network performances are fairly accurate except for remote end faults. Thus it is appropriate that the proposed scheme be operational only for low impedance faults. It is well known that special techniques have to be used for detecting high impedance faults and it holds true for this case as well.

9.4.4 ANN Performance for Different Source Impedances

The same networks were tested for their performance with different source impedances. As can be expected, the network performance was observed unsatisfactory when the sources were weaker than what they were trained for. They were also tested with stronger sources and the results for a pre-fault power flow level of 90% rated is shown in Figure 9.12. In the case of reverse power flow, the steady bus voltages of a strong system has helped to maintain higher network performance even for far end faults.

The positive and zero sequence impedances of the strong sources are half of those ones used originally for training. The test results are for the transmission system with strong sources at both ends.

Obviously, the best approach is to have different sets of weights trained for predictable large topological changes of the transmission system.

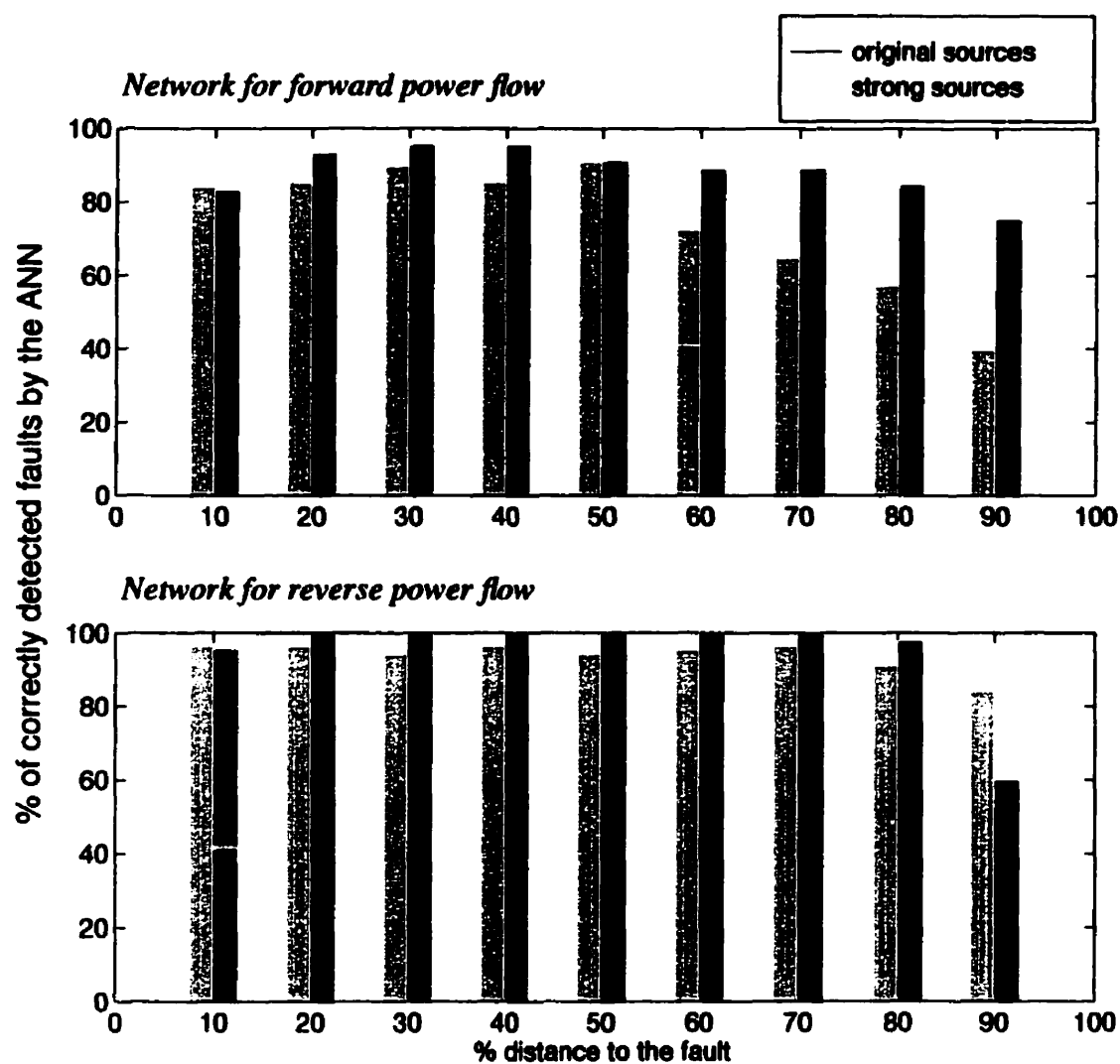


Figure 9.12: Network performance variation for strong sources at receiving and sending ends.

9.5 Comparison of the Trip Signals from the ANN and the APT Impedance Elements

In order to directly compare the performance of the artificial neural network unit and the ground and line impedance elements of the Alpha Power Technology relay, a few

fault cases are presented with their respective trip signals. The ANN which is issuing a trip signal to each individual faulted phase is compared with an equivalent zone-one and zone-two trip signal derived using the trip signals of the ground and line impedance elements of the APT relay. The logic that derives the zone trips for each phase, using the trip signals from the impedance elements are as follows.

$$(Zone-one\ trip)_{phase-a1,2} = G1_{a1,2} + L1_{a1,2b1,2} + L1_{c1,2a1,2} \quad 9.1$$

$$(Zone-one\ trip)_{phase-b1,2} = G1_{b1,2} + L1_{a1,2b1,2} + L1_{b1,2c1,2} \quad 9.2$$

$$(Zone-one\ trip)_{phase-c1,2} = G1_{c1,2} + L1_{b1,2c1,2} + L1_{c1,2a1,2} \quad 9.3$$

$$(Zone-two\ trip)_{phase-a1,2} = G2_{a1,2} + L2_{a1,2b1,2} + L2_{c1,2a1,2} \quad 9.4$$

$$(Zone-two\ trip)_{phase-b1,2} = G2_{b1,2} + L2_{a1,2b1,2} + L2_{b1,2c1,2} \quad 9.5$$

$$(Zone-two\ trip)_{phase-c1,2} = G2_{c1,2} + L2_{b1,2c1,2} + L2_{c1,2a1,2} \quad 9.6$$

$G1$ and $G2$ signals are the zone-one and zone-two ground impedance relay trip signals of the phases denoted by the subscripts. Similarly $L1$ and $L2$ are the line impedance relay trips for zone-one and two respectively, for the phases shown in subscripts. The + sign in the logic expressions is a logic OR operation. It should be noted that the trip signals from the directional impedance elements are excluded in these tests for ease of direct comparison.

The ANN used here is the one trained to detect faults for pre-fault power flow of 90% of the rated power in the reverse direction (i.e. from *McCalmont* to *Sprindale*). The pre-fault power flow is maintained at 90% of the rated value during the tests as well. However, the fault cases are not necessarily from the training or the test sets used during the training and testing phases of the ANN.

Figure 9.13 shows the comparison of the zone-one and two trip signals derived using the above equations (equation 9.1 to equation 9.6), with the ANN trip signals for a single-line to ground fault at 10% distance. The faulted phase is phase- a_1 and it is a zone-one fault. As seen in the figure, the ANN trip for the faulted phase comes faster than the zone-one trip from the impedance elements. It also issues a signal only for the faulted phase whereas the impedance trips come for both phases a_1 and c_1 , apparently due to a trip in a line impedance element.

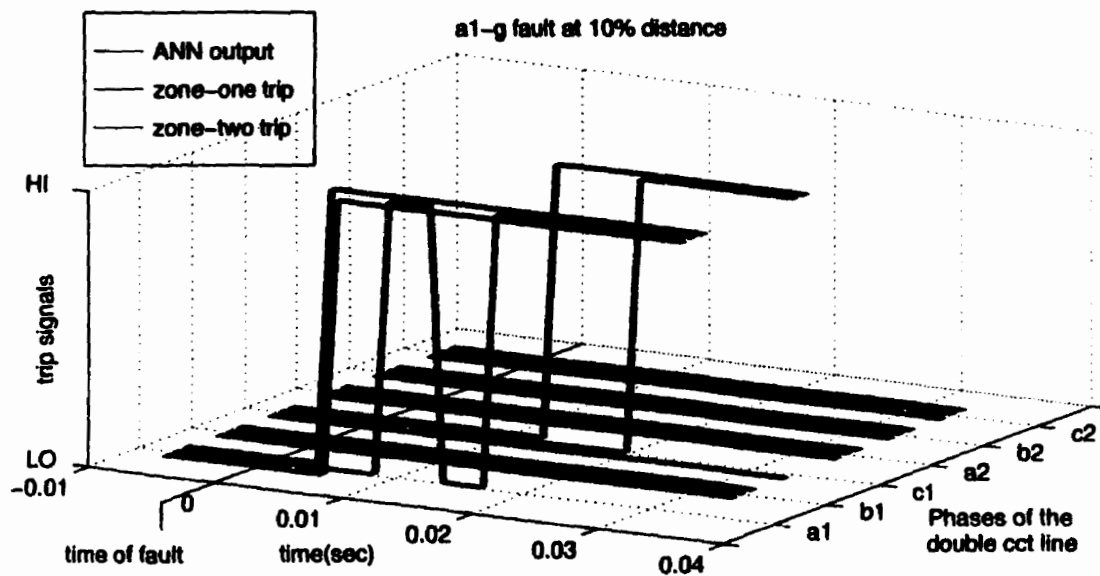


Figure 9.13: Comparison of trip signals from the ANN and the zone trips of the APT impedance elements, for a a1-g fault at 10% distance.

The following test results in Figure 9.14 to Figure 9.17 also demonstrate the same trend in the trip signals. That is, the ANN trips are confined to the faulted phases and they are in general faster than the impedance zone-one trips for both ground and non-ground faults. Zone-two trips, which generally have a time grading incorporated, will

actually occur later than when they are shown on the figures. Therefore they too generally will be slower than the ANN trips even if they seem faster on the figures.

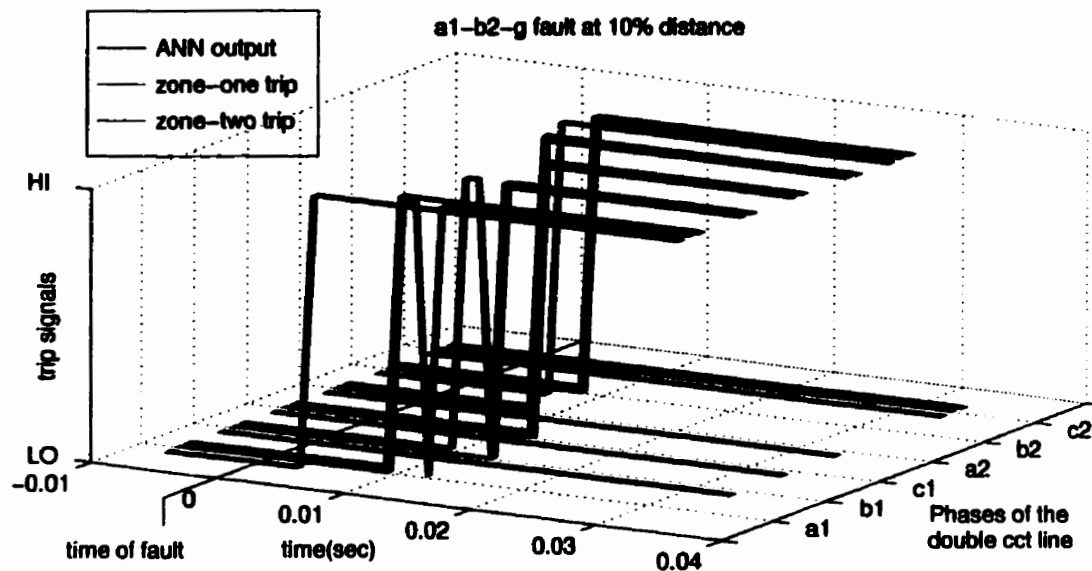


Figure 9.14: Comparison of trip signals from the ANN and the zone trips of the APT impedance elements, for a a1-b2-g fault at 10% distance.

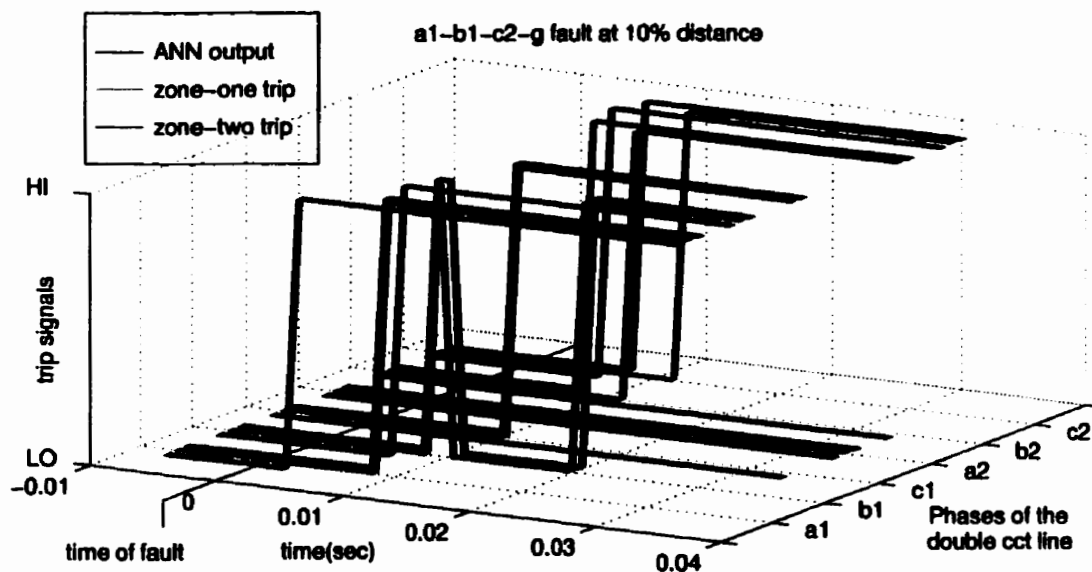


Figure 9.15: Comparison of trip signals from the ANN and the zone trips of the APT impedance elements, for a a1-b1-c2-g fault at 10% distance.

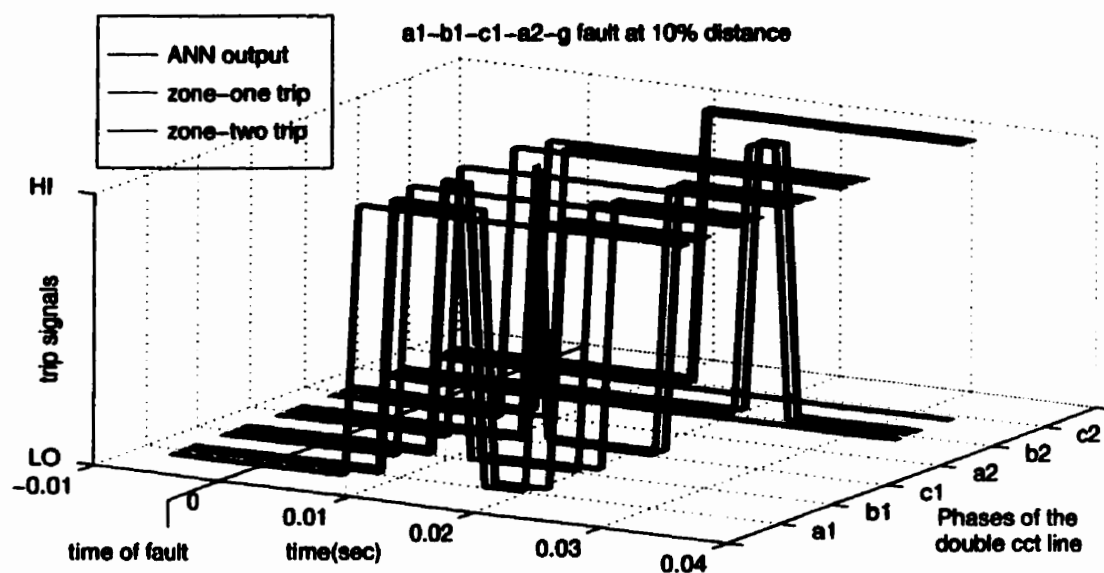


Figure 9.16: Comparison of trip signals from the ANN and the zone trips of the APT impedance elements, for a a1-b1-c1-a2-g fault at 10% distance.

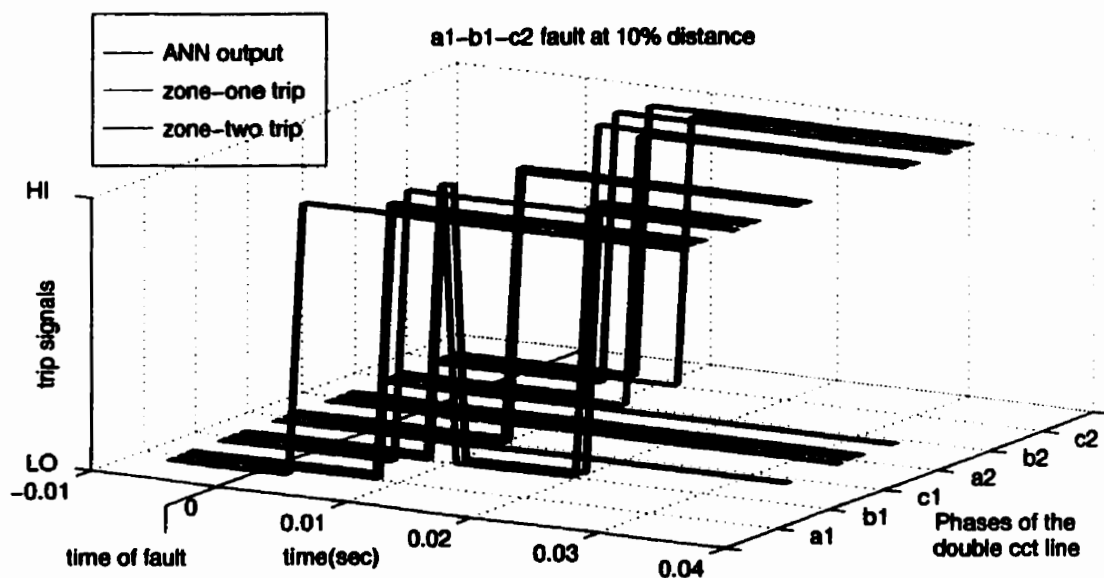


Figure 9.17: Comparison of trip signals from the ANN and the zone trips of the APT impedance elements, for a a1-b1-c2 fault at 10% distance.

Figure 9.18 and Figure 9.19 below are a repeat of the same comparison of ANN and APT trip signals, for remote faults at 90% distance.

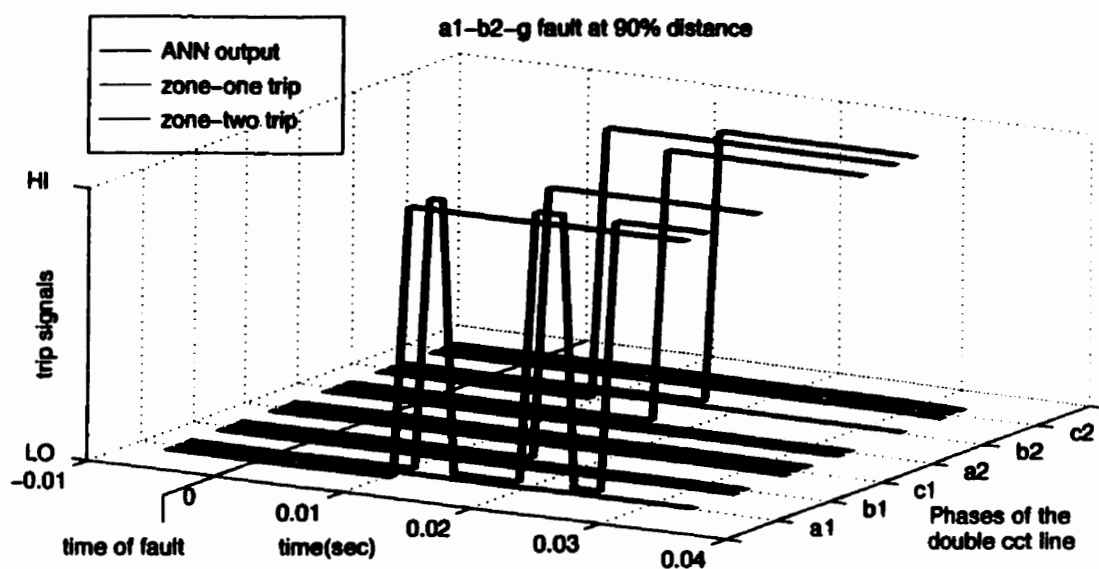


Figure 9.18: Comparison of trip signals from the ANN and the zone trips of the APT impedance elements, for a a1-b2-g fault at 90% distance.

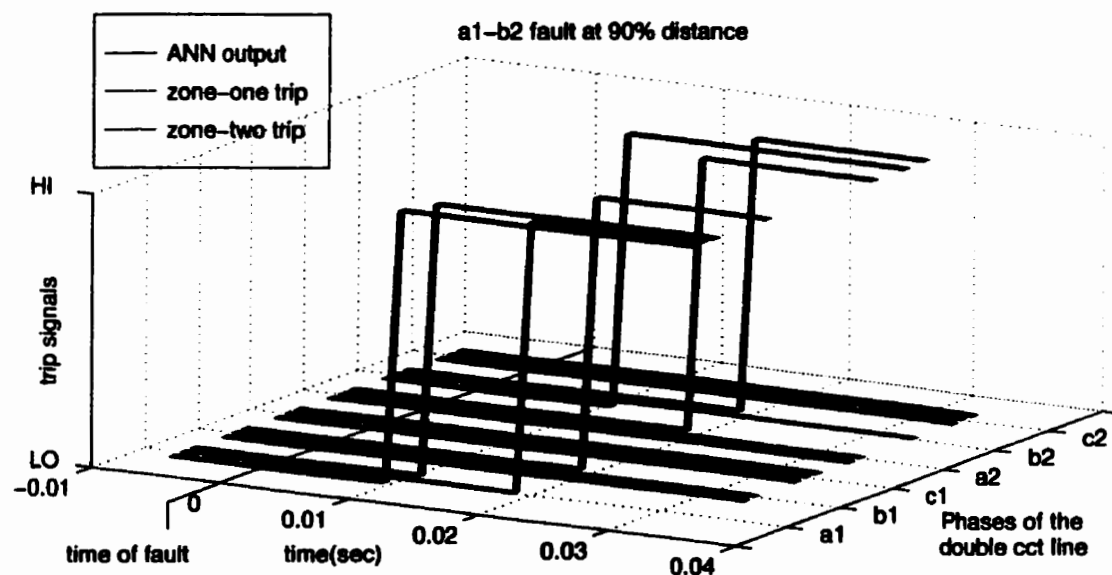


Figure 9.19: Comparison of trip signals from the ANN and the zone trips of the APT impedance elements, for a a1-b2 fault at 90% distance.

In these faults it is the zone-two trip that occurs for most of the fault situations and as can be seen, the ANN picks the faulted phases accurately for both ground and non-ground faults.

Thus the performance of the ANN is promising in this application. However, it remains to be perfected for other prefault operation conditions and system topologies. The trip signals from the ANN and the APT relay elements should then be optimally combined using a trip logic to issue the final trip signals to the circuit breaker.

9.6 Comparison of the Trip Signals from the ANN and the APT Single-Pole Trip Logic

During fault conditions where single pole tripping is possible, it is always desirable to have such provision in the relay algorithm. Thus the APT relay algorithm designed for application on single circuit lines has a special logic given in equation 9.7 to equation 9.9 that combines the ground and line impedance trips coming from the impedance elements for single pole tripping.

$$TripA = (G_a + L_{ab} + L_{bc} + L_{ca}) \cdot \overline{[G_b \cdot \overline{G_c} \cdot \overline{G_a}]} \cdot \overline{[G_c \cdot \overline{G_a} \cdot \overline{G_b}]} \quad 9.7$$

$$TripB = (G_b + L_{ab} + L_{bc} + L_{ca}) \cdot \overline{[G_c \cdot \overline{G_a} \cdot \overline{G_b}]} \cdot \overline{[G_a \cdot \overline{G_b} \cdot \overline{G_c}]} \quad 9.8$$

$$TripC = (G_c + L_{ab} + L_{bc} + L_{ca}) \cdot \overline{[G_a \cdot \overline{G_b} \cdot \overline{G_c}]} \cdot \overline{[G_b \cdot \overline{G_c} \cdot \overline{G_a}]} \quad 9.9$$

where

$TripA$, $TripB$ and $TripC$ are trip signals to the phases a , b and c respectively. $G_{a,b,c}$ signals are the zone-one ground impedance relay trip signals of the phases denoted by

the subscripts. Similarly $L_{ab,bc,ca}$ are the line impedance relay trips for zone-one, for the phases shown in subscripts. The + sign in the logic expressions is a logic OR operation and '.' is a logic AND. The bar over the signal denotes a negation. It should be noted that the trip signals from the directional impedance elements are excluded in these tests for ease of direct comparison.

Analytical fault studies of single circuit systems show that single line to ground faults can cause line impedance trajectories to move to the trip zones. This logic ensures that only the phase at fault is tripped during any single-line-to-ground fault even if some line impedance elements are tripped. All other fault conditions will result in a three-pole trip.

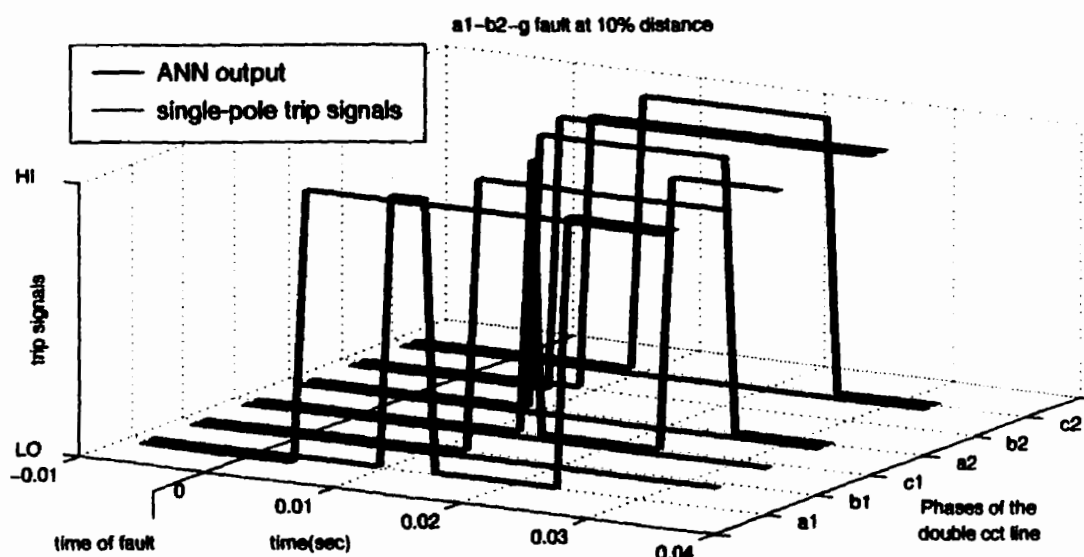


Figure 9.20: Comparison of trip signals from the ANN and the single-pole trip logic of the APT relay algorithm, for a a1-b2-g fault at 10% distance.

However, it proves inadequate for single pole tripping of double-circuit lines. An inter-circuit double-line-to-ground fault (a_1-b_2-g) is used to demonstrate the trip signals generated by the single pole trip logic used on the two circuits on a double-circuit transmission line. The ideal algorithm in such a fault condition is expected to only trip the two faulted phases a_1 and b_2 leaving all other poles in operation. However, the logic fails to do so as shown in Figure 9.20. The trip in the first circuit is due to two ground impedance elements coming in operation during the fault. The short duration trip of all poles on the second circuit is due to a single line impedance trip while all other impedance elements are indicating a no-trip. It initially trips both circuits completely whereas the ANN outputs shown on the same figure secure the operation of all the healthy lines for the same fault, tripping only the two faulted lines.

9.7 Conclusions

Two artificial neural networks have been trained to detect faulted phases on the *McCalmont-Springdale* double circuit transmission line. The ANN is proposed to be implemented with the digital distance relay under investigation. The network performance has shown promising use of artificial intelligence in distance relays particularly with respect to speed of operation and single pole tripping functions. The neural network designed by no means is the optimal and some suggestions for apparent improvement have been mentioned where appropriate. However, the results provided in this chapter provide a basis to find a solution to the complex problem of single ended protection on complex transmission networks.

Artificial intelligence seems to be a potential solution to the complex protection problem addressed in this study. However, it involves a long process of off-line training and testing before it can be implemented on an actual network. This technique can therefore only be justified if 100% accuracy can be achieved. Also, staged faults on the system are not the way to generate training or test data. Therefore, a simulation model of the power system is a pre-requisite for such a protection scheme. The model however can be simplified appropriately, since the inputs to the neural networks usually can tolerate a certain amount of noise.

Some experiments were done for designing a similar artificial neural network for a six-phase transmission line configuration. However, the experimentation did not mature to a reportable degree.

CHAPTER 10

CONCLUSIONS AND FUTURE WORK

10.1 Contributions

- Development of an off-line software model of the digital distance relay algorithms.

The models have been extensively tested on PSCAD/EMTDC Electromagnetic Transient Simulation Tool. They also have been compared with the actual relay responses for various transmission network models. The models consist of both general purpose data processing elements as well as the specific distance relay elements and are available for use in the form of a library.

- Models of a double circuit transmission line and a six phase transmission system were set up on the PSCAD/EMTDC simulation tool, with extensive details that simulate accurate transients during faults. Proper driving logic is set up to simulate faults at different distances, on different points on the wave, with three different fault resistances on the same system.

The digital distance relays are attached to each of these system models for testing.

- Off-line faults studies were carried out on the two compact transmission systems in order to identify the problems associated with the distance relays for short

circuit faults. The studies covered the complete spectrum of faults and revealed the imperfections of ground and line impedance relays as well as the directional impedance algorithms in the respective application.

- Modifications to the ground impedance relays have been proposed which significantly improved the performance of the relay on the two compact transmission line configurations discussed in the thesis.
- The successful exercise of modifying the APT relay with a current-balance algorithm for application on the *Winnipeg Hydro* double circuit transmission line has been demonstrated.
- A neural network solution is investigated for improving the reliability and the security of the distance relay scheme on double circuit transmission lines. Performance of the neural network designed is promising and eliminates doubts of its use as a solution to the complex protection problem on the compact transmission line configurations. However, it remains to be improved to flawlessly operate in various prefault operating conditions before any practical use is justified.

10.2 Future Work

- The current transformers and potential transformers were not modelled in the course of the study, because the relay algorithms are based on the fundamental

component of the voltages and currents. However, the saturation of the measuring transformers may have some effect on the performances of the algorithms investigated in the study. Therefore, these components have to be modelled for a more complete evaluation of the protective algorithms, at least for relatively severe fault conditions that run the measuring transformers into saturation.

- The system transformer saturation was also not modelled in the study, again for the reasons of keeping the initial studies within reasonable simplicity. However, system transformer saturation needs to be incorporated in the models for a complete evaluation of the protective apparatus.
- The artificial neural network technique, proposed for enhancing the relay performance on complex transmission configurations, is in its pre-mature stages for implementing on a relay. It needs further improvement to be functional for all operating power levels. It also has to be perfected to eliminate all possible mis-operations.
- The contributions made do not complete a distance relay scheme that can be applied to a double circuit transmission line without a trip logic that combines the decisions made by the independent data processing elements. The final trip signal issued to the circuit breaker needs to ensure single pole tripping wherever possible. Therefore, careful designing of a trip logic that uses all the information from the relay elements and the artificial neural network would be another task for the

future. Depending on the necessities, another neural network can be used for this purpose.

- Completion of the experiments on a neural faulted-phase detector for application on a six-phase transmission line. This exercise can also have an approach similar to that of the double circuit line.
- Finally, by testing a prototype relay customized for an actual transmission line, the proposals made in the course of the study can be validated.

10.3 Conclusions

The most common technique of enhancing transmission capability, by increasing the transmission voltage seem to have reached a plateau, due to the cost and environmental concerns. Multi-circuit transmission networks have been long known to the utilities all over the world as a remedy for the problem of acquiring right-of-way. In the search for more compact and efficient transmission systems with minimal electric fields and radio interferences, multi-phase lines have also emerged, although still in an experimental stage.

The widely used distance protection schemes are now asked to be adaptable to these various compact configurations of transmission lines. Implementation of many complementary protection algorithms is the best suited approach for enhancing the adaptability of modern micro-processor based digital relay algorithms. They can also benefit from the newly developed techniques, such as neural computing, for improving

their reliability and security. The proposals in the thesis exploit these philosophies to modify the digital distance algorithm to suit the double circuit and six phase transmission configurations, as a potential stand alone scheme, with suitable back up protection.

However, protection engineering is an area where no scheme with the slightest doubt is tolerated. Therefore, the proposed neural network scheme is still in its pre-mature stage for any practical use. Never the less, with the demanded speed of operation, neural networks which inherently have the parallel processing architecture is a promising approach to the problems as complex as the one addressed here in this project. The investigations are also in line with finding a more economical substitution to the use of multiple, top-of-the-line, dissimilar protections schemes on compact transmission systems.

REFERENCES

- 1 A. Clerici, G. Valtorta, L. Paris, "Overhead lines optimum conductor configuration for EHV AC transmission systems." *Publications of CIGRE Symposium Leningrad 1991*, Paper No: 300-08.
- 2 R.E. Kennon, "Determining the right-of-way power transfer capability" *Publications of CIGRE Symposium Leningrad 1991*, Paper No: 500-01.
- 3 L.O. Barthold, "Optimization of open-wire transmission" *Publications of CIGRE Symposium Leningrad 1991*, Paper No: 600-04.
- 4 A.C. Britten, D.H. Cretchley, K.J.Sadurski, B. Druif and H.A. Roets "The compaction of conductor-to-tower clearances on Eskom's 765 kV transmission lines." *Publications of CIGRE Symposium Leningrad 1991*, Paper No: 500-04.
- 5 J.H.M. Fernandes, J.G. Tannuri, W. Sato, N. Kabaf, J.M. Arimori, "Eletronorte Brazil - 500 kV and 230 kV compact lines: design and electrical aspects." *Publications of CIGRE Symposium Leningrad 1991*, Paper No: 300-07.
- 6 Yu.M. Gutman, N.I. Stepina, "Studies of the dielectric strength of phase-to-ground and phase-to-phase clearances EHV and UHV power transmission lines." *Publications of CIGRE Symposium Leningrad 1991*, Paper No: 300-06.
- 7 G.N. Alexandrov, A.V. Gorelov, A.I. Kurnosov, G.V. Podporkyn, I.M. Nosov, Ye.A. Khmel'nov, "Design features of the compact lines with enhanced surge impedance loading built in the USSR." *Publications of CIGRE Symposium Leningrad 1991*, Paper No: 300-05.
- 8 G.N. Alexandrov, "Scientific and Engineering principles of creating compact lines with increased natural capacity." *Publications of CIGRE Symposium Leningrad 1991*, Paper No: 300-04.

- 9 Y. Takagi, M. Sugihara, M. Adachi, "Technical development of reduced line inductance for bulk power transmission." *Publications of CIGRE Symposium Leningrad 1991*, Paper No: 300-01.
- 10 Navin B. Bhatt, Subrahmanyam S. Venkata, William C. Guyker, William H. Booth, "Six-Phase (Multi-Phase) Power Transmission Systems: Fault Analysis." *IEEE Transactions on Power Apparatus and Systems*, Vol. PAS-96, No:3, May/June 1977, pp 758-767.
- 11 J. R. Stewart, I. S. Grant, "High-Phase Order Ready for Application." *IEEE Transactions on Power Apparatus and Systems*. Vol. PAS-101, No:6, June 1982, pp 1757-1767.
- 12 James R. Stewart, Laurie J. Oppel, Gary C. Thomann, Thomas F. Dorazio, R. V. Rebbapragada, "Transformer winding selection associated with reconfiguration of existing double circuit line to six-phase operation." *IEEE Transactions on Power Delivery*, Vol. 7, No:2, April 1992, pp 979-985.
- 13 Alexander Apostolov, William George, "Protecting NYSEG's Six-Phase Transmission Line." *IEEE Computer Applications in Power*. Vol. 5, N0:4, October 1992, pp 33-36.
- 14 T.F. Dorazio, J.R. Stewart, D.D. Wilson, "Six-Phase Power Transmission: First Utility Application." *Publications of CIGRE Symposium Leningrad 1991*, Paper No: 600-01.
- 15 S. S. Vendata, W. C. Guyker, J. Kondragunta, N. K. Saini, E. K. Stanek, "138 kV Six-Phase Transmission System: Fault Analysis." *IEEE Transactions on Power Apparatus and Systems*, Vol. PAS-101, No:5, May 1982, pp 1203-1214
- 16 W. C. Guyker, D. F. Shankle, "138 kV Six-Phase uprating of a 138 kV Double Circuit Line." *IEEE Transactions on Power Apparatus and Systems*, Vol. PAS-104, No:9, September 1985, pp 2547-2554.
- 17 H. Becker, J. Nilges, H. Dittrich, "Distance protection of double-circuit lines with different rated voltages during intersystem faults." *Publications of CIGRE Symposium Paris 1990*,

Paper No: 34-206.

- 18 B. Clairmont, L. Zaffanella, L. Cabeza, G. Stillman, S. Zelingher, "Hybrid Transmission Corridors - Corona and Field Effects." *Publications of CIGRE Symposium Leningrad 1991*, Paper No: 600-03.
- 19 Rogerio T. Verdoline, *Over-voltage and coupling effects on an AC-DC hybrid transmission system*. Ph.D. Thesis.
- 20 H. Hapfauer, G. Koch, "An Enhanced Transmission Line Protection Concept for Multi-Circuit Lines." *5th International Conference on Developments in Power System Protection*, IEE Pub. No. 368, 1993, p145-8.
- 21 M. Aziz Pervez, V. Sorensen Henrik, Jan Van Der Spiegel, "An overview of Sigma-Delta Converters." *IEEE Signal Processing Magazine*, January 1996, pp. 61-68.
- 22 J.W. Cooley, J.W. Tukey, "An algorithm for the machine computation of complex Fourier series" *Mathematics of Computation*, 19 pp. 297-301, April 1965
- 23 Maurice Bellanger, *Digital Processing of Signals Theory and Practice*.
- 24 P.G. McLaren, G.S. Swift, E.N. Dirks, R.P. Jayasinghe, I. Fernando, "Accurate software model for off-line assesment of a digital relay." *IEEE Stockholm Power Tech '95, Conference Porceedings*, p582.
- 25 H. Lui, Y. Hu, P.G. McLaren, G.S. Swift, E.N. Dirks, "Efficient FFT/DFT Implementation Techniques for a TMS320C30-Based Numerical Relay for Power System Protection." *ICSPAT International conference on Signal Processing Applictions and Techniques*, 24-26th October, Boston USA.
- 26 P. G. McLaren, G. W. Swift, Z. Zhang, E. Dirks, R. P. Jayasinghe, I. Fernando, "A New Directional Element for Numerical Distance Relays.", *IEEE Transactions on Power Delivery*,

April 1995, Vol 10, No. 2, ITDPE5, p666.

- 27 K. S. Prakas, O. P. Malik, G. S. Hope, "Amplitude Comparator Based Algorithm for Directional Comparison Protection of Transmission Lines." *IEEE Transactions on Power Delivery*, Vol. 4, No. 4, October 1989.
- 28 Gabriel Benmouyal, Simon Chano, "Characterization of Phase and Amplitude Comparators in UHS Directional Relays." *IEEE Transactions PWRD*, July 1996.
- 29 A. Guzman, J. Roberts, D. Hou, "New Ground Directional Elements Operate Reliably for Changing System Conditions." *22nd Annual Western Protective Relay Conference*, Spokane, WA, October 1995.
- 30 Publication of Manitoba HVDC Research Centre, *User's Manuals on PSCAD/EMTDC Power Systems Simulation Software*.
- 31 P.G. McLaren, I. Fernando, H. Liu, E. Dirks, G.W. Swift, C. Steele, "Enhanced Double Circuit Line Protection." *IEEE Transactions PWRD*, July 1996.
- 32 W D Stevenson, *Elements of Power System Analysis*.
- 33 *Newnes Electrical Pocket Book* - 21st edition.
- 34 Alexander Redfern of Churchill College, *Signal Processing Techniques in Distance Protection Applications*. Ph.D Thesis.
- 35 Y. Ohura, T. Matsuda, M. Suzuki, M. Yamaura, Y. Kurosawa, T. Yokoyama, "Digital distance Relay with Improved Characteristics Against distorted Transient Waveforms." , *IEEE Transactions on Power Delivery*, Vol. 4, October 1989, pp 2025-2030.
- 36 M. S. Sachdev (Co-ordinator), *Micro-processor relays and Protection Systems*, *IEEE Tutorial Course Text*, Publication No.88EH0269-1-PWR, June 1986.

- 37 A.G. Phadke, T. Hlibka, M.G. Adamiak, M. Ibrahim, J.S. Thorp, "Micro Computer based ultra high speed distance relay: field test." *IEEE Transactions on Power Apparatus & Systems*, Vol PAS - 100, No 4 April 1981. pp 2026-2033.
- 38 Delano D. Wilson, James R. Stewart, "Switching surge characteristics of six-phase transmission lines." *IEEE Transaction on Power Apparatus and Systems*, Vol. PAS-103, NO. 11, November 1984, pp3393-3401.
- 39 A.G. Jongepier, L. van der Sluis, "Adaptive Distance Protection of Double Circuit line using artificial neural nets.", *Fifth International Conference on DPSP '93*, pp 157-160.
- 40 Bernad Widrow, Michael A. Lehr, "Backpropagation and its applications." Neural Network Computing for the Electric Power Industry, *Proceedings of the 1992 Inns Summer Workshop*. pp 21-29
- 41 Steven A. Harp and Tariq Samad, "Optimizing Neural Networks with Genetic Algorithms.", Neural Network Computing for the Electric Power Industry, *Proceedings of the 1992 Inns Summer Workshop*. pp 41-44.
- 42 Y. D. Lukic, C. R. Stevens, J. Si, "Application of a Real Time Artificial Neural Network for Classifying Nuclear Power Plant Transient Events.", Neural Network Computing for the Electric Power Industry, *Proceedings of the 1992 Inns Summer Workshop*. pp 59-62.
- 43 A. G. Jongepier, L. van der Sluis, "Adaptive Distance Protection of a Double-Circuit Line Using Artificial Neural Nets.", *Fifth international conference on Developments in Power System Protection (DPSP '93) conference Publication No: 368*. Power Division of IEE and CIGRE, pp 157 - 160.
- 44 D.S. Fitton, R.W. Dunn, R.K. Aggarwal, A.T. Johns, Y. H. Song, "The Application of Neural Network Techniques to Adaptive Autoreclosure in Protection Equipment.", *Fifth international conference on Developments in Power System Protection (DPSP '93) conference Publication No: 368*. Power Division of IEE and CIGRE, pp 161-164.

- 45 Thomas Dalsein, Bernd Kulicke, "Neural network approach to fault classification for high speed protective relaying." *IEEE Transactions on Power Delivery*, April 1994,
- 46 Thomas Dalsein, Thomas Friedrich, Bernd Kulicke, Dejan Sobajic, "Multi neural network based fault area estimation for high speed protective relaying." *IEEE Transactions on Power Delivery*, April 1995,
- 47 Mladen Kezunovic, Igor Rikalo, "Detect and Classify Faults Using Neural Nets." *IEEE Computer Applications in Power*, Volume 9, Number 4, October 1996, pp 42-47
- 48 Thomas Baumann, Alain Germnd, Daniel Tschudi, "Impulse test fault diagnosis on power transformers using Kohonen's self-organizing neural network." Neural Network Computing for the Electric Power Industry, *Proceedings of the 1992 Inns Summer Workshop*. pp 59-62.
- 49 E. Baum, D. Haussler, "What size net gives valid generalization?" *Neural Computation*, Vol. 1, pp. 151-160, spring 1989.
- 50 Jacques de Villiers and Etienne Barnard, "Backpropagation neural nets with one and two hidden layers." *IEEE Transactions on Neural Networks*, Vol. 4, No. 1, January 1992. , pp 136-141.
- 51 John Hertz, Anders Krogh, Richard G. Palmer, "Introduction to the Theory of Neural Computation"
- 52 Simon Haykin, "Neural Networks, A Comprehensive Foundation".
- 53 Drew van Camp, *A Users Guide for the XERION Neural Network Simulator*.

Appendix A

Positive Sequence Incremental Impedance Computations

A.1 Computation of the Positive Sequence Incremental Impedances for a Three-Phase Single-Circuit Transmission Line

This section shows the computation of the positive sequence incremental impedance at the *busbar M* for forward and reverse faults on a three-phase, single-circuit transmission line.

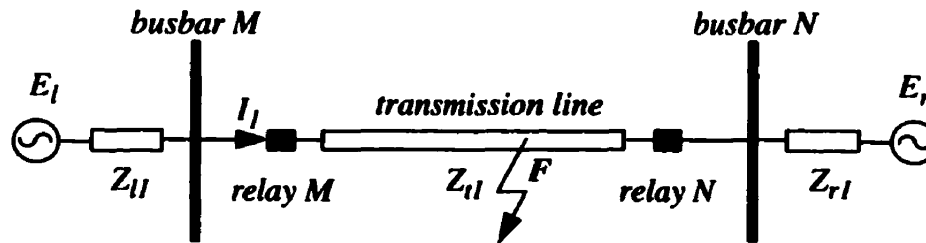


Figure A1: Positive sequence network of a three-phase single-circuit transmission line with a fault in front of the 'busbar M'.

The system parameters for the three phase single circuit transmission system shown in Figure A1 are as follows.

Positive sequence impedance of the local source (near busbar M) = Z_{l1} ,

Positive sequence impedance of the remote source (near busbar N) = Z_{r1} ,

Positive sequence impedance of the transmission line = Z_{l1} ,

Excitation voltage of the local source = E_l ,

Excitation voltage of the remote source = E_r ,

Prefault current into the transmission line = I_1

Then the prefault voltage at busbar M is given by:

$$V_1 = E_l - Z_{l1} I_1 \quad \text{A1}$$

The voltage at *busbar M* due to the fault at *F* (shown in Figure A1):

$$V_{1ff} = E_l - Z_{l1} I_{1ff} \quad \text{A2}$$

where

V_{1ff} = the positive sequence fault voltage at *busbar M* and

I_{1ff} = the positive sequence fault current measured into the transmission line at
busbar M.

If the incremental positive sequence voltage and current due to the fault at *F* are:

$$\Delta V_1 = V_{1ff} - V_1 \quad \text{and}$$

$$\Delta I_1 = I_{1ff} - I_1$$

From equations A1 and A5,

$$\Delta V_1 = V_{1ff} - V_1 = (E_1 - Z_{11} I_{1ff}) - (E_1 - Z_{11} I_1)$$

$$\Delta V_1 = -Z_{11} \cdot (I_{1ff} - I_1)$$

But,

$$\Delta I_1 = I_{1ff} - I_1$$

Therefore,

$$\frac{\Delta V_1}{\Delta I_1} = -Z_{11} \quad \text{A3}$$

For a forward fault, the positive sequence incremental impedance measured at the busbar M is equal to the positive sequence impedance of the local source with a sign reversal.

Similarly for a reverse fault at R,

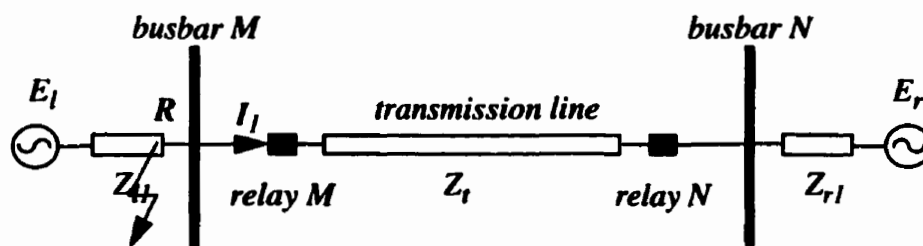


Figure A2: Positive sequence network of a three-phase single-circuit transmission line with a fault behind the busbar M

Then the prefault voltage at *busbar M* is given by:

$$V_1 = E_r + Z_{r1}I_1 + Z_{t1}I_1 \quad \text{A4}$$

The voltage at *busbar M* due to the fault at *R*:

$$V_{1fr} = E_r + Z_{r1}I_{1fr} + Z_{t1}I_{1fr} \quad \text{A5}$$

where

V_{1fr} = the positive sequence fault voltage at *busbar M* due to fault at *R* and

I_{1fr} = the positive sequence fault current measured into the transmission line at *busbar M*.

Therefore, the incremental positive sequence voltage and current due to the fault at *F* are:

$$\begin{aligned} \Delta V_1 &= V_{1fr} - V_1 \quad \text{and} \\ \Delta I_1 &= I_{1fr} - I_1 \end{aligned}$$

From equations A4 and A5,

$$\begin{aligned} \Delta V_1 &= V_{1fr} - V_1 = (E_r + Z_{r1}I_{1fr} + Z_{t1}I_{1fr}) - (E_r + Z_{r1}I_1 + Z_{t1}I_1) \\ \Delta V_1 &= (Z_{r1} + Z_{t1})(I_{1fr} - I_1) \end{aligned}$$

But,

$$\Delta I_1 = I_{1fr} - I_1$$

Therefore,

$$\frac{\Delta V_1}{\Delta I_1} = Z_{r1} + Z_{t1} \quad \text{A6}$$

The positive sequence incremental impedance measured at the *busbar M*, for a reverse fault is equal to the positive sequence impedances of the remote source and the transmission line.

The equations A3 and A6 which are derived for the positive sequence network can also be similarly derived for each phase on the three phase system. Therefore, these equations can be extended to phases *a*, *b* and *c* on a three phase system where all quantities are for the phase considered.

This derivation however, does not hold valid for double-circuit transmission line configurations.

A.2 Computation of the Positive Sequence Incremental Impedances for a Three-Phase Double-Circuit Transmission Line

The positive sequence incremental impedance seen by the directional relay on a double circuit-line varies depending on the nature of the fault. The incremental impedance seen due to three-phase-ground fault on one circuit is derived as follows.

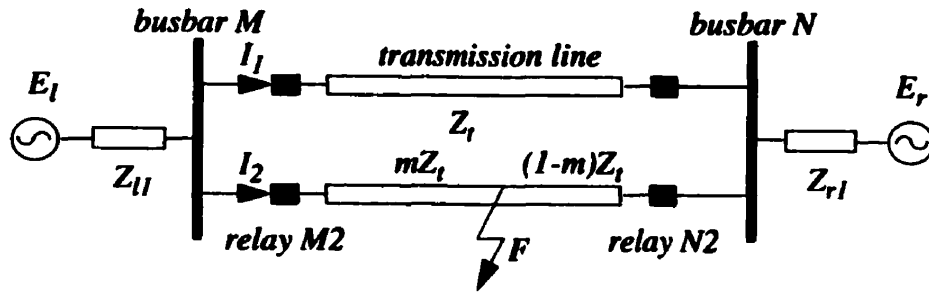


Figure A3: The double circuit transmission line and the positive sequence network impedances.

The Thevenin equivalent positive sequence incremental impedance network is shown in Figure A3, for a three phase to ground fault at F .

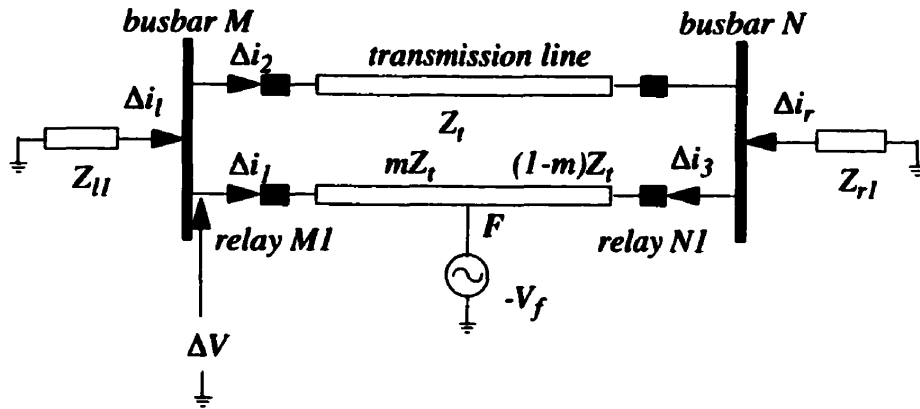


Figure A4: The Thevenin equivalent positive sequence incremental impedance network for the double circuit line in Figure A3, for a three-phase to ground fault at F .

The incremental current and voltage equations can be written as follows

$$\Delta i_1 + \Delta i_2 = \Delta i_l, \quad \text{A7}$$

$$\Delta i_3 - \Delta i_2 = \Delta i_r, \quad \text{A8}$$

also,

$$\Delta i_3 = \frac{m\Delta i_1 - \Delta i_2}{1-m}. \quad \text{A9}$$

also,

$$\Delta V = -Z_l \cdot \Delta i_l = -Z_l \cdot (\Delta i_1 + \Delta i_2),$$

$$\frac{\Delta V}{\Delta i_1} = -Z_l \cdot \left[1 + \frac{\Delta i_2}{\Delta i_1} \right], \quad \text{A10}$$

$$\Delta V = -Z_r \cdot \Delta i_r + Z_t \cdot \Delta i_2, \quad \text{A11}$$

from equation A10 + equation A11;

$$-Z_l \cdot \Delta i_1 \cdot \left[1 + \frac{\Delta i_2}{\Delta i_1} \right] = -Z_r \cdot \Delta i_r + Z_t \cdot \Delta i_2. \quad \text{A12}$$

Using equations A7 to A12, it can be shown that,

$$\Delta Z_l = \frac{\Delta V}{\Delta i_1} = \frac{-Z_l}{1 + \frac{Z_l}{Z_t} - \left\{ \frac{Z_l}{Z_t} \cdot \left[\frac{Z_l + \frac{m}{2} \cdot Z_t}{Z_r + \frac{1-m}{2} \cdot Z_t} \right] \right\}}. \quad \text{A13}$$

For $m=0$,

$$\Delta Z_1 = \frac{-Z_l \cdot (2Z_r + Z_t)}{Z_l + 2Z_r + Z_t} \text{ and}$$

$m=1$,

$$\Delta Z_1 = -2 \cdot Z_l.$$

Thus it is seen that the incremental positive sequence impedance is not always equal to the impedance of the local source for faults on a double circuit line configuration.

Appendix B

Transmission Line Data and Conductor Configurations

B.1 *McCalmont-Springdale* Transmission Line Data

The data used for modelling the *McCalmont-Springdale* double circuit and six-phase transmission lines are as follows.

Conductor Configuration:

The 345 *kV* 3-phase double circuit line has six bundles with two sub-conductors in each bundle. The line is 100 *km* in length. The conductor clearances are as shown in Figure B1 with a mid-span sag of 1.5 *m* [2] [32] [33].

Transmission line current rating is 2.5 *kA* based on its thermal operating limit of 3.2 *kA*, for a 3-phase double circuit operating configuration and an operating safety margin of 20% [2].

Line Conductors:

61 strands of all aluminium conductors of 24.5 *mm* diameter. The DC resistance of the conductors is 0.0807 Ω/km .

Ground Wires:

7/16 steel conductors with a conductor radius of 1.09728 *cm* and a DC resistance of 2.8645 Ω -*m*.

Ground Resistivity:

A value of 100 Ω -*m*, typical for Manitoba, is chosen for ground resistivity based on data provided by Manitoba Hydro.

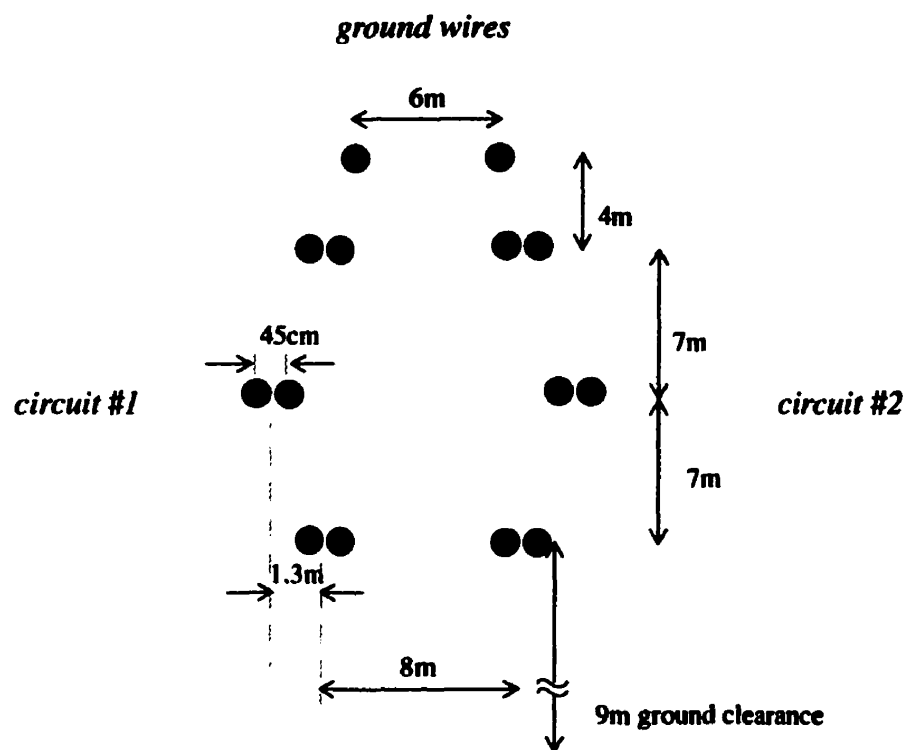


Figure B1: Conductor configuration for the three-phase double circuit line.

The same conductor configuration is used for the six phase transmission line without the ground wires.

B.2 Pointe du Bois Transmission Line Data

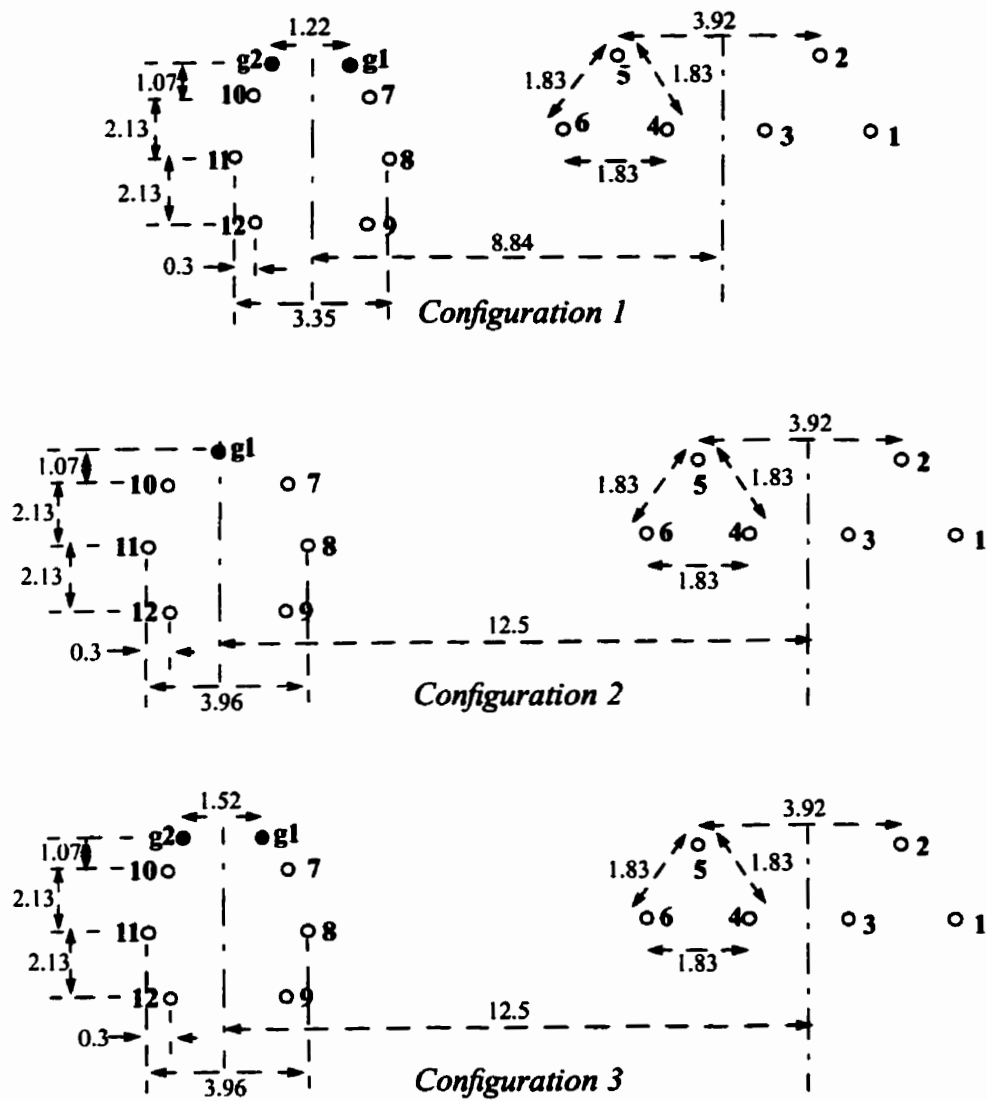


Figure B2: Conductor configurations of the Pointe du Bois transmission line (all lengths in meters)

The 69 kV three-phase transmission line runs on two sets of towers which are erected on the same right of way. These towers have varying configurations along the length of the line. The four circuits are named P1, P2, P3 and P4.

The tower structure and the spacing are such that four basic conductor configurations can be identified. Three of these shown in Figure B2, were with circuits P1 and P2 on one tower and the circuits P3 and P4 on another. The fourth configuration has all circuits on the same tower, but this was not modelled due to the insignificant distance of line covered by this tower structure.

Table B.1: Heights to Conductor Positions.

Conductors	Height (meters)
<i>1, 3, 4, 6,</i>	<i>13.95</i>
<i>2, 5</i>	<i>15.53</i>
<i>7, 10</i>	<i>14.33</i>
<i>8, 11</i>	<i>12.19</i>
<i>9, 12</i>	<i>10.06</i>
<i>g1, g2 (ground conductors)</i>	<i>15.39</i>

The complete line was broken down to 14 segments to be able to transpose and to change to correct conductor configurations in the model. The details of each segment are given in Table B.2.

Table B.2: Conductor Segment Information.

Segment	length (km)	distance (km)	conductor confi- guration	comments	phase order in positions 1-12
1	3.54	0.0	1	Rover	bca cab abc abc
2	3.86	3.54	2	change of conf.	bca cab abc abc
3	13.36	7.40	2	transpose P3 ,P4	bca cab cab cab
4	14.65	20.76	2	transpose all	cab bca bca bca
5	5.31	35.41	2	transpose P3,P4	cab bca abc abc
6	8.69	40.72	2	transpose P1,P2	abc abc abc abc
7	5.31	49.41	2	transpose P3,P4	abc abc cab cab
8	6.76	54.72	3	change of conf.	abc abc cab cab
9	14.48	61.48	3	transpose all	bca cab bca bca
10	6.12	75.96	3	transpose P3,P4	bca cab abc abc
11	6.92	82.08	3	transpose P1,P2	cab bca abc abc
12	15.13	89.00	3	transpose P3,P4	cab bca cab cab
13	12.39	104.13	3	transpose all	abc abc bca bca
14	7.08	116.52	3	transpose P3,P4	abc abc abc abc
		123.60		Pointe du Bois	abc abc abc abc

Conductor data for the Winnipeg transmission line are as follows:

Line Conductors:

278.6 kCM AAC - Consists of 19 aluminium strands (each 0.021" diameter), in three concentric rings of 1, 6 and 12 strands. The overall diameter of the line

conductors is approximately 0.605". DC resistance of the conductors is $0.2129 \Omega/km$.

Ground Conductors (P3 and P4):

3/8" Steel - Consists of 7 steel strands (each 0.120" diameter), in two concentric rings of 1 and 6 strands. The overall diameter of the ground conductors is approximately 0.360". DC resistance of the ground wires is $3.42 \Omega/km$.

Total length of transmission line:

123.6 km.

The self and mutual impedances of the transmission lines were provided for positive, negative and zero sequences. These same impedances were obtained using the transmission line set up on EMTDC 20 conductor 'Bergeron' line model, for comparison (Table B.3). The discrepancies were attributed to the possible assumption of perfect transposition etc. in the calculation of impedances that were provided.

Table B.3: Comparison of Impedances for the transmission lines.

	Data Provided	Model Data
<i>+/- seq. Self Impedance P1</i>	<i>22.9 + j55.2</i>	<i>27.1 + j 64.7</i>
<i>+/- seq. Self Impedance P2</i>	<i>22.9 + j55.2</i>	<i>27.1 + j 64.7</i>
<i>+/- seq. Self Impedance P3</i>	<i>22.9 + j58.9</i>	<i>29.3 + j 83.0</i>
<i>+/- seq. Self Impedance P4</i>	<i>22.9 + j58.9</i>	<i>29.3 + j 83.0</i>
<i>0 seq. Self Impedance of P1</i>	<i>54.8 + j218.4</i>	<i>80.0 + j321.0</i>
<i>0 seq. Self Impedance of P2</i>	<i>56.5 + j216.9</i>	<i>80.0 + j334.0</i>
<i>0 seq. Self Impedance of P3</i>	<i>64.6 + j204.4</i>	<i>91.0 + j342.0</i>
<i>0 seq. Self Impedance of P4</i>	<i>64.6 + j204.4</i>	<i>92.0 + j342.0</i>
<i>0 seq. Mutual Impedance of P1//P2</i>	<i>32.6 + j 142.2</i>	<i>44.0 + j183.0</i>
<i>0 seq. Mutual Impedance of P1//P3</i>	<i>35.8 + j105.7</i>	<i>30.0 + j120.0</i>
<i>0 seq. Mutual Impedance of P1//P4</i>	<i>35.8 + j98.9</i>	<i>28.0 + j111..0</i>
<i>0 seq. Mutual Impedance of P2//P3</i>	<i>37.1 + j114.4</i>	<i>35.0 + j120.0</i>
<i>0 seq. Mutual Impedance of P2//P4</i>	<i>36.9 + j104.9</i>	<i>33.0 + j118.0</i>

Appendix C

Validation Test of *Pointe du Bois* Transmission Line Model

Recorded data for different faults on the system were made available for testing the *Pointe du Bois* transmission line model. This section presents the results of the validation test cases.

The recording equipment coupled to the circuits P3 and P4, at the Rover terminal station, stores *0.3 seconds* of information in the event of a fault, with *0.1 sec* of it as pre-fault data. The sampling rate used is *16* samples per cycle.

Since fairly short transmission line segments are used a $10\ \mu\text{s}$ time step was used in the simulations. The frequency dependant line model has the limitation of a maximum of 10 conductors per corridor. Therefore, the Bergeron line model was used in the simulations. This transmission line model is not as accurate as the frequency dependent model for harmonics. Therefore only the *60 Hz* component of voltages and currents along with their sequence components were used for comparison of the recorded and simulation data.

Recorded pre-fault data exhibited a small degree of imbalance in the voltage at the Rover HV bus. The EMTDC source model was appropriately modified for simulation of this effect.

C.1 Case Studies

All pre-fault operating points were derived based on the pre-fault recorded information except in one case where the data were insufficient. The operating point for that particular case was from another set of data recorded around the same time of the day. Line impedances used are those derived from simulations. Circuits P1 and P2 are considered ON or OFF as appropriate.

In almost all of these faults, the distance to fault is unknown. Therefore the distance on the model is set by trial and error to give a best match of currents and voltages at fault. Considerable effort was made to maintain the angle of fault inception the same as in the recorded data, in all cases.

- Details of system operating point,
- dynamics on the system, identified according to the recorded data, approximate distance to the fault as found by trial and error (does not apply for other dynamics like circuit breaker operations etc.) and
- comparison of simulated and recorded data,

are briefly discussed.

The case is identified by the date it occurred. Scaling factors for voltage and current are *600:1* and *80:1* respectively. Operating point information was derived taking Rover end HV bus voltage as the reference phasor.

Results obtained using EMTDC simulations and the processed recorded data, for all the cases discussed above, are plotted on the same graphs for comparison. (Note: All angles corresponding to small amplitudes were set to zero).

C.1.1 Case 94-0330.000

- Operating point information

Rover source voltage $E_{rov} = 65.77 \angle -1.5^\circ \text{ kV}$ (line - line rms)

Pointe source voltage $E_{pin} = 8.47 \angle 15.94^\circ \text{ kV}$ (line-line rms on the LV bus)

Both circuits P1 and P2 were set 'ON'.

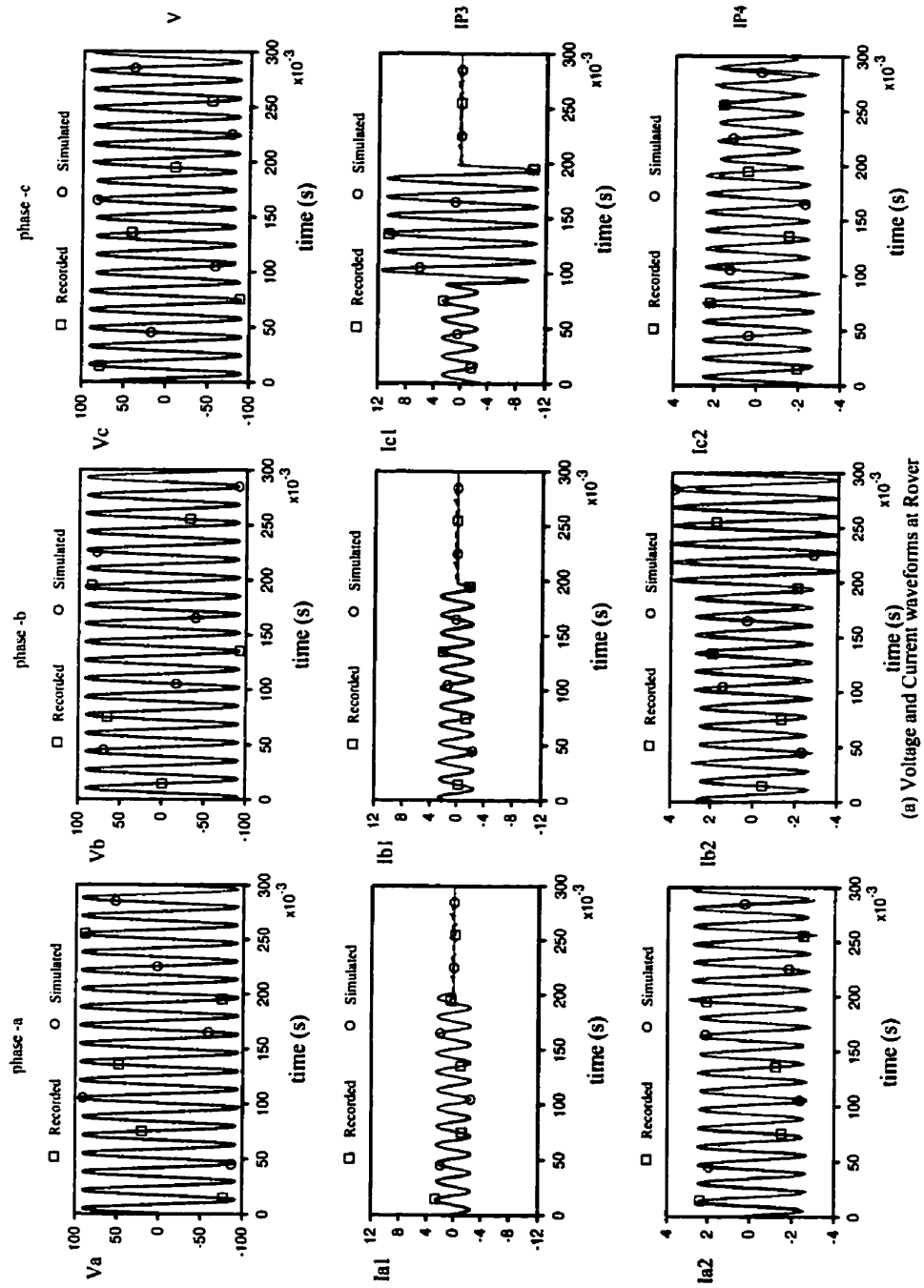
- Information on type of fault: c-phase to ground fault on circuit P3. Circuit breaker at Rover end is opened approximately $6\frac{1}{2}$ cycles after inception of fault.
- Approximate distance to fault is 45 km from Rover.
- Comparison of results.

The simulation data did not follow the decreasing trend the b-phase current of circuit P4 displays during fault.

The drop in current of b-phase of P3 and c-phase of P4 are not as much as in actual data.

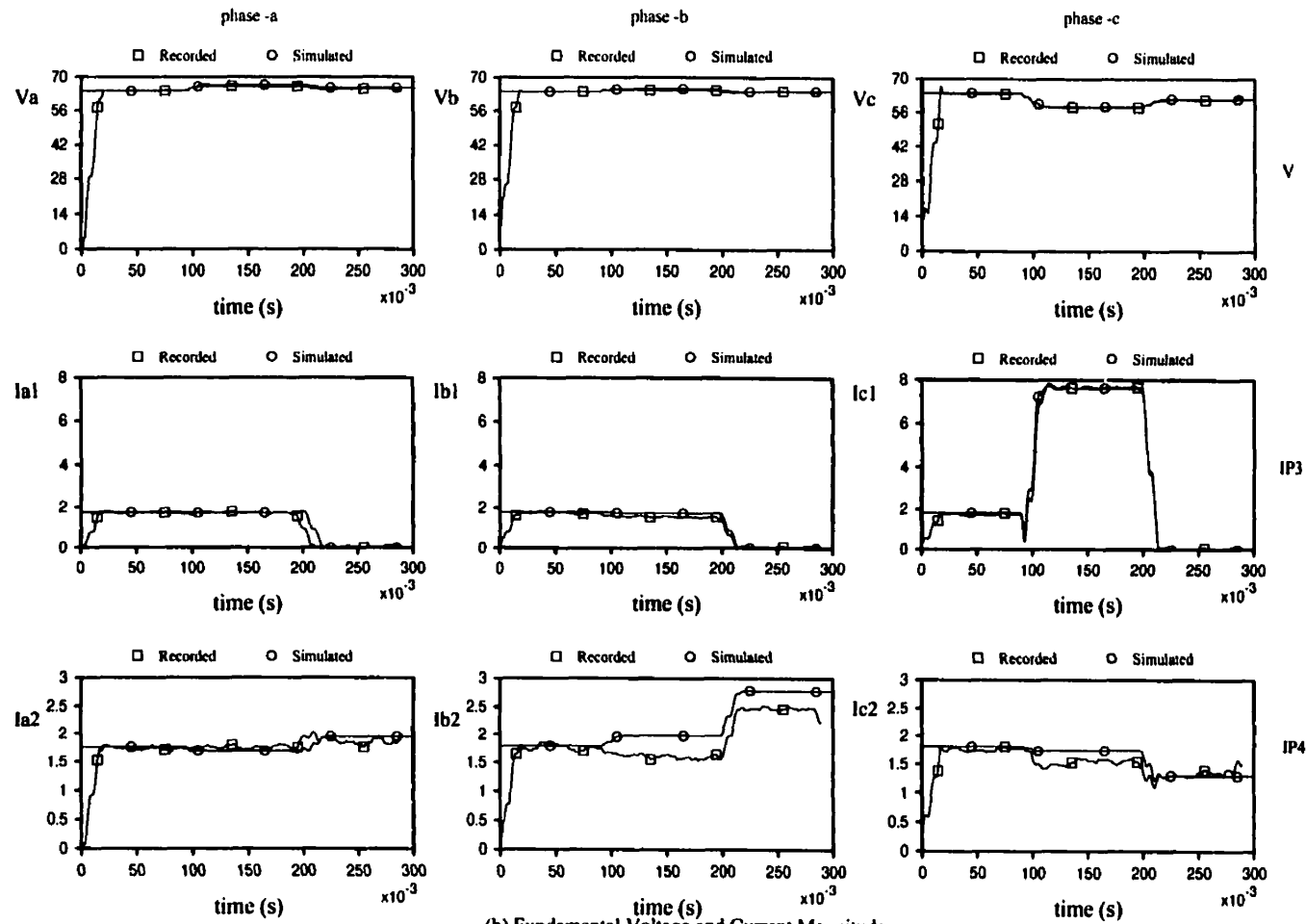
Zero sequence currents were more than expected, where as negative sequence currents were less than expected.

Sequence current errors were more in the circuit P4.



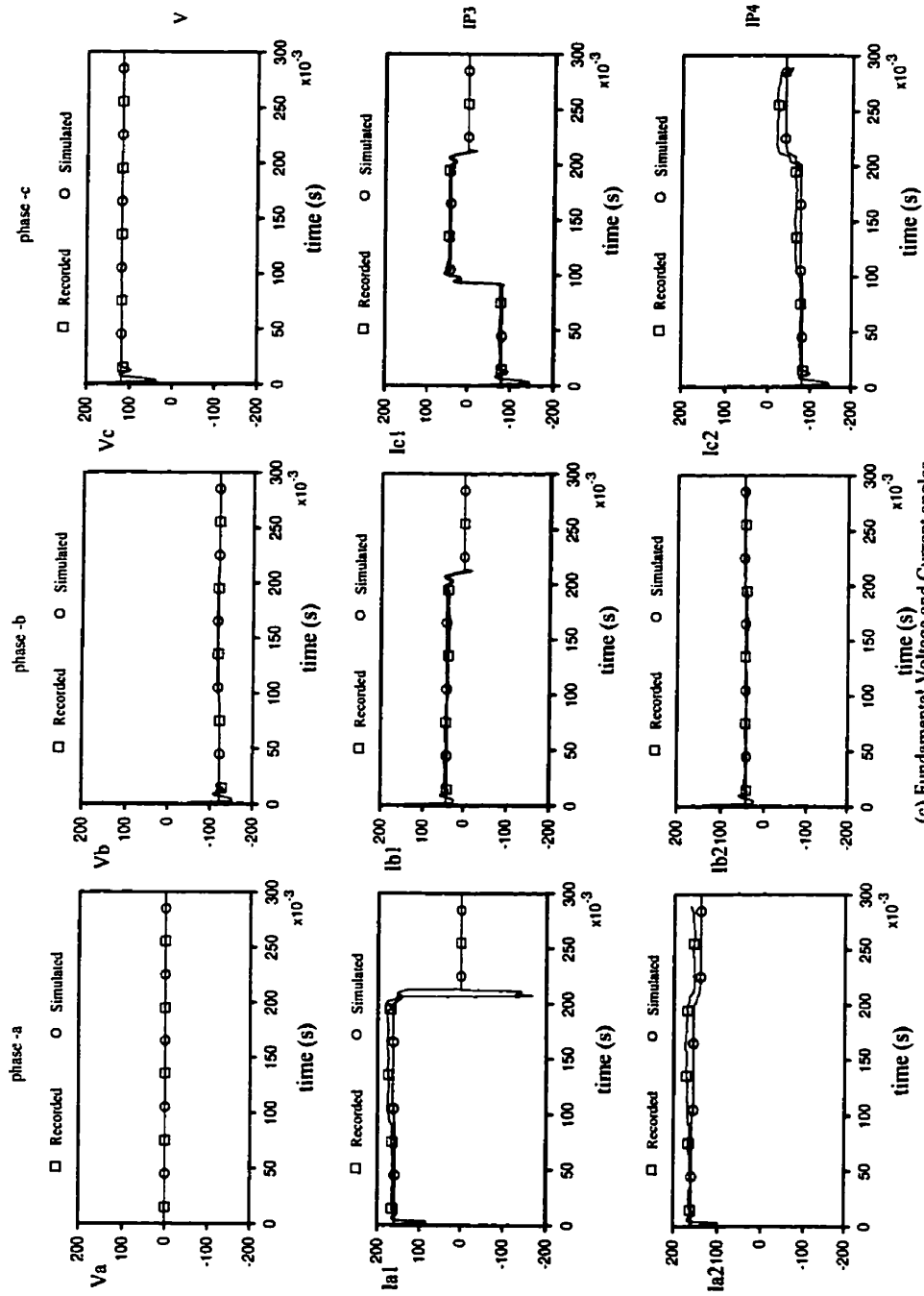
(a) Voltage and Current waveforms at Rover

Comparison of recorded and simulated voltage and current waveforms case 94-0330.000



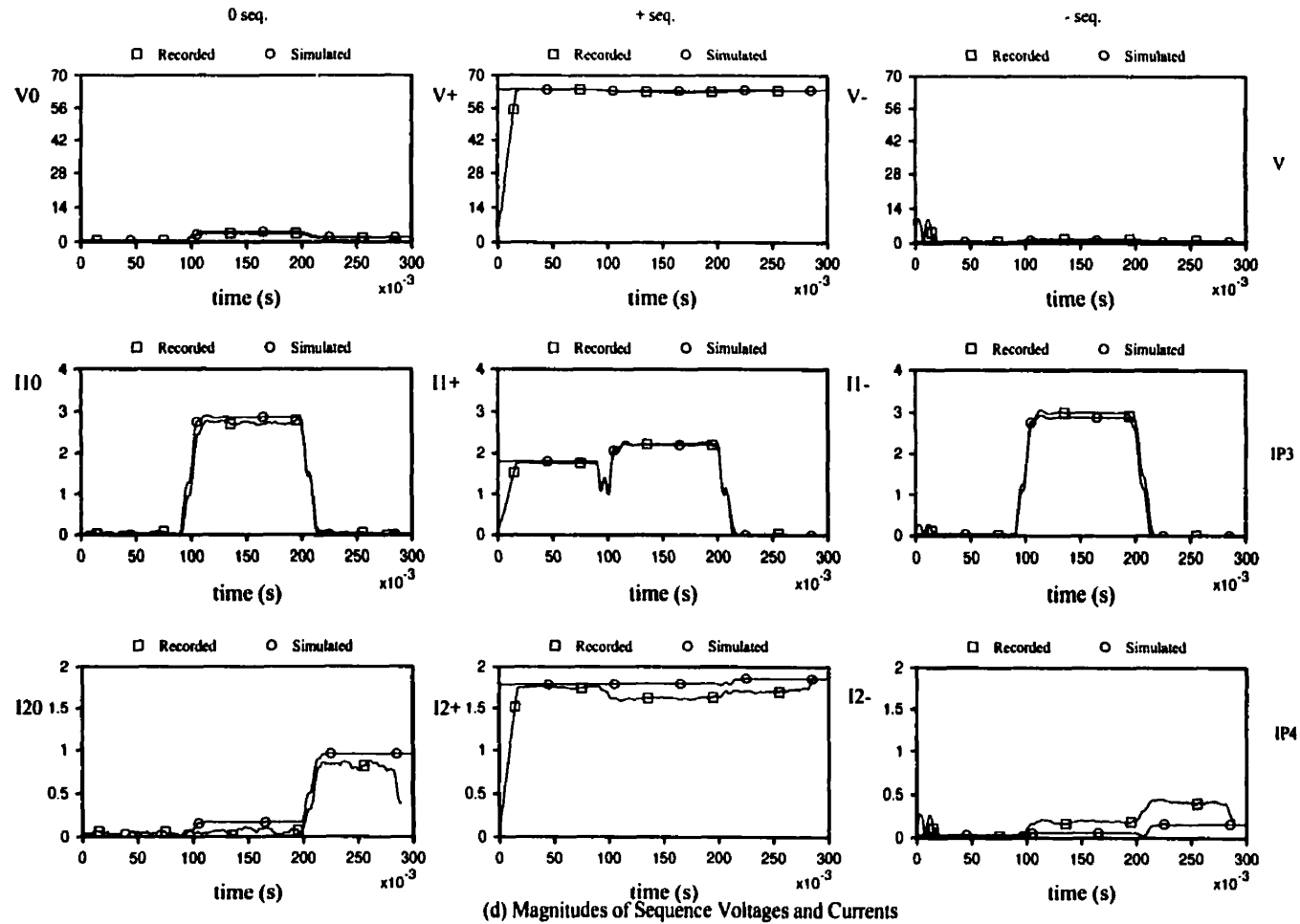
(b) Fundamental Voltage and Current Magnitudes

Comparison of recorded and simulated magnitudes of the fundamental voltages and currents case 94-0330.000

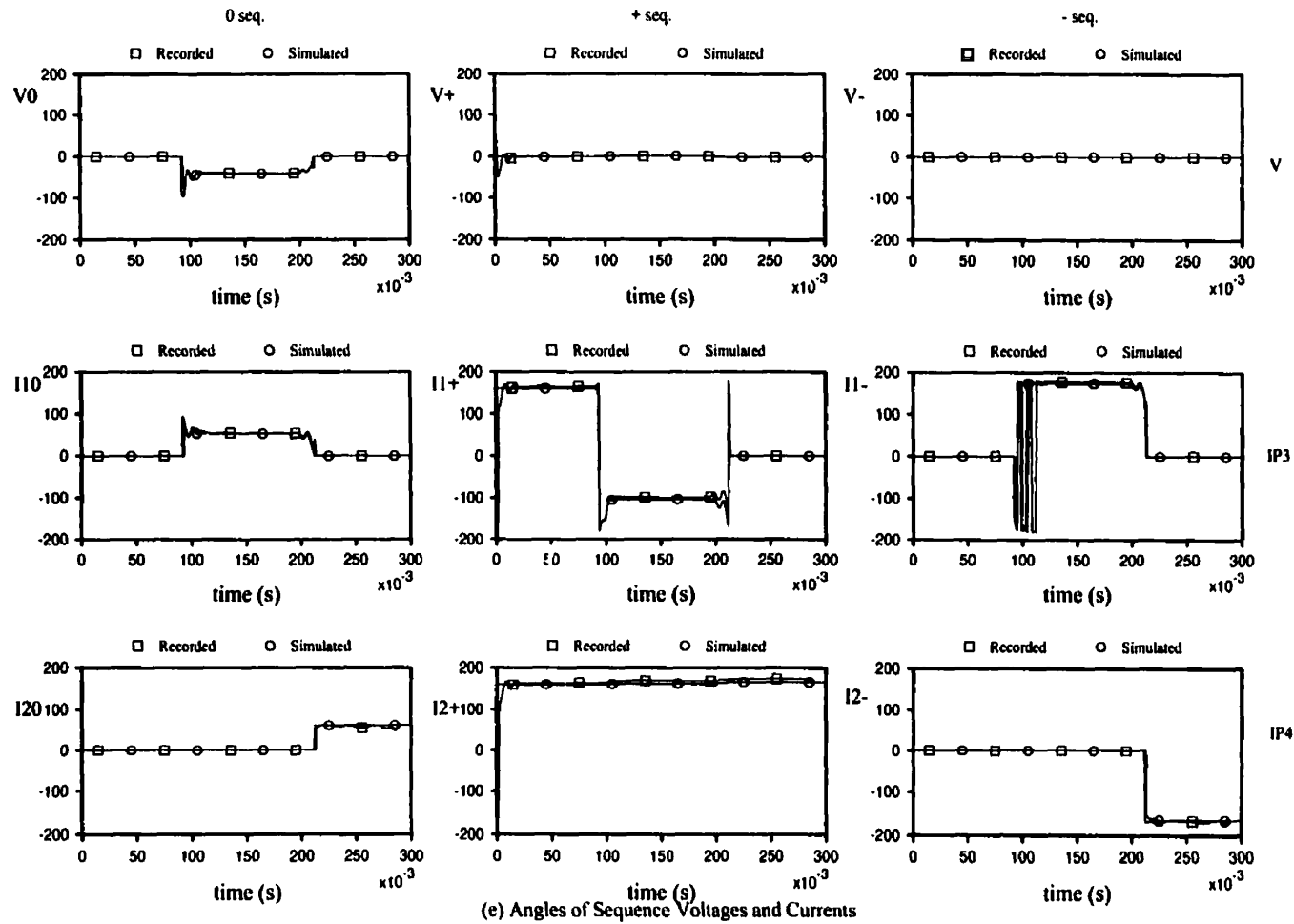


(c) Fundamental Voltage and Current angles

Comparison of recorded and simulated angles of the fundamental voltages and currents case 94-0330.000



*Comparison of recorded and simulated
magnitudes of the sequence voltages and currents case 94-0330.000*



*Comparison of recorded and simulated angles
of the sequence voltages and currents case 94-0330.000*

C.1.2 Case 94-0410.000

- Operating point information

Rover source voltage $E_{rov} = 66.18 \angle -1.22^\circ \text{ kV}$ (line - line rms)

Pointe source voltage $E_{pin} = 8.25 \angle 15.8^\circ \text{ kV}$ (line-line rms on the LV bus)

Both circuits P1 and P2 ON

- Information on type of fault: b-phase to ground fault on circuit P3. Circuit breaker at Rover is opened approximately $5 \frac{1}{2}$ cycles after inception of fault.
- Approximate distance to fault is 41 km from Rover.
- Comparison of results. (Results not attached)

The simulation data did not follow the decreasing trend the a-phase current of circuit P4 displayed, during fault.

The drop in currents of other phases were not as much as in actual data.

Zero sequence currents were greater in magnitude than expected, where as negative sequence currents were less.

Sequence current errors were more in the circuit P4 after fault clearance.

C.1.3 Case 94-0414.000

- Operating point information

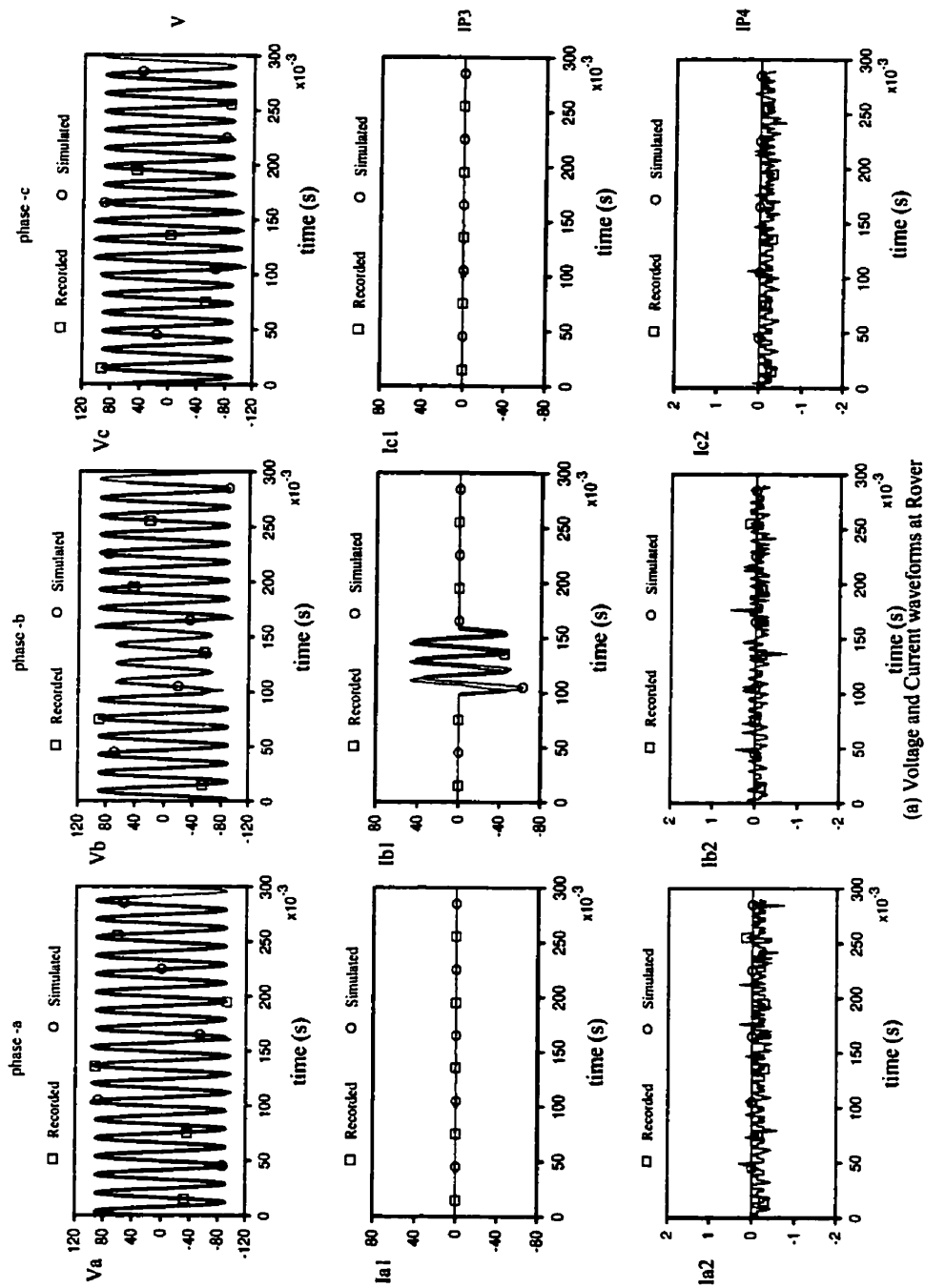
Same as for Case 94-0410.000, but circuit P4 is OFF

- Information on type of fault: Re-closure of Rover end circuit breaker on a b-phase to ground fault on circuit P3. Circuit breaker re-opens approximately $3 \frac{1}{2}$ cycles later.

- Approximate distance to fault is 9 *km* from Rover.
- Comparison of results.

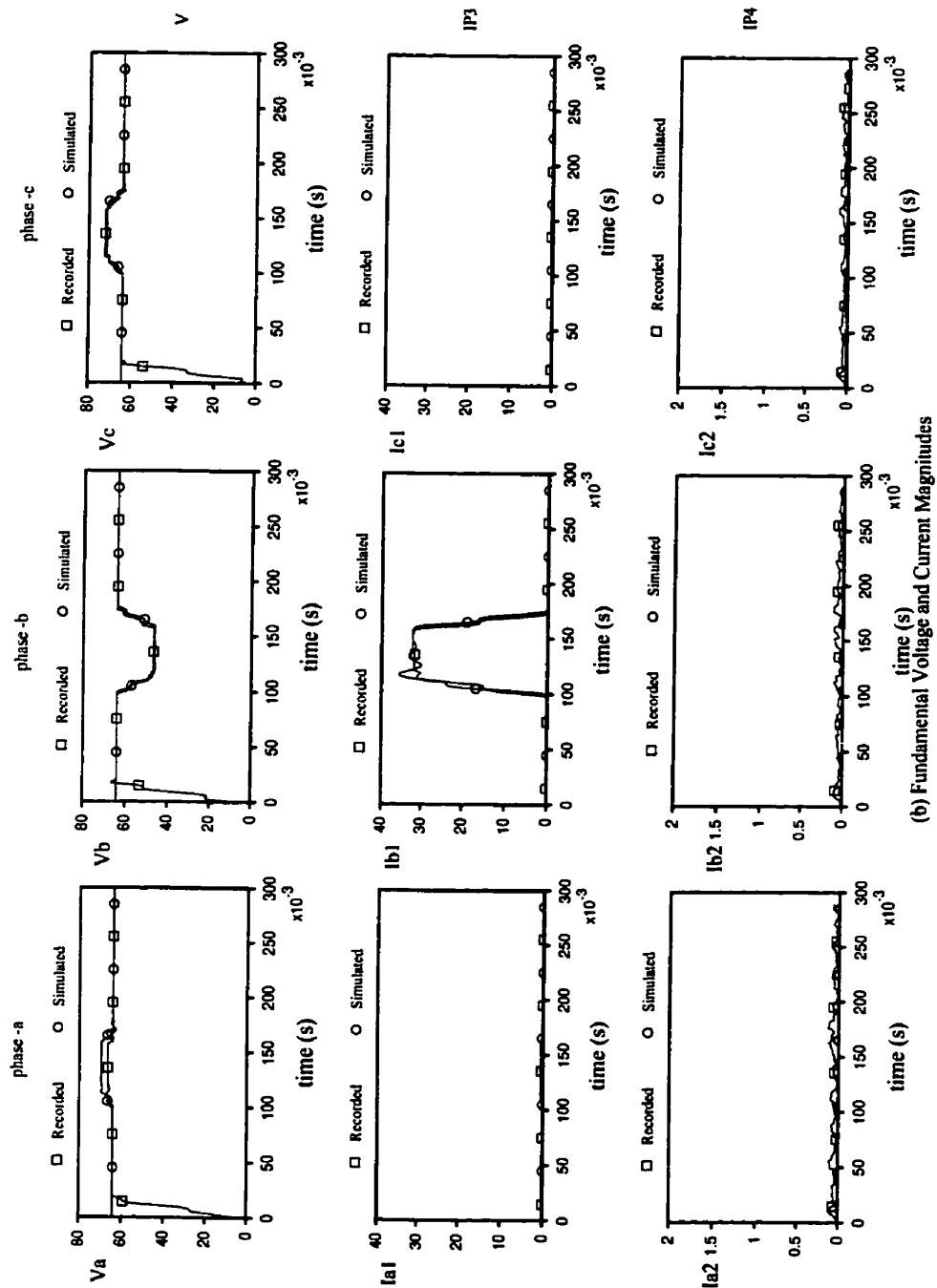
Fault phase current and the sequence current magnitudes were satisfactory. But the phase angle of these currents were off by about 18° .

The current transformer saturation seen in the recorded data was not simulated.



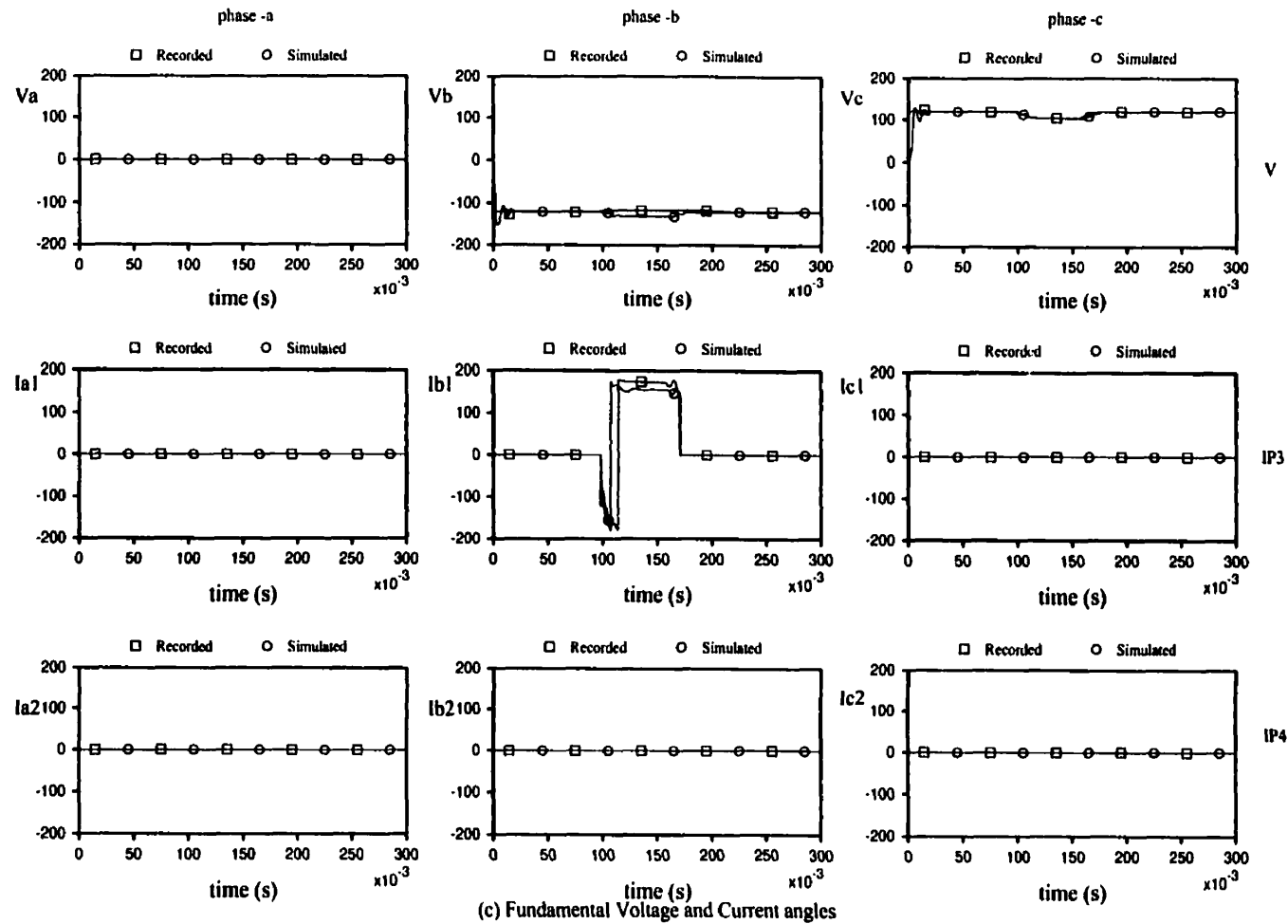
(a) Voltage and Current waveforms at Rover

Comparison of recorded and simulated voltage and current waveforms for case 94-0414.000

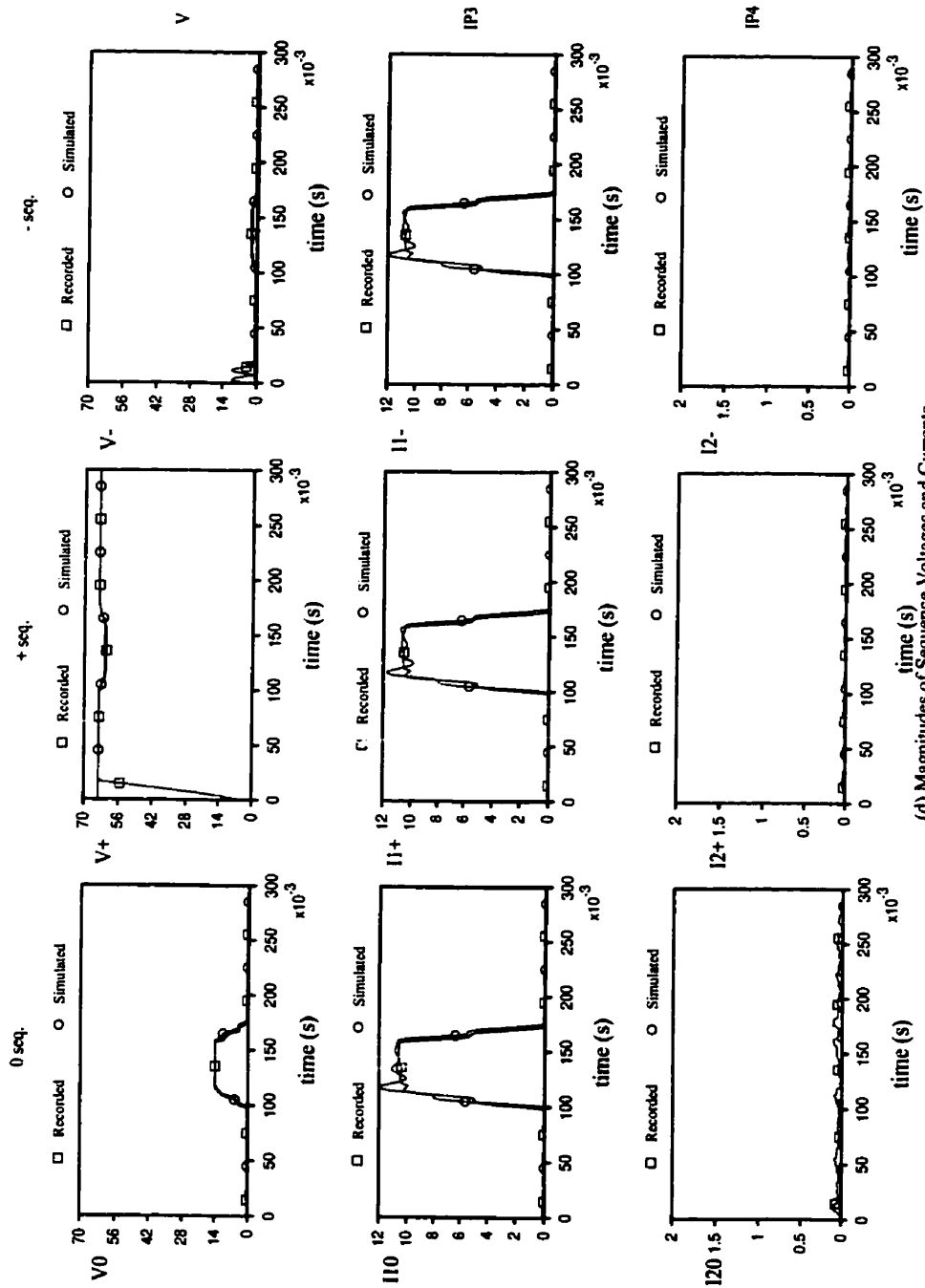


(b) Fundamental Voltage and Current Magnitudes

Comparison of recorded and simulated magnitudes of the fundamental voltages and currents for case 94-0414.000

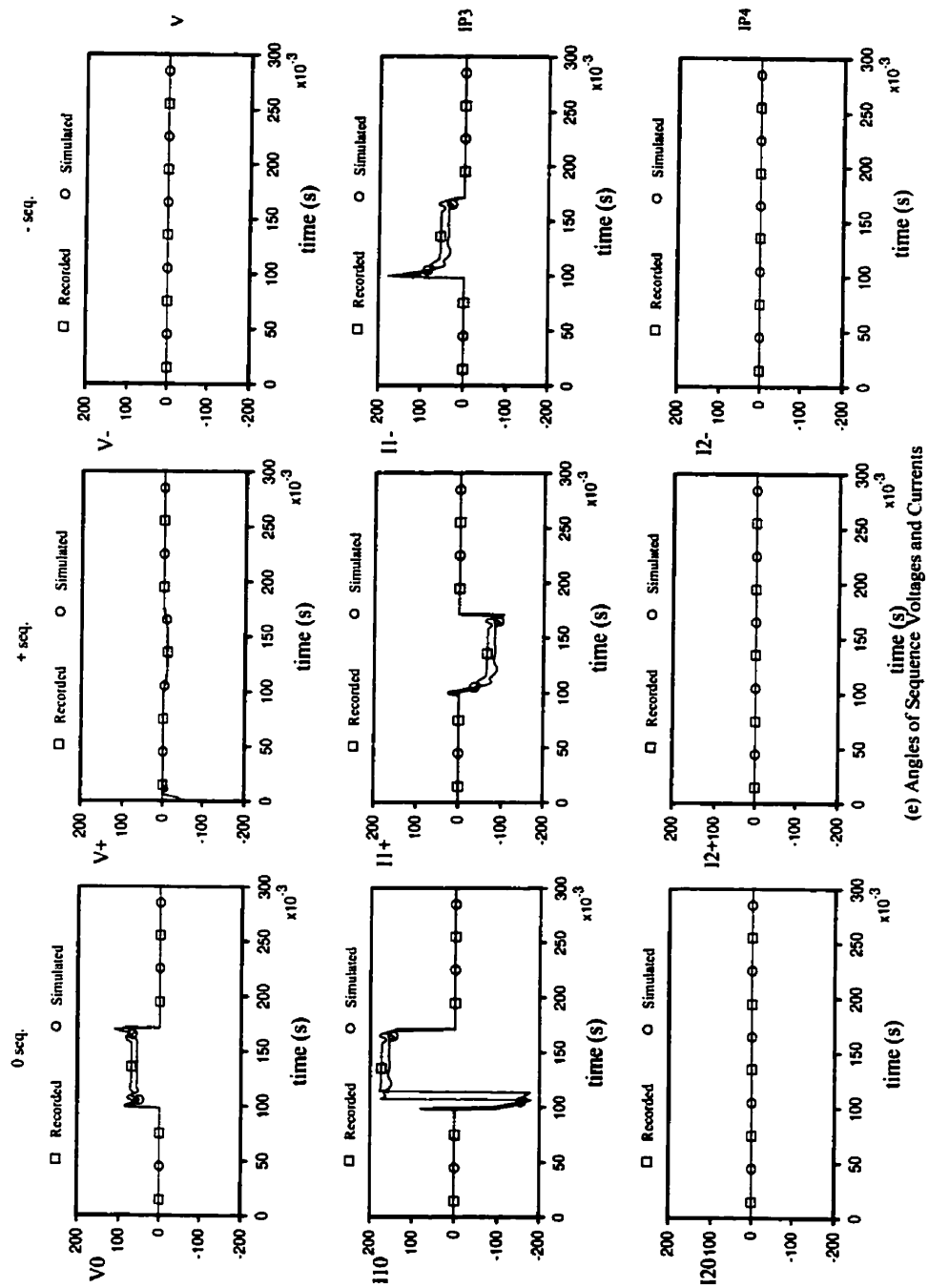


Comparison of recorded and simulated angles of the fundamental voltages and currents for case 94-0414.000



(d) Magnitudes of Sequence Voltages and Currents

*Comparison of recorded and simulated magnitudes
of the sequence voltages and currents for case 94-0414.000*



Comparison of recorded and simulated angles of the sequence voltages and currents for case 94-0414.000

C.1.4 Case 94-0608.000

- Operating point information

Rover source voltage $E_{rov} = 66.42 \angle -0.97^\circ \text{ kV}$ (line - line rms)

Pointe source voltage $E_{pin} = 8.14 \angle 10.91^\circ \text{ kV}$ (line-line rms on the LV bus)

Both circuits P1 and P2 ON

- Information on type of fault: c-phase to ground fault on circuit P4. Circuit breaker at Rover end is opened approximately $3\frac{1}{2}$ cycles after inception of fault.
- Approximate distance to fault is 10 km from Rover.
- Comparison of results.

Differences seen in this case were similar to all other cases of single line to ground faults discussed.

C.1.5 Case 94-0608.001

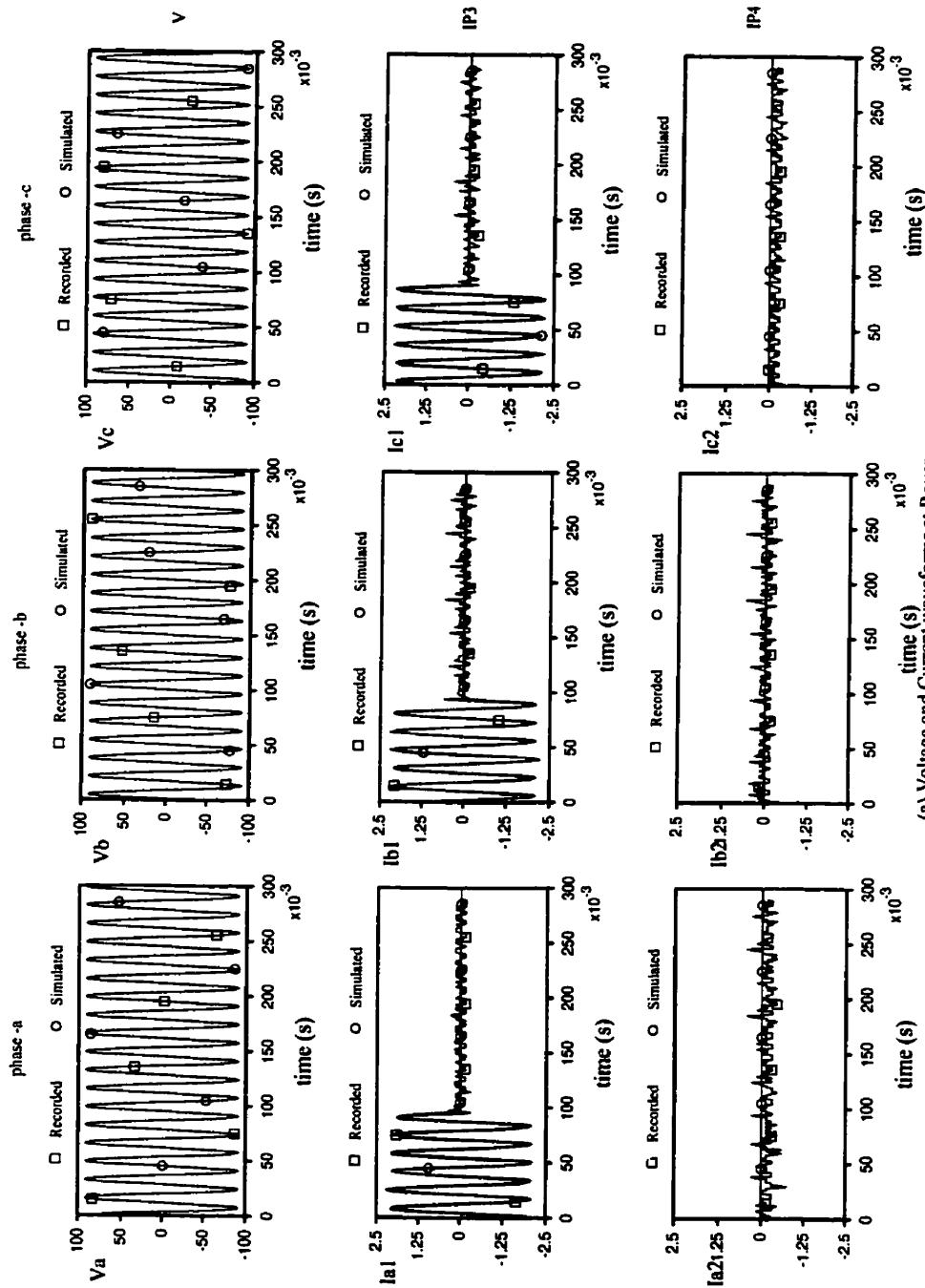
- Operating point information

This case follows from the Case 94-608.000. Therefore has the same operating point. The circuit P4 was not in operation. P1 and P2 were considered 'ON'.

- Information on type of event: Circuit breakers on P3 were opened.
- Comparison of results.

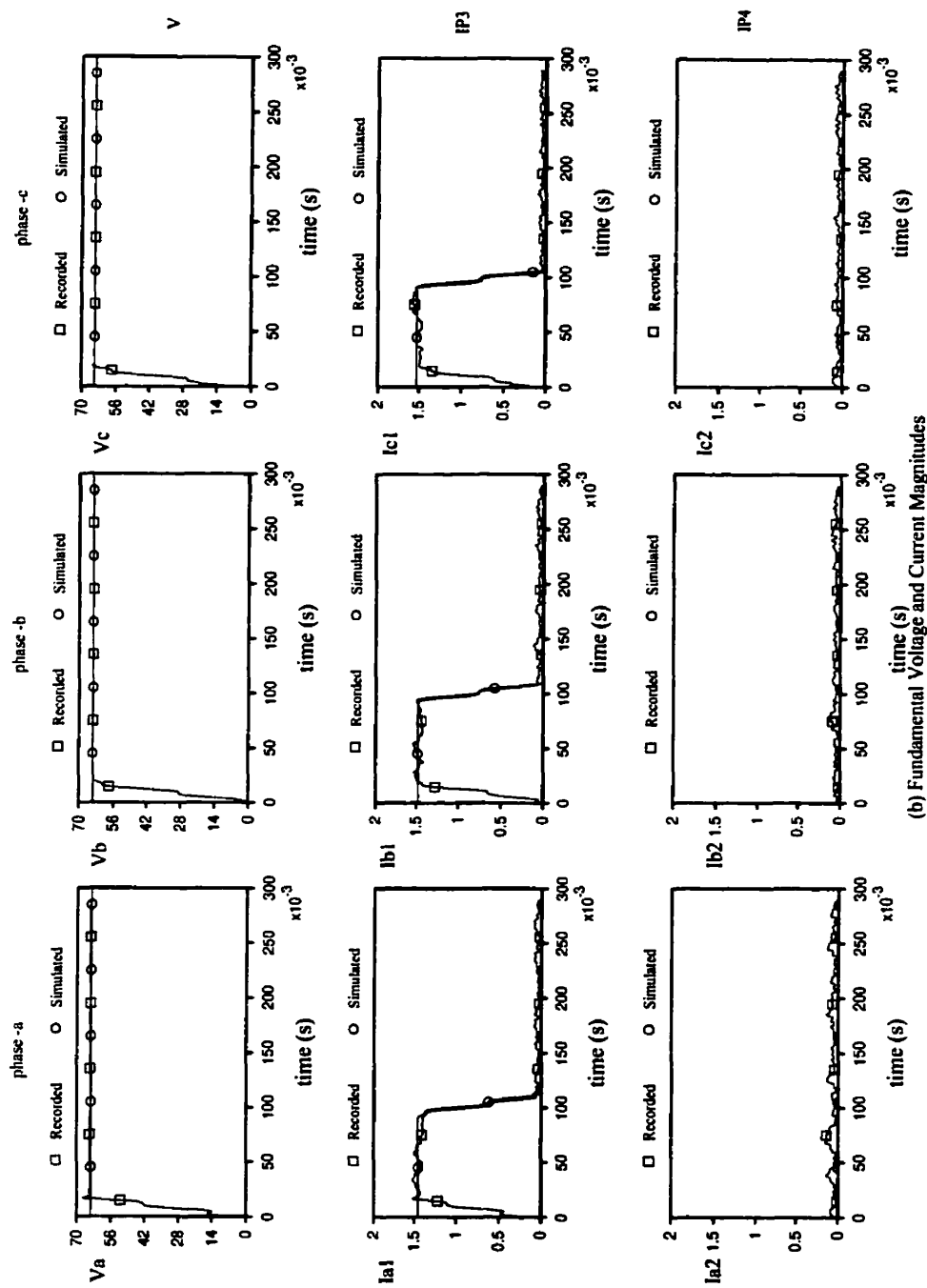
The information available was insufficient to judge the compatibility of results because both circuits did not have currents flowing through them after the event.

The match in voltages was good.

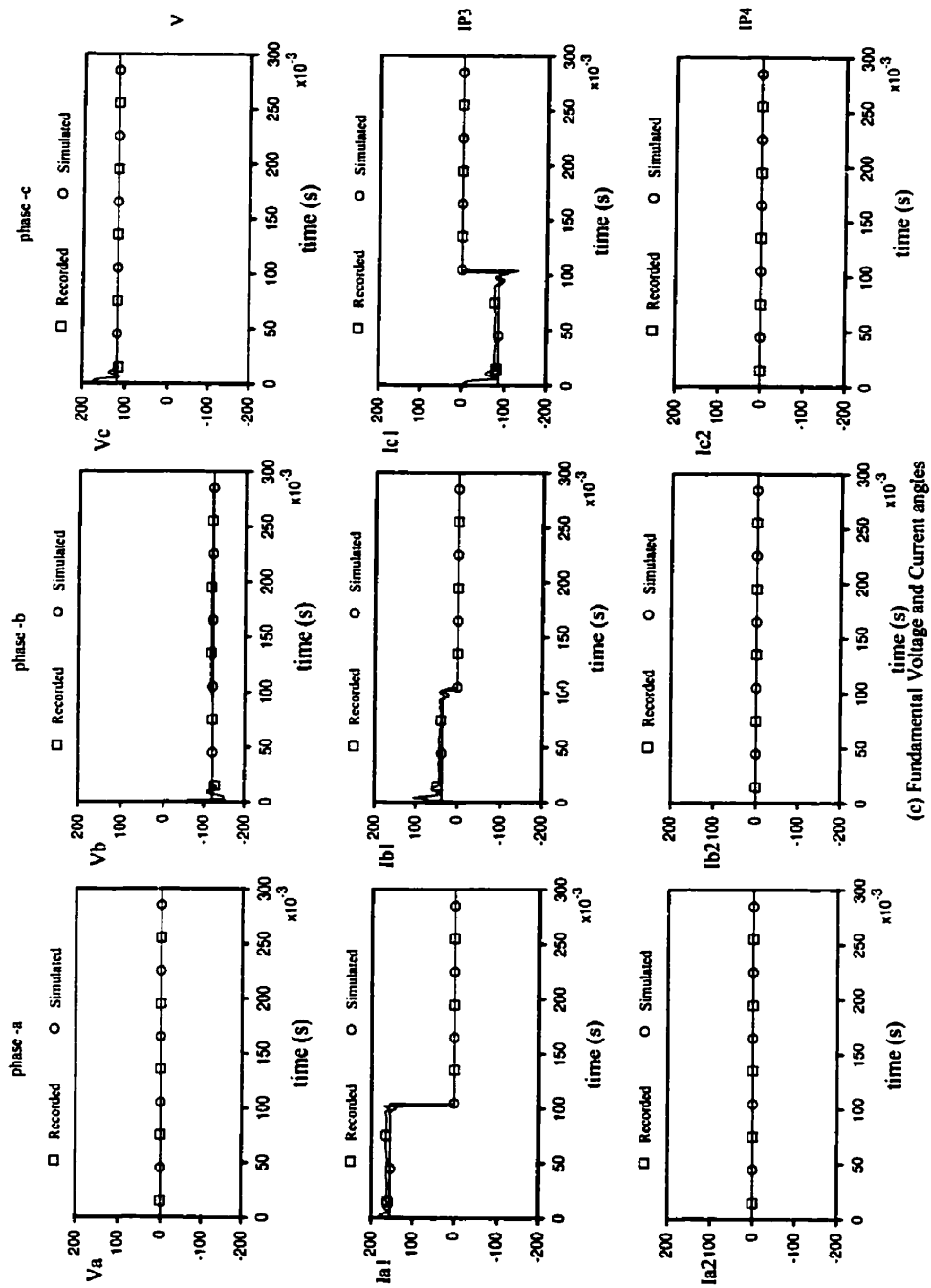


(a) Voltage and Current waveforms at Rover

Comparison of recorded and simulated voltage and current waveforms for case 94-0608.001

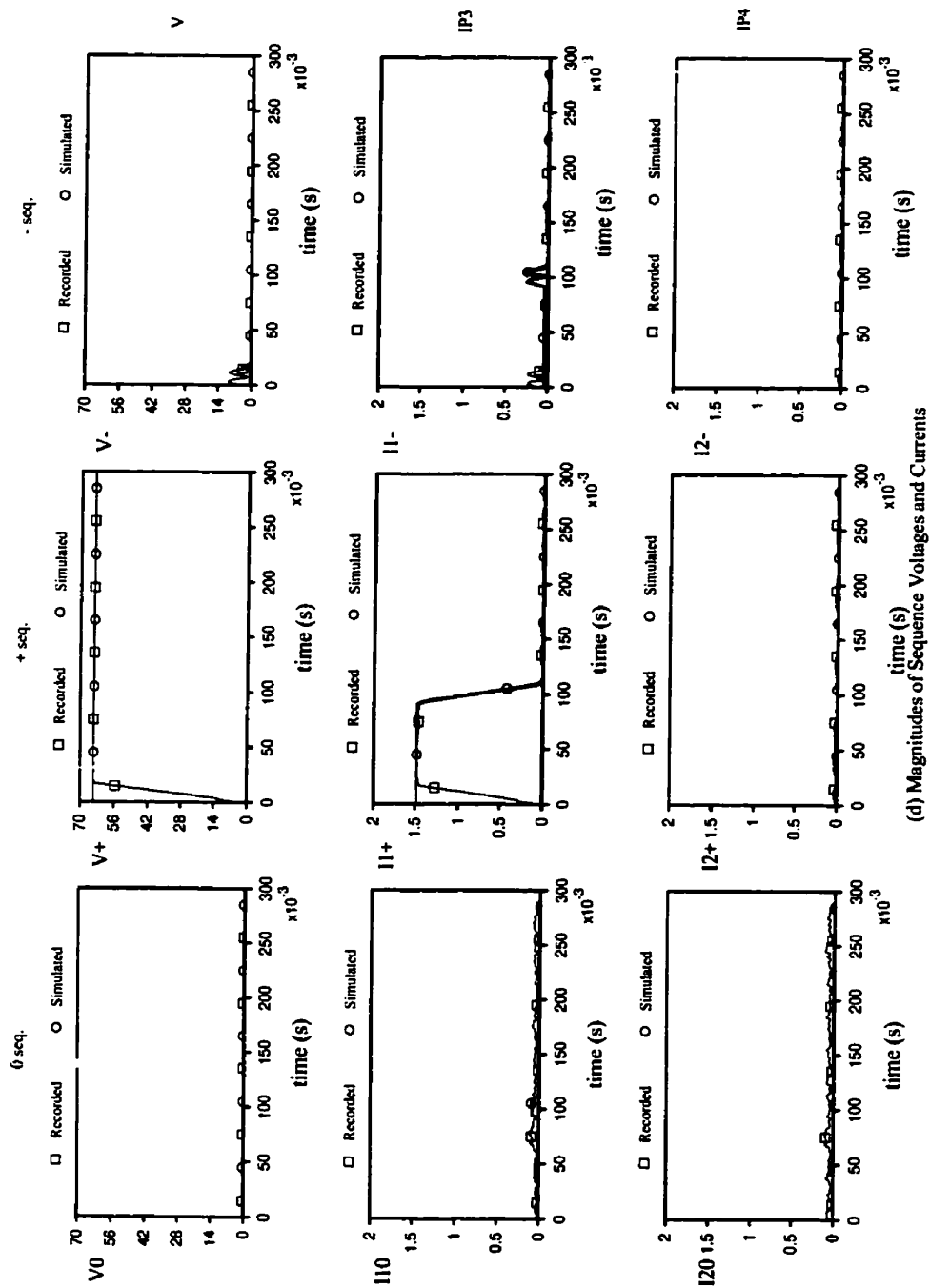


Comparison of recorded and simulated magnitudes of the fundamental voltages and currents for case 94-0608.001

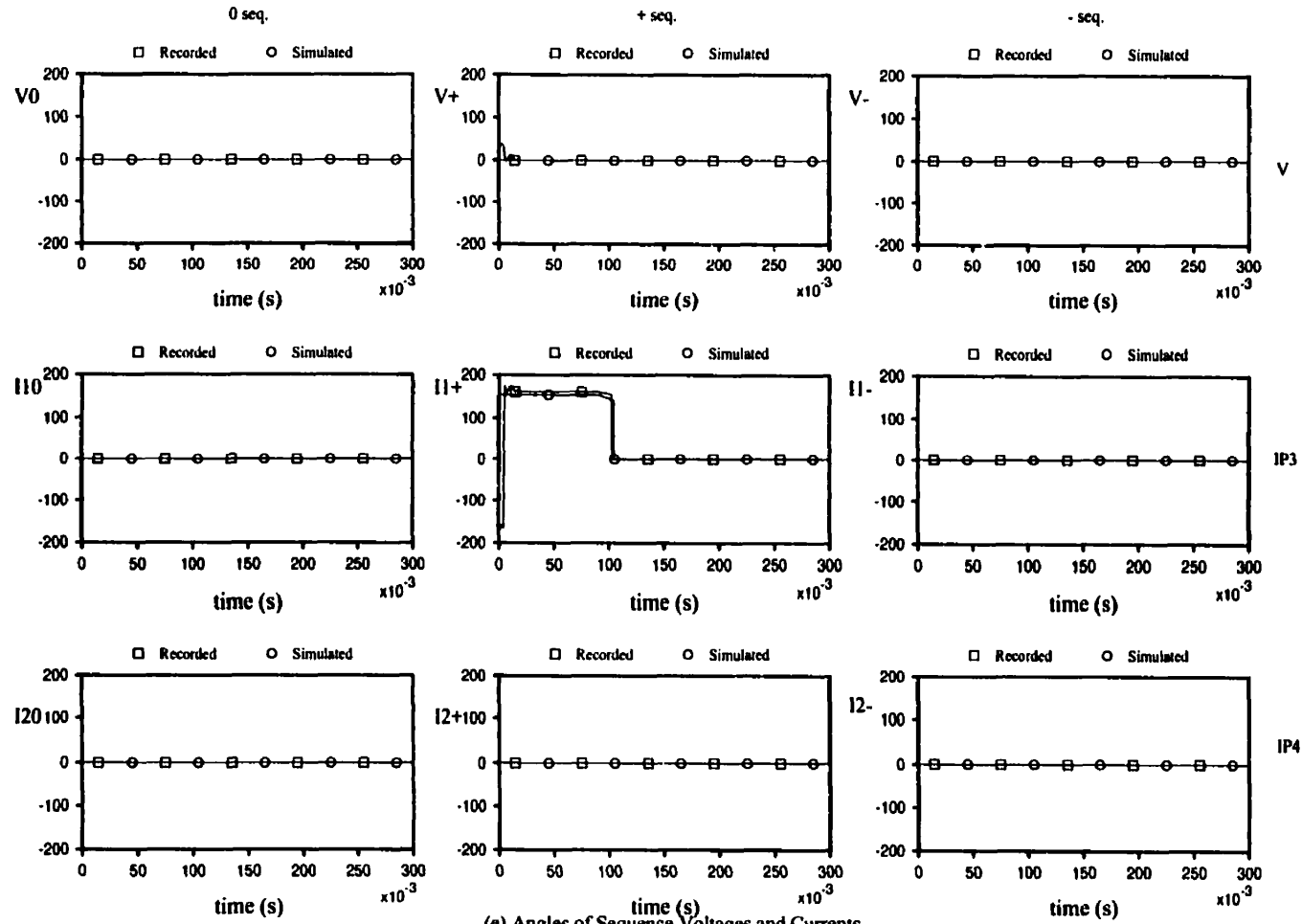


(c) Fundamental Voltage and Current angles

*Comparison of recorded
and simulated angles of the fundamental voltages and currents for case 94-0608.001*



Comparison of recorded and simulated magnitudes of the sequence voltages and currents for case 94-0608.001



(e) Angles of Sequence Voltages and Currents

Comparison of recorded and simulated angles of the sequence voltages and currents for case 94-0608.001

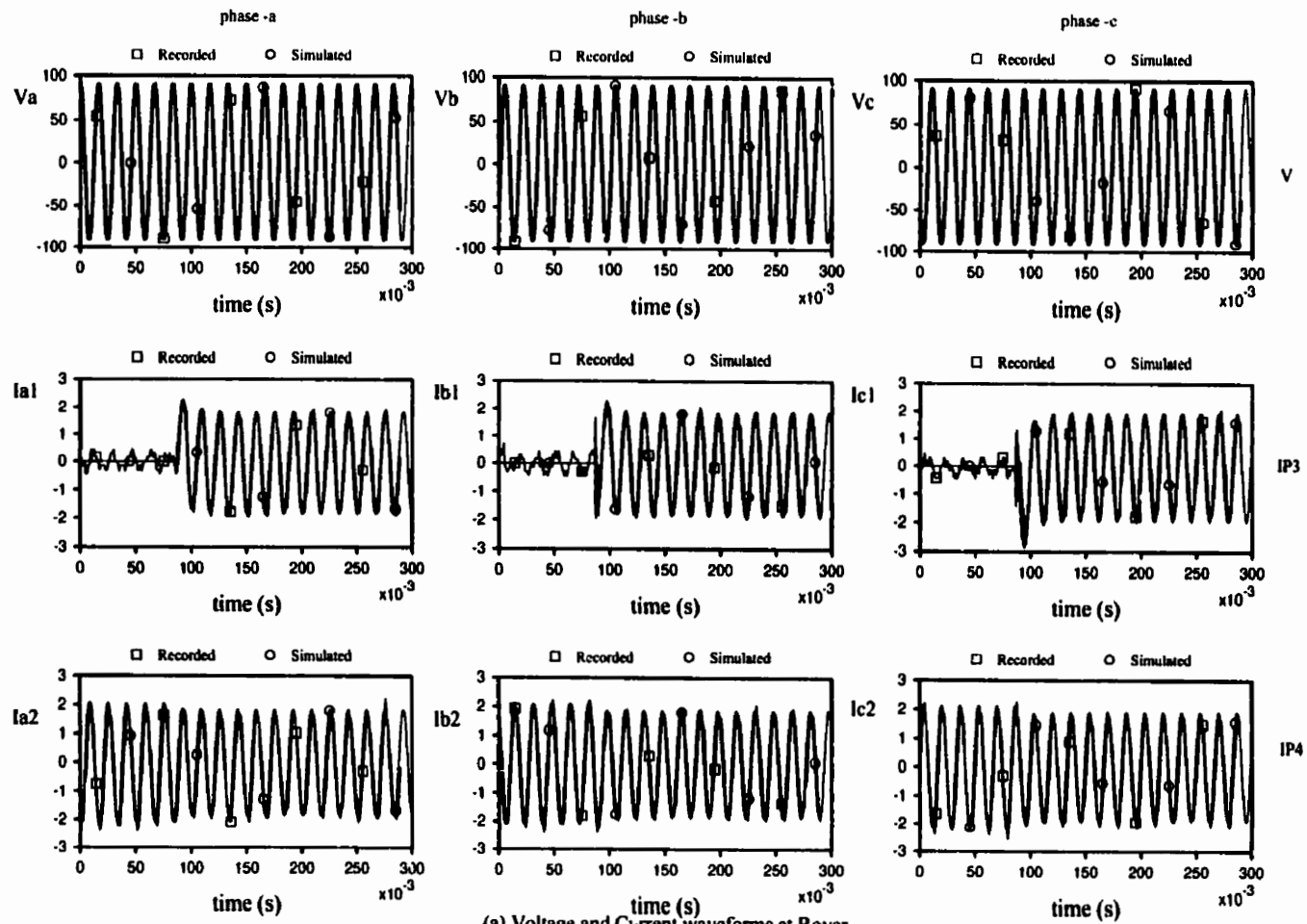
C.1.6 Case 94-0608.002

- **Operating point information**

Has the same operating point as for the two cases above. P1, P2 and P4 ON and P3 OFF.

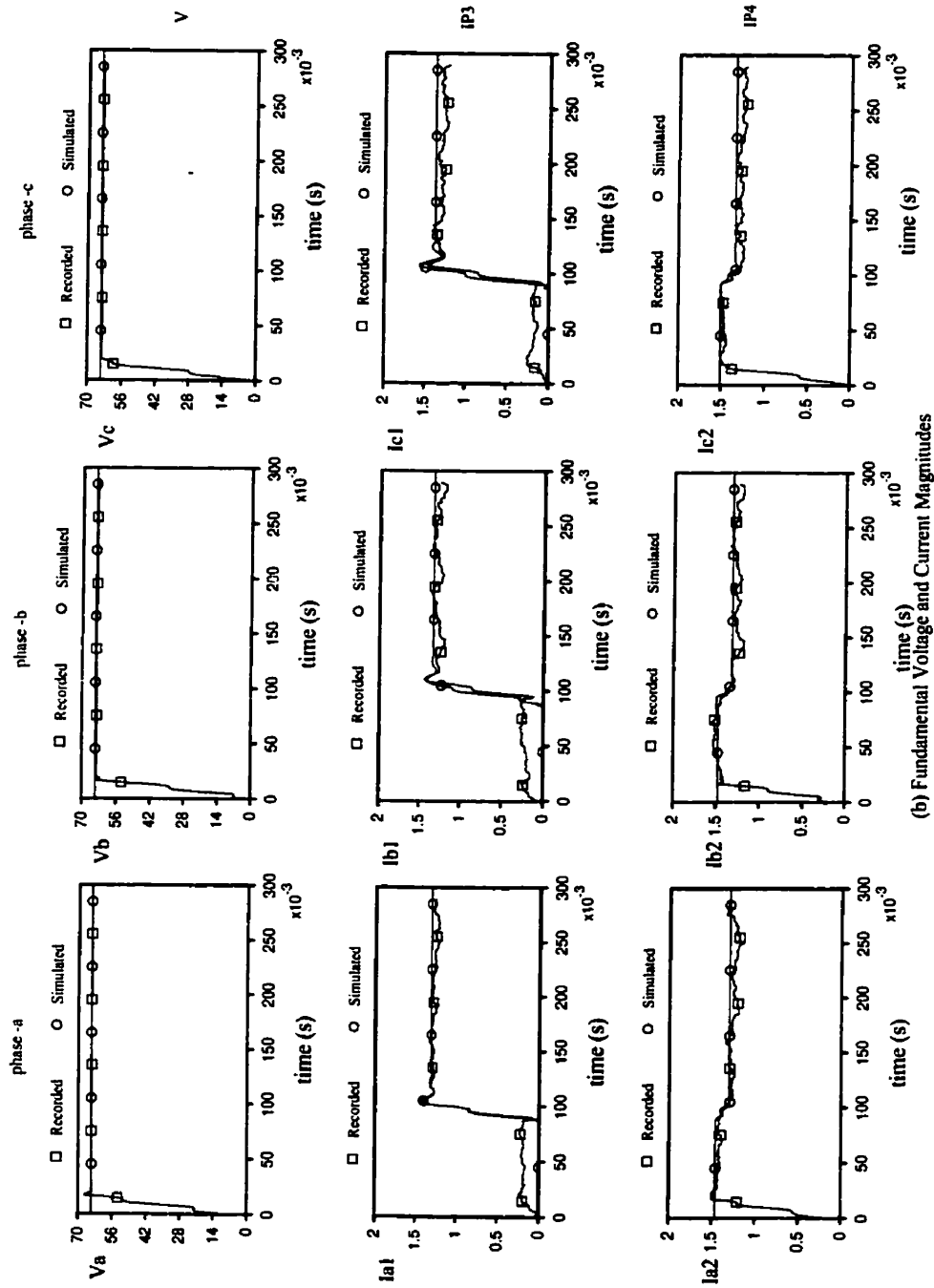
- **Information on type of event: P3 is put back in operation, this even was a follow up of event discussed in case 0608.001.**
- **Comparison of results.**

A fairly good match was seen in this case. Possibly because the dynamics does not involve any zero sequence currents which was the likely cause of most of the discrepancies. Also this case does not involve any ambiguous information such as the distance to the fault etc.

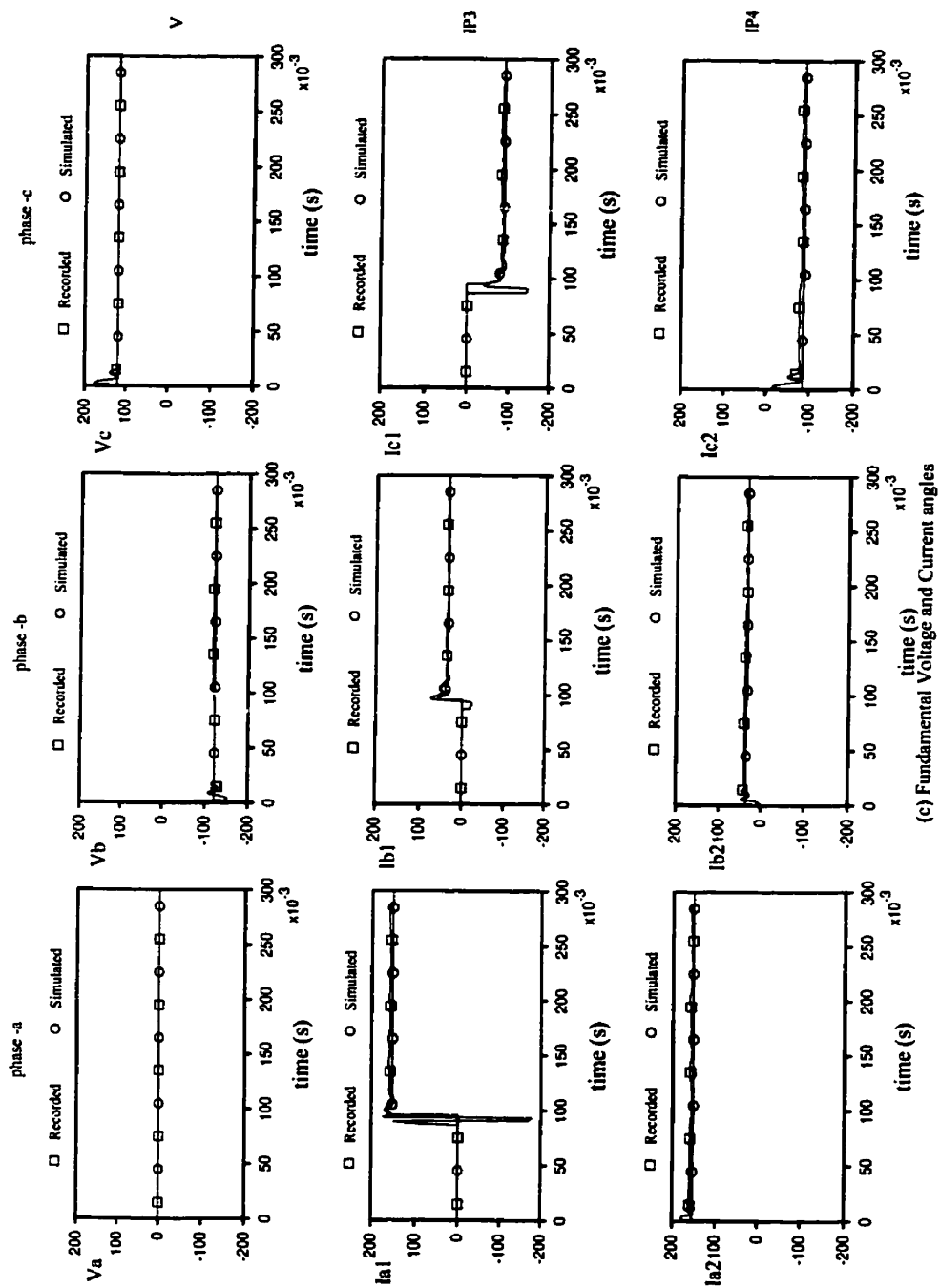


(a) Voltage and Current waveforms at Rover

Comparison of recorded and simulated voltage and current waveforms for case 94-0608.002

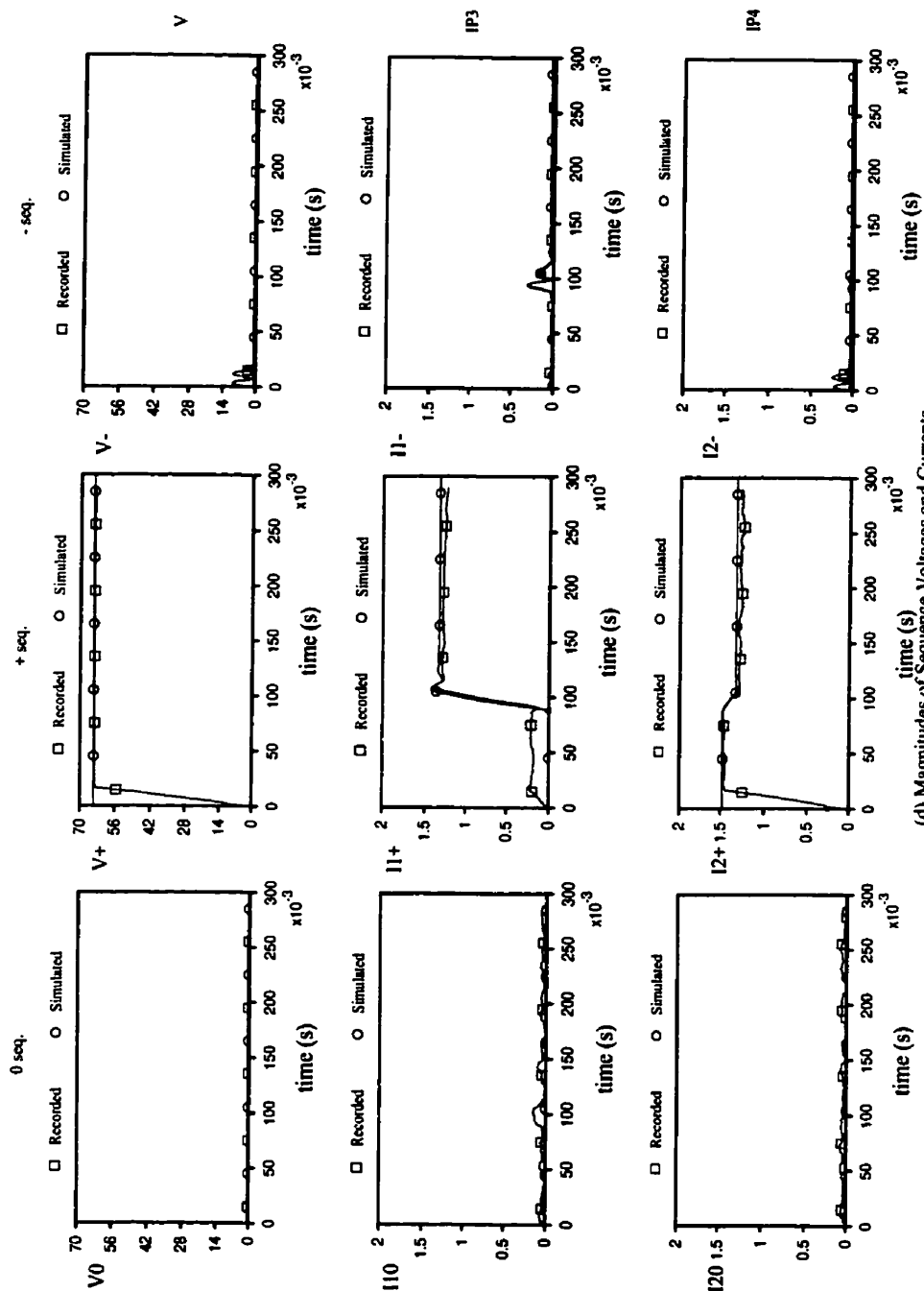


Comparison of recorded and simulated magnitudes of the fundamental voltages and currents for case 94-0608.002



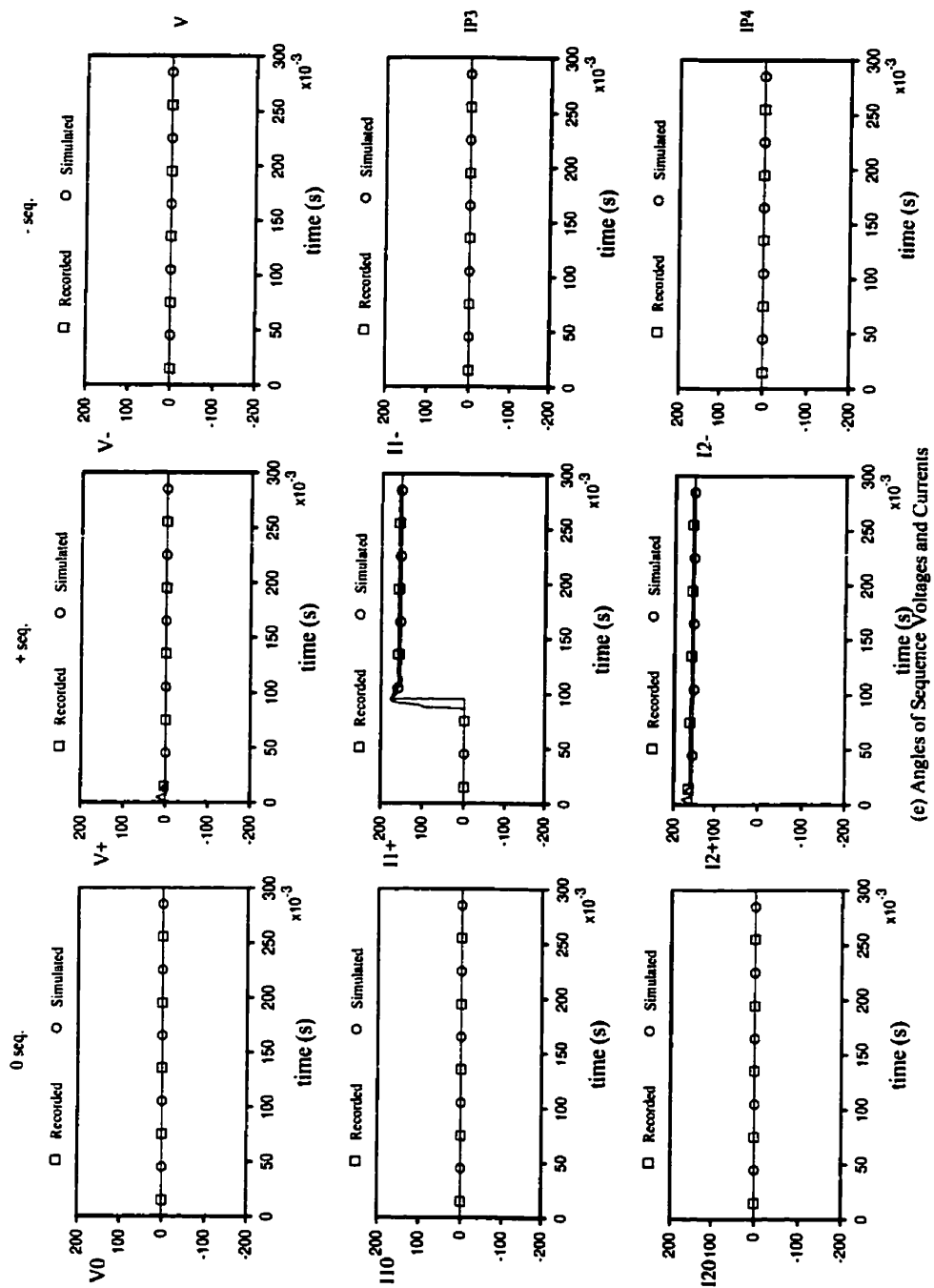
(c) Fundamental Voltage and Current angles

Comparison of recorded and simulated angles of the fundamental voltages and currents for case 94-0608.002



(d) Magnitudes of Sequence Voltages and Currents

Comparison of recorded and simulated magnitudes of the sequence voltages and currents for case 94-0608.002



(e) Angles of Sequence Voltages and Currents

Comparison of recorded and simulated angles of the sequence voltages and currents for case 94-0608.002

C.1.7 Case 94-0617.000

- Operating point information

Rover source voltage $E_{rov} = 66.86 \angle -0.79^\circ \text{ kV}$ (line - line rms)

Pointe source voltage $E_{pin} = 8.09 \angle 8.74^\circ \text{ kV}$ (line-line rms on the LV bus)

Both circuits P1 and P2 ON

- Information on type of fault: Seemed to be a three phase to ground fault on all four circuits. But it also displayed some imbalance in the system during fault. Another line to b-phase to ground fault was simulated on circuit P2 to account for the higher voltage drop exhibited on phase b. The exact type of fault was not clearly identifiable. The fault seemed to persist for approximately $3\frac{1}{2}$ cycles.

Approximate distance to fault:

The three-phase fault was simulated 27.2 *km* from Rover. b-g fault of P2 was set at 4.6 miles from Rover.

- Comparison of results.

No conclusive comparisons were made, since the fault was not exactly identified.

C.1.8 Case 94-0702.000

- Operating point information

Rover source voltage $E_{rov} = 66.65 \angle -0.86^\circ \text{ kV}$ (line - line rms)

Pointe source voltage $E_{pin} = 8.16 \angle 9.5^\circ \text{ kV}$ (line-line rms on the LV bus)

Both circuits P1 and P2 ON

- Information on type of fault: b-c-g fault on circuits P3 and P4. Approximately 2.6 cycles later a-g fault occurs on circuits P1 and P2.

The fault on circuits P3 and P4 are cleared 31/2 cycles after fault inception. The other fault seems uncleared.

- Approximate distance to fault:

b-c-g fault is approximately 10.46 *km* away from Rover. approximate distance to a-g fault is 20.76 *km*.

- Comparison of results.

The results do not match. This is most likely because the faults were not well identified.

C.2 Conclusions

The discrepancies in the simulated data are mostly visible in cases where there are zero sequence components of currents and voltages. It may be due to an over estimation of the zero sequence mutual impedances of the line or due to an error in the data of conductor configuration itself.

Other factors giving rise to considerable differences in simulations would be, current transformer saturation which is not modelled. The operating condition of the circuits P1 and P2 which cannot be derived using the available recorded data. Also mis-identification of the type and distance to fault. These problems could only be overcome with some staged faults on the system.

The operating point was preset based on calculations done for a completely balanced system. But since the voltage source had its own imbalance of phase angles, pre-fault conditions simulated were not perfectly the same as that of the recorded data.